Aquaporins in *Magnaporthe oryzae*

A thesis submitted for the degree of Doctor of Philosophy at the University of Oxford

Elizabeth Birch

Trinity Term 2013

Aquaporins in *Magnaporthe oryzae*

A thesis submitted for the Degree of Doctor of Philosophy
Trinity Term 2013

Elizabeth Birch
New College

The Ascomycete fungus *Magnaporthe oryzae* is the causative agent of Rice Blast, and has become the predominant model organism for study of fungal phytopathogens and other appressorium-forming fungi. I identified and attempted to elucidate the function of the six aquaporin genes in the *M. oryzae* genome. These small membrane channels have been implicated in the transport of water, glycerol, and a variety of other small molecules. We speculated that these functions might be important in the formation of the appressorium – a specialised infection structure that relies on the generation of turgor. The role of these proteins in general fungal biology is poorly understood, and this project endeavoured to correct this gap.

A phylogenetic analysis of aquaporins in extant fungi revealed the significant expansion of this gene family in Pezizomycete and Basidiomycete fungi, with up to 17 genes in some species. I characterised the expression pattern of the six identified aquaporins in the *M. oryzae* genome during pathogenic development and found there to be substantial up-regulation co-incident with appressorial turgor generation. Single knock-outs of each aquaporin gene were fully pathogenic, with normal infection-related development and axenic growth. I speculated that the absence of a strong phenotype may have been caused by functional redundancy, and used qRT-PCR investigate the incidence of transcriptional up-regulation of remaining family members in the knock-out backgrounds. This uncovered a putative reciprocal relationship between two genes *MoAQP1* and *MoAQP2*, suggesting that deletion of one results in up-regulation of the other. I subsequently tested the substrate permeability of this gene pair and found them to be permeable to hydrogen peroxide. However, deletion of one of these genes did not appear to affect the rate of flux of hydrogen peroxide across the plasma membrane. My attempt to characterise the cellular localisation of these proteins using GFP fusions was largely unsuccessful with the exception of a single gene, *MoAGP2*, which appears to be located on the endoplasmic reticulum.

Acknowledgements

First and foremost, I would like to offer my sincere thanks to my supervisor, Professor Sarah Gurr, who always believed in this project. Without her encouragement, I might never have completed this thesis. The opportunity to observe the power of her charisma and clear communication style was an invaluable experience.

I would also like to offer special thanks to Dr. Marketa Samalova. Her teaching and assistance with the day-to-day molecular biology was vital, as was her enthusiasm for a Guinness after work! I am grateful to my second supervisor, Dr. Mark Fricker for his wise perspective on science and would also like to thank my collaborator at the University of Copenhagen, Dr. Pai Pedas, for enabling me to spend time working in Denmark.

It has been a privilege to work alongside those on the Gurr / Preston / Moore corridor. The other members of the Gurr lab– Jasper, Sarena, Ivey and Molly – were always willing to offer advice and kept things interesting! A special mention must go to Sarah and Caroline for tolerating “the messiest student we’ve ever had”. I will miss coffee time with the other members of the corridor - Sarah, Michael, Anya, Helen, Brendan, Niloufer, Monika, Astrid and Charlotte - as well as friends from further afield in the department, Jon, Jim and Matt (to mention but a few).

Without the girls at Mansfield Road FC and OUWAFC, my DPhil would have been nowhere near as rich an experience. Last but not least, I would like to thank my family (including Dr. Sarah Rouse) for their love and encouragement, and without whom I would never have enjoyed so many opportunities.

Contents

Chapter 1 Introduction 1

1.1 The global significance of plant pathogens 1

1.2 Rice and Rice Blast Disease 2

1.3 The rice blast fungus, *Magnaporthe oryzae* 4

1.3.1 *M. oryzae* as a model pathogen 4

1.3.2 The life cycle of *M. oryzae* 4

1.3.3 Appressorial turgor 8

1.4 The importance of turgor 9

1.4.1 Regulation of turgor pressure 10

1.5 Aquaporins 11

1.5.1 Aquaporins in animals 15

1.5.2 Aquaporins in plants 16

1.5.3 Aquaporins in fungi 18

1.6 Objectives of this Thesis 21

Chapter 2 Materials and Methods 23

2.1 Materials and Methods 24

2.1.1 Materials 23

2.1.1.1 Suppliers 23

2.1.1.2 Chemical reagents 24
2.1.1.3 Equipment 24
2.1.1.4 Solutions and media 24
2.1.1.5 Oligonucleotide sequences 26
2.1.1.6 *Saccharomyces cerevisiae* strains 32
2.1.1.7 *Magnaporthe oryzae* strains 32
2.1.1.8 *Escherichia coli* strains 34
2.1.1.9 Important websites 34
2.2 Methods 34
2.2.1 Plant methods 34
2.2.1.1 Stock maintenance and routine growth 34
2.2.1.2 Barley epidermal peel preparation 34
2.2.1.3 Onion epidermal peel preparation 35
2.2.2 *Magnaporthe oryzae* methods 35
2.2.2.1 Routine growth and maintenance of stocks 35
2.2.2.2 *Magnaporthe oryzae* transformation 36
2.2.2.3 Pathogenicity assays 37
2.2.3 *Saccharomyces cerevisiae* methods 38
2.2.3.1 Routine growth and maintenance of stocks 38
2.2.3.2 *Saccharomyces cerevisiae* transformation 38
2.2.4 *Escherichia coli* methods 39
2.2.4.1 Preparation of DH5α competent cells 39
2.2.4.2 Transformation of DH5α competent cells 39
2.2.4.3 Plasmid DNA preparation 40
2.2.5 DNA methods 40

2.2.5.1 Genomic DNA extraction 40
2.2.5.2 PCR methods 41
2.2.5.3 Southern blotting 43
2.2.6 RNA methods 45
2.2.6.1 Maintenance of an RNA-free environment 45
2.2.6.2 Total fungal RNA extraction 45
2.2.6.3 gDNA removal 45
2.2.6.4 qRT-PCR methods 45
2.2.7 Microscopy 47
2.2.7.1 Light microscopy 47
Chapter 3 Putative aquaporins in *Magnaporthe oryzae* 48
3.1 Introduction 48
3.1.1 The evolution of the aquaporin gene family 48
3.1.2 Transcript abundance of *M. oryzae* aquaporin genes 53
3.2 Experimental aims 54
3.3 Methods specific to this chapter 56
3.3.1 Bioinformatic methods 56
3.3.2 qRT-PCR methods 57
3.4 Results 58
3.4.1 Identification of aquaporins in *Magnaporthe oryzae* 58
3.4.2 The phylogeny of fungal aquaporins 62
3.4.3 The phylogeny of fungal and plant MIPs 69
3.4.4 Aquaporins are expressed during pathogenic development 71
3.5 Discussion 78
3.5.1 Generating accurate phylogenies of the MIP protein family is challenging 78

3.5.2 Aquaporin MIPs are expressed during pathogenic development 79

Chapter 4 Generation and phenotyping of single aquaporin deletion mutants 80

4.1 Introduction 80

4.1.1 Study of gene function in filamentous fungi 80

4.1.2 Gene deletion in filamentous fungi 82

4.1.3 Pathogenicity and virulence 84

4.1.4 Vegetative growth and stress responses 85

4.2 Experimental aims 87

4.3 Methods specific to this chapter 87

4.3.1 Appressorial turgor measurement 87

4.4 Results 87

4.4.1 Generation of the *AQP1, AQP2, AQP3 & AGP1* 'split marker' deletion constructs. 87

4.4.2 Generation of Δ*agp2* using the 'whole' marker method 92

4.4.3 Generation and confirmation of aquaporin knockout strains 93

4.4.4 Pathogenicity and virulence 100

4.4.5 Infection-related development 103

4.4.6 Vegetative growth and stress tolerance 109

4.5 Discussion 115

4.5.1 Single aquaporin deletion mutants are fully pathogenic and appear to have normal pathogenic development 115

4.5.2 Deletion of Δ*aqp1* and Δ*aqp3* may affect vegetative growth 117

4.5.3 *AGP2* may be affected by the ion detoxification process 118

4.5.4 The split marker deletion strategy is not more effective in the Guy11 background 118

Chapter 5 Genetic redundancy among aquaporins 120

5.1 Introduction 120

5.1.1 Redundancy in gene families 120
5.1.2 qRT-PCR 122
5.2 Experimental objectives 126
5.3 Methods specific to this chapter 126
5.3.1 RNA extraction from Teflon surfaces 126
5.3.2 qRT-PCR methods in this chapter 129
5.4 Results 130
5.4.1 The combination of two individual biological replicates 131
5.4.2 Replicates 1 and 2 137
5.5 Discussion 142
5.5.1 A regulatory backup circuit may exist between *AQP1* and *AQP2* 142
5.5.2 The existence of other compensatory changes cannot be ruled out 143
Chapter 6 Aquaporin permeability 147
6.1 Introduction 147
6.1.1 Heterologous expression of aquaporin proteins 147
6.2 Experimental aims 149
6.3 Methods specific to this Chapter 149
6.3.1 *Saccharomyces cerevisiae* assays 149
6.3.2 Grx-roGFP2 confocal imaging 153
6.4 Results 155
6.4.1 Aquaporin structure/function characteristics 155
6.4.2 *Saccharomyces cerevisiae* expression assays 162
6.4.3 Deletion of an H_2O_2 permeable aquaporin does not affect the rate of roGFP-redox response to H_2O_2 perfusion 168
6.5 Discussion 172

6.5.1 The *Magnaporthe oryzae* 70-15 gene annotations are of poor quality 172

6.5.2 Predictions based on the primary sequence are partially correct 172

6.5.3 Deletion of the H_2O_2 permeable *AQP2* does not affect the rate of H_2O_2 diffusion across germling plasma membranes 174

Chapter 7 GFP tagging of aquaporins in *M. oryzae* 177

7.1 Introduction 177

7.1.1 Aquaporin localisation 177

7.2 Experimental aims 177

7.3 Methods specific to this Chapter 178

7.3.1 Yeast recombinational cloning 178

7.3.2 Confocal microscopy 180

7.3.3 Western blots 180

7.4 Results 182

7.4.1 C-terminal aquaporin fusion proteins are not expressed or mislocalise 182

7.4.2 An *AGP1* fusion with *eGFP* on an internal loop has no detectable fluorescence .. 188

7.4.3 Some aquaporin promoters drive the expression of cytosolic eGFP 192

7.4.4 Only *AGP2* is expressed by the pRP27 promoter with a C-terminal eGFP tag 196

7.4.5 N-terminal aquaporin eGFP fusion proteins mislocalise 201

7.5 Discussion 204

7.5.1 The *pRP25*::*AGP2*::*eGFP*-expressing strains display membrane-localised fluorescence and a germ tube emergence phenotype 205

Chapter 8 Discussion 208

8.1 Summary 208

8.2 MIP family expansions 210

8.3 Regulation of expression 211

8.4 Further Work 212

8.5 Concluding remarks 214

Chapter 9 References 215

Chapter 1 Introduction

1.1 The global significance of plant pathogens

The human population is predicted to continue to grow until the middle of this century before reaching a plateau of some 9 billion people (Tilman et al., 2011). A major correlate of this growth deceleration is increased wealth; and this, in turn, is associated with consumption of more resource-intensive foods such as meat, dairy, and fish (Godfray et al., 2010). This demand-driven expansion of the global food supply will present a significant challenge in the coming decades. It is thought that global food production may need to triple over the next fifty years to accommodate the increase in demand (Godfray et al., 2010).

The problem of increasing demand is compounded by supply constraints. As global fisheries are mostly over- or fully-exploited, much of this additional food must be produced from the land (Sumaila et al., 2012). It is estimated that land degradation, urbanisation, and the appropriation of farmland for non-food production, will reduce the global food agricultural area by 8-20% in the next forty years (Nellemann, 2009). Therefore, the productivity of land stocks must increase. Raising the productivity of farm land can take two forms – increasing yields, or reducing losses.

The use of better quality inputs such as high quality seed stocks and fertilisers is central to increasing the productivity of farmland in any given environment (Jaggard et al., 2010). During the mid-20th Century the cross-breeding of semi-dwarf Indica rice lines with high-yielding cultivars, in the so-called “green revolution”, brought about some 10-fold increases in yield. Similar increases across a wide variety of crops continued throughout the 20th century (Duvick & Cassman, 1999, Reilly & Fuglie, 1998, Silvey, 1994). However, emerging evidence suggests that yield increases from plant breeding have slowed in the 21st Century (Allen et al., 2005, Spink et al., 2009).

There is a substantial gap between the 'theoretical' and 'actual' yields, which varies widely between different regions of the world (Lobell et al., 2009). Much of the yield gap derives from poor farming practices – a problem that is largely structural where it is most acute (Godfray et al., 2010, Jaggard et al., 2010); that is, lack of education and technical skills, poor access to markets, lack of infrastructure, or scant access to capital. These combine to make reducing the yield gap challenging where its impact could have the most benefit (Godfray et al., 2010).

The main factors contributing to crop losses are outlined in Figure 1.1. Losses attributable to abiotic factors are largely caused by use of poor quality and environmentally unsuited crop varieties; or lack of, or inappropriate use of, nutritional supplements such as fertilisers. An increase in attainable yields is often associated with greater vulnerability to biotic losses (Oerke, 2006). Therefore, efforts to raise yields must go 'hand-in-hand' with efforts to reduce losses caused by weeds, animal pests and pathogens. These losses are substantial – a study of six major crops in, found that between 2001 and 2003, 32% of annual yield was lost to these biotic factors globally (Oerke, 2006). Losses due to weeds contributed 8.8%, animal pests 10.1% and pathogens 12.5%.

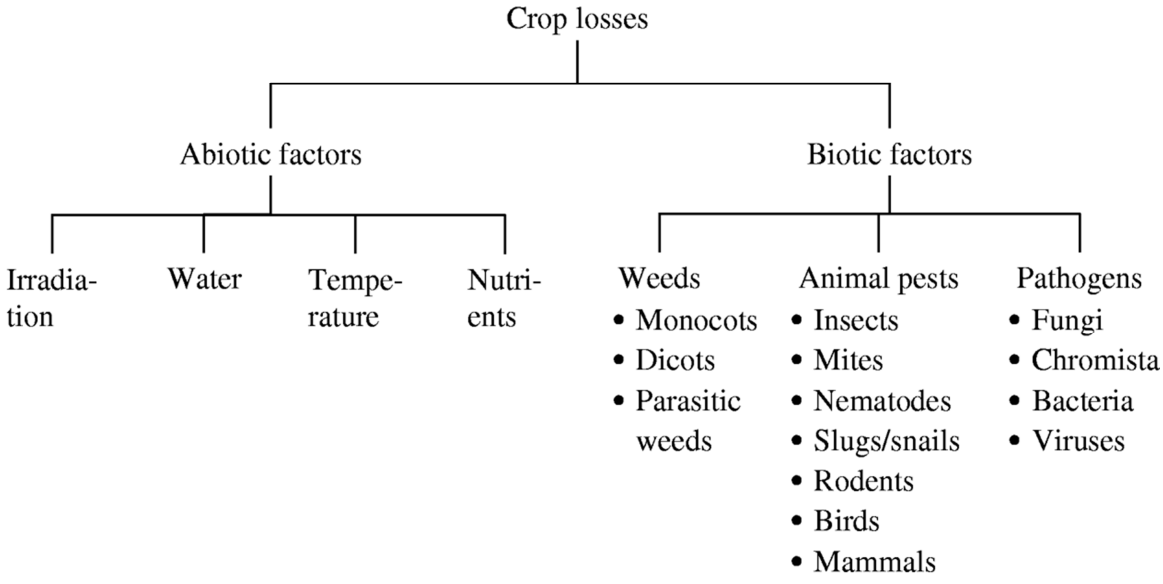

Figure 1.1: Abiotic and biotic factors causing crop losses. *Reproduced with permission from E. Oerke, Crop Losses to Pests, Journal of Agricultural Science, Vol 144, Issue 1, p32*

1.2 Rice and Rice Blast Disease

Rice (*Oryza sativa*), provides ~19% of global dietary energy (Ray et al., 2013), and it is estimated to be the staple food crop for 3 billion people (Goff, 1999). However, the rate of production growth

has slowed, and mean yield change of rice production per year is now only 1.0%, down from a rate of 2.49% from 1970-1990 (Khush & Jena, 2009, Ray et al., 2013). In areas where rice represents a high proportion of calorie intake rice yields are decreasing (Ray et al., 2013). World rice stocks are at historically low levels, and the price of rice is increasing and becoming more volatile (FAO Food Price Index 2010).

It is estimated that 37% of rice yields are lost to abiotic factors each year – 10.2% to weeds, 15.1% to animal pests and 12.2% to pathogens (Oerke, 2006). However, in some parts of the world, yield losses can be as much as 51%. Rice Blast Disease, caused by the filamentous heterothallic ascomycete fungus *Magnaporthe oryzae* (Hebert) Barr [anamorph: *Pyricularia oryzae* Sacc.], (Barr, 1977) is the most significant biotic disease burden on rice (Khush & Jena, 2009, Skamnioti & Gurr, 2009).

Rice blast affects all rice-growing areas, but losses are most significant in temperate and upland regions (Khush & Jena, 2009). Even in advanced farming systems, rice blast is a significant problem. The breakdown of gene-for-gene disease resistance in Japan, results frequently in yield losses from 20-100% in some cultivars (Miah et al., 2013). *M. oryzae* adapts rapidly to infect new resistant rice varieties, and new resistance genes are frequently compromised after only a few years under cultivation (Koide et al., 2009). Rice is the most globally significant host, but the *M. oryzae* species complex is also capable of infecting, and causing disease on, over 50 species of grass and sedge, including barley (*Hordeum vulgare*), wheat (*Triticum aestivum*) and finger millet (*Elusine coracana*) (Talbot, 2003).

Yield losses in rice are most severe when the panicle neck node becomes infected (Bonman, 1992). However, the fungus can also infect the leaves, collars, panicles and roots (Marcel et al., 2010, Roumen, 1992), and there is some evidence that certain isolates have become tissue-specialised (Ghatak et al., 2013).

1.3 The rice blast fungus, *Magnaporthe oryzae*

1.3.1 *M. oryzae* as a model pathogen

A high degree of genetic tractability and its significance as a global pathogen has made *M. oryzae* the predominant model species for the study of fungal phytopathogens, and a model for all appressorium-forming fungi (Talbot, 2003, Wilson & Talbot, 2009b). The fungus is easy to culture axenically on simple medium and the entire pre-penetration phase development can be induced on inductive coverslips, which mimic the surface of a rice leaf, further facilitating microscopy and expression profiling (Oh et al., 2008). The complete genome sequence of both *M. oryzae* and its primary host *O. sativa* are available, as are re-sequenced genomes for several field isolates (Dean et al., 2005, Goff et al., 2002, Xue et al., 2012).

A number of large-scale studies have substantially widened the toolkit available for studying *M. oryzae*. A SuperSAGE study by Soanes et al. (2012) provides open-source information on the expression levels of all annotated *M. oryzae* genes, during infection-related development and on standard medium. The use of *Agrobacterium*-mediated transformation to generate large mutant libraries is facilitating the rapid identification of novel pathogenicity determinants (Choi et al., 2007). As the availability of such resources increases, the ease with which this pathogen can be studied also increases.

1.3.2 The life cycle of *M. oryzae*

M. oryzae is capable of reproducing sexually under suitable environmental conditions, producing perithecia containing eight-celled asci (Valent et al., 1991). However, female-fertile strains are only found in limited areas of Asia, and it is the asexual reproduction cycle that causes disease (Saleh et al., 2012, Talbot, 2003).

The asexual life cycle, shown in Figure 1.2, is initiated when a three-celled spore lands on a host surface in the presence of free water (Talbot, 2003). Conidia adhere to the plant surface by effusion of spore tip mucilage from the apical compartment – a mixture of α-linked mannosyl and glucosyl residues, lipids, and proteins (Hamer et al., 1988, Koga & Nakayachi, 2004).

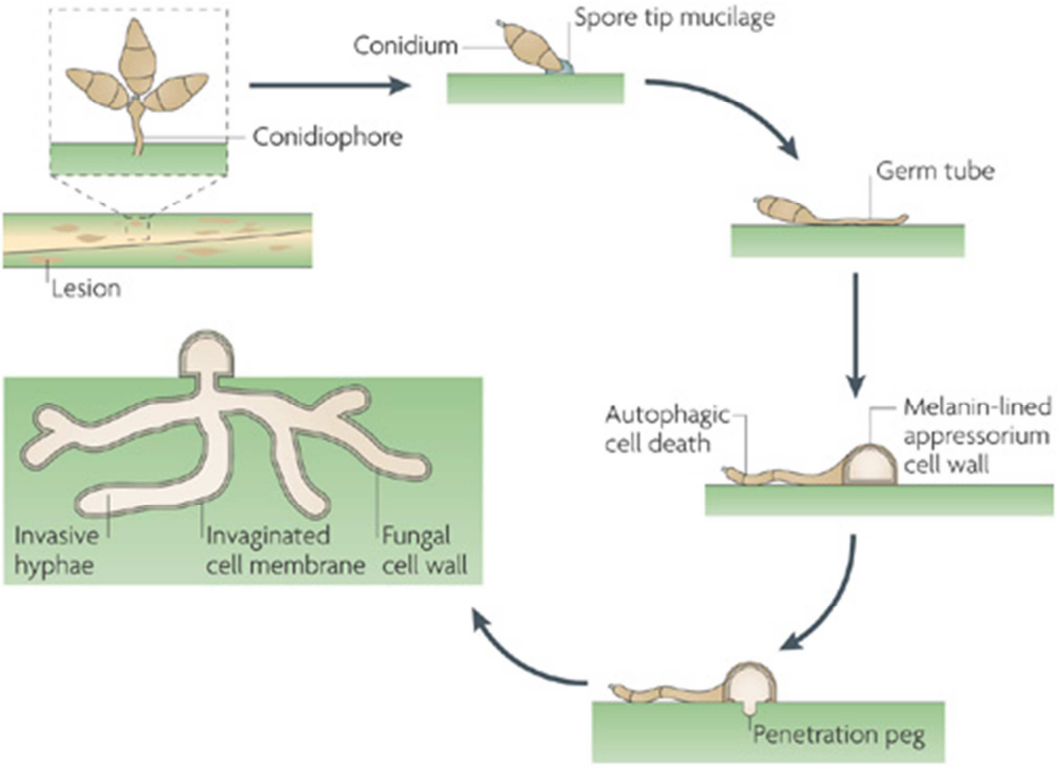

Figure 1.2: The asexual disease cycle begins when a three-celled conidium lands on a compatible host surface. The spore adheres to the cuticle and germinates, forming a short germ tube which flattens and hooks against the substrate. After surface recognition events occur, signalling cascades are activated that culminate in the differentiation of an appressorium. The contents of the conidium are degraded and trafficked into the developing appressorium in an autophagy-dependent manner. The appressorium becomes melanised and develops substantial turgor pressure via the accumulation of internal glycerol. The turgor-derived physical force is used to puncture the host cell wall with a narrow penetration peg that emerges from the base of the appressorium. The penetration peg invaginates the host cell membrane, and the fungus grows biotrophically, moving from cell-to-cell by plasmodesmata, suppressing host defences and deriving nutrition via secretion of effectors. Necrotic disease lesions producing aerial conidiophores become apparent 72-96h after infection. Conidia are transferred to new host plants by dewdrop splash. *Reprinted with permission from MacMillan Publishers Ltd: Nature Reviews Microbiology, (Talbot, 2009), copyright 2009*

Approximately 2 h after adhesion, a narrow germ tube emerges from the apical or distal cell of the conidium and grows for 15-30 µm (Talbot, 2003). The germ tube subsequently undergoes a stage of development known as 'hooking', thought to constitute a 'recognition phase' during which the fungus senses the external environment (Bourett & Howard, 1990). Germination can occur only in the absence of exogenous nutrients on a hard, hydrophobic surface (Dean, 1997). However, it can be induced on non-inductive surfaces by the addition of soluble cutin or lipid monomers such as cis-9,10-epoxy-18-hydroxyoctadecanoic acid or 1,16-hexadecanediol (Gilbert et al., 1996). These physical and chemical cues activate signalling pathways that culminate in the formation of a

specialised dome-shaped infection structure – the appressorium. Initiation and subsequent maturation of the appressorium is regulated by progression through specific cell cycle checkpoints. A DNA replication checkpoint is an essential for initiation of appressorium formation, and subsequent maturation of the appressorium requires entry into mitosis (Saunders et al., 2010). Septation between the developing appressorium and the germ tube occurs after a single daughter nucleus, from the unusual spatially-asymmetric cell division that occurs prior to appressorium development, migrates to the tip of the germ tube (Veneault-Fourrey et al., 2006). The remaining daughter nucleus is transported back into the conidium, which eventually collapses and is degraded in an autophagy-dependent process (Kershaw & Talbot, 2009, Veneault-Fourrey et al., 2006)

Appressorium development is regulated by at least two important signalling pathways: cyclic-AMP (cAMP) dependent signalling and the Pmk1 MAP kinase pathway (Wilson & Talbot, 2009b, Zhao et al., 2005). The cAMP signalling pathway has been implicated in surface recognition and regulation of appressorium formation (Choi & Dean, 1997, Mitchell & Dean, 1995). Targeted replacement of *MAC1*, a putative adenelylate cyclase, results in null mutants that are unable to form appressoria and are therefore unable to cause disease (Choi & Dean, 1997). This defect can be restored by the addition of exogenous cAMP. Furthermore, appressorium formation on non-inductive surfaces can be induced by addition of cAMP (Adachi & Hamer, 1998, Choi & Dean, 1997). cAMP signal generated by Mac1 is transduced by protein kinase A (PKA) – a tetrameric holoenzyme which phosphorylates target proteins (Kronstad, 1997).

The Pkm1 MAP kinase pathway is comprised of the Pkm1 MAP kinase (MAPK), which operates downstream of the Mst1 MAPK kinase (MAPKK), and the Mst11 MAPKK kinase (MAPKKK) (Xu & Hamer, 1996). The Pkm1 pathway is orthologous to the Kss1 pathway in yeast, and in *M. oryzae* this pathway integrates environmental signals via heterotromeric G-proteins and other upstream activators (Fang & Dean, 2000, Liu et al., 2011). Pkm1 deletions strains can be cultured axenically but are unable to elaborate appressoria or grow *in planta,* even when inoculated directly into wounded rice tissue (Xu & Hamer, 1996, Zhao et al., 2005).

The appressorium is a single dome-shaped cell with a highly specialised cell wall rich in chitin, and containing a melanised layer approximately 100 nm thick adjacent to the plasma membrane but

absent from the region in contact with the substrate (Bourett & Howard, 1990, Howard & Valent, 1996). This melanin layer is thought to act as an impermeable barrier to the efflux of osmotically active solutes that accumulate inside the appressorium during maturation (Chumley & Valent, 1990). The accumulation of these solutes, thought to be predominantly glycerol (up to 3.2 M), cause water to move into the appressorium by osmosis, raising the internal pressure as high as 8.0 MPa (Chumley & Valent, 1990, de Jong et al., 1997, Howard et al., 1991).

Coincident with maximal turgor pressure a narrow hypha 700-800 nm in diameter known as a penetration peg, emerges from the base of the appressorium and pierces the cell wall of the host plant (Dagdas et al., 2012, Howard & Valent, 1996). The site of penetration peg formation is can be distinguished early in appressorium development by the clustering of vesicles and the absence of a cell wall (Zeigler et al., 1994). As the appressorium reaches approaches maturation the F-actin cytoskeleton is reorganised at the base of the appressorium in a septin-dependent manner. Septins organise the F-actin network directly and indirectly via RM proteins, linking the actin to the membrane and organising the Rvs167 I-BAR proteins and the WASP/WAVE complex involved in membrane curvature at the tip of the emerging penetration peg (Dagdas et al., 2012).

After the fungus has mechanically penetrated the host cell wall, host cells are initially invaded by narrow primary infection hyphae (IH) that invaginate the host plasma membrane and subsequently develop into bulbous secondary IH (Kankanala et al., 2007). The fungus grows biotrophically for up to three days before switching to a necrotrophic growth form (Wilson & Talbot, 2009b). The secondary IH fills the first infected cell 8-12h post inoculation, and spreads to neighbouring cells within 36hpi via plasmodesmata (Kankanala et al., 2007).

During biotrophic invasion, *M. oryzae* secretes many low molecular-weight 'biotrophy-associated' (Bas) proteins which facilitate undetected invasive growth and nutrition (Mosquera et al., 2009, Saitoh et al., 2012, Valent & Khang, 2010). A recent study by Giraldo et al. (2013), defined two types of effector – apoplastic effectors and cytoplasmic effectors. The former do not enter host cells, but are retained within the extra-invasive hyphal membrane compartment enclosing IH in rice cells. The latter preferentially accumulate in the biotrophic interfacial complex (BIC) – a membrane-rich structure adjacent to primary hyphal tips, shown by the authors to be plant-derived but directly associated with fungal IH cells that are enriched in secretion machinery components (Giraldo et al.,

2013). The secretion of apoplastic effectors involves the canonical fungal ER-Golgi secretion pathway, but the secretion of cytoplasmic effectors requires a novel system involving exocyst components and the Sso1 t-SNARE (Giraldo et al., 2013).

After 72h typical disease lesions become visible, and it has been estimated that fungal biomass accounts for up to 10% of infected leaf biomass (Talbot et al., 1993). These necrotic lesions sporulate profusely, and conidia dislodged from conidiophores are transferred to new hosts by dew drop splash (Kim & Lee, 2012, Wilson & Talbot, 2009b). Yield losses in rice are most severe when the panicle neck node becomes infected (Bonman, 1992). However, the fungus can also infect the leaves collars, panicles and roots (Marcel et al., 2010, Roumen, 1992), and there is some evidence that isolates become tissue-specialised (Ghatak et al., 2013).

1.3.3 Appressorial turgor

Host penetration via an appressorium is relatively common amongst plant pathogenic fungi such as rusts and powdery mildews (Deising et al., 2000). Appressorium-mediated penetration occurs in the absence of exogenous nutrients, therefore all metabolism and structural remodelling must be carried out using only the contents of the conidium (Wilson & Talbot, 2009a).

M. oryzae condia contain several storage carbohydrates, principally mannitol, trehalose and glycogen (Bourett & Howard, 1990, Dixon et al., 1999). Early studies of *M. oryzae* appressoria measured their contents using gas-liquid chromatography and reported that they contained as much as 3.22±0.4M glycerol (de Jong et al., 1997). It was subsequently proposed that this glycerol might be produced from these storage carbohydrates (Foster & Talbot, 2000). However, temporal imaging of cellular glycogen showed that stocks are mostly degraded during spore germination, with glycogen largely absent by the time of appressorium formation (Thines et al., 2000). Trehalose - another storage carbohydrate – was also considered as a glycerol precursor. However, deletion of two trehalsases, *TRE1* and *NTH1,* abolishes trehalose metabolism, but does not prevent appressorium-mediated penetration (Foster et al., 2003).

Thines et al. (2000) demonstrated that storage carbohydrate metabolism enzymes are not up-regulated during turgor generation relative to levels in mycelium. They showed that glycerol is instead generated by the activity of triacylglycerol lipases. Lipid bodies are mobilised and trafficked

into the nascent appressorium, in a manner dependent on the activity of the Pkm1 MAPK (Thines et al., 2000). The formation of these lipid bodies was shown to be dependent on autophagic degradation of the conidium (Liu et al., 2007). Although individual deletion of any of the eight putative intracellular triacylglycerol lipase-encoding genes does not abolish pathogenicity, their activity is substantially up-regulated during turgor generation (Soanes et al., 2012, Thines et al., 2000). In addition, both the glyoxcylate shunt and the fatty oxidation β-oxidation pathway are important for the elaboration of functional appressoria (Wang et al., 2003, Wang et al., 2007). These pathways facilitate the release of carbon units from fatty acids, which may subsequently be used to synthesis sugars or glycerol (Soanes et al., 2012).

The synthesis of glycerol proceeds only after the appressorial cell wall is melanised (Wilson & Talbot, 2009a). This melanin layer prevents efflux of synthesised glycerol into the surrounding water environment but permits the diffusion of water up the concentration gradient into the appressorium (Wilson & Talbot, 2009b). The increase in turgor is associated with remodelling of the cell wall and cytoskeleton at the point of penetration peg emergence (Dagdas et al., 2012).

1.4 The importance of turgor

The basic principle of appressorium-mediated penetration – the remodelling of cell wall properties coupled with pressure-driven expansion – is thought to be the mechanism by which hyphal growth proceeds (Lew, 2011). In walled cells, turgor pressure provides both structural support for free standing cell networks and a force that can be used to drive substrate penetration, cellular expansion, or other processes (Money, 1998). An extreme example of the use of turgor pressure in fungi is the high-velocity spore discharge processes, common among the Ascomycota and Zygomycota, that can propel spores with accelerations of between 20,000 and 180,000 *g* (Trail, 2007, Yafetto et al., 2008).

In tip-growing fungal species, growth is thought to be caused by expansion of the extensible tip by hydrostatic force (Bartnicki-Garcia et al., 2000). The turgor pressure is created by osmosis, which occurs because the concentration of osmotically active solutes is higher inside the hypha than in the surrounding environment. In a theoretical closed system, the relationship between pressure, volume and solute concentrations can be modelled with the ideal gas law, where $PV = nRT$ (where

P = pressure, *V* = volume, *n* = number of moles of osmotically active solutes, *R* is the gas constant and *T* is temperature) (Cosgrove, 1981).

These factors are affected by two further properties: the extensibility of the cell wall and the rate of water flux across the membrane. The dynamics of pressure and volume changes also depend on the rate of water flux across the membrane, which in turn depends on the hydraulic conductance of the cell membrane and wall (Lew, 2011).

In reality, the extensibility of the cell wall is equally as important as the rate of supply of new cell wall material (Bartnicki-Garcia, 2006). Studies in *Achlya bisexualis*, a hyphal oomycete demonstrated that the incorporation of new wall and membrane material was driven by turgor pressure, but modulation of the cell wall extensibility was used to moderate the rate of growth (Lockhart, 1965, Money & Harold, 1992). This was demonstrated by artificially increasing turgor pressure in hyphae, resulting in an initial increase in the rate of elongation followed by a decline back to the original rate despite the sustained pressure elevation. (Money & Harold, 1992).

1.4.1 Regulation of turgor pressure

The HOG1 (high osmolarity glycerol) MAPK signalling system is a conserved mechanism for controlling cellular turgor in eukaryotes (Han et al., 1994, Han et al., 1998, Popping et al., 1996). In *S. cerevisiae*, active Hog1 responds to osmotic stress via regulation of protein translation and cell cycle progression, in addition to modulating the synthesis of glycerol and flux of ions (Saito & Tatebayashi, 2004, Lew et al., 2006, Lew, 2010, Hohmann, 2002).

Extracellular hyperosmolarity in *S. cerevisiae* is detected by two plasma membrane osmosensors, Sln1 and Sho1 (Reiser et al., 2006). Signals from these are integrated by the MAPKK Pbs2, which acts via phosphorylation of the Hog1 MAPK. The transmembrane Sln1, has an extracellular sensor domain and an internal histidine kinase domain that, following autophosphorylation of Sln1 in conditions of low osmolarity, results in the phosphorylation of Ypd1, then Ssk1 (Posas et al., 1996). This osmosensor relay then activates the upstream MAPKKKs (SKK2S/SK22) and downstream MAPKK Pbs2 (Maeda et al., 1995).

Sho1 is a four transmembrane domain that interacts with Pbs2 via an SH3 domain (Cheetham et al., 2007). Under high osmolarity conditions. The Sho1-dependent phosphorylation of Pbs2 under, also requires Ste11, Ste20, Ste50 and Cdc42 (Posas et al., 1998, Raitt et al., 2000, Reiser et al., 2006, Saito & Tatebayashi, 2004). Cdc42 is a small G protein that activates Ste20, a p21-activated protein kinase (PAK). Ste20 then phosphorylates the MAPKKK Ste11, which is present in a complex with Ste50. The Ste11 MAPKKK then phosphorylates the Pbs2 MAPKK.

Deletion of the *HOG1* homolog in *M. oryzae*, *OSM1,* also results in drastically reduced growth, relative to the wild type Guy11, after exposure to hyperosmotic stress (Dixon et al., 1999). The authors of this study also determined that arabitol, rather than glycerol, is the principal osmoprotectant that accumulates in response to high external osmolarity, and were unable to identify any other amino acids or non-carbohydrate sources via ^{13}C NMR or gas liquid chromatography. However, a separate study identified glycerol, rather than arabitol, as the major compatible solute accumulated under osmotic stress, although the profile of accumulated substrates varied between salt and sugar stress (Motoyama et al., 2005). At the time of the study, the importance of ion flux in response to osmotic stress was not known, therefore this, the only study of the HOG1 pathway in *M. oryzae*, did not investigate this component of the osmo-response. Appressorial turgor was not affected in the Δ*osm1* strain, therefore turgor pressure in the appressorium is Osm1-independent (Dixon et al., 1999)

Interestingly, deletion of the *M. oryzae SLN1* homologue resulted in loss of pathogenicity due to a penetration defect (Zhang et al., 2010). However, the explanation proposed by the authors was not well-substantiated by the data presented. Deletion of both the *M. oryzae SSK1* homolog and its paralogue *SKN7,* results in sensitivity to high external osmolarity, and deletion of *SKK1* resulted in a reduction in disease severity (Motoyama et al., 2008), but the cause of the pathogenicity defect was not elucidated.

1.5 Aquaporins

The rate of water flux across membranes can be dynamically controlled by the expression of aquaporins. These proteins are present in the plasma and intracellular membranes of all major taxa in extant prokaryotes, eukaryotes and archaea (Zardoya, 2005). The numbers of aquaporins

in the genomes of different organisms varies widely, from 0 in some bacteria to 55 in the tree, *Populus trichocarpa* (Gupta & Sankararamakrishnan, 2009, Tanghe et al., 2006). In animals and plants, aquaporins are most highly expressed in tissues and organs with a high degree of water flux (Agre, 2006) reflecting their role as passive water diffusion channels. However, in addition to water they have been implicated in permeability of a wide range of small molecules. These include many small uncharged molecules and some gases, as shown in Table 1.1.

Table 1.1: The best-characterised aquaporin substrates and their physical structures. *References are examples where permeability for that substrate has been experimentally demonstrated*

Substrate	Structure	Example reference
Water	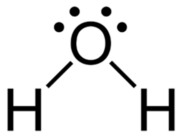	Yakata et al. (2011)
Glycerol and other small polyols	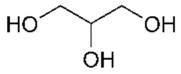	Wallace et al. (2002)
Urea	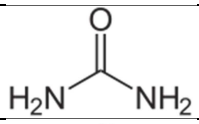	Ma et al. (1997)
Ammonia/ammonium	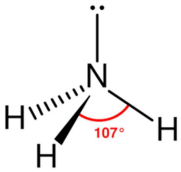	Litman et al. (2009)
Methylamine	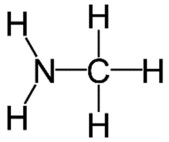	Beitz et al. (2006)
Formamide	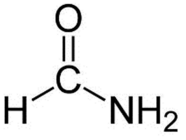	Wallace and Roberts (2005b)
CO_2	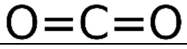	Endeward et al. (2006)
NO	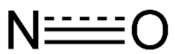	Herrera et al. (2006)
H_2O_2	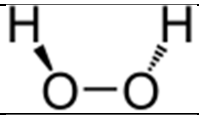	Bienert et al. (2007)
Boric acid	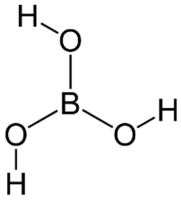	Katsuhara et al. (2002)

Silicic acid	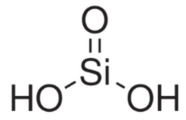	Ma et al. (2006)
Lactic acid	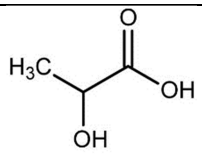	Bienert et al. (2013)
Nitrate ions	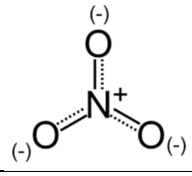	Ikeda et al. (2002)

Aquaporin proteins are hourglass-shaped channels composed of six membrane spanning α-helices and two hemi-helices that enter and leave the bilayer on the same side of the membrane (Hachez & Chaumont, 2010), as shown in Figure 1.3. The N and C termini are internal, and the re-enterent helices carry the conserved asparagine-proline-alanine (NPA) motifs that are highly conserved in the aquaporin protein family. The core aquaporin domain is approximately 250 aa, but the proteins often carry long terminal extensions implicated in regulation (Hachez & Chaumont, 2010)

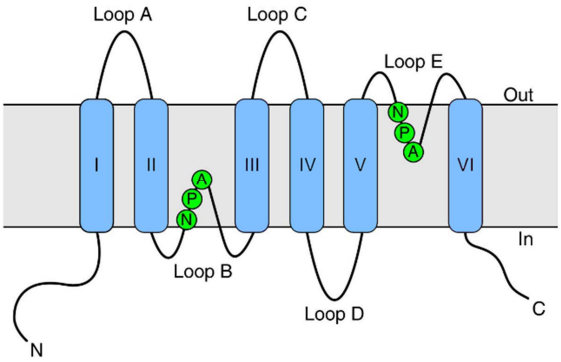

Figure 1.3: Topology of an aquaporin membrane protein. *Each protein consists of six transmembrane helices (I-VI) that span the membrane and two hemi-helices with the characteristic NPA motif that enter and re-emerge from the membrane on the same side of the bilayer. N, amino terminus; C, carboxyl terminus. The diagram is modified from Kruse et al. (2006)*

These helices wrap around in a right-handed bundle to form an hourglass-shaped channel, with the narrowest region of the pore formed by the NPA hemi-helices, as shown in Figure 1.4A. Channel permeability is determined by the physical and electrical properties of the amino acids in the pore region (Harries et al., 2004, Heymann & Engel, 2000). Aquaporin genes are present in the membrane as homo- or heterotetramers, as shown in Figure 1.4B (Mathai & Agre, 1999). The

tetrameric assembly appears important for the proper folding, stability, localisation and function of aquaporins (Ringler et al., 1999). Although each monomer functions independently, the composition of the tetramer has been reported to influence transport (Otto et al., 2010), and there are reports that the central pore has tertiary transport capability (Yool & Weinstein, 2002, Yu et al., 2006).

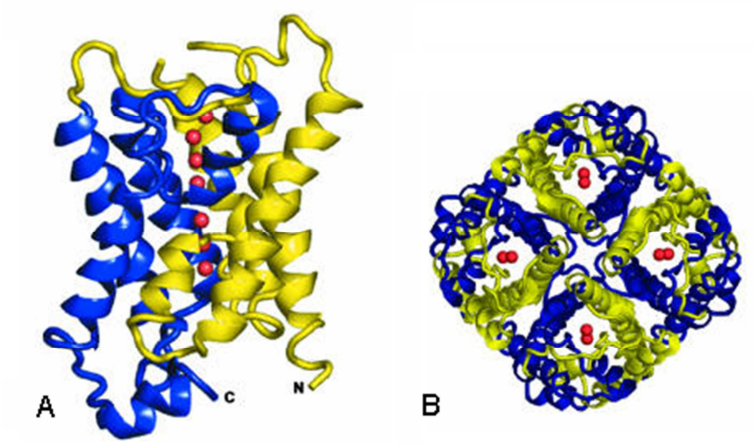

Figure 1.4 The monomer (A) and tetramer (B) structure of bAQP0, a canonical aquaporin. A shows the bAQP1 monomer in side view, with the extracellular side uppermost. B) shows the bAQP0 tetramer looking down the z axis from the extracellular side of the protein. Red spheres represent water molecules. Structures are reproduced from Harries et al. (2004). © 2004 by The National Academy of Sciences of the USA

The term ‘aquaporin’ is something of a misnomer, as it is used in the literature to refer to both aquaporins and aquaglyceroporins. These constitute two early diverging homologous groups with in the Major Intrinsic Protein (MIP) superfamily, but ‘aquaporin’ is used today to refer to both groups. The evolutionary divergence of aquaporins (AQPs) and aquaglyceroporins (AGPs) pre-dates the divergence of the prokaryotes and eukarotes, but their distribution in the archaea is subject to debate (Araya-Secchi et al., 2011, Danielson & Johanson, 2010).

The two protein families have a similar secondary and tertiary structure but low amino acid similarity at the protein level (Engel & Stahlberg, 2002). Traditionally, AQPs have been considered to be water channels and AGPs were considered to be glycerol facilitators; however, recent evidence reveals this to be too simplistic (Hub & de Groot, 2008, Wu & Beitz, 2007). MIPs instead are permeable to diverse permeants with some notable phenotypic effects upon their deletion.

1.5.1 Aquaporins in animals

A total of 13 aquaporin genes have been identified in *Homo sapiens,* designated AQP0-AQP12 (Ishibashi et al., 2009). These can be grouped phylogenetically into four categories – AQP1-like (6 genes), AQP8-like (1 gene), AQP3-like (4 genes) and AQP11-like (2 genes) (Soto et al., 2012). Members of one of these categories, the AQP3-like genes, are considered to be AGP proteins and the remainder are considered to be AQPs (Ishibashi et al., 2009). As no specific, non-toxic inhibitors are available, most mammalian aquaporins are investigated using null mice and humans (Haddoub et al., 2009).

Abnormal water flux is demonstrable in AQP1, 2, 3, 4, and 5 null mice (Verkman, 2005). AQP1 is expressed widely (Magni et al., 2008), and null mice suffer from a mild urine concentration defect, sensory dysfunction, fat malabsorption and low ocular pressure (Meyrial et al., 2001, Oshio et al., 2006). The vasopressin-stimulated AQP2 null phenotype in mice manifests as fatal *diabetes insipidus* (Lloyd et al., 2005), whereas deletion of AQP3 causes dry skin and a urine concentration defect (Hara-Chikuma & Verkman, 2005, Ma et al., 2000). Deletion of AQP4 causes sensory defects, a reduction in injury-related brain oedema and a slight urine concentration defect (Lu et al., 2008, Papadopoulos & Verkman, 2007). AQP5 null mice suffer from dry mouths, thin corneas and reduced sweating (Burghardt et al., 2003, Satoh et al., 2013).

Abnormal glycerol transport in AQP3, AQP7 and AQP9 aquaglyceroporin deletion mice caused several glycerol-related phenotypic effects. AQP3 mice suffer from dry skin, and AQP7 mice are prone to obesity, secrete excess glycerol in the urine and have reduced glycerol metabolism (Hara-Chikuma et al., 2005, Hibuse et al., 2005, Matsumura et al., 2007, Sohara et al., 2006). AQP9 null mice have a lower ability to take up glycerol in the liver but are otherwise normal (Rojek et al., 2007).

AQP0 mice suffer from cataracts but, interestingly, this is likely to result from a cell-adhesion role for AQP0, rather than a transport role (Kumari et al., 2011). AQP11 null mice die shortly after birth from uraemia caused by severely polycystic kidneys (Morishita et al., 2005). However, AQP6, 8, 10 and 12 null mice are almost normal (Ishibashi et al., 2009, Morinaga et al., 2002, Nagase et al., 2007).

The expression and function of members of the MIP gene family in animals is extremely diverse, and has been the subject of several recent reviews (Loreto & Reggio, 2010, Papadopoulos & Verkman, 2013, Tradtrantip et al., 2009). It is clear that the expansion of the gene family in humans reflects their wide physiological importance.

1.5.2 Aquaporins in plants

The MIP superfamily in plants is widely expanded, with 23 MIPs in the genome of even the early-diverging moss, *Physcomitrella patens* (Danielson & Johanson, 2008). Plant MIPs have been divided into seven subfamilies (Danielson & Johanson, 2008)

1) Plasma-membrane intrinsic proteins (PIPs)
2) Tonoplast intrinsic proteins (TIPs)
3) Nodulin-26 like intrinsic proteins (NIPs)
4) Small basic intrinsic proteins (SIPs)
5) GlpF-like intrinsic protein (GIPs)
6) Unrecognised intrinsic proteins (XIPs)
7) Hybrid intrinsic proteins (HIPs)

Higher plants have previously been reported to lack AGP-type genes (Zardoya, 2005). However, a comprehensive recent phylogeny suggests this to be incorrect, and that the NIPs are actually AGP-like proteins (Soto et al., 2012). The HIPs and the GIPs are only present in early-branching taxa and the phylogenetic distribution of the XIPs is uncertain (Danielson & Johanson, 2008, Soto et al., 2012).

PIPs and TIPs represent the most abundant classes of plant MIPs and are thought to be important for water relations (Maurel, 2007). The PIPs are expressed on the plasma membrane and the TIPs are expressed on internal vacuolar membranes (Negishi et al., 2012). In addition to water, it has been proposed that PIPs are permeable to CO_2, although the physiological relevance of this is debated (Flexas et al., 2006, Uehlein et al., 2003). TIPs are also reported to facilitate urea, ammonia and hydrogen peroxide transport (Liu et al., 2003, Loque et al., 2005).

In higher plants, the NIPs are a divergent subfamily with a long N-terminal domain implicated in pore gating. NIPs have been shown to be important in membrane transport of silicon and boron (Ma et al., 2006) and they are reportedly permeable to glycerol, ammonia and lactic acid (Choi & Roberts, 2007, Jahn et al., 2004, Wallace & Roberts, 2005a). They are thought to be expressed in the ER (Mizutani et al., 2006), but there is also some evidence of plasma membrane localisation (Choi & Roberts, 2007).

SIPs are localised on the ER membrane (Ishikawa et al., 2005). Some SIPs have been shown to be permeable for water; however, their physiological relevance is poorly understood (Maeshima & Ishikawa, 2008). Similarly, the HIPs, which are unique to early-evolving plants, are not well characterised. The name, 'hybrid' intrinsic proteins derives from several conserved residues that show intermediate properties between TIPs and PIPs; however, this is poorly substantiated (Danielson & Johanson, 2008)

The XIPs are plasma-membrane localised channels that are permeable to glycerol, urea, hydrogen peroxide and boric acid (Bienert et al., 2011). Their substrate specificity is similar to NIPs but they appear to be predominantly localised on the plasma membrane rather than ER. The role of the XIPs remains to be characterised as does their evolutionary history.

The GIPs have only been identified in a limited range of moss species (Gustavsson et al., 2005). These genes have very low similarity to other plant MIPs but are thought to be similar to bacterial AGPs, leading to the suggestion that they were acquired by horizontal gene transfer. The role of these proteins is largely unknown.

The involvement of plant aquaporins in several important processes is well understood. In plants, long distance water transport occurs mostly through vascular tissue, and therefore movement does not encounter significant membrane barriers (Maurel et al., 2008). However, water flux across cells can take any of three paths: the apoplastic path, the symplastic path, and the transcellular path. It is transport across this final path that predominantly involves aquaporins. The water transport function of aquaporins in plants has been implicated in transpiration (Hachez et al., 2006), tissue expansion (Ludevid et al., 1992), and tissue desiccation and imbibition (Pina et al., 2005).

Plant MIPs have also been implicated in nitrogen source assimilation and micronutrient acquisition. Some genes are strongly induced by nitrate (Gaspar et al., 2003) or under conditions of nitrogen starvation (Loque et al., 2005). Direct evidence is still not available but the demonstrable permeability of these genes to nitrogen compounds implies a role in their uptake, equilibration or mobilisation (Kojima et al., 2006).

There is strong evidence for a role for plant MIPs in boron uptake under conditions of boron limitation (Takano et al., 2006). A similar role has been proposed for silicon uptake, where a mutant screen in rice identified a NIP homologue null mutant as being defective in silicon uptake (Ma et al., 2006).

Once again, the highly expanded protein families in plants endorse their physiological importance. The aquaporins are widely-studied owing to their fundamental importance in plant physiology. Their importance primarily reflects the essentiality of water in plant development. However, the secondary transport properties of aquaporin permeability are extremely important. For a review of plant aquaporins see (Forrest & Bhave, 2007).

1.5.3 Aquaporins in fungi

Relative to plant and animal aquaporins, fungal aquaporins are poorly studied (Pettersson et al., 2005). Several studies have attempted to characterise the distribution of aquaporins amongst fungal species (Pettersson et al., 2005, Tanghe et al., 2006, Xu et al., 2013). These analyses suggest that both subfamilies of aquaporins (aquaporins and aquaglyceroporins) are spread throughout the major fungal clades. In some species, the families are highly-expanded. However, they are best studied in the model organism, *Saccharomyces cerevisiae*, which carries two aquaporin ORFs and two aquaglyceroporin ORFs in its genome (Will et al., 2010).

1.5.3.1 AQP-like genes in *Saccharomyces cerevisiae*

1.5.3.1.1 Aquaporins in yeast

The *S. cerevisiae* genome codes for two aquaporin genes, *AQY1* and *AQY2*. Aqy1 is thought to be plasma membrane localised, but Aqy2 is thought to be ER-localised based on the localisation pattern of the GFP-tagged proteins (Meyrial et al., 2001). However, many industrial and laboratory

strains harbour non-functional *AQY2* alleles, and some strains also have non-functional *AQY1* alleles (Karpel & Bisson, 2006, Laizé et al., 2000).

In strains with functional *AQY1* and *AQY2*, such as Σ1278b, the *AQY1* mRNA is up-regulated during meiosis and sporulation (Chu et al., 1998, Sidoux-Walter et al., 2004), under heat stress (Karpel & Bisson, 2006) and during nitrogen limitation (Backhus et al., 2001), collectively suggesting a role for Aqy1 during stress responses. Heterologous expression of Aqy1 and Aqy2 in *Xenopus laevis* oocytes indicates that both are water permeable (Soveral et al., 2010). Interestingly, the activity of Aqy1 appeared to be regulated by membrane tension, suggesting some form of tension-gating (Soveral et al., 2008). Aqy2 was found to be highly-expressed in proliferating cells in rich medium but the transcript abundance of Aqy2 rapidly diminishes after nutrient depletion (Meyrial et al., 2001).

A screen of wild yeast species showed that the presence of functional aquaporin alleles correlates very strongly with their ability to survive freezing and thawing (Will et al., 2010). Loss of freeze tolerance is strongly associated with species that live in warm environments (where freezing is rare) with high (~25% w/v) sugar concentrations (Will et al., 2010). This corroborates with evidence suggesting that loss of aquaporin function provides a selective advantage under high osmolarity (Will et al., 2010).

Phenotypic analysis of laboratory aquaporin knockouts show reduced tolerance to freeze-thaw cycles (Tanghe et al., 2005b), but greater survival following rapid changes in osmolarity (Bonhivers et al., 1998, Carbrey et al., 2001a). Lack of Aqy1 reduces spore fitness, but it is not clear whether this defect manifests during sporogenesis or during subsequent dormancy or germination (Sidoux-Walter et al., 2004). Experiments with *Saccharomyces chevalieri* demonstrated that double aquaporin null cells had a greater tendency to aggregate, and their surfaces were more hydrophobic (Carbrey et al., 2001a). From experiments with double aquaporin deletion strains, Soveral et al. (2006) proposed that aquaporins in *S. cerevisiae* could be important for sustaining water permeability at low temperatures, whereas diffusion of water across the lipid bilayer is sufficient at high temperatures. This may explain the absence of a mutant phenotype in laboratory null strains as experiments are rarely conducted at low temperatures.

1.5.3.1.2 AGP-like genes in *Saccharomyces cerevisiae*

The yeast genome contains two ORFs encoding aquaglyceroporin genes – *YFL054* and *FPS1* (Pettersson et al., 2005). The Yfl054-encoding gene is poorly studied, but encodes a 646 aa protein with a long N-terminal extension conserved amongst yeast species (Pettersson et al., 2005). Expression of this protein is repressed by the redundant Mig1 and Mig2 glucose repressors, but its physiological role remains unknown (Lutfiyya et al., 1998).

The second aquaglyceroporin, *FPS1*, was identified in a screen for cell fusion defects during mating (Philips & Herskowitz, 1997). This mating defect manifests itself because cells are unable to regulate the osmotic balance during fusion events. The 669 aa Fps1 protein is localised in the plasma membrane and is functional as a homotetramer (Tamas et al., 1999). It is known to be permeable to glycerol, xylitol, acetic acid and the trivalent metalloids, arsenite and antimonite (Tamas et al., 1999, Hedfalk et al., 2004, Thorsen et al., 2006, Mollapour & Piper, 2007).

The most prominent phenotype of *FPS1*-null *S. cerevisiae* cells is strong sensitivity to hypo-osmotic shock following prolonged incubation at high osmolarity (Tamas et al., 1999). In response to high exogenous osmolarity, *S. cerevisiae* produces glycerol from the glycolytic intermediate dihydroxyacetonephosphate (Brown, 1990). Glycerol efflux occurs in under five seconds after cells are shifted to low osmolarity to protect the cells from bursting following influx of water (Tamas et al., 1999). The N and C terminal extensions of Fsp1 have been implicated in gating of the protein during normal growth (Hedfalk et al., 2004, Tamás et al., 2003). Both proteins carry short amphiphilic domains that, if deleted, produce a constitutively active Fps1 channel. This mutant displays a growth defect on high-osmolarity medium, caused by the loss of accumulated glycerol into the medium (Tamas et al., 1999). The speed of response to osmolarity shift indicates that the gating of Fsp1 is likely mechanical (Tamás et al., 2003). However, the exact mechanism of this regulation is not well understood.

Fsp1 has also been implicated in arsenite detoxification in a Hog1 dependent manner (Thorsen et al., 2006). The channel permeable to arsenite, but, counter-intuitively, deletion of the protein reduces arsenite tolerance and overexpression increases tolerance (Maciaszczyk-Dziubinska et al., 2010).

1.5.3.2 Aquaporins in other fungi

The *Candida albicans* genome contains a single ORF with homology to aquaporin-type MIPs (Carbrey et al., 2001b). *C. albicans* aquaporin null mutants are less sensitive to osmotic shock than the wild type and the cell surface was less hydrophobic, but there was no effect on virulence in murine models for systematic candidiasis. Presence of an aquaporin also enhanced tolerance to freeze-thawing but the *in vivo* relevance of this effect is not clear (Tanghe et al., 2005a).

Other than *S. cerevisiae*, the fungus in which aquaporins are best-studied is the ectomycorrhizal Basidiomycete, *Laccaria bicolor* (Dietz et al., 2011). This fungus forms mutualistic interactions with tree roots, and this symbiotic relationship enables the plant to optimise nutrient acquisition in exchange for carbohydrates (Smith & Read, 2010). Infected plant roots are covered in hyphae that participate in the transpiration-driven flow of water from the soil into the atmosphere (Plamboeck et al., 2007). ECM fungi can also obtain water from the plant host in a process known as 'hydraulic lift' (Querejeta et al., 2003). There is even evidence of inter-plant water transfer via ECM intermediates (Egerton-Warburton et al., 2007).

Beitz and colleagues (2011) investigated the permeability and expression levels of six of seven identified major intrinsic protein genes in the genome. The genes were differentially regulated, with two genes highly expressed in ectomycorrhizas. Permeability assays indicate that these genes are permeable to a range of molecules, but both ectomycorrhizum-expressed genes are permeable to ammonia. From this, it has been speculated that these proteins may be an integral part of the nitrogen nutritional exchange between ECM fungi and plant hosts (Dietz et al., 2011). A role for aquaporins in the flow of water and other nutrients has also been proposed (Dietz et al., 2011).

1.6 Objectives of this Thesis

Little is known about the role of aquaporins in fungi, and nothing is known about aquaporins in fungal phytopathogens. Regulation of turgor is essential for during pathogenic and filamentous growth of *M. oryzae*. The dynamics of water flux across the appressorium are completely unknown, and the high concentrations of glycerol inside the appressorium suggest several possible roles for glycerol channels. The internal distribution of this osmolyte must presumably be uniform to prevent bursting of organelles, perhaps necessitating the expression of an aquaporin on internal

membranes. A second possibility is the requirement for a ‘pressure valve’ to prevent explosive extrusion of the fungal cytoplasm into the first-invaded plant cell, following rapid equilibration between the internal turgor of the appressorium and the plant cell. There is no microscopic evidence of this, therefore the proposed pressure inside the appressorium must be released at moment of emergence through the plant cell wall. The role of aquaporins during normal filamentous growth is also unknown in pezizomycete fungi.

The myriad other molecules to which aquaporins are often also permeable allows speculation on the other roles that aquaporins might play in fungi. Using the model phytopathogen *M. oryzae,* in this thesis, I will attempt to address the question: why do these fungi retain a large and diversified family of aquaporin genes?

Chapter 2 Materials and Methods

2.1 Materials and Methods

2.1.1 Materials

2.1.1.1 Suppliers

Table 2.1: Contact details for materials suppliers

Company	Contact address
Abcam PLC	330 Cambridge Science Park, Cambridge, CB4 0FL, UK
Agilent Technologies	610 Wharfedale Road, Wokingham, Berkshire, RG41 5TP, UK
Ambion	3 Fountain Drive, Paisley, PA4 9RF, UK
Beckmann Coulter	Oakley Court, Kingsmead Business Park, London Road, High Wycombe, HP11 1JU
Becton, Dickinson & Co.	Sparks, MD 21152, USA
Bio-Rad Laboratories Ltd.	Bio-Rad House, Maxted Road, Hemel Hempstead, HP2 7DX
Eppendorf	Eppendorf House, Gateway 1000 Whittle Way, Arlington Business Park, Stevenage, SG1 2FP, UK
Fischer Scientific	Bishop Meadow Road, Loughborough, LE11 5RG
ForMedium	Hunstanton, PE36 5JQ, UK
GE Healthcare Life Sciences	Amersham Place , Little Chalfont , Buckinghamshire, HP7 9NA UK
Life Technologies	3 Fountain Drive, Paisley, PA4 9RF, UK
Media Cybernetics Inc.	4340 East-West Hwy, Suite 400, Bethesda, MD, 20814-4411 USA
Menzel	Gerhard Menzel, Glasbearbeitungswerk GmbH & Co., Braunschweig, Germany
Merck	64271 Darrmstadt, Germany
New Brunswick Scientific	175 Freshwater Boulevard, Enfield, CT, 06082-4444, USA
New England Biolabs	Wilbury Way, Hitchin, SG4 0TY, UK
Olympus Microscopy,	KeyMed House, Stock Road, Southend-on-Sea
QI Imaging Corporation	19535 56th Avenue, Suite 101 Surrey, BC, Canada
Qiagen Ltd.	Skelton House, Lloyd Street North, Manchester, M15 6SH, UK
Roche Diagnostics Ltd.	Charles Avenue, Burgess Hill, RH15 9RY, UK
Sanyo	1300 Michael Drive, Suite A, Wood Dale, IL 60191 USA
Sigma Aldrich	New Road, Gillingham, SP8 4XT, UK
Thermo scientific	Unit 9 Altey Way, Cramlington, NE23 1WA, UK
VWR International Ltd.	Hunter Boulevard, Magna Park, Lutterworth, Leicestershire LE17 4XN, UK
Weiss-Gallenkamp	Units 37 - 38, The Technology Centre, Epinal Way, Loughborough, Leicestershire, LE11 3GE, UK

Whatman	Springfield Mill, James Whatman Way, Maidstone, Kent, ME14 2LE, UK

2.1.1.2 Chemical reagents

Chemicals were purchased from Sigma Aldrich or VWR International Ltd., unless specified otherwise in the text.

2.1.1.3 Equipment

Table 2.2: Details of routinely-used laboratory equipment

Equipment	Brand	Model
Autoclaves	Midas	PriorClave 40
Centrifuges	Beckmann Coulter	Allegra X-15R
	Biofuge (Thermo Scientific)	Heraeus Pico
Fungal growth chambers	New Brunswick Scientific	Innova 4230
	Sanyo	MLR 350
	Panasonic	MLR 352H
Gel tanks	GeneFlow	Multi Sub Choice
Nanodrop	NanoDrop	ND-1000
Plant growth chambers	Gallenkamp	Fi-totron PG660
Power supply for electrophoresis	BioRad	PowerPac 300
Spectrophotometer	BioRad	SmartSpec 3000
Thermal cyclers	Biometra	T-gradient
	BioRad	PTC-100

2.1.1.4 Solutions and media

Solutions listed in Table 2.3 were autoclaved at 121^{o}C and 15lb.sq.in^{-1} for 20-30 min where indicated.

Table 2.3: Media and solutions used in this thesis

Complete medium (CM)	Liquid	10 g D-glucose, 2 g Peptone (Becton, Dickinson & Co.), 1 g yeast extract, 1 g casamino acids (Becton, Dickinson and Co.), 50 ml 20x nitrate salts, 1 ml 1000x vitamin solution & 1 ml 1000x trace elements. pH to 6.5 with 1 M NaOH, made up to 1 l with dH_20. Autoclaved
	Solid	As above with 1.5% agar (w/v)
Minimal medium (MM)	Liquid	10 g D-glucose, 50 ml 20x nitrate salts, 1 ml 1000x trace elements, 1 ml 1% thiamine (w/v), 50 µl 0.05% biotin (w/v). pH to 6.5 with 1 M NaOH, made up to 1 l with dH_2O. Autoclaved
	Solid	As above with 1.5% agar (w/v)
20x nitrate salts	120 g $NaNO_3$, 10.4 g KCl, $MgSO_4$.7H2O (Fischer Scientific), 30.4 g KH_2PO_4. Made up to 1 l with dH_2O. Autoclaved and stored at 4^{O}C	
20x non-nitrate salts	10.4 g KCl, 10.4 g $MgSO_4.7H_2O$, 30.4 g KH_2PO_4. Made up to 1 l with dH_2O. Autoclaved and stored at 4^{o}C	
1000x vitamin mix	0.01 g of biotin, pyridoxine, thiamine, riboflavin, *p*-aminobenzoic	

	acid & nicotinic acid. Made up to 100 ml with dH_2O. Autoclaved and stored at 4^oC	
1000x trace elements	80 ml dH_2O, 2.2 g $ZnSO_4$.7H2O, 1.1 g H_3BO_3, 0.5 g $MnCl_2.4H_2O$, 0.5 g $FeSO_4$.7H2O, 0.17 g $CoCl_2.6H_2O$, 0.16 g $CuSO_4.5H_2O$, 0.15 g $Na_2MoO_4.2H_2O$ & 5 g NaEDTA. Components added in order, boiled and adjusted at 60^oC to pH 6.5 with 1 M KOH. Made up to 100 ml with dH_2O. Autoclaved and stored at 4^oC	
YPD medium	Liquid	10 g yeast extract (Merck), 20 g peptone, 20 g D-glucose. Made up to 1 l with dH_2O. Autoclaved. Where appropriate, Ampicillin (dissolved in 1M sodium bicarbonate) was added to a final concentration of 100 µg/ml
	Solid	As above with 1.5% agar (w/v)
YPG medium	As for YPD, with 20 g D-galactose instead of D-glucose	
SD medium	With ammonium sulphate	6.9 g yeast nitrogen base without amino acids. 20 g agar if required. Made up to 900 ml with ddH_2O and autoclaved. 20 g D-glucose was dissolved in 100 ml ddH_2O, filter-sterilised and added to the medium after autoclaving
	Nitrogen minimal	As above, with 1.9 g yeast nitrogen base without amino acids or ammonium sulphate instead of yeast nitrogen base without amino acids.
SG medium	As for SD medium with D-galactose instead of glucose	
Luria-Bertaini (LB) medium	Liquid	10 g NaCl, 10 g bacto-tryptone, 5 g yeast-extract. pH to 7 with 1 M NaOH. Made up to 1 l with dH_2O. Autoclaved
	Solid	As above with 1.5% agar (w/v)
X-broth	20 g tryptone, 5 g yeast-extract, 0.5 g NaCl & 10 ml 250 mM KCl. pH to 7 with 1 M NaOH, make up to 975 ml and autoclave. Prior to use add 5 ml filter-sterilized 2 M $MgCl_2$ & 20 ml 1 M D-glucose. Final volume 1 l	
SOC	0.5% yeast extract, 2% tryptone, 10 mM NaCl. 2.5 mM KCl, 10 mM $MgCl_2$, 10 mM $MgSO_4$, 20 mM D-glucose. Glucose was filter-sterilised and added after autoclaving	
Water agar	1.5% agar (w/v). Made up to 1 l with dH_2O and autoclaved	
Genomic DNA extraction buffer	20 ml 1M Tris HCl pH 7.5, 5 ml 5M NaCl, 5 ml 500mM EDTA & 5 ml 10% SDS. Made up to 100 ml with dH_2O	
50x Tris acetate EDTA buffer (TAE)	242 g Trizma base (Tris), 57.1 ml glacial acetic acid & 100 ml 0.5 M EDTA pH 8. Made up to 1 l final volume	
6x DNA loading dye	0.25% (w/v) bromophenol blue, orange G and xylene cyanol FF. 40% (w/v) sucrose	
TE buffer	0.5 ml 1 M Tris pH 7.6 & 100 µl 0.5 M EDTA. Made up to 50 ml with dH_2O and autoclaved	
Neutralisation buffer	87.66 g NaCl & 60.5 g Trizma base (Tris). pH to 7.5 with conc. HCl. Made up to final volume 1 l with dH_2O	
Denaturation buffer	87.66 g NaCl & 20 g NaOH; pH to 7.5 with conc. HCl. Made up to final volume 1 l with dH_2O	
Depurination buffer	11 ml Conc. HCl; Made up to final volume 1 l with dH_2O	
20x SSC buffer	88.23 g Tri-sodium Citrate & 175.32 g NaCl. pH to 7-8 with 1 M NaOH. Made up to final volume 1 l with dH_2O and autoclaved	
10x TE buffer	0.5 ml 1 M Tris pH 7.6 & 100 µl 0.5 M EDTA. Made up to final volume 50 ml with dH_2O and autoclaved	
1x phosphate buffered saline (PBS)	8.0 g NaCl, 0.2 g KCl, 1.33 g Na_2HPO_4, 0.24 g KH_2PO_4. pH to 7.4 with 1 M HCl. Made up to final volume 1 l with dH_2O and autoclaved	
1x radioimmunoprecipitation assay buffer (RIPA)	0.5 ml Igepal CA-630, 0.25 g sodium deoxycholate, 0.05 g SDS, 49.5 ml 1x PBS. Just prior to 10 mM β-mercaptoethanol and, per 10 ml buffer 1x cOmplete ULTRA EDTA-free mini tablet (Roche Diagnostics Ltd)	
10x TBS	24.23 g Trizma-HCl, 80.06 g NaCl. Made up to 1 l with dH_2O and	

	adjusted pH to 7.6 with conc. HCl
1x TBS-T	100 ml 10x TBS, 899 ml dH_2O, 1 ml Tween20
1x Western running buffer	14.4 g glycine, 3 g Tris, 1.0 g SDS (Bio-Rad Laboratories Ltd.). Made up to 1 l with dH_2O
1x Western transfer buffer	200 ml methanol, 3 g Tris, 14.4 g glycine. Made up to 1 l with dH_2O
1x blocking buffer	5 g skimmed milk powder, 1 g BSA, 100 µl goat serum. Made up 10 100 ml with 1x TBS-T. Added 0.5 ml Tween 20 and mixed for 30 min
5x MOPS buffer	83.72 g of MOPS and 8.23 g sodium acetate was added to 1.6 l of DEPC-treated water. Added 20 ml of DEPC-treated 0.5 M EDTA and the pH adjusted to 7.0 with 10 M NaOH. Made up to final volume of 2 l with DEPC-treated water and autoclaved in 200 ml aliquots
RNA sample buffer	10 ml formamide, 3.5 ml 37% formaldehyde, 2 ml 5x MOPS buffer. Aliquotted and stored at -20^oC for up to 6 months
RNA loading dye	50% glycerol, 1 mM EDTA, 0.4% bromophenol blue, made up to final volume with nuclease-free H_2O. Aliquotted and stored at -20^oC
OM lysis buffer	44.37 g $MgSO_4$, 1 ml 1 M $NaH_2PO_4.H_2O$ & 2.1 g lysing enzymes from *Trichoderma harzianum*. pH to 5.8 with dibasic Na_2HPO_4. Made up to 150 ml with dH_2O and filter-sterilised
ST buffer	54.66 g sorbitol & 50 ml 1M Tris-HCl pH 7.0. Made up to 500 ml with dH_2O & autoclaved.
STC buffer	109.32 g sorbitol, 5 ml 1 M Tris-HCl pH 7.5 & 5 ml 1 M $CaCl_2$. Made up to 500 ml with dH_2O & autoclaved.
PTC buffer	40 g PEG 4000, 18.22 g sorbitol, 1 ml 1 M Tris-HCl pH 7.5 & 1 ml 1 M $CaCl_2$. Made up to 100 ml with dH_2O & autoclaved.
Defined Complex Medium (DCM)	1.7 g Yeast nitrogen base without amino acids (ForMedium), 2 g L-asparagine, 1 g ammonium nitrate & 10 g D-glucose. pH 6 with dibasic Na_2HPO_4, add 1.5% agar (w/v. Made up to 1 l with dH_2O and autoclaved
BDCM Bottom Layer	1.7 g yeast nitrogen base without amino acids or ammonium sulphate, 1 g L-asparagine, 2 g ammonium nitrate, 10 g D-glucose, 273.84 g sucrose. Made up to 1 l with ddH_2O and pH to 6 with 1 M Na_2HPO_4. Added 15 g agar per litre and autoclaved
BDCM Overlay	1.7 g yeast nitrogen base without amino acids or ammonium sulphate, 1 g L-asparagine, 2 g ammonium nitrate, 10 g D-glucose. Made up to 1 l with 1 M Na_2HPO_4 and added 10 g agar per litre. Autoclaved
SOB medium	2% (w/v) tryptone, 0.5% (w/v) yeast extract, 10 mM NaCl, 2.5 mM KCl, 10 mM $MgCl_2$, 10 mM $MgSO_4$. Make up to 1 l and autoclave
TB	10 mM PIPES, 15 mM $CaCl_2$, 250 mM KCl. Made up to 0.5 l and adjusted pH with KOH. Added 55 mM $MnCl_2$. All salts were added as solids

2.1.1.5 Oligonucleotide sequences

Oligonucleotide primers used in this thesis were synthesised by Sigma Aldrich.

Table 2.4: Complete list of oligonucleotides used in this thesis

Primer Name	PRIMER SEQUENCE
B-tubulin F	CTCTGCCATCTTCCGTGGA
B-tubulin R	ACGAAGTACGACGAGTTCTTGTTGT
EF-F	TCAACGGTGACCACATGATCTCG
EF-R	CCTAACGCTCCTTGGTACAAGG
qPCR1_03904F	GGACCCTGTGTCGTTACC
qPCR1_03904R	GTTGGCCATCTCGTACTC

qPCR1_04162F	GAAGCACAGGTTGACATA
qPCR1_04162R	CAGTATATCCAGTGGTAGG
qPCR1_05880F	GCAGCATACTTTTCTTCATCA
qPCR1_05880R	TTGACTGAGGAGGTGGAC
qPCR1_13332F	TTGGATCTATTGGGCTGGAC
qPCR1_13332R	CACTCTCCAGATCCCTGCTC
qPCR1_13615F	GCAGGATGCCTTTTCAGAGT
qPCR1_13615R	GCAGTAGACGCCAAACATGA
13615WCHyg-F	GTCGACGTTAACTGATATTGAAGGAG
13615WCHyg-R	GTCGACGTTAACTGGTTCCCGGTCGGC
136153'H-F	GATGCCGACCGGGAACCAGTTAACGTCGACCGCGACTTTGGCCCCAGGTTGGTTTC
136153'H-R	AATGCTCCTTCAATATCAGTTAACGTCGACGCCTTGTAGTTGCCGTACACGATTGCCG
13615WC-F	CGTTTTCTTTGAGAAATTCATTCCTGCG
13615WC-R	AACTGCAACTGGACTGTTTTTATGC
SM05880-F1	CCAGCGGTTGACGAAAAATATTTCGTTAG
SM05880-F2	CTACCATTCAAACTATACCATGGGTCGACAGAAGATGATATTGAAGGAG
SM05880-F3	GCTGCTTGGTGCACGATAACTTGG
SM03904-F1	TGGGGAGAGCCTCTTTTTAGAAACAGCC
SM03904-F2	CAAGCGACATCCACGGTAGCAGGTCGACAGAAGATGATATTGAAGGAG
SM03904-F3	GCTGCTTGGTGCACGATAACTTGG
SM03904-F4	CTGCCCGTCACCGAGATTTAGGTCGACGGACAATGATCCAACTCAGAATCCGGCC
SM03904-R1	CTCCTTCAATATCATCTTCTGTCGACCTGCTACCGTGGATGTCGCTTGC
SM03904-R2	AGCAGGTGGGTGTAGAGCGTGGAGCC
SM03904-R3	GGCCGGATTCTGAGTTGGATCATTGTCCGTCGACCTAAATCTCGGTGACGGG
SM03904-R4	CGAAAGTAGACATGTTCACATGCGC
SM05880-F4	CTGCCCGTCACCGAGATTTAGGTCGACTTTTAATAAAGCGGAGGAACAGAACAAC
SM05880-R1	CTCCTTCAATATCATCTTCTGTCGACCCATGGTATAGTTTGAATGGTAG
SM05880-R2	AGCAGGTGGGTGTAGAGCGTGGAGCC
SM05880-R3	GTTGTTCTGTTCCTCCGCTTTATTAAAAGTCGACCTAAATCTCGGTGACGGG
SM05880-R4	TTGCGGACGAGTATAATAAATATATCGTATAAC
SM13332-F1	ACGCCTGTATATGCCGGTGAATGG
SM13332-F2	CAGGATTCGTCCATCAGCGCCGTCGACAGAAGATGATATTGAAGGAG
SM13332-F3	GCTGCTTGGTGCACGATAACTTGG
SM13332-F4	CCCGTCACCGAGATTTAGGTCGACGGATGCCGCTCACCCGGACGAAG
SM13332-R1	CTCCTTCAATATCATCTTCTGTCGACGGCGCTGATGGACGAATCCTG
SM13332-R2	AGCAGGTGGGTGTAGAGCGTGGAGCC
SM13332-R3	CTTCGTCCGGGTGAGCGGCATCCGTCGACCTAAATCTCGGTGACGGG
SM13332-R4	CTACTGTGGCACCGGCTGCAACCC
SM10783-F1	GACGACGGTGACAGGGCGGG
SM10783-F2	GAGTTTGTCGGCACCTTTTTGTTCGTCGACGTTAACTGATATTGAAGGAGC
SM10783-F3	AGACCTGCCTGAAACCGAACTGCCC
SM10783-F4	GATGCCGACGGGAACCAGTTAACGTCGACGTTTCTGGGCTCGGCCTTGGGTGCAGGG
SM10783-R1	GCTCCTTCAATATCAGTTAACGTCGACGAACAAAAAGGTGCCGACAAACTC
SM10783-R2	AATGCGGAGCATATACGCCCGGAG
SM10783-R3	CCCTGCACCCAAGGCCGAGCCCAGAAACGTCGACGTTAACTGGTTCCCGGTCGGCATC
SM10783-R4	CTGGCTGTTTTCGGCATTGCTCGCTC

SM04162-F1	GGGGGTTTTCTTCCATCAAAGCTTGTG
SM04162-F2	CACCACAACACACGTTAGCCCCACGTCGACGTTAACTGATATTGAAGGAG
SM04162-F3	AGACCTGCCTGAAACCGAACTGCCC
SM04162-F4	GATGCCGACCGGGAACCAGTTAACGTCGACCGAATGGTTCTCAAAGATGAAAGTTGC
SM04162-R1	CTCCTTCAATATCAGTTAACGTCGACGTGGGGCTAACGTGTGTTGTGGTG
SM04162-R2	AATGCGGAGCATATACGCCCGGAG
SM04162-R3	GCAACTTTCATCTTTGAGAACCATTCGGTCGACGTTAACTGGTTCCCGGTCGGCATC
SM04162-R4	GACGTTGGTTTCTTTCCCATTGCG
SM13615-R4	CGAGTTGGTTTAGTCTCGTTACATTTCCAC
13332_IP3F	CAGCCTGCCGGTTCCGCC
13332_IP3R	CCAGCGCCGTAAGCCCTCCTC
10783_IP5F	AGGCCCACGAAACAACCATC
10783_IP5R	CGCACCAAGTTATCGTGCACC
10783_IP3F	CGTACACAAATCGCCCGC
10783_IP3R	CCATGCACCCAACAGCAATATC
13332_IP5F	GCGGATACCGAAGTCGGAG
13332_IP5R	ATGAACCATCTTGTCAAACGACAC
05880_IP5F	TGTAATTTCAGCCTGCTCCGC
05880_IP3F	CGGGAACTGGCATGACGTGG
05880_IP3R	TCGAGGGAGTGTCGTGGCTGG
05880_IP5R	ATGAACCATCTTGTCAAACGACAC
04162_IP5F	CCTTGAGTGGTCAAGGGGGTG
04162_IP5R	GCTGCATCATCGAAATTGCCGTC
04162_IP3F	CGGCGCTCGAAGTGTGAC
04162_IP3R	GAGAAAATGGGGGCTGATGTG
13615_IP5F	ACCCTCTTGTACCCGCATGTC
13615_IP5R	CAAGTTATCGTGCACCAAGCAG
13615_IP3F	GATGCAGCTTGGGCGCAGG
13615_IP3R	CCGACCAGTTGCGGACAGG
03904_IP5F	TGAACATACACCGTACACATCCG
03904_IP5R	GTGCACCAAGCAGCAGATG
03904_IP3F	GTGGGTTTCTGGCAGCTGG
03904_IP3R	CTGGTCCGAACTCAAAACCGTC
qPCR2_04162F	CGAAACCAGAAGACCAGAGC
qPCR2_04162R	GTTGCGGAGGATAGGAGACA
qPCR2_05880F	CATCCCTGCGACTTTGTTC
qPCR2_05880R	TGCCGACAATCATCAAACTG
qPCR2_13332F	CCTACGGGTTTTCTCTGCTG
qPCR2_13332R	GGTGACAGCGGGATTAAAGA
qPCR2_13615F	GCACCAAGGGTGAATATCAGA
qPCR2_13615R	CGGATTTCATGGAGCAGTAGA
Actin_F	ACAATGGTTCGGGTATGTGC
Actin_R	CGACAATGGACGGGAAGAC
40S_F	ACAAGCTCAAGACCCTCGTC
40S_R	GGTGGTGATGGTGAAGCAG
iGFP58us F	AAAAGGCGCGCCGATAATAAGTGTAGCTTTTCTCGATAGAAAAGTAAG
iGFP58us R	CCACCCCGGTGAACAGCTCCTCGCCCTTGCTCACAATATGGACGCCGGAGTG
iGFP58eG F	CGCTGGTCGGCTCGCACACTCCGGCGTCCATATTGTGAGCAAGGGCGAGGAG
iGFP58eG R	AGCCTAGGTTCTGGTCTGGGTGCGGGTAGGAGCAGCTTGTACAGCTCGTCCATGC
iGFP58ds F	GCCGGGATCACTCTCGGCATGGACGAGCTGTACAAGCTGCTCCTACCCGCACCC

iGFP58ds R	AAAAGCGGCCGCCAGACAGGTCTCCGACTGC
iGFP58us F	AAAAGGCGCGCCGATAATAAGTGTAGCTTTTCTCGATAGAAAAGTAAG
iGFP58us R	CCACCCCGGTGAACAGCTCCTCGCCCTTGCTCACAATATGGACGCCG GAGTG
C03904F	AAAAAGGCGCGCCGATCAGACGAGTGTGTG
C03904R	AAAAACCTGCAGGCTTGGCATCAAAGCCACC
C04162F	AAAAGGCGCGCCAGCTTGTGATTTTGCATCGTTCTAC
C04162R	AAAACCTGCAGGAGCGACCCTCGTCAAGGGATCGCGG
C05880F	AAAAGGCGCGCCTGTCTAAACCCGAGTCCGAGATGAG
C05880R	AAAAGGCGCGCCTGCCTTTATGCCCTGCTCCTCGTC
C13332F	AAAAGGCGCGCCATTAGACACTGTATTTGCAGC
C13332R	AAAACCTGCAGGTCTAGACTCGGTGGCAACTC
C13615F	AAAAGGCGCGCCGTATTACCTTCCACGTCCG
C13615R	AAAACCTGCAGGGACGTTGCTGATCTCTTTG
N03904F	AAAAAGCGGCCGCAGCATCAAATCCTGATCCAG
N03904R	AAAAAATTTAAATTTACTTGGCATCAAAGCC
N04162F	AAAAGGATCCGCCAGCGACGAACAGACCTCAACTACCC
N04162R	AAAATACGTATCAAGCGACCCTCGTC
N05880F	AAAAGGATCCCGCCGATACGGTAGCTCCCGTG
N05880R	AAAATACGTATTATGCCTTTATGCCCTGCTC
N13332F	AAAAGCGGCCGCATCGCCAACCCACAATCTCC
N13332R	AAAATACGTACTATCTAGACTCGGTGGCAACTCCACTCTCCAGATCCCT G
N13615F	AAAAGGATCCGCACACGTCACGGAGATATATACCGTC
N13615R	AAAATACGTACTAGACGTTGCTGATCTC
FG Vector_[39]Promoter_F	AACTGTTGGGAAGGGCGATCGGTGCGGGCCATATTTGGAACTGATGG CGATAAG
FG [39]Promoter_R	GATGATTAGATGTTTCCCACTCCTG
FG [39]Promoter_eGFP_F	GGCCCCAGGAGTGGGAAACATCTAATCATCATGGTGAGCAAGGGCGA GGAGCTG
FG eGFP_R	TTACTTGTACAGCTCGTCCATGCC
FG eGFP_[39]Term_F	ACTCTCGGCATGGACGAGCTGTACAAGTAATGACACCGAAGCAAACTC AACAGTTC
FG [39]Term_R	GGCAAGATAAGGGGGCGGGGGTCTG
FG [39]Term_sulph_F	ACCTACAGACCCCCGCCCCCTTATCTTGCCGTCGACGTGCCAACGCCA CAGTGC
FG Vector_sulph_R	TTCACACAGGAAACAGCTATGACCATGATTGTCGACGTGAGAGCATGC AATTCC
FG Vector_[41]Promoter_F	AACTGTTGGGAAGGGCGATCGGTGCGGGCCAAGTTGCTTTAGTGGGT TGGGCGAG
FG [41]Promoter_R	CGTGGCTTCTTTCTTGTCCTCCTC
FG [41]Promoter_eGFP_F	AAGGAGAGGAGGACAAGAAAGAAGCCACGATGGTGAGCAAGGGCGA GGAGCTG
FG eGFP_R	TTACTTGTACAGCTCGTCCATGCC
FG eGFP_[41]Term_F	ACTCTCGGCATGGACGAGCTGTACAAGTAAGCAACCAACCAGCCGCA CTTGGATG
FG [41]Term_R	GCATCCTATCACATCGTTCTCGTGG
FG [41]Term_sulph_F	CCTTCCACGAGAACGATGTGATAGGATGCGTCGACGTGCCAACGCCA CAGTGC
FG Vector_sulph_R	TTCACACAGGAAACAGCTATGACCATGATTGTCGACGTGAGAGCATGC AATTCC
FG Vector_[58]Promoter_F	AACTGTTGGGAAGGGCGATCGGTGCGGGCCGCCCGGCGTTAACTAAT ACTACTAC

FG [58]Promoter_R	CCTGCTTTCATCGTCTAGAACCAAC
FG [58]Promoter_eGFP_F	TCGCTGTTGGTTCTAGACGATGAAAGCAGGATGGTGAGCAAGGGCGAGGAGCTG
FG eGFP_R	TTACTTGTACAGCTCGTCCATGCC
FG eGFP_[58]Term_F	ACTCTCGGCATGGACGAGCTGTACAAGTAAGACACCGCTCACACTAATGATTAC
FG [58]Term_R	GCAACCAAGAAAAAAAACGACGATC
FG [58]Term_sulph_F	TTTGGGATCGTCGTTTTTTTTCTTGGTTGCGTCGACGTGCCAACGCCACAGTGC
FG Vector_sulph_R	TTCACACAGGAAACAGCTATGACCATGATTGTCGACGTGAGAGCATGCAATTCC
FG Vector_[133]Promoter_F	AACTGTTGGGAAGGGCGATCGGTGCGGGCCCTGGCGGCCATCAACTTCTCGGGC
FG [133]Promoter_R	TGTTTCGTCGGTGGGCGGCGATTG
FG [133]Promoter_eGFP_F	AGACTCCAATCGCCGCCCACCGACGAAACAATGGTGAGCAAGGGCGAGGAGCTG
FG eGFP_R	TTACTTGTACAGCTCGTCCATGCC
FG eGFP_[133]Term_F	ACTCTCGGCATGGACGAGCTGTACAAGTAAATTGACGTGTTTTTTAACTTGATTG
FG [133]Term_R	CTCCTTCGTCGACCGCCAAGATTTC
FG [133]Term_sulph_F	CGGGGGAAATCTTGGCGGTCGACGAAGGAGGTCGACGTGCCAACGCCACAGTGC
FG Vector_sulph_R	TTCACACAGGAAACAGCTATGACCATGATTGTCGACGTGAGAGCATGCAATTCC
FG Vector_[136]Promoter_F	AACTGTTGGGAAGGGCGATCGGTGCGGGCCCGTGCTTTTGTTCCTTGCCGATGG
FG [136]Promoter_R	GTTTTATAGACAAGAGAAAGATCG
FG [136]Promoter_eGFP_F	GAGATCGATCTTTCTCTTGTCTATAAAACATGGTGAGCAAGGGCGAGGAGCTG
FG eGFP_R	TTACTTGTACAGCTCGTCCATGCC
FG eGFP_[136]Term_F	ACTCTCGGCATGGACGAGCTGTACAAGTAAAACAATACCTTGGCGCAGCTGTTC
FG [136]Term_R	CTAGACTAGGGGTTGTGGGGGCC
FG [136]Term_sulph_F	CCCTCAAGGCCCCCACAACCCCTAGTCTAGGTCGACGTGCCAACGCCACAGTGC
FG Vector_sulph_R	TTCACACAGGAAACAGCTATGACCATGATTGTCGACGTGAGAGCATGCAATTCC
CSVector_pRP27_F	AACTGTTGGGAAGGGCGATCGGTGCGGGCCATAAATGTAGGTATTACCTGTACA
CSpRP27_R	TTTGAAGATTGGGTTCCTACGAAAG
CSpRP27_[39]_F	CTTGGCTTTCGTAGGAACCCAATCTTCAAAATGGCATCAAATCCTGATCCAGGAG
CSLinker_[39]_R	GGCGCCGCCGGCGCCGCCCTCTTTGTGTAGGTATTCCCTCTG
CS[39]_linker_eGFP_F	CAAAGAGGGCGGCGCCGGCGGCGCCGTGAGCAAGGGCGAGGAGCTGTTCACCGG
CSeGFP_R	TTACTTGTACAGCTCGTCCATGCC
CSeGFP_[39]term_F	ACTCTCGGCATGGACGAGCTGTACAAGTAAACTGTGGTACTGCCTCGCCATCATC
CS[39]term_R	TTGGCATAGCTCCTTCCGATATC
CS[39]term_sulph_F	AAAAAAAGATATCGGAAGGAGCTATGCCAAGTCGACGTGCCAACGCCACAGTGC
CSVector_sulph_R	TTCACACAGGAAACAGCTATGACCATGATTGTCGACGTGAGAGCATGC

	AATTCC
CSVector_pRP27_F	AACTGTTGGGAAGGGCGATCGGTGCGGGCCATAAATGTAGGTATTACCTGTACA
CSpRP27_R	TTTGAAGATTGGGTTCCTACGAAAG
CSpRP27_[41]_F	CTTGGCTTTCGTAGGAACCCAATCTTCAAAATGGCCAGCGACGAACAGACCTC
CSLinker_[41]_R	GGCGCCGCCGGCGCCGCCAGCGACCCTCGTCAAGGGATCGCG
CS[41]_linker_eGFP_F	GGTCGCTGGCGGCGCCGGCGGCGCCGTGAGCAAGGGCGAGGAGCTGTTCACCGG
CSeGFP_R	TTACTTGTACAGCTCGTCCATGCC
CSeGFP_[41]term_F	ACTCTCGGCATGGACGAGCTGTACAAGTAAGCAACCAACCAGCCGCACTTGGATG
CS[41]term_R	GCATCCTATCACATCGTTCTCGTG
CS[41]term_sulph_F	CCCTTCCACGAGAACGATGTGATAGGATGCGTCGACGTGCCAACGCCACAGTGC
CSVector_sulph_R	TTCACACAGGAAACAGCTATGACCATGATTGTCGACGTGAGAGCATGCAATTCC
CSVector_pRP27_F	AACTGTTGGGAAGGGCGATCGGTGCGGGCCATAAATGTAGGTATTACCTGTACA
CSpRP27_R	TTTGAAGATTGGGTTCCTACGAAAG
CSpRP27_[58]_F	CTTGGCTTTCGTAGGAACCCAATCTTCAAAATGCGCCGATACGGTAGCTCCCG
CSLinker_[58]_R	GGCGCCGCCGGCGCCGCCTGCCTTTATGCCCTGCTCCTCGTC
CS[58]_linker_eGFP_F	TAAAGGCAGGCGGCGCCGGCGGCGCCGTGAGCAAGGGCGAGGAGCTGTTCACCGG
CSeGFP_R	TTACTTGTACAGCTCGTCCATGCC
CSeGFP_[58]term_F	ACTCTCGGCATGGACGAGCTGTACAAGTAAGACACCGCTCACACTAATGATTAC
CS[58]term_R	CAAGAAAAAAAACGACGATCCC
CS[58]term_sulph_F	GATAATTTGGGATCGTCGTTTTTTTCTTGGTCGACGTGCCAACGCCACAGTGC
CSVector_sulph_R	TTCACACAGGAAACAGCTATGACCATGATTGTCGACGTGAGAGCATGCAATTCC
CSVector_pRP27_F	AACTGTTGGGAAGGGCGATCGGTGCGGGCCATAAATGTAGGTATTACCTGTACA
CSpRP27_R	TTTGAAGATTGGGTTCCTACGAAAG
CSpRP27_[133]_F	CTTGGCTTTCGTAGGAACCCAATCTTCAAAATGTCGCCAACCCACAATCTCCTC
CSLinker_[133]_R	GGCGCCGCCGGCGCCGCCTCTAGACTCGGTGGCAACTCCACTC
CS[133]_linker_eGFP_F	GTCTAGAGGCGGCGCCGGCGGCGCCGTGAGCAAGGGCGAGGAGCTGTTCACCGG
CSeGFP_R	TTACTTGTACAGCTCGTCCATGCC
CSeGFP_[133]term_F	ACTCTCGGCATGGACGAGCTGTACAAGTAAATTGACGTGTTTTTTAACTTGATTG
CS[133]term_R	CTTCGTCGACCGCCAAGATTTCC
CS[133]term_sulph_F	CATCGGGGGAAATCTTGGCGGTCGACGAAGGTCGACGTGCCAACGCCACAGTGC
CSVector_sulph_R	TTCACACAGGAAACAGCTATGACCATGATTGTCGACGTGAGAGCATGCAATTCC
CSVector_pRP27_F	AACTGTTGGGAAGGGCGATCGGTGCGGGCCATAAATGTAGGTATTACCTGTACA
CSpRP27_R	TTTGAAGATTGGGTTCCTACGAAAG
CSpRP27_[39]_F	CTTGGCTTTCGTAGGAACCCAATCTTCAAAATGGCACACGTCACGGAGATATATAC
CSLinker_[39]_R	GGCGCCGCCGGCGCCGCCGACGTTGCTGATCTCTTTGCGCTG
CS[39]_linker_eGFP_F	*CAACGTC*GGCGGCGCCGGCGGCGCCGTGAGCAAGGGCGAGGAGCTGTTCACCGG
CSeGFP_R	TTACTTGTACAGCTCGTCCATGCC

CSeGFP_[39]term_F	ACTCTCGGCATGGACGAGCTGTACAAGTAAAACAATACCTTGGCGCAGCTGTTC
CS[39]term_R	GACTAGGGGTTGTGGGGGCCTTG
CS[39]term_sulph_F	TTGCCCTCAAGGCCCCCACAACCCCTAGTCGTCGACGTGCCAACGCCACAGTGC
CSVector_sulph_R	TTCACACAGGAAACAGCTATGACCATGATTGTCGACGTGAGAGCATGCAATTCC
cDNA 03904R	AAAAAAGCGGCCGCTTACTTGGCATCAAAGCCACC
cDNA 04162F	AAAAGAATTCATGGCCAGCGACGAACAG
cDNA 04162R	AAAAACTCGAGTCAAGCGACCCTCGTCAAG
cDNA 05880F	AAAAGAATTCATGCGCCGATACGGTAGC
cDNA 05880R	AAAACTCGAGTGCCTTTATGCCCTGCTC
cDNA 13332F	AAAAGAATTCATGTCGCCAACCCACAATCTCC
cDNA 13332R	AAAACTCGAGTCTAGACTCGGTGGCAACTCC
cDNA 13615F	AAAAGAATTCATGGCACACGTCACGGAGATATATACC
cDNA 13615R	AAAACTCGAGGACGTTGCTGATCTCTTTGC

2.1.1.6 *Saccharomyces cerevisiae* strains

All strains were acquired from EUROSCARF (http://web.uni-frankfurt.de/fb15/mikro/euroscarf/), with the exception of Δ*mep1-3* which was a gift from Dr. Pai Pedas (University of Copenhagen).

Table 2.5: A list of *Saccharomyces cerevisiae* strains used in this thesis

Mutant	Background	Genotype	Phenotype
BY4741 wild type	BY4741	MATa; his3Δ 1; leu2Δ 0; met15Δ 0; ura3Δ 0	
Δ*dur3*	BY4741	Mat a; his3D1; leu2D0; met15D0; ura3D0; YHL016c::kanMX4	Lacks *DUR3*, a high affinity urea/H^+ symporter responsible for urea uptake
Δfps1	BY4741	Mat a; his3D1; leu2D0; met15D0; ura3D0; YLL043w::kanMX4	Lacks *FPS1,* an endogenous aquaglyceroporin
Δ*mep1-3*	31019b	MATa ura3 mep1Δ mep2Δ::LEU2 mep3Δ::KanMX	Lacks all endogenous ammonium transporters
Δ*yap1*	BY4741	Mat a; his3D1; leu2D0; met15D0; ura3D0; YML007w::kanMX4	High sensitivity to oxidative stress resulting from loss of the Yap1 transcription factor
DS94 wild type	DS94	MATα ura3-52 trp1-1 leu2-3 his3-11 lys2-801	

2.1.1.7 *Magnaporthe oryzae* strains

Table 2.6: A list of *Magnaporthe oryzae* strains used in this thesis

Strain	**Background Strain**	**Source**	**Description**	**Resistance Marker**
Guy11	N/A	N. Talbot, University of Exeter	Wild type strain	None
Δ*Ku70*	Guy11	N. Talbot, University of Exeter	Non-homologous recombination impaired	SUR

Δ*aqp1*	Guy11	This study	Aquaporin knockout	BAR
Δ*aqp2*	Guy11	This study	Aquaporin knockout	HYG
Δ*agp1*	Guy11	This study	Aquaporin knockout	BAR
Δ*mgg_10783*	Guy11	This study	Aquaporin knockout	HYG
Δ*aqp3*	Guy11	This study	Aquaporin knockout	BAR
Δ*agp2*	Guy11	This study	Aquaporin knockout	HYG
Δ*agp1* Δ*agp2*	Guy11	This study	Aquaporin knockout	BAR & HYG
pAQP1::*AQP1*::eGFP	Δ*aqp1*	This study	C terminal eGFP fusion, native promoter	BAR & HYG
pAQP2::*AQP2*::eGFP	Δ*aqp2*	This study	C terminal eGFP fusion, native promoter	BAR & HYG
pAGP1::*AGP1*::eGFP	Δ*agp1*	This study	C terminal eGFP fusion, native promoter	BAR & HYG
pAQP3::*AQP3*::eGFP	Δ*aqp3*	This study	C terminal eGFP fusion, native promoter	BAR & HYG
pAGP2::*AGP2*::eGFP	Δ*agp2*	This study	C terminal eGFP fusion, native promoter	BAR & HYG
pRP27::*AGP1*::*eGFP*	Δ*agp1*	This study	Internal eGFP fusion, native promoter	BAR & HYG
pRP27::*AQP1*::*eGFP*	Δ*aqp1*	This study	N terminal eGFP fusion, strong promoter	BAR & HYG
pRP27::*AQP2*::*eGFP*	Δ*aqp2*	This study	N terminal eGFP fusion, strong promoter	BAR & HYG
pRP27::*AGP1*::*eGFP*	Δ*agp1*	This study	N terminal eGFP fusion, strong promoter	BAR & HYG
pRP27::*AQP3*::*eGFP*	Δ*aqp3*	This study	N terminal eGFP fusion, strong promoter	BAR & HYG
pRP27::*AGP2*::*eGFP*	Δ*agp2*	This study	N terminal eGFP fusion, strong promoter	BAR & HYG
pRP27::*eGFP*::*AQP1*	Guy11	This study	C terminal eGFP fusion, strong promoter	SUR
pRP27::*eGFP*::*AQP2*	Guy11	This study	C terminal eGFP fusion, strong promoter	SUR
pRP27::*eGFP*::*AGP1*	Guy11	This study	C terminal eGFP fusion, strong promoter	SUR
pRP27::*eGFP*::*AQP3*	Guy11	This study	C terminal eGFP fusion, strong promoter	SUR
pRP27::*eGFP*::*AGP2*	Guy11	This study	C terminal eGFP fusion, strong promoter	SUR
pAQP1::eGFP	Guy11	This study	Cytosolic eGFP under the AQP1 promoter	SUR
pAQP2::eGFP	Guy11	This study	Cytosolic eGFP under the AQP2 promoter	SUR
pAGP1::eGFP	Guy11	This study	Cytosolic eGFP under the AGP1 promoter	SUR
pAQP3::eGFP	Guy11	This study	Cytosolic eGFP under the AQP3 promoter	SUR
pAGP2::eGFP	Guy11	This study	Cytosolic eGFP under the AGP2 promoter	SUR
Grx1-roGFP2	Guy11	M. Samalova, University of Oxford	Redox sensitive GFP probe	BAR
Δ*aqp2* Grx1-roGFP2	Δ*aqp2*	This study	Δ*aqp2* expressing Grx1-roGFP2	BAR & HYG

2.1.1.8 *Escherichia coli* strains

Table 2.7: A list of *Escherichia coli* strains used in this thesis

Strain	Source	Genotype
DH5α	Unknown	FΦ80*lacZ*ΔM15 Δ(*lac*ZYA-*arg*F) U169 *rec*A1 *end*A1 *hsd*R17(R_k^-, m_k^+) *pho*A *sup*E44 *thi*-1 *gyr*A96 *rel*A1 *ton*A

2.1.1.9 Important websites

Table 2.8: A list of websites used in this thesis

Website	URL
Autodimer	http://yellow.nist.gov:8444/dnaAnalysis/primertoolspage.do
Broad Institute	http://www.broadinstitute.org/
InterProScan	http://www.ebi.ac.uk/Tools/pfa/iprscan/
Jalview	http://www.jalview.org/
MUSCLE alignment web server	http://www.ebi.ac.uk/Tools/msa/muscle/
NCBI	http://www.ncbi.nlm.nih.gov/
NCBI BLAST server	http://blast.ncbi.nlm.nih.gov/Blast.cgi
Primer3	http://bioinfo.ut.ee/primer3-0.4.0/
UniProt	http://www.uniprot.org/

2.2 Methods

2.2.1 Plant methods

2.2.1.1 Stock maintenance and routine growth

Barley (*Hordeum vulgare* L. cv. Golden Promise) was grown in a 50:50 mixture of Erin Multipurpose Compost and John Innes No. 2 loam-based compost. Rice (*Oryzae sativa* cv. CO-39) was grown in John Innes No 3 compost and silver sand in a 3:1 ratio. Rice and Barley were incubated under a 14/10h light/dark photoperiod. Barley was incubated at 20^{o}C and 84% humidity for seven days and rice at 25^{o}C and 90% humidity for 21 days.

2.2.1.2 Barley epidermal peel preparation

Barley leaves were removed from the plant and placed adaxial side up on a cutting tile. A single edge blade (Fischer Scientific) was used to cut vertically down through each leaf leaving the lower epidermis intact. The lower epidermis could then be removed by carefully flexing and pulling away the upper leaf material.

2.2.1.3 Onion epidermal peel preparation

White onions were cut into quarters and the outer sheaths removed. The epidermis was gently separated from the inner surface of each layer and placed epidermal-side up onto a 2% (w/v) water agar plate.

2.2.2 *Magnaporthe oryzae* methods

2.2.2.1 Routine growth and maintenance of stocks

M. oryzae strains were cultured on solid media at 24^{o}C with a 14/10 hour light/dark photoperiod. In liquid culture strains were grown at 24^{o}C, 150 rpm in darkness. Plates were sealed with micropore tape to prevent contamination.

For long-term storage, strains were inoculated onto solid CM media and surrounded by small pieces of sterile filter paper (Whatman Plc). After 10 days, the filters were collected and desiccated over silica gel for one week and stored at -20^{o}C.

2.2.2.1.1 Conidial harvesting

Conidia were harvested from 10 day old fungal cultures grown on CM. Five millilitres of sterile dH_2O was pipetted onto each plate and conidia were extracted by gently scraping the surface of the culture using a sterile microscope slide. The liquid was passed through a double layer of sterile Miracloth (Merck Chemicals Ltd) to remove mycelial fragments and centrifuged for 5 min at 2095 xg (3000 rpm). The supernatant was poured off and the conidia resuspended in 1 ml sterile ddH_2O. Conidial concentration was measured using a haemocytometer and adjusted appropriately.

2.2.2.1.2 Radial growth assays

To each 10 cm round Petri dish was added 35 ml of the specified media under sterile conditions. An 8mm circular plug was removed using a sterile cork borer from a 10-day old CM culture and placed, mycelial-side down, at the centre of the Petri dish. Plates were sealed using micropore tape and incubated for 10 days under normal growth conditions unless specified otherwise.

2.2.2.2 *Magnaporthe oryzae* transformation

2.2.2.2.1 Protoplast release

Conidia were harvested from a 10-day old CM plate and inoculated into 300 ml liquid CM containing 100 µg/ml penicillin and streptomycin. These flasks were incubated in the dark for 66 h at 25^{o}C and shaken at 150 rpm.

After incubation, the unmelanised mycelial cultures were filtered through a double-layer of sterile Miracloth (Merck). The mycelium was squeezed dry in sterile paper towelling and split into two Falcon tubes. Each mycelial plug was homogenised with a sterile scalpel in 50 ml filter-sterilised OM buffer and digested in the dark at 30^{o}C for 3-4 h, shaking at 150 rpm.

Following digestion, the protoplast suspension from each tube was split into two 50 ml Falcon tubes and gently overlaid with ice-old ST buffer to a final volume of 50 ml. The tubes were centrifuged at 2744 xg (5000 rpm) for 15 min at 4^{o}C, before the released protoplasts were collected at the OM/ST interface. The protoplasts were overlain with at least 10 ml STC buffer and centrifuged for 10 min at 2095 xg (3000 rpm) at 4^{o}C. The supernatant was poured off and the protoplasts were resuspended in 10ml ice cold STC buffer and recentrifuged at 2095 xg (3000 rpm) at 4^{o}C. This washing step was repeated a further three times.

Following the final wash, the pellet was resuspended in 1 ml STC buffer and the protoplast concentration measured using a haemocytometer. The concentration was adjusted using ice cold STC buffer to a final concentration of 6.5x10^{6} /ml.

2.2.2.2.2 PEG-mediated protoplast transformation

Double-distilled water containing 2-10 µg DNA was added to 140 µl protoplast suspension and incubated at room temperature. After 15-25 min, 1 ml filter-sterilised PTC buffer was added and mixed gently by inverting before incubation at room temperature for 20 min. The transformed protoplasts were added to 200 ml molten (48^{o}C) OCM agar (hygromycin B (Merck) and bialophos (GoldBio)) or BDCM (chlorimuron ethyl), mixed gently and poured into 10 sterile 9 cm round petri dishes. The protoplasts were regenerated in the dark for 24 h at 24^{o}C before being overlaid with antibiotic selective medium. hygromycin-resistant strains were isolated by overlaying sets of 10 plates with 400 ml MM supplemented with 300 µg/ml hygromycin B and bialophos-resistant strains

were overlaid with 400 ml DCM containing 100 µg/ml bialophos. chlorimuron ethyl resistant strains were overlaid with 400 ml BDCM upper layer supplemented with 75 µg/ml chlorimuron ethyl (sulphonylurea). Solid chlorimuron ethyl was solubilised in dimethyl sulfoxide for use as a 100 mg/ml stock solution; the chlorimuron ethyl stock was a gift from Dr Michael Kershaw (University of Exeter).

Single colonies growing through the upper layer within 7-14 days were removed with a sterile scalpel and put through a second round of selection on the overlaying medium, supplemented with the relevant antibiotic at half the original concentration.

2.2.2.3 Pathogenicity assays

The 3rd emergent leaf from seven day old CO-39 rice plants were harvested and trimmed to 9 cm. Leaves were washed in 2% sodium hypochlorite (bleach) solution and rinsed for 30 s in sterile ddH_2O three times to sterilise the surface. Six leaves were placed adaxial-side up on 120 mm square Petri-dishes filled with 2% (w/v) water agar. The tips and base of the leaves were covered with a sterile microscope slide to affix the leaves securely to the agar.

Conidia were harvested from three 10-day old CM plates, washed as described in section 2.2.2.1.1 and resuspended in 2 ml ddH_2O. The concentration was adjusted to 6.4x10^5 spores per ml using a haemocytometer. One millilitre of this spore solution mixed with 1 ml 0.4% (w/v) gelatine solution and sprayed evenly over the leaf surfaces using compressed air (Maxim Air) and an artist's airbrush. Before and between sprays the airbrush was cleaned with 70% ethanol and washed three times in sterile distilled water.

After spraying, plates were incubated for five days under rice growth conditions and photographed. The pathogenicity of each strain was analysed using image analysis software written by Dr. Mark Fricker (University of Oxford). A minimum of three biological replicates were carried out per genotype.

2.2.3 *Saccharomyces cerevisiae* methods

2.2.3.1 Routine growth and maintenance of stocks

Yeast strains were propagated on SD/SG medium, supplemented with the necessary amino acids or in YPD medium. Strains were incubated at 28^{o}C in the dark and liquid cultures were shaken at 220 rpm.

For long-term storage, yeast cells were collected using a sterile 10 µl inoculating loop and resuspended in 1 ml 15% glycerol (Fischer Scientific) and stored at -80^{o}C.

2.2.3.2 *Saccharomyces cerevisiae* transformation

2.2.3.2.1 LiAC/SS carrier DNA/PEG transformation

Yeast strains for transformation were streaked out and grown for 2-4 days on YPD plates. A 10 µl inoculating loop full of cells was inoculated into 10ml liquid YPD in a 50 ml Falcon tube and grown for 4-6 h at 28^{o}C, 200 rpm. The Falcon tube was spun down at 931 xg (2000 rpm) for 3 min and the supernatant poured off. The pellet was gently resuspended in 1 ml sterile ddH_2O. An aliquot of 100-300 µl of this suspension in a 1.5 ml sterile Eppendorf tubes was centrifuged at 931 xg (2000 rpm) for 50 sec. The supernatant was pipetted off and cells were resuspended by vortexing in 1 ml 100 mM LiAc. Cells were incubated for 5 min at room temperature before centrifugation at 931 xg (2000 rpm) for 50 sec and the supernatant pipetted off. 300 µl 50% PEG 3500, 36 µl 1 M LiAc, 50 µl boiled salmon sperm single-stranded carrier DNA (2 mg/ml) and 1 µg transformation plasmid in 36 µl H_2O were added to each Eppendorf tube. The SS-carrier DNA was boiled and flash cooled prior to use up to a maximum of four times. The transformation mixture was vortexed to resuspend and incubated at 42^{o}C for 20-40 min. The cells were pelleted at 931 xg (2000 rpm) for 50 sec and the supernatant carefully pipetted off. The cells were resuspended in 200µl ddH_2O and spread over an SD plate. Plates were sealed and incubated upside down at 28^{o}C in the dark for 3-5 days until visible colonies appeared. Single colonies were re-plated by streaking out selection medium.

2.2.4 *Escherichia coli* methods

2.2.4.1 Preparation of DH5α competent cells

2.2.4.1.1 Subcloning efficiency cells

A sterile culture of DH5α cells were streaked across an LB plate and incubated at 37^{o}C for 16 h. A single colony was inoculated into 5 ml liquid LB medium and grown for 16 h at 37^{o}C, 150 rpm, and 500µl of this culture was inoculated into 50ml fresh liquid LB and shaken at 37^{o}C until the OD_{600} reached 0.45-0.55. The flask was cooled on ice for 5 min and the culture was split into two pre-cooled 50 ml Falcon tubes. The cells were centrifuged at 4^{o}C for 5 min, 2851 xg (3500 rpm), the supernatant was poured off and the pellet was gently resuspended in 25 ml of filter-sterilised 0.1 M $CaCl_2$. The cells were kept on ice for 30 min before being centrifuged at 4^{o}C for 5 min at 2851 xg (3500 rpm). After centrifugation, the supernatant was poured off and each pellet was gently resuspended in 5 ml filter-sterilised 0.1 mM $CaCl_2$ with 12.5% glycerol. The cells were aliquoted into pre-cooled Eppendorf tubes and flash-frozen immediately in liquid nitrogen.

2.2.4.1.2 High efficiency cells

A single DH5α colony was inoculated into 5ml liquid SOB medium and grown for 16h at 37^{o}C and 220 rpm. A 250ml conical flask containing 50ml liquid SOB was inoculated with 0.5ml of this culture and incubated at 18^{o}C until the OD_{600} reached exactly 0.6. The flask was cooled on ice for 10 min the cells were decanted to a sterile 50ml Falcon tube and centrifuged at 2095 xg (3000 rpm) for 10 min at 4^{o}C. The supernatant was discarded and the cells were resuspended gently in 50ml TB and incubated on ice for 10 min. The cells were re-centrifuged at 3000 rpm for 10 min at 4^{o}C, the supernatant discarded and the cells resuspended in 0.04x the original culture volume. DMSO was added to a final concentration of 7% and the cells were aliquotted and immediately frozen in liquid nitrogen.

2.2.4.2 Transformation of DH5α competent cells

Up to 20 µl ligation reaction was added to up to 200 µl thawed DH5α *E. coli* cells, with the final volume of ligation reaction mixture not exceeding 10% of the total volume. The mixture was incubated on ice for 30 min before heat-shocking at 42^{o}C for exactly 2 min (for subcloning efficiency cells) or 30 sec (for ultra-competent cells). Heat-shocked cells were cooled on ice for 2 min before 1 ml of X-broth was added. Cells were incubated at 37^{o}C, 150 rpm for 30m-1h. Cells

were briefly centrifuged at 1164 xg (3500 rpm) in a microcentrifuge and all but 200 µl of the supernatant was pipetted off. Cells were resuspended by gently tapping the tube and plated out on LB agar plates containing 100 µg/ml ampicillin and incubated overnight at 37^{o}C.

2.2.4.3 Plasmid DNA preparation

Single DH5α *E. coli* colonies were inoculated into 5 ml of 100 µg/ml ampicillin selective LB liquid medium and grown for 16 h at 37^{o}C, 200 rpm. Cultures were centrifuged for 15 min at 5251 xg (4750 rpm) and plasmid DNA was extracted from the pelleted cells using a QIAprep Spin Miniprep Kit (Qiagen) according to manufacturers' instructions.

2.2.5 DNA methods

DNA samples were stored at -20^{o}C unless stated otherwise. DNA concentrations were determined using a Nanodrop machine.

2.2.5.1 Genomic DNA extraction

For "high quality" genomic DNA, fungal material was collected by scraping the surface of a 10 day old culture on complete medium with a sterile scalpel. This tissue was flash-frozen in liquid nitrogen and ground using a sterile ceramic pestle and mortar. gDNA was extracted using a Qiagen DNEasy Plant Minikit according to the manufacturers' instructions.

For "low quality" genomic DNA, around 1cm^{2} of plate-grown fungal mycelium was collected in a 1.5ml Eppendorf tube using a sterile scalpel and ground in 400µl genomic DNA extraction buffer using a sterile micropestle (Eppendorf). The sample was vortexed for 10 sec and incubated at room temperature for 15 min. The sample was centrifuged at 17,900 xg (13,000 rpm) for 60 sec and 300 µl supernatant transferred to a new 1.5 ml tube. An equal volume of isopropanol was gently mixed with the supernatant before centrifuging at 17,900 xg (13,000 rpm) for 5 min. The supernatant was pipetted off and the pelleted DNA left to dry at room temperature for up to 30 min. The dry pellet was resuspended in 50 µl 1x TE buffer and stored at 4^{o}C.

2.2.5.2 PCR methods

2.2.5.2.1 High-fidelity PCR

The high-fidelity proofreading enzyme Herculase II Fusion DNA polymerase (Agilent Technologies) was used where template fidelity was required. Reactions were carried out in 50 µl volumes with the following components:

10 µl	5x Herculase buffer
1.25 µl	100 pM forward primer
1.25 µl	100 pM reverse primer
1 µl	dNTP mix (25 mM each dATP, dTTP, dCTP, dGTP)
100-300 ng	DNA template(s)
1 µl	Herculase II Fusion DNA polymerase
Up to 50 µl	ddH2O

PCR reactions with Herculase II were carried out with the following cycling conditions:

Step 1	Denaturation	94°C	4 min	
Step 2	Denaturation	94 °C	20 sec	Repeat steps 2-4 35x
Step 3	Annealing	55-64 °C	20 sec	
Step 4	Elongation	72 °C	3 min	
Step 5	Final elongation	72 °C	3 min	
Step 6	Cooling	4 °C	∞	

2.2.5.2.2 Low-fidelity PCR

Where template fidelity was not essential, recombinant Taq DNA polymerase (Fermentas) was used. PCR reactions were carried out in 25 µl volumes with the following components:

0.5 µl	100 pM forward primer
0.5 µl	100 pM reverse primer
2.5 µl	10x Taq buffer ($(NH_4)_2SO_4$)
2.5 µl	25 mM $MgCl_2$
50-150 ng	DNA template
0.25 ul	dNTP mix (25 mM each dATP, dTTP, dCTP, dGTP)
0.5 µl	Recombinant Taq DNA polymerase
Up to 25 µl	ddH_2O

PCR reactions with recombinant Taq DNA polymerase were carried out with the following cycling conditions:

Step 1	Denaturation	94°C	5 min	
Step 2	Denaturation	94 °C	30 sec	Repeat steps 2-4 35x
Step 3	Annealing	55-64 °C	30 sec	
Step 4	Elongation	72 °C	130 min	
Step 5	Final elongation	72 °C	10 min	
Step 6	Cooling	4 °C	∞	

2.2.5.2.3 PCR fragment purification

PCR fragments were purified using a Qiagen QIAquick PCR Purification kit according to the manufacturers' instructions.

2.2.5.2.4 Agarose gel electrophoresis

0.8 – 2% agarose (w/v) was added to 1x TAE buffer and microwaved to dissolve the agarose. Prior to pouring rthidium bromide was added to a final concentration of 0.5 µg per ml. DNA samples were pre-mixed with 6x loading dye and loaded into the gel together with an appropriate DNA ladder where required. A voltage of 80-100 V was applied to separate the DNA molecules along a size gradient.

2.2.5.2.5 Gel extraction of DNA fragments

DNA bands were illuminated on a UV transilluminator (λ=254 nm) and excised with a scalpel, taking care to minimise the amount of excess agarose and UV exposure time. DNA was extracted from the gel using a Qiagen QIAquick Gel Extraction Kit according to the manufacturers' instructions.

2.2.5.2.6 Restriction endonuclease digestion

Restriction enzymes were supplied by New England Biolabs, and digests were performed according to the manufacturers' instructions, unless specified otherwise in the text. For multiple enzyme digests, experimental strategies were designed to facilitate buffer compatibility. When circularising vectors were digested, termini were dephosphorylated using Antarctic Phosphatase (NEB) according to manufacturers' instructions to prevent re-circularisation. Enzymes were heat inactivated after use wherever possible.

2.2.5.2.7 DNA ligation

Following digestion and dephosphorylation, where necessary, the insert and vector digests were cleaned with QIAquick PCR purification kit to remove protein and buffer contamination. Ligation reactions were performed using T4 DNA ligase (Sigma) according to the manufacturers' instructions. Ligation reactions were carried out overnight in water cooled from room temperature to 4^{o}C in a refrigerator.

2.2.5.2.8 Ethanol precipitation of DNA

DNA was dissolved in 200 µl ddH_2O and gently mixed with 6 µl 5 M NaCl and 618 µl 100% ethanol. The mixture was kept at -20^oC for at least 30 min before centrifugation at 17,900 xg (13,000 rpm) at 4^oC for 60 min. The supernatant was pipetted off and the pellet washed with ice cold 70% ethanol. The pellet was then dried for up to half an hour and eluted in sterile ddH_2O.

2.2.5.2.9 Phenol/chlorophorm DNA extraction

DNA eluted in 200 µl ddH2O was added to 200 µl phenol:chloroform:isoamyl alcohol 25:24:1 saturated with 10 mM Tris (pH 8.0). The mixture was vortexed for 30 sec and centrifuged for two min at 17,900 xg (13,000 rpm) to separate the liquid phases. The upper aqueous phase was pipetted off into a new Eppendorf tube, taking care not to disturb the protein débris.

2.2.5.2.10 DNA sequencing

Plasmid and PCR samples were sent to Source BioScience (Department of Biochemistry, University of Oxford) for sequencing via Illumina GAIIx and HiSeq 2000 sequencing machines. Sequencing lengths were assembled using BioEdit Sequence Alignment Editor.

2.2.5.3 Southern blotting

High quality genomic DNA was extracted from 10 day old CM plates as detailed in Section 2.2.2.1. DNA concentration was checked using a Nanodrop machine and a minimum of 2 µg DNA was digested overnight with the relevant enzymes.

An ethidium bromide-free 0.8% (w/v) gel was poured, and the samples together with a 1 kb DNA ladder were mixed with 20x loading dye and added to the wells. The ladder was pre-mixed with ethidium bromide to allow visualisation. The gel was run until the ladder had distributed along the length of the gel.

Following electrophoresis, the ladder and wells were excised from the gel and the gel was agitated in depurination buffer. After 20 min, the depurination buffer was poured off and replaced with denaturation buffer for another 30-60 min. Finally the gel was treated with neutralisation buffer and gently shaken for another 30-60 min.

A capillary transfer tower was constructed as described in Sambrook and Russell (3rd edition, 2001) on an elevated plastic tray, with a double layer of Whatman 3M filter paper as the wick with

the ends submerged in 10x SSC buffer. The gel was placed upside down on top of the 10x SSC dampened filter paper. A nylon Hybond N+ membrane (Amersham) was cut to the dimensions of the gel and placed carefully on top. Three identical pieces of Whatman 3M filter paper, pre-wetted in 10x SSC, were placed on top of the membrane. A stack of pre-cut paper towels were placed on top of the filter papers and weighted down with a 900 g weight. After 16 h, the tower was disassembled and the DNA was cross-linked to the membrane using a Stratagene UV Stratalinker 2400.

After cross-linking the membrane was pre-hybridised in a rotating oven for 1 h at 65^{O}C in 10 ml Perfect HYB Plus Hybridisation buffer (Sigma Aldrich).

The DNA probe was radiolabelled using an Amersham Ready-To-Go DNA Labelling Kit (GE Healthcare) according to the manufacturers' instructions. The ^{32}P α-dCTP labelled probe was separated from unincorporated nucleotides using Illustra NICK columns (GE healthcare). Columns were washed with 3 ml 1x TE buffer before the probe, pre-mixed with 50 µl dextran blue, was pipetted into the centre of the column. The blue mixture was allowed to run through the column and collected and stored on ice.

The labelled probe was boiled for 10 min then flash cooled on ice before being carefully pipetted into the pre-hybridisation mixture. The membrane and probe were hybridised overnight at 65^{0}C in a rotating oven.

Following hybridisation, the probe was poured off and the membrane washed as detailed below:

Wash 1 and 2:	30 min	2x SSC, 0.1% SDS
Wash 3:	20 min	1x SSC, 0.1% SDS
Wash 4 and 5:	20 min	0.1x SSC, 0.1% SDS

All washing was carried out at 65^{o}C in 50 ml of the washing solutions.

After washing the membrane was air dried and, in a darkroom, placed in a lead cassette with an Amersham Hyperfilm MP (Amersham) for 24 h at -80^{o}C. The film was developed using Kodak GBX fixer and developer (Sigma Aldrich).

2.2.6 RNA methods

RNA was aliquotted and frozen at -80^{o}C for long-term storage or -20^{o}C for short-term storage. RNA for use immediately was stored on ice to reduce the activity of RNases.

2.2.6.1 Maintenance of an RNA-free environment

Work surfaces and pipettes were cleaned with RNAse-ZAP wipes (Ambion) and rinsed with diethylpyrocarbonate-treated (DEPC) RNase-free water. Disposable RNase/DNase-free plastic equipment was used where possible. Other plasticware was treated with 0.2% (v/v) DEPC overnight at 37^{o}C before autoclaving. Ceramic pestles and mortars and metal equipment were baked at 200^{o}C for a minimum of 6 h.

2.2.6.2 Total fungal RNA extraction

Fungal RNA was extracted from tissue flash frozen in liquid nitrogen and ground in a pre-cooled RNase-free pestle and mortar. Tissue was used immediately or stored at -80^{o}C. RNA was extracted using a Qiagen RNeasy Minikit according to the manufacturers' instructions.

2.2.6.3 gDNA removal

Genomic DNA was removed using an Ambion TURBO DNA-*free* kit (Life Technologies) according to the manufacturers' instructions. The 'rigorous' DNase treatment protocol was followed.

2.2.6.4 qRT-PCR methods

2.2.6.4.1 Preparation of cDNA

cDNA was prepared using a First Strand cDNA Synthesis Kit (Thermo Scientific) according to the manufacturers' instructions. Per reaction, 500 ng RNA was used or replaced with water for a 'no template control' (NTC). When generating a 'minus reverse transcriptase' control (-RT), the reverse transcriptase was omitted and replaced with water.

2.2.6.4.2 Transcript quantification with qRT-PCR

Relative transcript abundance was quantified in an ABI Prism 7300 Sequence Detection System (Applied Biosystems) with SYBR Green (Invitrogen) as a double stranded DNA-binding reporter dye.

Primers were designed using Primer3 software (http://primer3.wi.mit.edu/). Primer pairs with a T_m within 1°C and amplicons of 60-100 bp were imported into Autodimer (http://yellow.nist.gov:8444/dnaAnalysis/primertoolspage.do). Primer pairs forming dimers or secondary structures with a Gibbs free energy ≤ -2.0 were discarded. Primer specificity within the *M. oryzae* genome was checked using primer-BLAST (http://www.ncbi.nlm.nih.gov/tools/primer-blast/). Sequences with >15 bp homology to another genomic region were discarded.

DNA quantification was performed using a QuantiTect SYBR Green RT-PCR kit (Qiagen). Each PCR reaction contained the following components in a total volume of 25 µl:

12.5 µl	SYBR Green master mix
2.5 µl	100 pM forward primer
2.5 µl	100 pM reverse primer
2.5 µl	cDNA template
8 µl	Nuclease-free water

The reaction was carried out using the following cycling conditions:

Step 1	AmpliTaq Gold Polymerase Activation	95°C	10 min	
Step 2	Denaturation	95°C	15 sec	Repeat steps 2-3
Step 3	Anneal/Extend	60°C	20 sec	x40
Step 4	Melting curve	Range		

Primer efficiency was calculated using a 10-fold dilution series of the pooled cDNA templates from all time-points. The mean quantification cycle (C_q) of three replicates for each dilution was plotted against the $\log_{10}$ [relative cDNA concentration]. C_q was automatically assigned using the ABI software and manually checked for error. The primer efficiency (E) for each primer pair was calculated from the gradient of the best fit line according to the equation $E=10^{(-1/slope)}$ (Pfaffl 2001). Primer pairs with an E of less than 0.9 or greater than 1.1 were discarded and redesigned.

Primer specificity was checked by analysis of the melting curve. The fluorescence/temperature profile of a completed qPCR reaction can identify nonspecific amplification. Nonspecific amplicons are unlikely to have the same melting temperature as the specific sequence and can be identified by the presence of multiple fluorescence peaks in the melting curve. Primer pairs with multiple significant peaks were discarded.

The relative transcript abundance of each target gene at each time point was quantified relative to constitutively-expressed reference genes. Where indicated, the reference genes used were: β-tubulin (MGG_00604) and elongation factor 1α (MGG_03641) (Skamnioti and Gurr 2007) or Actin (MGG_03982) and 40S ribosomal protein S27 (MGG_02872) (Sarena Che Omar et al., manuscript in preparation 2013).

The transcript abundance of target genes was expressed relative to a given condition as stated in the text. Relative transcript abundance was calculated according to the equation:

$$\text{Ratio} = \frac{(\text{E}_{\text{gene}})^{\Delta \text{C}_\text{q}\ \text{gene}}}{(\text{E}_{\text{reference}})^{\Delta \text{C}_\text{q}\ \text{reference}}}$$

where E represents the calculated efficiency of that primer pair. Details of calculations in specific experiments can be found in the relevant chapters.

For each primer pair a 'no template control' (NTC) reaction was carried out, and for each RNA sample a 'no reverse transcriptase' (-RT) control was included. These tested for the presence of primer dimers and gDNA contamination respectively.

2.2.7 Microscopy

2.2.7.1 Light microscopy

Light microscopy was conducted using an Olympus BX50 microscope (Olympus Microscopy). Images were captured using a Q Image Retiga Exi digital camera (QI Imaging Corporation) and Image-Pro 6 software (Media Cybernetics Inc.). Post-processing and analysis of images was performed using ImageJ software (http://rsbweb.nih.gov/ij/index.html).

Chapter 3 Putative aquaporins in *Magnaporthe oryzae*

3.1 Introduction

This chapter investigates the aquaporin gene family in *Magnaporthe oryzae* and considers these genes in the context of the wider cross-kingdom aquaporin phylogeny. Evidence is presented – from published next-generation sequencing methods and microarray data – and from experimental quantitative PCR assays, that a subset of *M. oryzae* aquaporins are transcriptionally up-regulated during germling morphogenesis and coincident with the initiation of host infection.

3.1.1 The evolution of the aquaporin gene family

The basic aquaporin structure is shown in Figure 3.1. The protein comprises of two halves that are thought to have fused following an ancient gene duplication event (Pao et al., 1991, Park & Saier, 1996). Phylogenetic analysis of the major intrinsic protein (MIP) family reveals that the two major clades, the aquaporins and aquaglyceroporins, evolved prior the divergence of the prokaryotes and eukaryotes (Zardoya et al., 2002, Zardoya & Villalba, 2001). It has been proposed that these two subfamilies originated from an archaeon-like ancestral sequence (Araya-Secchi et al., 2011, Kozono et al., 2003). This hypothesis is based on the intermediate characteristics of the *AqpM* gene from the Archaeon *Methanothermobacter marburgensis* (Araya-Secchi et al., 2011). However, the nature of the evolutionary relationship between the archaea, the eukarya and the prokarya remains controversial, and the ancestral phylogeny implicit in this hypothesis may be incorrect (Gribaldo et al., 2010, Harish et al., 2013).

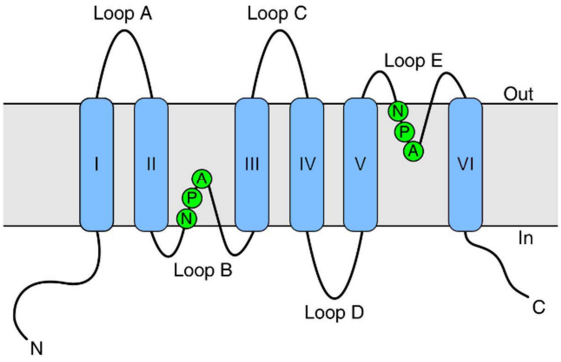

Figure 3.1: Topology of an aquaporin membrane protein. *Each protein consists of six transmembrane helices (I-VI) that span the membrane and two hemi-helices carrying the characteristic NPA motifs that enter and re-emerge from the membrane on the same side of the bilayer. N, amino terminus; C, carboxy terminus. The diagram is modified from Kruse et al. (2006).*

Although certain bacteria have both aqua- and aquaglyceroporin-type MIPs, some report that other bacterial species that lack MIPs (Tanghe et al., 2006). Indeed, some species have either aquaporins or aquaglyceroporins (Zardoya, 2005); of these, Gram-positive bacteria appear to have more aquaglyceroporin-type MIPs, whilst Gram-negative bacteria typically have more aquaporin-type MIPs.

The bacterial MIP genes typically cluster as outgroups at the base of the eukaryotic aquaporin and aquaglyceroporin phylogenetic trees (Zardoya, 2005). However, the most recent comprehensive study dates predates much of our current genome-based knowledge (2005); hence the “within-group” evolutionary history of bacterial MIPs is not well resolved.

3.1.1.1 The phylogenetic framework of eukaryotic aquaporins

The greatest expansion of MIP proteins is seen in vertebrates and plants (Zardoya, 2005). Plant MIPs are classified into seven groups – tonoplast intrinsic proteins (TIPs), plasma membrane intrinsic proteins (PIPs), NOD26-like intrinsic proteins (NIPs), small basic intrinsic proteins (SIPs), unrecognised intrinsic proteins (XIPs), hybrid intrinsic proteins (HIPs) and GlpF-like intrinsic proteins (GIPs), (Gupta & Sankararamakrishnan, 2009). The TIPs, PIPs, XIPs, SIPs and HIPs are all considered to be aquaporins (Maurel et al., 2008). The NIPs have aquaglyceroporin-like characteristics, and were originally thought to have evolved convergently from bacterial aquaporins, following a horizontal gene transfer (HGT) event (Zardoya et al., 2002). However, recent phylogenetic evidence suggests that this hypothesis is incorrect and they should actually be

classified as true aquaglyceroporins (Soto et al., 2012). As shown in Figure 3.2, the HIPs and GIPs are extant only in mosses and are thought to have been lost during the evolution of higher plants (Danielson & Johanson, 2008). The XIPs, which have a very weak amino acid similarity to other MIPs, are thought to have been lost in the monocot lineage.

The phylogenetic clustering of GIPs and bacterial glycerol facilitators has led to the proposal that these proteins were also acquired by HGT from bacteria (Gustavsson et al., 2005). However, evidence that GIP-like proteins are also present in trebouxiophyceae algae (a crown class of green algae) but not in algal outgroups, blurs this initial interpretation (Anderberg et al., 2011). A second independent gene duplication even has been proposed to explain this diversity (Anderberg et al., 2011). However, no supporting evidence for this second hypothesis, such as presence on genomic islands or use of specialised algorithms to detect HGT events, is provided and it is possible that this may be a classification or phylogenetic artefact.

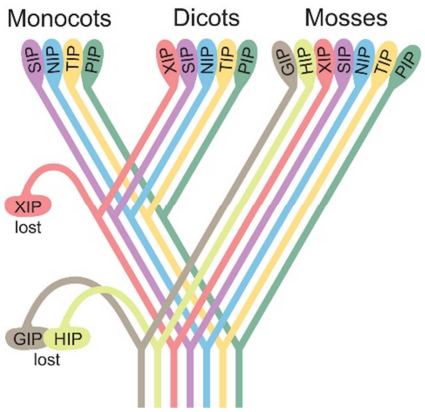

Figure 3.2: A schematic of the evolution of the MIP family in plants. *The ancestral plant is thought to have all groups of the MIP superfamily found in extant mosses. The GIPs and HIPs were lost in the higher plant lineage and the XIPs were lost during the evolution of monocots. Diagram from Danielson and Johanson (2008).*

Phylogenetic analysis of the animal MIPs suggests four conserved subfamilies: AQP1-like, AQP8-like, AQP3-like and AQP11-like (Danielson & Johanson, 2010, Soto et al., 2012). In *Homo sapiens*, the AQP1-like cluster contains HsAQP5, 2, 6, 10, 1, and 4, the AQP8-like subfamily contains only HsAQP8, the AQP3-like subfamily contains HsAQP3, 7, 10 and 8, and the AQP11-like subfamily contains HsAQP11 and HsAQP12 (Soto et al., 2012). The AQP1-like, 8-like and 11-like subfamilies are considered to be aquaporins and the AQP3-like subfamily are considered to be

aquaglyceroporins (Echevarria et al., 1994, Ishibashi, 2009, Ishibashi et al., 1997, Ishibashi et al., 2002, Ishibashi et al., 1994, Tsukaguchi et al., 1998).

Phylogenetic studies of MIP sequences are hampered by the low amino acid identity (<15%) between divergent family members (Soto et al., 2012). Assuming of deep homology many studies include divergent sequences in the same phylogenetic tree, often resulting in incongruence between the organismal tree and the MIP tree (Zardoya, 2005, Zardoya & Villalba, 2001). A recent study by Soto et al. (2012) used only eukaryotic MIP sequences with >25% amino acid identity and was able to circumvent this problem. This subset included all animal MIP groups but excluded the divergent XIPs, GIPs and HIPs from plants. The authors demonstrated that the four animal subfamilies are orthologous to four of the subfamilies in plants. Moreover, they proposed that the PIPs are orthologous to the AQP1-like proteins, the TIPs to the AQP8-like proteins, the NIPs to the AQP3-like proteins and the SIPs to the AQP11-like proteins. This indicates that the last common ancestor of plants and animals carried these same four subfamilies, as shown in Figure 3.3.

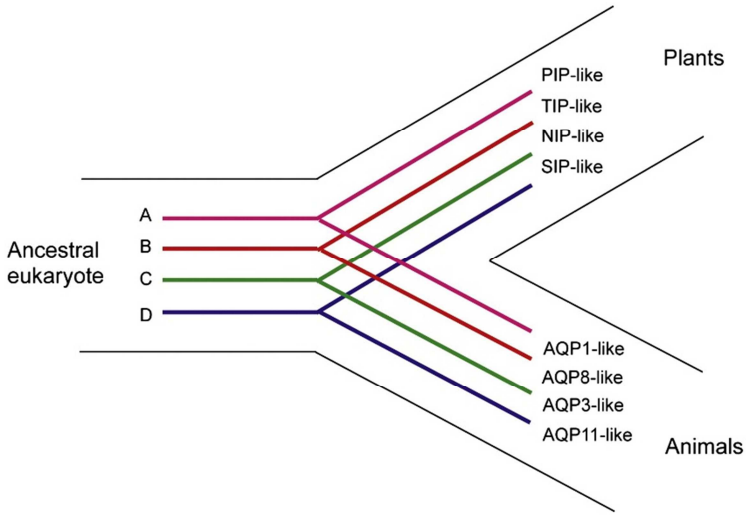

Figure 3.3: The evolution of the MIP protein family in plants and animals. *The ancestral eukaryote of these groups also had at least these four groups. Reprinted from Gene, 503 Soto et al., New insights into the evolution of aquaporins from flowering plants and vertebrates: orthologous identification and functional transfer is possible, Copyright (2012), with permission from Elsevier*

This analysis refutes several prior proposed phylogenetic relationships between eukaryotic MIPs. Previously, it had been hypothesised that higher plants lack aquaglyceroporins, but NIPs, acquired horizontally from bacteria, convergently evolved to fulfil the function of AGPs in plants (Zardoya et

al., 2002). However, the new phylogeny from Soto et al. (2012) shows this is incorrect as the NIP-family is orthologous to the AQP3-like family of aquaglyceroporins. The HGT hypothesis was strongly-supported by statistics (Danielson & Johanson, 2010, Park & Saier, 1996, Zardoya et al., 2002), and these findings demonstrate the importance of input sequence quality and thence use of appropriate phylogenetic inference techniques.

3.1.1.2 The phylogeny of fungal aquaporins

There is strong phylogenetic support for the position of plants as an out-group to animals and fungi in the phylogeny of the eukaryotes (Hampl et al., 2009). Therefore, if the last common ancestor of plants and animals had a minimum of four subfamilies, we assume this would also be true for fungi.

The most recent comprehensive phylogeny of fungal MIPs from 88 species groups them into four clusters – orthodox aquaporins, aquaglyceroporins, facultative aquaporins and XIPs (Xu et al., 2013). This contrasts with the first phylogenetic analysis of 19 yeast and three filamentous fungal species by Pettersson et al. (2005), which classified fungal aquaporins into: orthodox aquaporins, Fsp1-like aquaglyceroporins, Yfl054c-like aquaglyceroporins (equivalent to the facultative aquaporin categorisation in Xu et al., 2013) and 'other' aquaporins (equivalent to the facultative aquaporins in Xu et al., 2013). In 2009, Gupta and Sankararamakrishnan identified sequences in fungal genomes with homology to plant XIP genes. More recently, Dietz et al. (2011) used sequences of 29 fungal species to define four different groups: Fps1-like aquaglyceroporins, other aquaglyceroporins, classical aquaporins and fungal XIPs.

The existence of four groups – two aquaglyceroporin groups and two aquaporin groups – is common to these phylogenetic studies of fungal MIPs. However, the quality of the analyses is questionable given the difficulties associated with building phylogenies of divergent gene families. All three phylogenies used complete amino acid sequences to generate the evolutionary trees. The degree of conservation of aquaporin proteins varies along the sequence, with the helical residues being more conserved, but the loop and terminal domains are poorly conserved (Bansal & Sankararamakrishnan, 2007). Inclusion of these regions in the analysis may significantly reduce the quality of the phylogeny in three ways (Wu et al., 2012); i) by inclusion of large regions of

ambiguous alignment; ii) by introducing gaps from terminal extensions and group-specific insertions, and iii) by inclusion of amino acid positions that are evolving at enormously different rates (rate heterogeneity).

In the family phylogeny described by Xu et al. (2013), all representative plant MIPs (a PIP, TIP, SIP and a XIP) and a bacterial AqpZ gene cluster with the fungal XIPs. However, this likely represents a clustering of genes that are dissimilar to the other sequences in the alignment rather than similar to one another. These groupings, and numerous similar examples, suggest that the phylogeny employed by these authors does not adequately address the problems described above.

In this chapter, I attempt to generate a fungal aquaporin phylogeny that accurately depicts the evolutionary relationship within the fungi and in the wider eukaryotic kingdom. I invoke sequence selection criteria and strict editing of the input alignment to improve the quality of the input sequences relative to previous published attempts. From this robust input, I will thence use accurate probabilistic tree inference software to generate a phylogeny.

3.1.2 Transcript abundance of *M. oryzae* aquaporin genes

As laid out in the Introduction, this thesis aims to uncover a role for MIP genes in the infection process of *M. oryzae.* The relative transcript abundance of genes has been routinely used to identify genes that might influence infection or disease progression (Donofrio et al., 2006, Kim et al., 2010, Mosquera et al., 2009). Given the importance of water and glycerol, we were specifically interested in any increase in transcriptional abundance associated with the development of the appressorium through to early infectious growth. Any such increase might suggest that these genes are functionally important during this process. We examined the published large-scale sequence data available, and used qRT-PCR to validate this data *in planta.* I quantified the relative transcript abundance of each *M. oryzae* MIP gene in the wildtype Guy11 background, over the early stages of germling morphogenesis and infectious growth on barley leaves (*Hordeum vulgare* L. cv. Golden Promise) – an alternative host for *M. oryzae* (Leung et al., 1988).

qPCR can be a very accurate and sensitive tool for measuring gene expression levels. The transcript abundance is calculated based on the monitoring of product formation during the PCR cycles by measuring the fluorescence level of dsDNA-binding fluorophores. Figure 3.4A,

reproduced from Karlen et al. (2007), shows a typical amplification curve on a linear scale. There are three phases: the lag phase, the exponential phase, and the plateau. The lag phase is usually below the background fluorescence and is used to evaluate the baseline noise of the PCR amplification. The exponential phase corresponds to the linear phase of the amplification when plotted on a log scale (see Figure 3.4B) and the plateau occurs when reagents become exhausted. The cycle number at which each reaction reaches an arbitrary fluorescence threshold, the $C_{T,}$ is used to calculate the original transcript number with the equation:

$$T_{C_t} = T_0 . E_T^{C_t} \quad (1)$$

where T_{Ct} is the number of target molecules producing the threshold fluorescence, T_0 is the initial number of target molecules and E_T is the amplification efficiency of the target amplicon. The cycle threshold (C_T) is set in the exponential phase, manually or by various computational strategies. The C_T fluorescence threshold must be identical for all samples to be compared in a run.

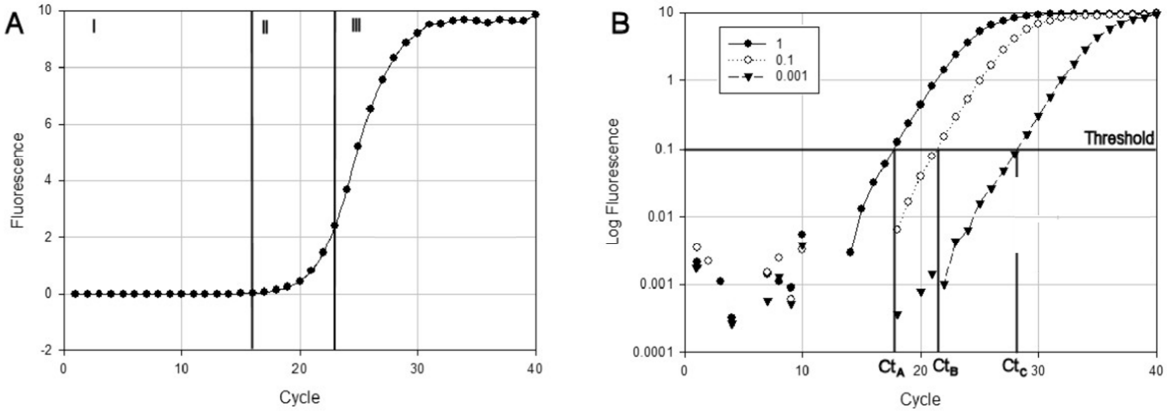

Figure 3.4: Representations of real-time PCR amplification curves on a linear (A) and log (B) scale. *Panel B shows a 10-fold dilution series of the same sample either undiluted (1), 10-fold diluted (0.1) or 1000-fold diluted (0.001). The figure is adapted from Karlen et al. (2007)*

There are two types of quantification strategy – absolute and relative quantification. In absolute quantification, the absolute mRNA copy number is quantified by reference to an appropriate external calibration curve (Pfaffl & Hageleit, 2001). Relative quantification is based on the expression ratio of a target gene to a reference gene. In its simplest form, relative quantification expresses the relative abundance of the target mRNA as the ratio r_i between the initial number of molecules T_0 and the initial number of reference mRNA molecules R_0:

$$r_1 = \frac{T_0}{R_0} \quad (2)$$

From equation (1), it can be shown that

$$r_1 = \frac{T_0}{R_0} = \frac{{}^{T}C_T T.E_T^{-C_T T}}{{}^{R}C_T R.E_R^{-C_R R}} \quad (3)$$

In the same experiment, $T_{C_t T}$ and $R_{C_T R}$ are constants, therefore:

$$r_1 = \frac{T_0}{R_0} = k.\frac{E_T^{-C_T T}}{E_R^{-C_R R}} \quad (4)$$

Where *k* is a constant that depends on various factors, including the type of reagents, the size and sequence of the PCR products and the fluorescence threshold (Livak & Schmittgen, 2001). Here, we assume that the constant *k* is equal to 1, therefore the relative transcript abundance will be expressed as a proportion of the abundance of the geometric mean of two constitutive housekeeping genes (Vandesompele et al., 2002).

We extracted RNA from infected leaves to investigate transcript abundance throughout the early stages of infectious development *in planta*. We selected seven time points, corresponding with different stages in the fungal developmental time course (Skamnioti et al., 2007). These are shown in Table 3.1 and were confirmed by light microscopy.

Table 3.1: The fungal developmental time course on barley epidermis

RNA extraction time point	Developmental stage
Spores	Ungerminated spores
1hpi	Germ tube emergence
2hpi	Hooking of the germ tube
4hpi	Appressorium development
8hpi	Appressorium maturation
12hpi	Penetration peg emergence
24hpi	Early infection hyphae

3.2 Experimental aims

1) To identify putative MIP genes in the *Magnaporthe oryzae* genome
2) To examine the evolutionary history of fungal aquaporins
3) To validate published expression data of *Magnaporthe oryzae* MIPs *in planta* using qRT-PCR

3.3 Methods specific to this chapter

3.3.1 Bioinformatic methods

3.3.1.1 Sequence discovery

MIP sequences were identified using iterative Hidden Markov Model (HMM) searches performed against a database of 59 fungal proteomes shown in Table 3.2. The protein family (PFAM) seed domain for the major intrinsic proteins (PF00230) was converted into a HMM profile and used to search the database with the Hmmer programme (Eddy, 1998). Hits were filtered using an e-value threshold of $1x10^{-10}$ and aligned using MAFFT (Katoh et al., 2005). Columns with >50% gaps were removed to prevent subgroup specific insertions biasing the models (Collingridge & Kelly, 2012).

This alignment was then used to generate the HMM for the next search iteration, with the search being terminated when no further hits passed the *e*-value threshold. To prevent biasing of the HMM towards any over-represented organisms, the gap-parsed alignments were re-parsed for >95% identity to other sequences within the alignment.

Sequence discovery algorithms and searches were written and performed with the help of Dr. Steve Kelly (University of Oxford).

Table 3.2: A list of fungal genomes from which MIP sequences were retrieved

Ajellomyces capsulatus	*Microsporum canis*
Ashbya gossippi	*Mucor circinelloides*
Aspergillus fumigatus	*Mycosphaerella graminicola*
Aspergillus nidulans	*Neurospora crassa*
Batrachochytrium dendrobatidis	*Paracoccidioides brasiliensis*
Blastomyces dermatitidis	*Penicillium chrysogenum*
Blumeria graminis	*Phaeosphaeria nodorum*
Botryotinia fuckeliana	*Phanerochaete chrysosporium*
Candida albicans	*Phycomyces blakesleeanus*
Candida dubliniensis CD36	*Pichia pastoris GS115*
Candida glabrata CBS138	*Pichia stipitis*
Chaetomium globosum	*Puccinia graminis*
Coccidioides immitis Rs 3	*Pyrenophora tritici-repentis*
Cochliobolus heterostrophus	*Rhizopus oryzae*
Colletotrichum graminicola	*Saccharomyces cerevisiae*
Coprinus cinereus okayama	*Schizosaccharomyces pombe*
Cryptococcus neoformans var JEC21	*Sclerotinia sclerotiorum*
Debaryomyces hansenii CBS767	*Spizellomyces punctatus*
Encephalitozoon cuniculi	*Sporobolomyces roseus*
Eremothecium gossypii	*Sporotrichum thermophile*
Fusarium oxysporum	*Thielavia terrestris*
Gaeumannomyces graminis var. tritici	*Trichoderma reesei*

Gibberella zeae	*Trichophyton rubrum*
Kluyveromyces lactis NRRL Y 1140	*Tuber melanosporum*
Laccaria bicolor	*Uncinocarpus reesii*
Lachancea thermotolerans CBS 6340	*Ustilago maydis*
Magnaporthe oryzae	*Verticillium dahliae*
Magnaporthe poae	*Yarrowia lipolytica CLIB122*
Melampsora laricispopulina	*Zygosaccharomyces rouxii CBS 732*

3.3.2 qRT-PCR methods

qRT-PCR is a highly sensitive method for determining the relative transcript abundance of a specific target mRNA relative to the expression of endogenous control genes. The qRT-PCR analysis in this chapter was carried out as described in the Materials and Methods, with Set 1 of qPCR primers. The two endogenous control genes, the β-tubulin β-chain gene (MGG_00604) and the elongation factor 1α (MGG_03641) gene were used as endogenous *M. oryzae* reference genes (Skamnioti et al., 2007).

RNA was extracted from spores, and from infected barley epidermis at specific time-points corresponding with six developmental stages – 1 hpi, 2 hpi, 4 hpi, 8 hpi, 12 hpi and 24 hpi. Conidia were harvested from 3x 10-day old CM plates and resuspended in 5 ml sterile ddH_2O. The conidial suspension was spray inoculated onto 7-day old barley plants (*Hordeum vulgare* L. cv. Golden Promise, susceptible to *M. oryzae* strain Guy11) and incubated as described in the materials and methods.

Barley leaves were removed from the plant and placed adaxial side up on a cutting tile. A single edge blade (Fischer Scientific) was used to cut vertically down through each leaf leaving the lower epidermis intact. The lower epidermis could then be removed by carefully flexing and pulling away the upper leaf material. This reduced the quantity of plant material in the final RNA preparation, thus increasing the ratio of fungal to plant RNA. Each epidermal peel was frozen in liquid nitrogen immediately to prevent degradation by RNases.

Initial quantification and quality assessment of RNA was carried out using a NanoDrop machine. The A_{260}/A_{280} and A_{260}/A_{230} ratios were used to provide an indication of RNA purity. RNA was considered to be of reasonable quality if the A_{260}/A_{280} ratio was close to 2.0 and the A_{260}/A_{230} ratio was above 1. The quality of RNA further assessed by running on a 1% (w/v) agarose/formaldehyde gel to check for the presence of two rRNA bands. The gel was prepared using 20 ml 5x MOPS

buffer, 72 ml RNase-free water and 1 g agarose, heated to boiling point, cooled to around 55^{o}C. To the cooled gel was added 17.6 ml 37% (v/v) formaldehyde and 5 µg ethidium bromide. 3.3 µl RNA was mixed with 6.7 µl RNA sample buffer and heated to 65^{o}C for 5 minutes then cooled on ice for 2 minutes. Prior to loading, 2 µl 5x RNA loading buffer was added.

cDNA was prepared as described in the Materials and Methods. Each experiment was carried out in triplicate with a single full experimental replicate.

3.4 Results

3.4.1 Identification of aquaporins in *Magnaporthe oryzae*

The *M. oryzae* MIP sequences were identified from annotation 8 of the *M. oryzae* genome (Broad Institute). The sequences were identified using BLASTP searches of the *M. oryzae* predicted protein set using the human MIP sequences as the query (Altschul et al., 1997). The retrieved sequences were reciprocally BLASTed against the *M. oryzae* genome to recover any additional sequences. The presence of an MIP domain was confirmed using InterPROscan (http://www.ebi.ac.uk/Tools/pfa/iprscan/). No domains were identified other than the MIP domain.

The sizes of the *M. oryzae* proteins identified ranged from 298 aa to 536 aa. The nature of the MIP proteins was further confirmed by checking the secondary structure conformed to the canonical ‘six transmembrane domain and two re-enterant helices’ structure. The secondary structure was predicted using MEMSAT-SVM – a support vector machine-based TM topology predictor with the ability to predict re-enterant helices (Nugent & Jones, 2009). A diagram of the secondary structure of each MIP is shown in Figure 3.5.

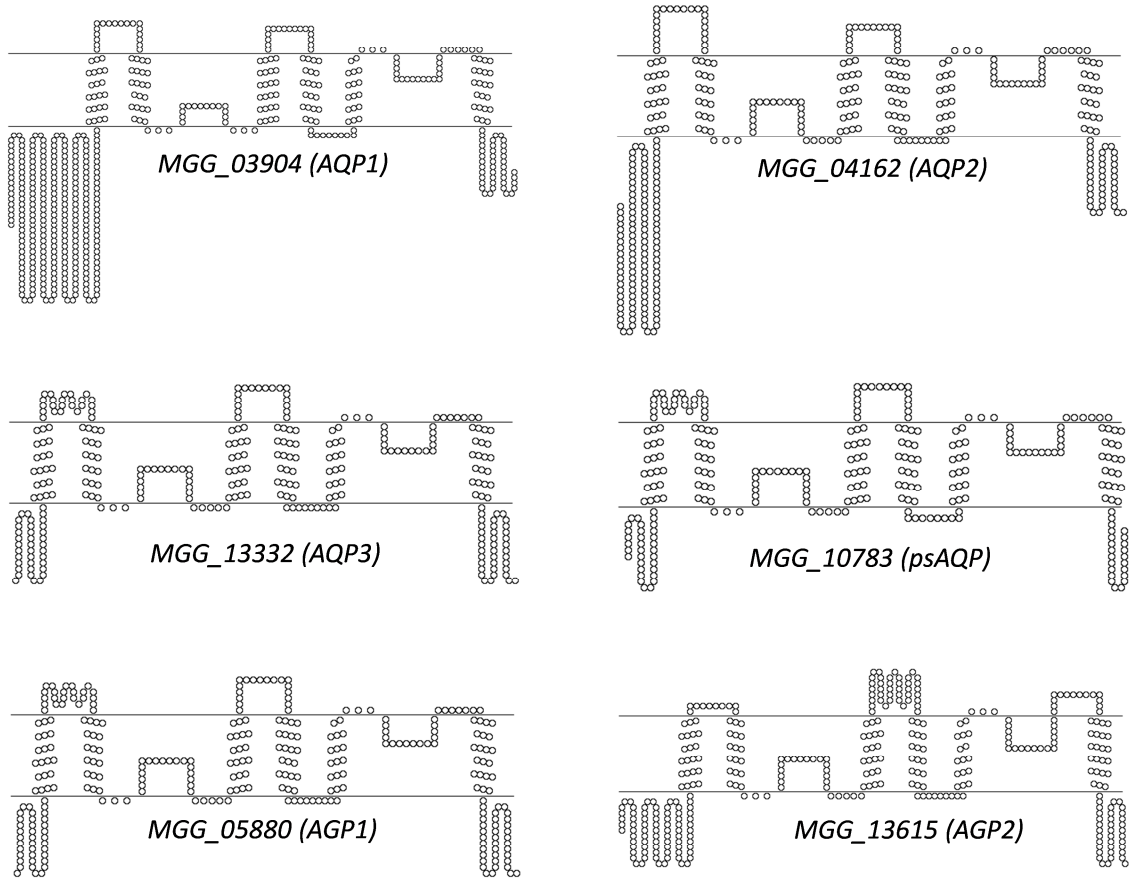

Figure 3.5: The topology of the six MIP genes in the Magnaporthe oryzae genome, as predicted by MEMSAT_SVM topology prediction software. Diagrams are displayed using TOPO2 (http://www.sacs.ucsf.edu/TOPO2/).

Each gene was classified as an aquaporin or an aquaglyceroporin by phylogenetic analysis with two canonical bacterial MIP genes: AqpZ as a representative of the aquaporins and GlpF as a representative of the aquaglyceroporins. The sequences were aligned using MUSCLE alignment software and a phylogeny was constructed using MEGA5 (Tamura et al., 2011). The evolutionary history was inferred by using the Maximum Likelihood method based on the Poisson correction model (Zuckerkandl & Pauling, 1965). The tree with the highest log likelihood is shown in Figure 3.6.

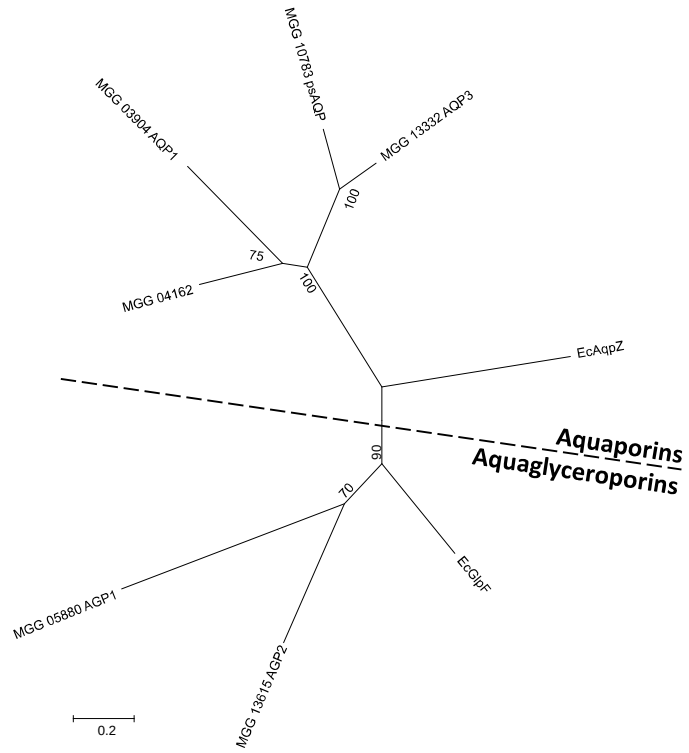

Figure 3.6: The molecular phylogeny of Magnaporthe oryzae MIPs and two reference sequences using Maximum Likelihood inference. *The evolutionary history was inferred using the ML method based on the Poisson correction model. The tree with the highest log likelihood (-3673.3491) is shown. Initial trees for the heuristic search were obtained automatically by applying Neighbor-Join and BioNJ algorithms to a matrix of pairwise distances estimated using a JTT model, and then selecting the topology with superior log likelihood value. A discrete Gamma distribution was used to model evolutionary rate differences among sites (5 categories (+G, parameter = 3.3011)). The tree is drawn to scale, with branch lengths measured in the number of substitutions per site. All positions containing gaps and missing data were eliminated. There were a total of 202 positions in the final dataset. Evolutionary analyses were conducted in MEGA5.*

The molecular phylogenetic analysis suggests that the genes *MGG_03904, MGG_04162* and *MGG_13332* are aquaporins, and *MGG_05880* and *MGG_13615* are aquaglyceroporins. *MGG_10783* is an aquaporin-type protein but, as discussed in Section 3.4.4.2, is thought to be a pseudogene. The *M. oryzae* aquaporin genes will be referred to using the prefix *AQP* for aquaporin-type genes and *AGP* for aquaglyceroporin-type genes. These names are shown in Table 3.3.

Table 3.3: The thesis nomenclature and corresponding Broad Institute reference numbers of Magnaporthe oryzae MIP genes.

Broad Institute Reference	Reference in this thesis
MGG_03904	AQP1
MGG_04162	AQP2
MGG_13332	AQP3
MGG_05880	AGP1
MGG_13615	AGP2
MGG_10783	psAQP

To further confirm the classification of these genes as aquaporins and aquaglyceroporins, we used MUSCLE alignment software to align the *M. oryzae* sequences, together with two canonical sequences representing the aquaporins (*HsAQP1*) and the aquaglyceroporins (*EcGlpF).* Using the reference sequences we identified the specific residue positions that have reportedly conserved properties in the aquaporin and aquaglyceroporin lineages (Hub & de Groot, 2008). These four residues, P2 to P5 (shown in Table 3.4), were identified based on the comparison of 153 MIP sequences from a wide range of distantly-related organisms and are thought to be conserved on the basis of function (Froger et al., 1998). Canonical aquaporins have two uncharged residues in P2 and P3, and two aromatic residues in P4 and P5. Canonical aquaglyceroporins carry two residues of opposite charge in P2 and P3 and two non-aromatic residues in P4 and P5. Substitution of aquaporin-type P2-P5 residues for aquaglyceroporin-type residues can abolish water permeability and lead to the gain of glycerol permeability by an aquaporin proteins (Lagrée et al., 1999). These residue properties of *M. oryzae* MIPs, shown in Table 3.4, fit correctly with our phylogenetic classification

Table 3.4: The profile of residues P2-5 that are differentially associated with aquaporins and aquaglyceroporins. Magnaporthe oryzae aquaporins are shown with two canonical aqua- and aquaglyceroporins. *Residues in P2 and P3 are coloured yellow if they are negatively charged, red if they are positively charged and grey if they are not charged. Residues in P4 and P5 are coloured green if they are aromatic and blue if they are not aromatic residues.*

Gene	P2	P3	P4	P5
AQP1	S	C	Y	W
AQP2	S	A	Y	W
AQP3	S	A	Y	W
AGP1	D	R	N	I
AGP2	D	R	P	M
HsAQP1	S	A	F	W
EcGlpF	D	K	P	L

As shown Figure 3.7, the identified genes typically carry two introns within their sequence, which ranges from 1875 bp (*AQP1*) from 1174 bp (*AQP3*). *AGP1* has a single large intron (391 bp) at the N-terminal of the genomic sequence. The majority of *M. oryzae* genes have between 0 and 2 introns – a typical number of *M. oryzae* protein-coding genes (Dean et al., 2005). It should be noted that the gene sequences were substantially corrected following sequencing of cDNAs as detailed in chapter 6. All sequence analysis work is carried out on the corrected DNA and protein sequences.

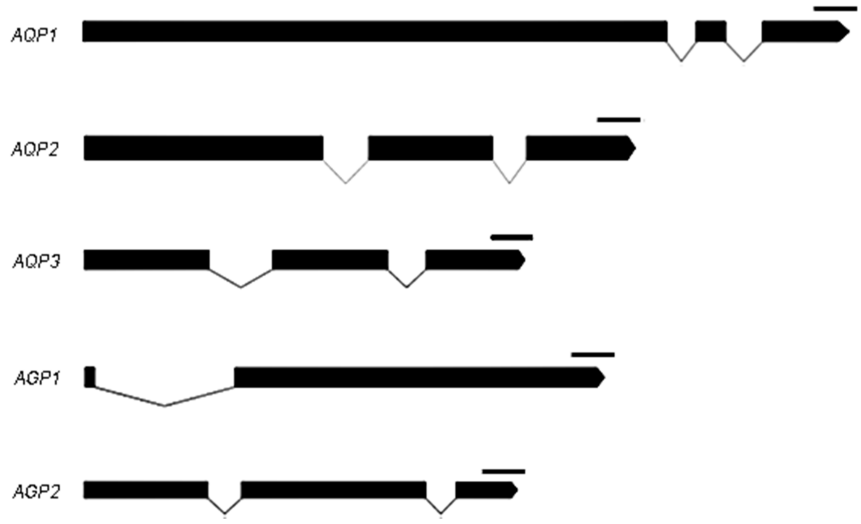

Figure 3.7: The intron-exon structure of M. oryzae MIP genes. Scale bars represent 100 nucleotides

3.4.2 The phylogeny of fungal aquaporins

In this chapter we attempt to generate a robust phylogenetic tree of fungal aquaporins and contextualise this tree within the established evolutionary relationships of eukaryotic MIPs. To do this, we took advantage of the large number of sequenced fungal genomes to extract MIP sequences from a range of different species covering a wide taxonomical distance.

The genomes of the species shown in Table 3.2 were mined using a fully-automated approach as detailed in the Materials and Methods section of this chapter. An iterative Hmmr search of the database with an HMM of the MIP Pfam domain (PF00230) was performed automatically thereby reducing the user bias in sequence selection. Comparison of the retrieved sequences from several genomes were checked manually, showing that this method recovered all sequences with an MIP domain. Truncated sequences or those with large internal deletions were removed manually.

The full-length sequences were aligned using MAFFT alignment software (Katoh et al., 2005). The alignment was inspected visually and extremely divergent sequences were removed. Although this means the protein set is incomplete, it improves the quality of the overall alignment and increases the likelihood that the alignment will represent the 'true' evolutionary history of the protein family (Philippe et al., 2005).

In addition to divergent sequences, ambiguously-aligned or highly variable amino acid positions, and sequence- or clade- specific inserts were removed. It has been repeatedly shown that the

quality of an input alignment greatly effects the quality of subsequent phylogenetic analysis (Kjer, 1995, Morrison & Ellis, 1997, Ogden & Rosenberg, 2006, Smythe et al., 2006, Xia et al., 2003). This is particularly true when, as with the MIPs, the sequences are of different lengths necessitating the introduction of gaps (Talavera & Castresana, 2007). We therefore sought to improve the quality of the phylogenetic inferences relative to previously published studies by robust curation of the input alignment.

The evolutionary history of all MIP proteins was inferred by using the Maximum Likelihood method, based on the rtREV+ Freq. model (Dimmic et al., 2002). This model had the highest 'goodness-of-fit' score as calculated with the model fitting software of MEGA5 (Tamura et al., 2011).

The bootstrap consensus tree, inferred from 500 replicates (Felsenstein, 1985), is displayed as two trees in Figure 3.8 and Figure 3.9. Each tree is rooted on the divergence point of the pair, representing the split between aquaporins and aquaglyceroporins. On the right hand side of each figure, branches corresponding to partitions reproduced in less than 50% of bootstrap replicates are collapsed to show weakly supported regions of the tree.

The percentage of bootstrap replicate trees in which the associated taxa clustered together is shown next to the branches. Initial trees for the heuristic search were obtained by applying the Neighbor-Joining method to a matrix of pairwise distances estimated using a JTT model. A discrete Gamma distribution was used to model evolutionary rate differences among sites (5 categories (+G, parameter = 1.6484)). The analysis involved 186 amino acid sequences, and there were a total of 198 positions in the final dataset.

To facilitate comparison of the organismal tree and the MIP tree, a phylogeny of the species from which the sequences were extracted, is shown in Figure 3.10.

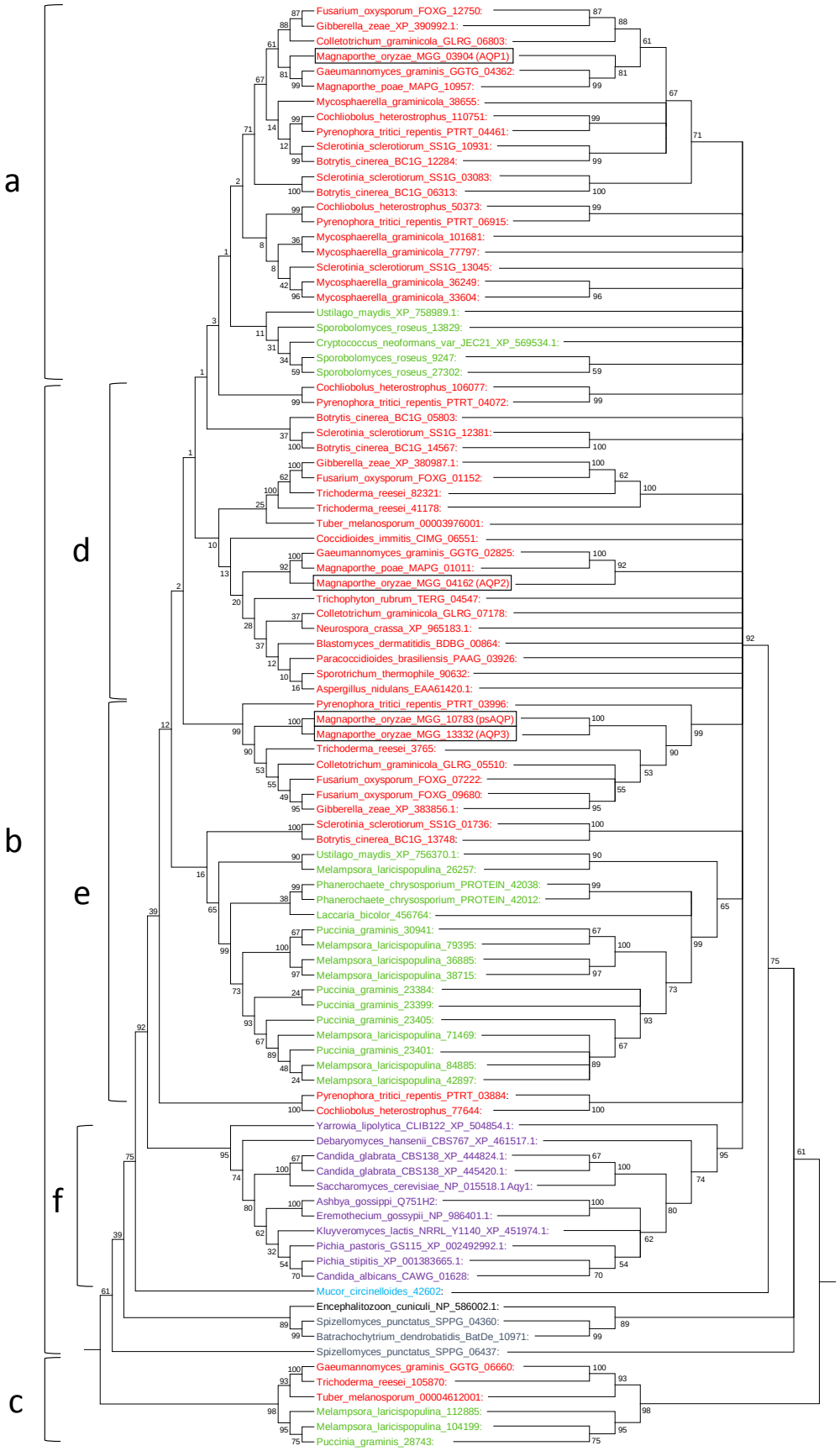

Figure 3.8: A phylogeny of the fungal aquaporin-like MIPs. *Legend continues on page 66*

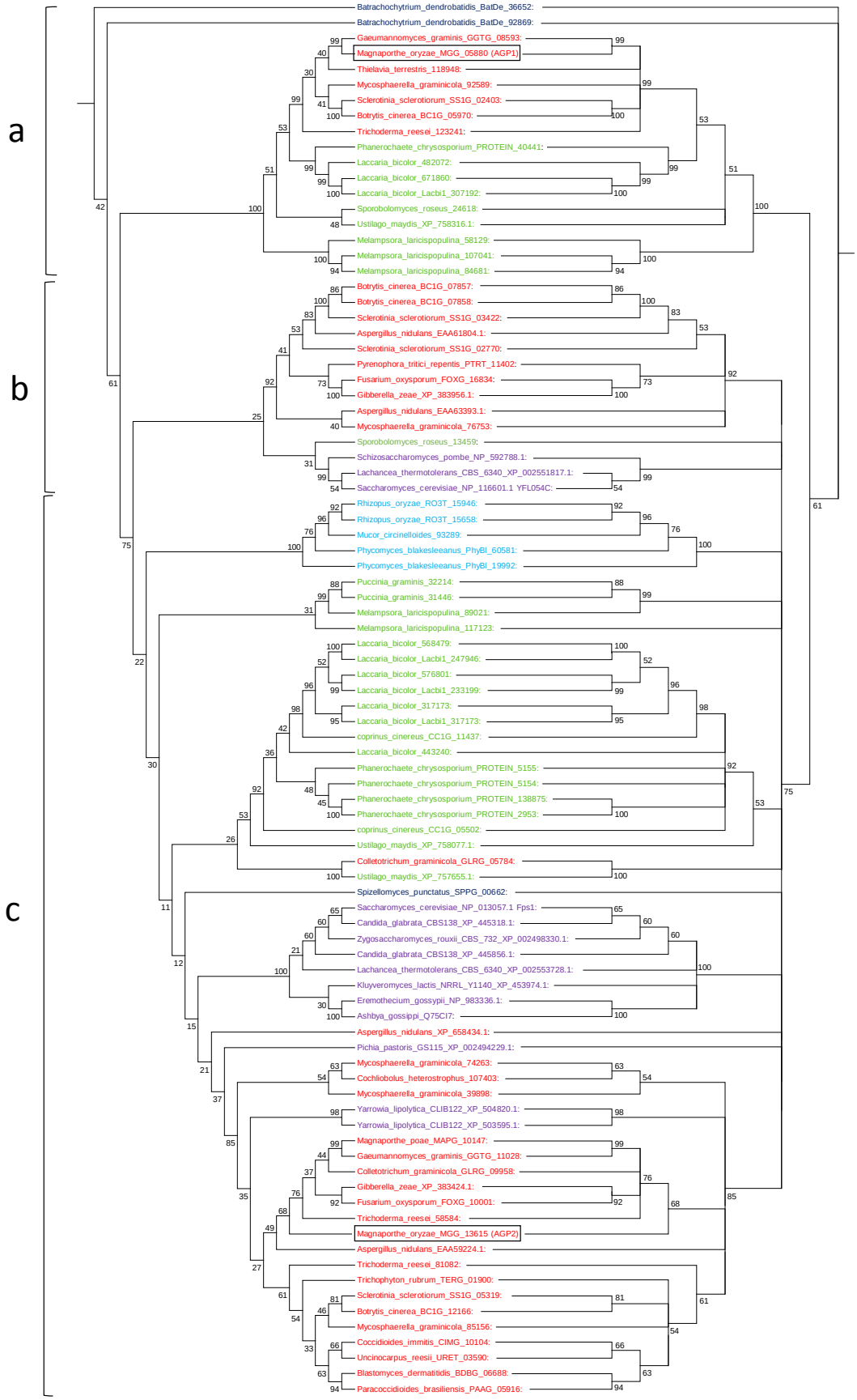

Figure 3.9: A phylogeny of the fungal aquaglyceroporin-like MIPs. *Legend continues on p. 66*

Figure 3.8 legend continued: *The evolutionary history of the MIP proteins was inferred using the Maximum Likelihood method based on the rtREV + Freq. model. A subset of all aquaglyceroporin-like sequences from the full bootstrap consensus tree from 500 replicates is shown. The tree is rooted on the branch to the other MIP tree. In the right hand trees, branches corresponding to partitions reproduced in less than 50% bootstrap replicates are collapsed. The percentage of trees in which the associated taxa clustered together is shown next to the branches. A discrete Gamma distribution was used to model evolutionary rate differences among sites (5 categories (+G, parameter = 1.6484)). The complete analysis involved 186 amino acid sequences. There were a total of 198 positions in the final dataset.*

Figure 3.9 legend continued: *The evolutionary history of the MIP proteins was inferred using the Maximum Likelihood method based on the rtREV + Freq. model. A subset of all aquaporin-like sequences from the full bootstrap consensus tree from 500 replicates is shown. The tree is rooted on the branch to the other MIP tree. In the right hand trees, branches corresponding to partitions reproduced in less than 50% bootstrap replicates are collapsed. The percentage of trees in which the associated taxa clustered together is shown next to the branches. A discrete Gamma distribution was used to model evolutionary rate differences among sites (5 categories (+G, parameter = 1.6484)). The complete analysis involved 186 amino acid sequences. There were a total of 198 positions in the final dataset.*

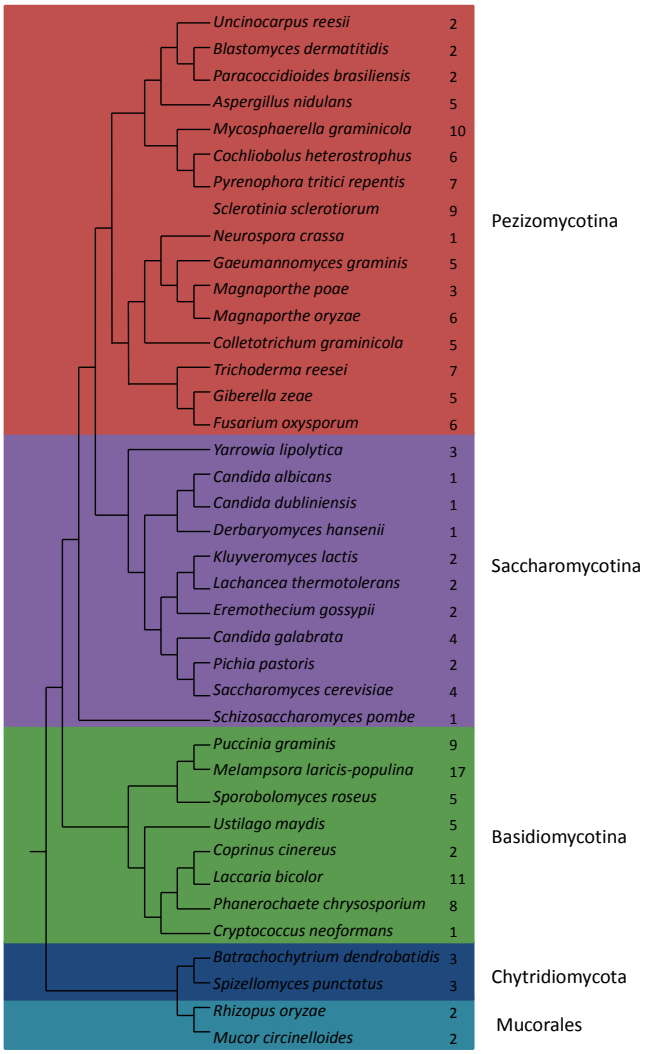

Figure 3.10: A cladogram showing the evolutionary relationships between the species used to construct the MIP phylogeny. The number of MIP-domain containing genes is shown to the right of the species name. *Pezizomycetes are highlighted in red, Saccharomycetes are shown in purple, Basidiomycetes are shown in green, Chytridomycetes are shown in dark blue and mucormycotina are shown in light blue.The tree is re-constructed from Ebersberger et al. (2011) and Wang et al. (2009).*

A general overview of the phylogeny allows several inferences to be made. Although some divergent sequences were removed, the number of MIP sequences associated with each species in Figure 3.10 is shown prior to their removal. This shows that no single species has lost the complete MIP family. Furthermore, no major clade, as colour coded in the phylogeny, has entirely lost either the aquaporins or the aquaglyceroporins.

Although the species selection is biased towards the "higher" fungi (that is the basidiomycetes and the ascomycetes), it is also immediately apparent that there has been a significant expansion of the gene family across the fungal clades. The mean number of MIP proteins is 5.3 in the pezizomycotina, 2.0 in the saccharomycotina, 7.3 in the basidiomycotina, 2 in the chytridomycotina and 3.0 in the muromycotina. The evolutionary relationship between these clades (not to scale) is shown in Figure 3.11.

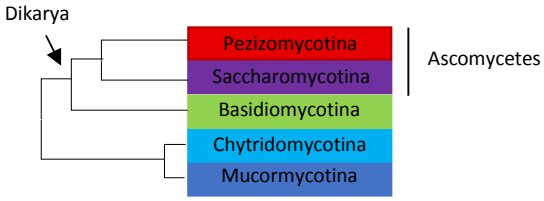

Figure 3.11: The evolutionary relationship between the colour-coded fungal clades shown in the MIP phylogenetic trees. *Branch lengths are arbitrary.*

In particular, many of the duplication events appear to be very recent in the basisiomycete lineages. This suggests that this expansion occurred after the divergence of the five groups shown in Figure 3.11, and that the ancestral state is a smaller number of MIPs. The expansion of the gene family in pezizomycetes and basidiomycetes does not appear to correlate with the fungal mode of nutrition or lifestyle.

This small number of ancestral proteins is consistent with the hypothesis proposed by Soto et al. (2012) that LCA of plants and animals had a small number of genes that subsequently increased during the radiation of those clades. Using each tree individually, it is possible to attempt to derive the ancestral fungal state.

3.4.2.1 The aquaporin-like phylogeny

Our phylogeny of the fungal aquaporin-like genes supports its origins in a single ancestral aquaporin gene that has undergone subsequent duplications in the radiation of the fungi. Shown in Figure 3.8, group b. represents this original gene family (with nested duplications). Starting at the base of the tree, the c. group genes are very likely to represent a long branch attraction (LBA) outgroup. Moving up the tree, as would be expected from the organismal tree, the muromycotina species and chytridomycotina species are basal. However, the f. group of saccharomycotina genes are positioned as an outgroup to the basidiomycetes and pezizomycetes, which is incongruent with the phylogeny in Figure 3.11. This is likely to be an artefact, resulting because the yeast genes are more similar to one another than they are to the basidiomycetes or pezizomycetes. Based on the very different numbers of gene family members, it is likely that aquaporin genes in the saccharomycetes are under different selection pressures to those in the other two families. This often results in significant rate heterogeneity across the amino acid positions being compared, possibly causing this artefactual grouping (Kolaczkowski & Thornton, 2004).

The a., d. and e. groups likely represent clusters resulting from two gene duplication events. The deeper branches in this region of the tree are, however, poorly supported. The position of some basidiomycete species in group a. may suggest that one of these divergences occurred before the branching of the dikarya, with subsequent loss in the saccharomycetes. However, it is more likely that these basidiomycete genes are incorrectly separated from the larger basidiomycete cluster. This would imply that both gene duplications occurred early in the evolution of the pezizomycetes. This is reflected in the *M. oryzae* gene complement with one gene in each duplicated cluster (and an additional species specific duplication event). Loosely interpreted, the ancestral gene in group e. duplicated to form group d., which duplicated again to form group a. This is also reflected in the *M. oryzae* phylogeny in Figure 3.6.

3.4.2.2 The aquaglyceroporin-like phylogeny

The aquaglyceroporin phylogeny is more challenging to interpret than the aquaporin phylogeny. The c. group most-likely represents an ancestral clade, as the topology is entirely consistent with

the organismal tree. This group corresponds to the 'fsp1-like' clade from Deitz et al., (2012) or the 'aquaglyceroporin' clade from Xu et al., (2013).

The a. and b. groups are more difficult to interpret. It is possible that they represent a second or possibly even third ancestral aquaglyceroporin gene cluster(s) that have experienced significant gene loss events during the radiation of the fungi. Together the a. and b. groups represent the 'YFL054c-like' or 'facultative aquaporins' groupings from previous phylogenetic studies (Pettersson et al., 2005). However, in this instance there is insufficient evidence to resolve their evolutionary history.

3.4.3 The phylogeny of fungal and plant MIPs

Having examined the ancestral gene complement of the fungi, I attempted to relate these clusters to the proposed aquaporin groupings in the last common ancestor of plants and animals (Soto et al., 2012). I attempted to build a global alignment of fungal and plant MIP sequences and generate a phylogeny to identify any deep homology between the clusters. Plant sequences, rather than animal sequences, were chosen to attempt to shed light on the proposed similarity between plant and fungal XIP-like proteins (Gupta & Sankararamakrishnan, 2009).

We repeated the sequence discovery process, as described in the materials and methods of this chapter with a database of plant genomes curated by Dr. Steven Kelly (University of Oxford). The sequences were aligned using MAFFT and ambiguously-aligned regions and divergent sequences were removed. A 100 replicate bootstrapped maximum likelihood phylogenetic tree was inferred using FastTree (Price et al., 2010) employing the JTT model of sequence evolution with a Bayesian mixture model for across-site heterogeneities in the amino-acid replacement matrix (CAT) (Lartillot & Philippe, 2004). A majority rule consensus tree was constructed from these 100 replicate trees using DendroPy (Sukumaran & Holder, 2010).

The inferred plant and fungal tree, collapsed for at nodes with less than 50% bootstrap support, is shown in Figure 3.13. It is apparent from this tree that no support for groupings between plant and fungal MIP clades can be inferred.

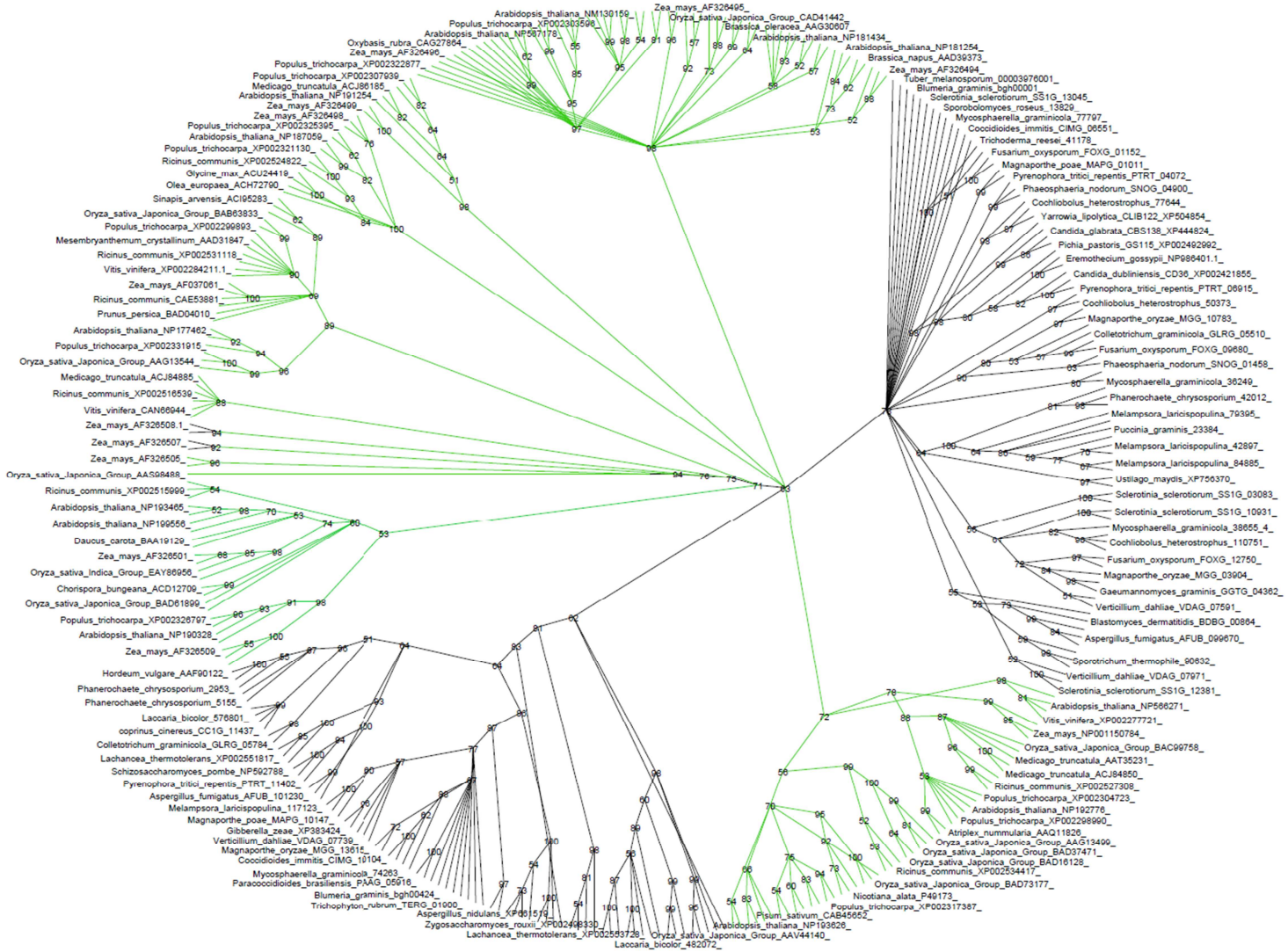

Figure 3.12: A phylogeny of the MIP proteins from plants and fungi. Overlapping taxon names are hidden. *Legend continues overleaf…*

Figure 3.13 continued: A phylogeny of the MIP proteins from plants and fungi. *A 100-replicate bootstrapped maximum likelihood phylogenetic tree was inferred using FastTree with the JTT model of sequence evolution with* ***a*** *Bayesian mixture model for across-site heterogeneities in the amino-acid replacement matrix (CAT). A majority rule consensus tree was constructed from these 100 replicate trees using DendroPy. Lineages with less than 50% bootstrap support are collapsed. Plant lineages are coloured in green. Overlapping taxon names are hidden.*

3.4.4 Aquaporins are expressed during pathogenic development

3.4.4.1 *Magnaporthe oryzae* MIPs in the literature

The transcriptome of *M. oryzae* during infection-related development has been the subject of several publications (Mathioni et al., 2011, Oh et al., 2008, Soanes et al., 2012). I reviewed these papers for references and information on the transcript abundance of *M. oryzae* MIPs. This revealed two studies carrying information on the MIP transcript abundance – one microarray-based experiment (Mathioni et al., 2011) and a High-Throughput SuperSAGE experiment (Soanes et al., 2012).

The first microarray study by Mathioni et al. (2011), compared gene expression during fungal growth under three nutrient-limited conditions (minimal medium (MM), MM minus carbon (MM-C) and MM minus nitrogen (MM-C), two *in planta* conditions (growth 72hpi in rice and barley) and under two stress conditions (oxidative stress and temperature stress). Although no data were supplied for independent analysis, this paper specifically noted that AGP2 (MGG_13615) was transcriptionally upregulated under three conditions – rice growth, barley growth and MM-C. No other MIP gene was described in main manuscript or in supplementary information.

The second high-throughput SuperSAGE analysis by Soanes et al. (2012), published all SuperSAGE data. I was thus able to download transcript information for all MIP genes (http://cogeme.ex.ac.uk/supersage). The authors extracted RNA from germlings developing on hydrophobic glass slides (inductive to appressorium formation) after 4, 6, 8, 14 and 16h. These time- points reportedly correspond with two broad phases – a “development” phase (4-8h) during which the germ tube tip swells, and the appressorium forms and melanises, and a “maturation” phase, during which the appressorium becomes pressurised. Two mycelial liquid-culture data points were also included – one from mycelia grown in complete medium and one from nutrient

minimal medium. The transcript abundance data from the SuperSAGE experiment is shown in Figure 3.14.

These data show that MIP genes in *M. oryzae* have different regulatory patterns. The three *AQP* genes and *AGP2* are expressed at very low levels in mycelium. However, *AGP1* is expressed at extremely high levels in mycelial culture, especially in nutrient-limiting conditions. As a point of comparison, the four housekeeping genes used in qRT-PCR analysis in this thesis and chosen on the basis of their high constitutive expression levels, are expressed at a geometric mean of 4000 and 5040 in CM and MM respectively.

The abundance of *AQP1* during infection-related development is highest during the later time points corresponding with appressorium maturation. Conversely, *AQP2,* whilst present throughout germling development, has higher abundance at the 'developmental' stages (4-8h). *AQP3* is expressed at a low and relatively invariant level throughout development.

Of the aquaglyceroporins, *AGP1* expression is almost imperceptible during germling development relative to mycelial growth. However, the expression pattern of *AQP2* is particularly interesting as it correlates with maturation and turgor generation in the appressorium. This pattern was also detected in the microarray assay of Mathioni et al. (2011).

3.4.4.2 qRT-PCR analysis of *M. oryzae* spores on susceptible barley plants

The SuperSAGE data was collected from RNA isolated from germlings on an infection-related surface, that is, on an artificial surface inductive to appressorium formation. To validate these results *in planta* I performed a qRT-PCR assay on samples extracted from barley leaves inoculated with *M. oryzae* spores. As listed in Table 3.1, the developmental time points selected cover a similar developmental range to those used in the SuperSAGE assay, but do not correspond exactly as the rate of germling development differs on plants and artificial surfaces (Skamnioti et al., 2007, Soanes et al., 2012).

The qRT-PCR transcript abundance data, expressed as a proportion of the geometric mean abundance of the two housekeeping genes, is shown in Figure 3.15.

A single transcript, *MGG_10783* (psAQP), could not be detected with any of five sets of primers tested, even with highly concentrated cDNA. The primers were also tested on genomic DNA and found to be fully-functional. Phylogenetic analysis shows this gene to be an *M. oryzae* specific gene duplication. qRT-PCR is a highly sensitive technique and the complete absence of any amplification suggests this gene is not expressed. *psAQP* is positioned close to the end of a chromosome – a region which in yeast is often transcriptionally silenced and enriched in pseudogenes (Doheny et al., 2008, Harrison et al., 2002). Gene duplication frequently result in the inactivation and subsequent loss of one of the sister genes (Cliften et al., 2006). Although there are no apparent inactivating mutations, the absence of transcript suggests that *MGG_10783* may also be in the process of becoming a pseudogene.

Although the unknown error term, *k,* derived in equation (4), renders comparisons between genes inexact, comparisons of the trend within a single transcript over the developmental conditions are possible. The *AQP1* transcript is expressed at very low levels until after 8hpi, where expression increases significantly and remains high through 24hpi. *AQP2* transcript abundance is highest in the early developmental phases, but decreases significantly after germ tube emergence. The *AQP3* transcript is relatively constitutive, but with a peak abundance at 1hpi.

The *AQP1* transcript appears to be expressed at its highest level in spores and then is barely detectable at other time points. However, given the enormously high abundance of the *AGP1* transcript in mycelium this expression peak may be caused by mycelial contamination. Mycelial fragments would not adhere to the leaves, thus would not be detected in leaf RNA preparations, but would be present at a low level in the spore preparation.

The *AGP2* transcript, as with the SuperSAGE data and the microarray data, shows an expression peak at 12 hpi, coincident with penetration peg emergence and maximal turgor pressure.

3.4.4.1 Comparison of SuperSAGE and qRT-PCR

An approximate comparison can be made between the SuperSAGE and qRT-PCR data by expressing the SuperSAGE data as a percentage of the geometric mean of the two housekeeping genes used in the qRT-PCR experiment. These data, plotted together with the qRT-PCR data, are

shown in Figure 3.16. No time points earlier than 4 hpi were measured in the SuperSAGE assay so the spore measurements and 1-2 hpi could not be compared. However, the 6 hpi data point in the SuperSAGE analysis broadly corresponds with the 4 hpi data point in the qRT-PCR experiment, 8hpi with 8 hpi and 14 hpi with 12 hpi. The 16 hpi and 24 hpi time points are included for reference but do not correspond very well, as the early stages of host infection cannot be mimicked on infection-related surfaces, as the penetration pegs do not form. Although the comparisons are not exact, overall trends can be compared.

The *AQP1* and *AQP2* SuperSAGE and qRT-PCR relative transcript profile trends correlate well. The profiles of the *AGP2* transcript also correlate reasonably well. However, the *AQP3* and *AGP1* profiles are more dissimilar.

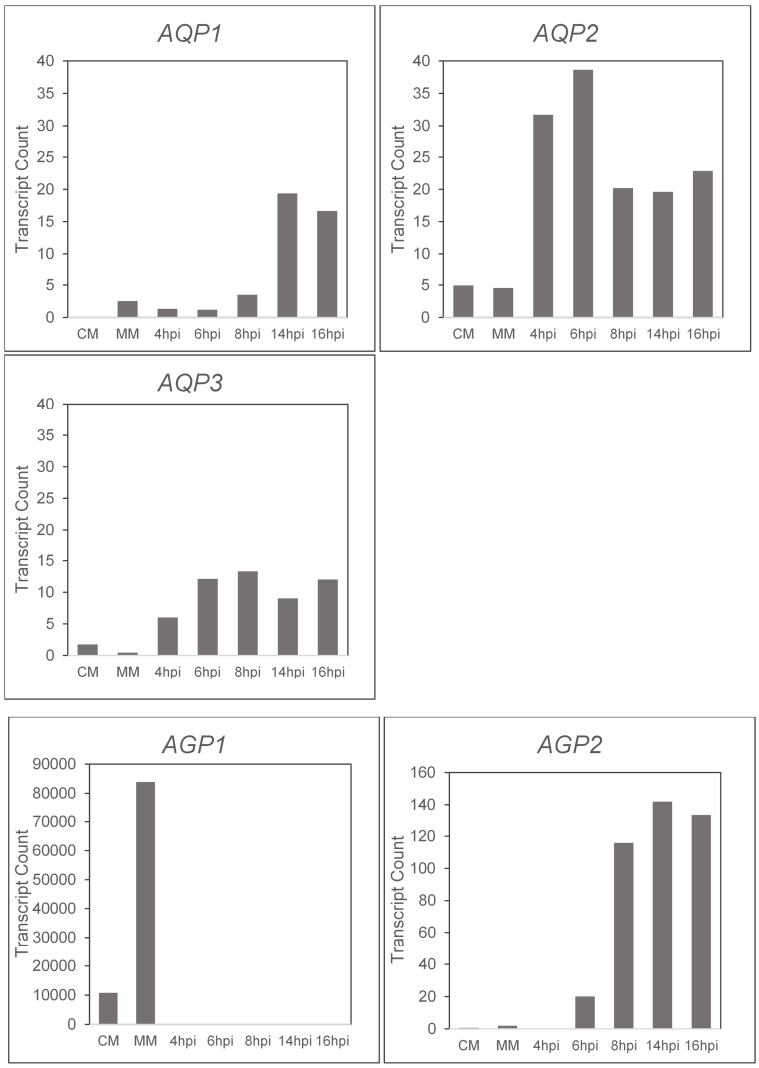

Figure 3.14: SuperSAGE transcript abundance during mycelial and infection-related development. *Aquaporin transcripts are expressed on the same axis, aquaglyceroporin transcripts are expressed on different axes to facilitate comparison. Data retrieved from Soanes et al. (2012). 'hpi' refers to the number of hours post inoculation on barley leaves.*

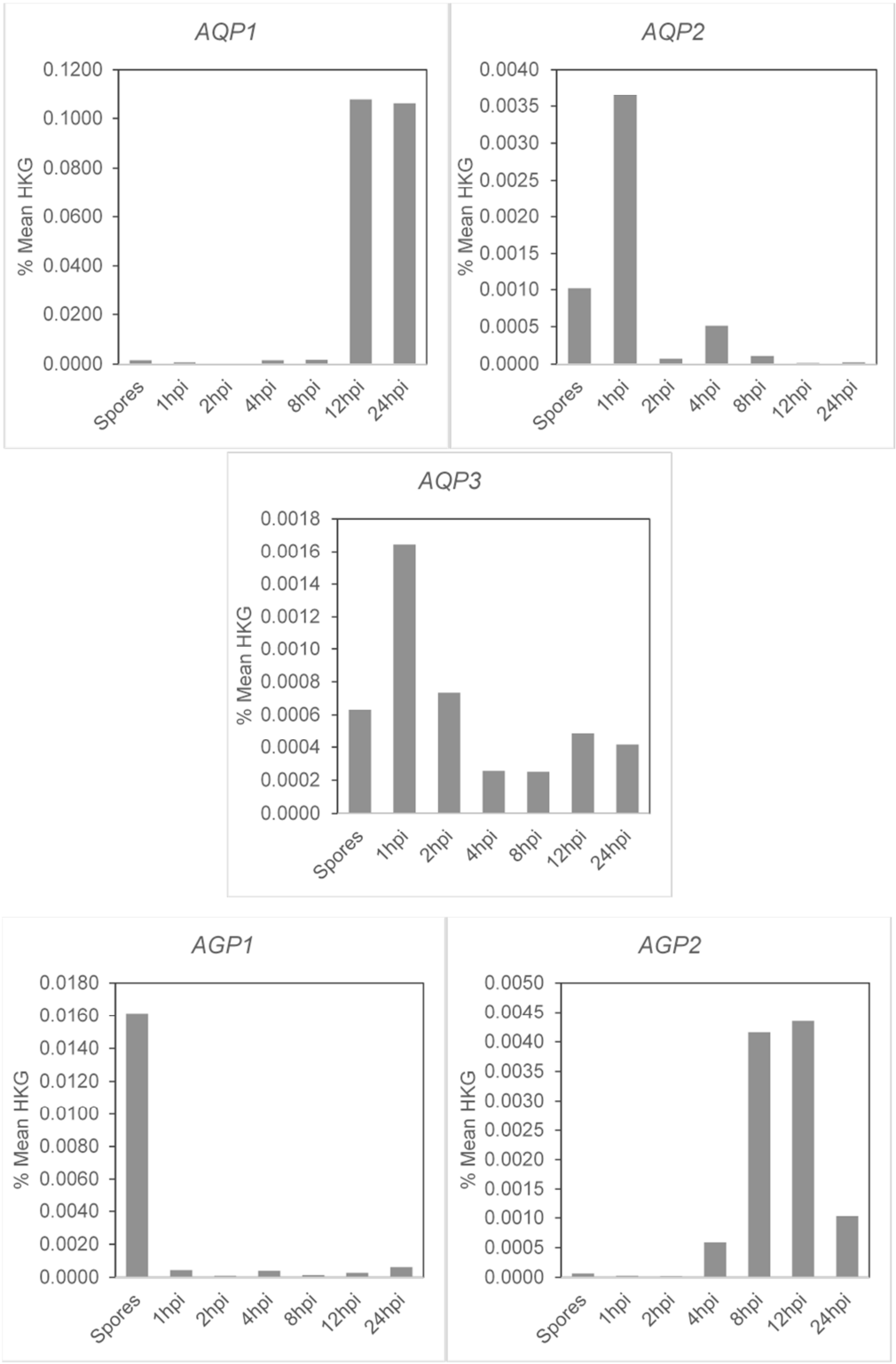

Figure 3.15: Expression of MIP genes in M. oryzae Guy11 wildtype conidia, and inoculated barley leaves, expressed as a percentage of the geometric mean of two housekeeping genes, β-tubulin and elongation factor 1α.

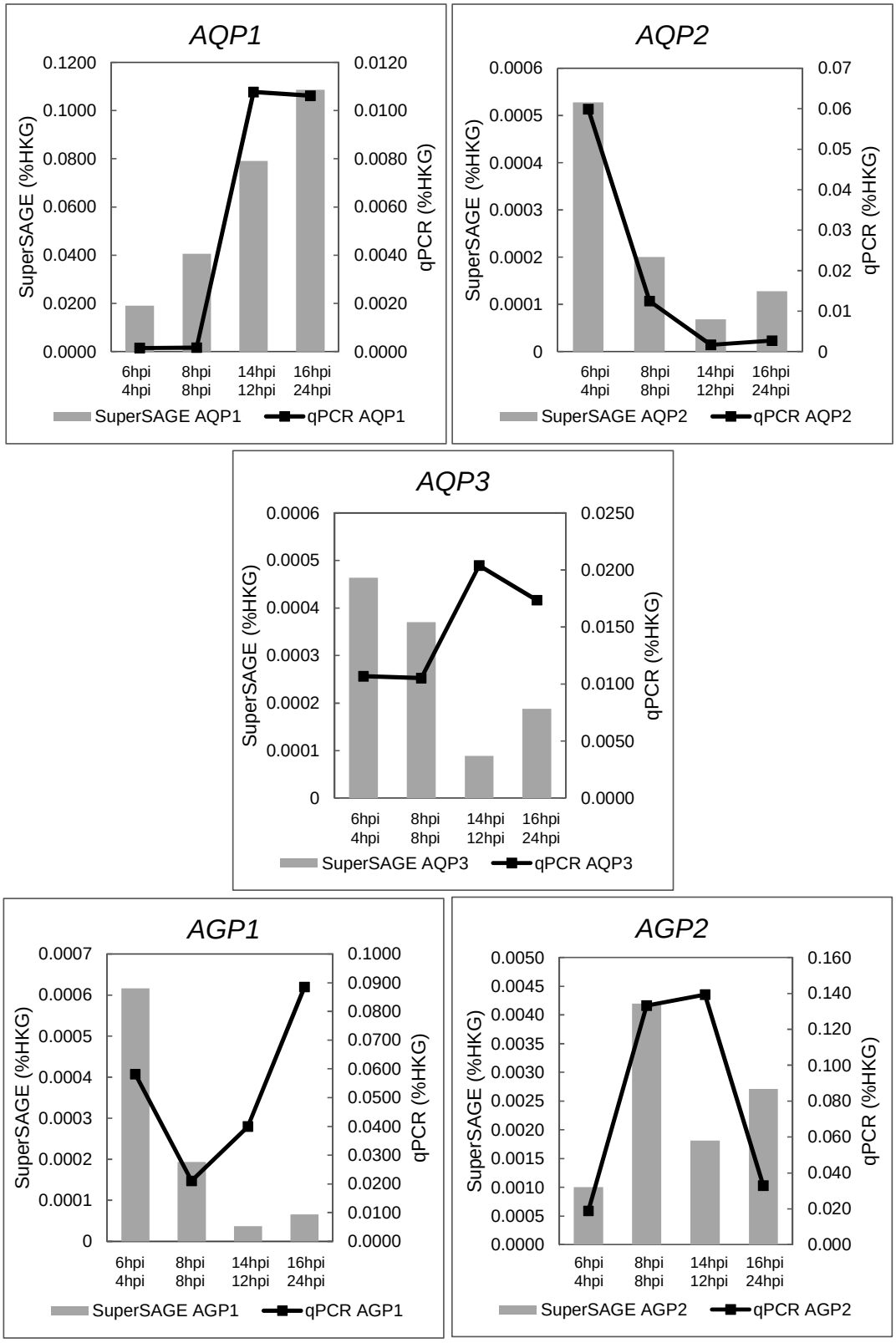

Figure 3.16: The transcript abundance of each MIP gene in M.oryzae WT strain Guy11 germlings at comparable developmental stages, expressed as a percentage of the geometric mean of the abundance of β-tubulin and elongation factor 1α, as determined by SuperSAGE (Soanes et al., 2012) or by qRT-PCR. SuperSAGE time points are shown above the qRT-PCR time points.

3.5 Discussion

3.5.1 Generating accurate phylogenies of the MIP protein family is challenging

In this chapter, we aimed to generate a robust phylogeny of the fungal aquaporins and to identify any deeper phylogenetic relationships between the fungal clades. We identified a single aquaporin-type gene cluster in the LCA of extant fungi, and were able to find no evidence supporting the claim that fungi have XIP-like genes in common with plants. We were unable to determine the number of aquaglyceroporin-like genes in the fungal LCA, but postulated a number between 1 and 3. The complement of *M. oryzae* aquaporins covers the full range of pezizomycota MIP genes, thus *M. oryzae* represents an excellent model for studying the role of these genes.

The phylogeny generated in this thesis represents an improvement on previous published attempts (Dietz et al., 2011, Pettersson et al., 2005, Xu et al., 2013). Our phylogeny displays a greater degree of congruence with the organismal tree and the taxonomic groupings have a higher degree of bootstrap support.

However, like many MIP phylogenies we were unable to appropriately resolve the deep phylogenetic relationships between taxa, and there were still problems with incongruent groupings (Soto et al., 2012). Probabilistic tree inference methods such as maximum likelihood or Bayesian inferences approaches are the most accurate, but also the most computationally demanding (Philippe et al., 2011). The fungal MIP tree, for example, required 50h of computing time.

Probabilistic models also make use of pre-specified models of sequence evolution, and selection of an inappropriate model can result in an erroneous phylogeny. We used specialised software to select a model but could not perform iterative refinements without access to more significant computing power.

The particular problems of MIP phylogeny construction make accurate phylogenies difficult to estimate. Our attempt represents an improvement on previous efforts. However, generation of a phylogeny by specialists with access to significant computing power could undoubtedly improve upon this further

3.5.2 Aquaporin MIPs are expressed during pathogenic development

Published SuperSAGE data indicates that some MIP genes in *M. oryzae* are upregulated during the elaboration and maturation of the appressorium. We used qRT-PCR to confirm and validate this data.

The differences between the SuperSAGE data and qRT-PCR data could be the result of three factors.

i) The measurements may be erroneous

ii) The time-point comparisons are inexact and the transcripts change rapidly

iii) There may be genuine differences between expression *in planta* and expression on artificial surfaces

The qRT-PCR experiment was performed with relatively low stringency (Bustin et al., 2009). Fungal transcripts are rare in the RNA preparations relative to contaminating plant RNA, thus the C_T values obtained for fungal aquaporin transcripts are relatively high (C_T = 28-34). This correlates with higher error values as the initial transcript number is small and thus more susceptible to stochastic variation (Caraguel et al., 2011). This, and the discrepancies between developmental comparisons, may explain why the identified trends do not correlate well for some genes.

Despite the methodological and comparability problems, two genes - *AQP1* and *AGP2* appear to have regulatory patterns that suggest a role in appressorium-mediated pathogenesis. These results suggest that further experimental work on *M. oryzae* MIPs is worthwhile, in order to establish whether these regulatory trends have functional implications.

Chapter 4 Generation and phenotyping of single aquaporin deletion mutants

4.1 Introduction

I previously identified six aquaporin genes in the *M. oryzae* genome (chapter 3), five of which are expressed and one is likely a pseudogene. The five aquaporins showed different regulatory patterns with two significantly up-regulated during pathogenic development. This chapter describes:

- The generation of aquaporin single deletion mutants in a *M. oryzae* WT Guy11 background.
- Their phenotypic characterisation, as compared with Guy11, in terms of:
    - i) Pathogenicity / virulence, as attested by disease lesion formation on rice leaves
    - ii) The effect of gene deletions on infection-related development on inductive surfaces
    - iii) Vegetative growth and tolerance to different imposed stresses

4.1.1 Study of gene function in filamentous fungi

In order to understand *in vivo* the role of specific protein-coding genes, a method for altering their function must be adopted. This can take several forms – altering the function of the protein through permanent or transient modification, or altering the expression of the protein temporally, spatially or quantitatively. I considered, but eventually discounted, the idea of using chemical blockers,

inducible promoters and RNAi with *M. oryzae* aquaporins, ultimately deciding to use targeted gene deletion to eliminate each individual aquaporin transcript.

Despite the significant pharmacological interest, selective non-toxic aquaporin inhibitors have not been developed (Verkman 2011, Martins et al. 2012). Although various mercurial compounds such as $HgCl_2$ have been shown to inhibit these proteins, their non-selective mode of action and toxicity limit their use when studying the role of novel proteins (Preston et al. 1993). Furthermore the *M. oryzae* aquaporins appear to lack the conserved cysteine residue with which mercurial, and other metalloid inhibitors such as $AgNO_3$ and $HAuCl_4$, interact (Niemietz and Tyerman 2002). The efficacy of other putative aquaporin inhibitors such as acetylsulfanilamide or acetazolamide is highly controversial (Yang et al. 2008). The lack of specific, non-pleiotropic aquaporin chemical inhibitors led us to rule out this approach to study the proteins in *M. oryzae.*

Altering the expression of proteins can help elucidate their functions. *M. oryzae* is genetically tractable and can be stably transformed with exogenous DNA constructs (Wilson and Talbot 2009). Inducible promoters, to which genes-of-interest can be fused, are frequently used to study gene function and exist for *M. oryzae*. However, the best available promoter is the acetate-inducible ICL1 isocitrate lyase promoter which has significant pleiotropic effects (Wang et al. 2003). The difficulty in distinguishing the acetate-associated changes from those of the induced protein limit the usefulness of this tool.

RNAi can be used to simultaneously silence multiple members of a conserved gene family. For example, RNAi-mediated silencing has successfully been used to silence the seven members of the rice *OsRac* gene family (Miki et al. 2005). The seven genes were silenced, to varying efficiencies, using two inverted repeat (IR) constructs expressing RNA hairpins of a highly conserved *OsRac* region. In *M. oryzae* RNAi has been used successfully to uncover the role in virulence of endo-β-1,4 xylanase genes using a single artificial silencing construct designed to target ten of the 11 endoxylanase genes (Nguyen et al. 2011). Cytosolic xylanase activity was reduced by 60% in the most strongly silenced line.

Despite the advantage of potentially being able to simultaneously target multiple gene family members, there are numerous problems associated with RNAi in fungi. Although a single construct

to target all five aquaporin genes in *M. oryzae* could plausibly be designed, silencing efficiency is often very low (Dr. M. Kershaw, pers. comm.) and highly variable (Nguyen et al. 2008). An attempt to simultaneously silence six hydrophobin genes in *Cladosporium fulvum* encountered significant pleiotropic changes in the expression level of non-target genes as well as surprising upregulation (up to 30-fold) of some 'silenced' targets (Lacroix and Spanu 2009). Despite extensive and time-consuming screening, the authors were unable to report a single line where all gene family members were significantly silenced. Even when silencing efficiency is high, phenotypic differences between knockout and knock-down mutants have also been reported. The reduction of the *PAN-2* transcript, for example, is not sufficient to recapitulate the *pan-2* knockout phenotype in *Neurospora crassa* (Goldoni et al. 2004).

Differential regulation of the *M. oryzae* aquaporin genes may mean that the function of the genes does not significantly overlap. Given the inherent weaknesses of alternative mechanisms for studying the *in vivo* role of aquaporins, gene deletion via allelic replacement was selected as a strategy to study their function in *M. oryzae.*

4.1.2 Gene deletion in filamentous fungi

Foreign DNA constructs can be introduced into *M. oryzae* by permeabilising protoplasts with PEG3000 and $CaCl_2$. After uptake, *M. oryzae* has two pathways for integrating DNA – homologous recombination (HR) and non-homologous end joining (NHEJ) (Villalba et al. 2008). The process of HR requires the 5'-3' degradation and subsequent priming of DNA synthesis using the homologous region as a template after DNA strand invasion. This newly-synthesised stretch of DNA can then be joined with the 5' end of the resected strand forming a Holliday junction (Huertas 2010). Conversely, NEHJ can occur without sequence homology, where broken DNA ends are directly ligated. The HR pathway involves the Rad52 epistasis group, whereas the NHEJ pathway ligates double-stranded breaks via the Ku heterodimer (Ku70/Ku80-protein complex) and the DNA ligase IV-Xrcc4 complex (Dudasova et al. 2004, Krogh and Symington 2004).

In *M. oryzae,* targeted gene disruption can be achieved by HR. The fungus is transformed with a disruption cassette containing a selectable marker flanked by sequences from the disruption target

(see Figure 4.1B). When HR occurs at the flanking regions, the region between the flanks will be replaced by the selectable marker (Weld et al. 2006).

The most commonly used selectable markers in *M. oryzae* are hygromycin B, bialophos and sulphonylurea (Mitchel 2002). Hygromycin B is an aminoglycoside antibiotic which acts by inhibiting protein synthesis at the translocation step, causing mis-reading of mRNA. The hygromycin B resistance cassette (HYG) used in this study encodes the *Escherichia coli hph* gene under the control of the *Aspergillus nidulans gpdA* promoter and flanked by the *A. nidulans trpC* terminator. Bialophos is a tripeptide that is broken down into phosphinothricin – an inhibitor of glutamine synthesis. The Bialophos resistance gene (BAR) encodes a phosphinothricin acetyltransferase isolated from *Streptomyces hygroscopius*. Sulphonylurea (chlorimuron ethyl) inhibits acetolactate synthase, an enzyme involved in the synthesis of valine and isoleucine. Interestingly the resistant allele was isolated from *M. oryzae* and is a variant of the *ILV1* gene. However, the Guy11 strain is susceptible and sulphonylurea can be used as a selectable marker.

When targeted gene deletion in *M. oryzae* is attempted, gene replacement occurs at a low frequency (average 7%) relative to non-homologous integration of the deletion construct (Villalba et al. 2008). In other fungal species deletion of either the *KU70, KU80* or *LIG4* genes significantly reduces the frequency of non-homologous recombination (Carvalho et al. 2010). The Δk*u80* and Δ*ku70* strains are widely used in *M. oryzae* research. However, work in our laboratory has suggested that there are detectable differences between the Δ*ku70* strain and the wildtype Guy11. A recent paper by Jeon et al. (2013) suggests that oxidative and UV radiation cause significant DNA damage during normal laboratory growth and subculture. As the Δ*ku70/ku80* strains are hypersensitive to DNA damage, it may be difficult to distinguish a deletion-induced phenotype from accumulated DNA damage. This is a particular problem with the use of NHEJ-impaired strains, as the absence of non-homologous integration complicates the construction of recomplemented strains. In recomplemented strains, the original gene is reintroduced to see whether the WT phenotype is restored. This ensures that the observed phenotype is caused by the gene deletion and not by cryptic changes elsewhere.

Higher frequency of homologous recombination in *M. oryzae* has been reported using the 'split marker' method of targeted gene replacement (Jeong et al. 2007). Using this technique, the

antibiotic selectable marker is 'split' into two parts with an overlapping region in the middle. As shown in Figure 4.1A, an additional recombination event – between the overlapping regions of the marker – must occur for the resistance phenotype to be observed. It has been reported that this method increases the frequency of successful homologous replacements in *M. oryzae*.

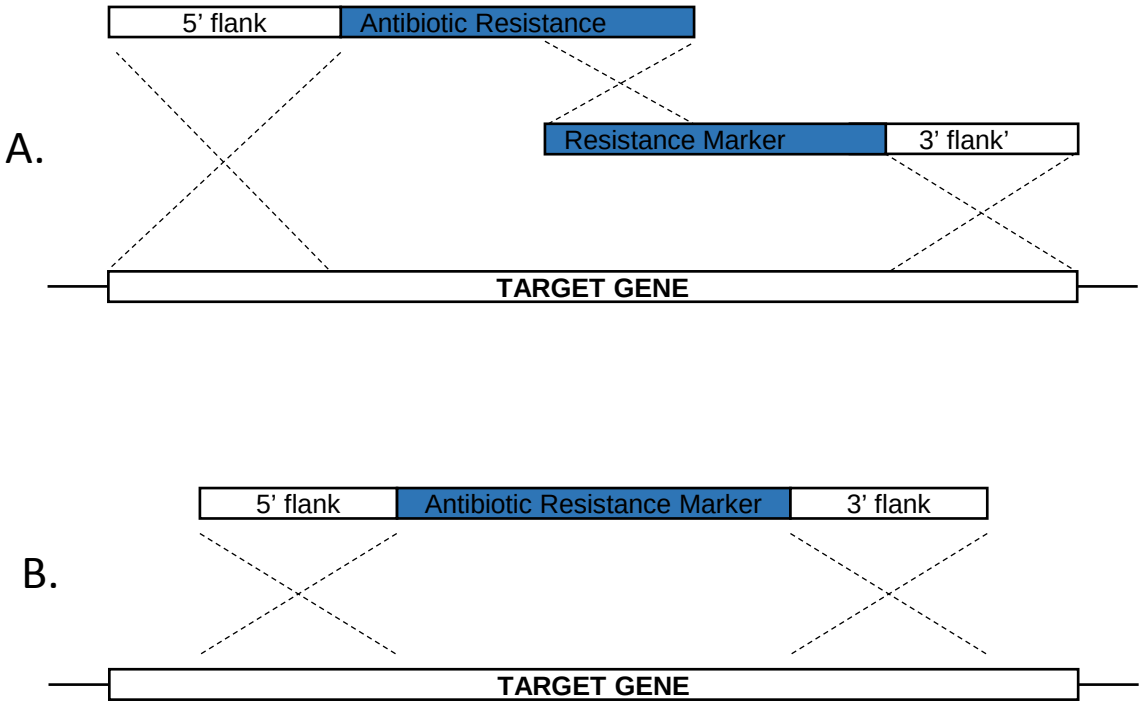

Figure 4.1: **Recombination events involved in the 'split' marker deletion method (A) and the 'whole' marker deletion method (B).**

4.1.3 Pathogenicity and virulence

M. oryzae infects via a specialised infection cell – the appressorium. As detailed in chapter 1, the appressorium harnesses enormous turgor pressure to force a penetration hypha through the leaf cuticle and into the cell beneath. Appressorial turgor pressure is generated by the influx of water into the cell against a concentration gradient generated by the accumulation of osmotically active glycerol (de Jong et al. 1997).

In chapter 3, I ascertained that the transcriptional abundance of a subset of these proteins is significantly upregulated over the course of pathogenic development. Given the importance of

water and glycerol in penetration, I hypothesised that there might be a role for aquaporins at the initiation of plant infection. As water channels, the aquaporins might facilitate water flux across the appressorial plasma membrane. As glycerol channels, the proteins may be required for equilibration of glycerol concentration gradients across internal membranes, or for diffusion of glycerol from the site of production.

If aquaporins are essential for pathogenic development, this can be determined by examining the ability of Δ*aquaporin* strains to cause disease. This can be tested experimentally by inoculating susceptible rice leaves with mutant strains and comparing the number of pathogenic lesions to leaves inoculated with the Guy11 wildtype.

4.1.3.1 Infection-related development

M. oryzae is capable of forming a melanised appressorium, on hard, hydrophobic surfaces in the absence of external nutrients (Liu et al. 2007). An infection-like developmental programme can be induced on glass coverslips and readily imaged on a microscope. Gene deletions that partially or completely abolish pathogenicity often have aberrant infection-like development (Xu and Hamer 1996, Liu et al. 2007). Conversely, some mutants, such as the Δ*des1* and Δ*abc1* strains, have reduced pathogenicity but no obvious defects in appressorium-mediated penetration (Urban, et al. 1999, Chi et al. 2009).

Infection-related development on artificial surfaces can be used to interpret any role for aquaporins in the ability to cause disease. The development of *M. oryzae* Δ*aquaporin* strains on inductive surfaces will be examined and compared to the wildtype strain.

4.1.4 Vegetative growth and stress responses

M. oryzae is predominantly studied as a model appressorium-forming phytopathogen. However, characterising the phenotype of targeted deletion mutants involves assaying many different aspects of their growth. Examining how deletion strains grow vegetatively and respond to stress can help elucidate the roles of the deleted proteins.

4.1.4.1 Osmotic stress

Eukaryotic cells respond to acute and chronic hyperosmotic stress by accumulating compatible solutes to prevent water loss. Plants tend to accumulate proline or glycine betanine, and mammalian cells accumulate betanine, sorbitol, glycerophosphorylcholine, inositol or ionic solutes (Garcia-Perez and Burg 1991, Xiong and Zhu 2002). Fungi predominantly accumulate polyols including erythritol, ribitol, arabinitol, xylitol, sorbitol, mannitol and galacticol (Hohmann 2002). In response to acute osmotic stress, *M. oryzae* has been shown to accumulate high concentrations of arabitol and somewhat lower concentrations of glycerol (Dixon et al. 1999). Interestingly, this osmoadaptive response, controlled by the MAP kinase *OSM1* (a homolog of the *S. cerevisiae HOG1* MAPK), is independent of appressorial turgor generation.

Using different osmostressors, I aim to test the possibility that deletion of putative water or polyol channels might alter the *M. oryzae* response to osmotic stress.

4.1.4.2 Oxidative stress

Some aquaporin channels are permeable to hydrogen peroxide (Bienert et al. 2007), and as described in chapter 6, two *M. oryzae* aquaporins, *AQP1* and *AQP2,* are putative peroxyporins. I tested the growth of *Δaquaporin* strains relative to the WT strain Guy11 under conditions of hydrogen peroxide stress to investigate whether the absence of these genes affected the ability to tolerate oxidative stress.

4.1.4.3 pH stress

In *S. cerevisiae,* the response to pH stress is mediated by the Cell Wall Integrity pathway (CWI). This interacts with the High Osmolarity Glycerol (HOG) MAPK kinase pathway, which is controlled by Hog1p in response to osmotic shock (de Lucena et al. 2012). The HOG pathway may be acting as a signal amplifier, or the damage caused by acid or alkali damage may expose the cell membrane, resulting in a loss of cellular turgor. The HOG pathway detects and responds to changes in cell turgor (Cheetham et al. 2007). If changes in cellular turgor homeostasis are caused by deletion of aquaporin genes in *M. oryzae,* it may alter the response to growth at non-optimal pH.

4.2 Experimental aims

- To generate single deletion strains of all expressed aquaporins in *M. oryzae.*
- To characterise the pathogenicity and pathogenic development of these knockouts.
- To characterise the vegetative growth and stress tolerance of these Δ*aquaporin* strains.

4.3 Methods specific to this chapter

4.3.1 Appressorial turgor measurement

The concentration at which 50% of appressoria undergo cytorrhysis (cell collapse) can be used to provide an estimate of the internal glycerol concentration. Conidia were inoculated onto inductive glass Menzel coverslips and incubated in a humidity chamber at 24^{o}C to produce melanised appressoria. The water droplet was gently removed using filter paper and replaced with 200 µl glycerol at a range of concentrations (0-4 M). After 10 min, the coverslip was photographed and the number of collapsed and un-collapsed appressoria was counted. Spores were harvested from three independent plates and at least 100 spores from each plate were counted at every glycerol concentration.

4.4 Results

4.4.1 Generation of the *AQP1, AQP2, AQP3* and *AGP1* 'split marker' deletion constructs

Constructs for the four genes deleted using the 'split marker' method were generated using overlap-extension PCR. To create the pair of deletion constructs shown in Figure 4.1B, six PCR reactions were required. The generic PCR steps required are shown in Figure 4.2.

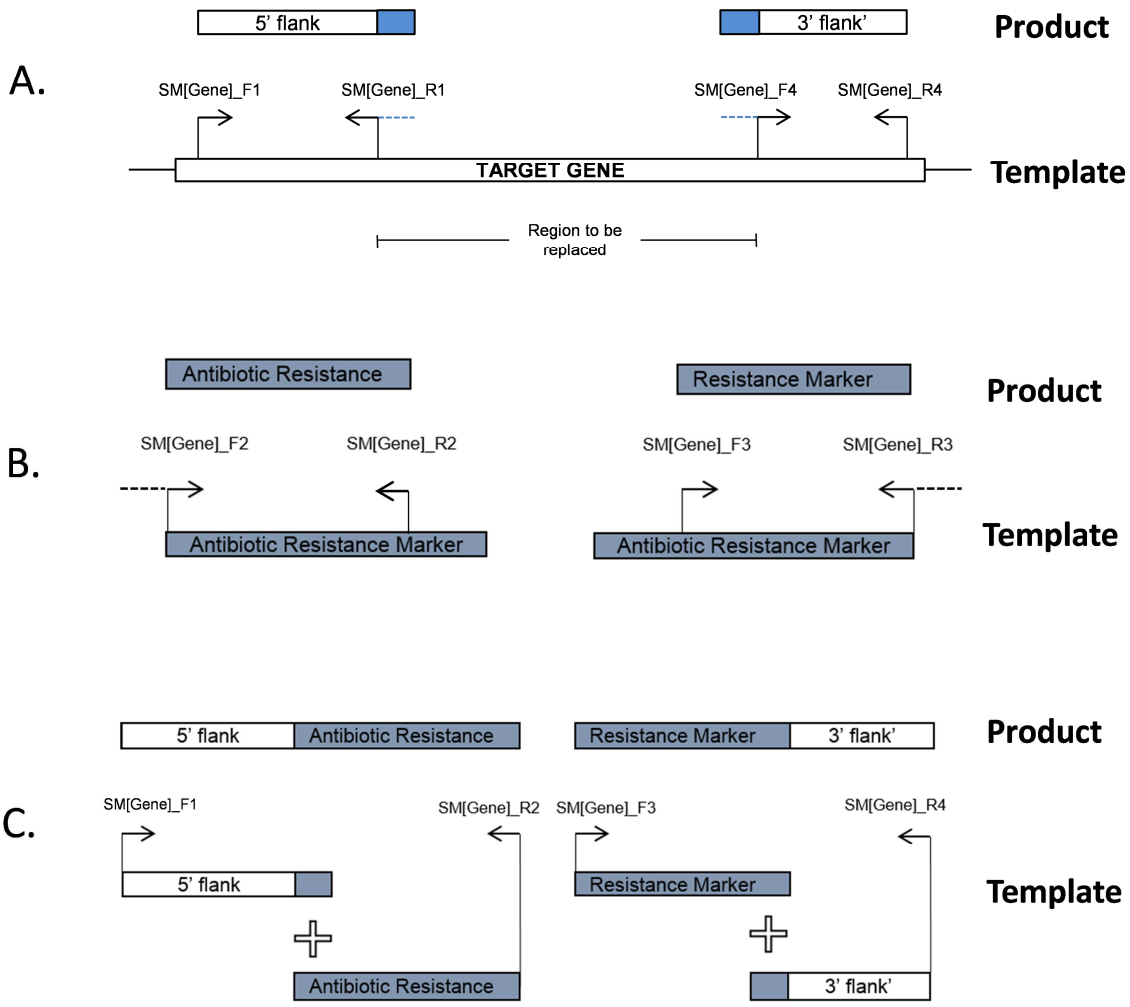

Figure 4.2: The PCR steps to create the two DNA constructs required to delete a M. oryzae gene using the 'split marker' method.

A. generates the two homologous flanking regions (1.0 - 1.5kb) up- and downstream of the genomic region to be replaced by the antibiotic resistance marker. At their 5' ends, the SM[Gene]_R1 primer and the SM[Gene]_F4 primer have 20-30 bp homology with, respectively, the 5' and 3' ends of the resistance marker. This creates an overhang that is complementary to the end of the resistance marker to which each fragment will be joined.

B. generates the two partially overlapping fragments of the antibiotic resistance marker. The SM[Gene}_F2 and SM[Gene]_R3 primers are, respectively, the reverse complement of the SM[Gene]_R1 and SM[Gene}_F4 primers, therefore creating a short complementary sequence to the homologous flanks. The two fragments overlap in the middle of the marker with a region of 0.48-0.51kb homology.

C. joins the homologous flanks and partial resistance markers to create the two final constructs.

4.4.1.1 Generation of the *AQP1* deletion constructs

The *AQP1* deletion strategy was designed to replace 1610 bp of the 1875 bp gene with a bialophos-resistance cassette. The replaced region was 82 bp downstream of the original start codon and 183 bp upstream of the original stop codon.

The 5' flanking region was amplified from Guy11 gDNA with SM03904F1 and SM03904R1 primers to generate a 1506 bp fragment with a 27 bp overhang at the 3' end complementary to the first

27 nucleotides of the BAR promoter. The 3' flanking region was amplified with SM03904F4 and SM03904R4 to generate a 1166 bp fragment with a 24 bp overhang at the 5' end complementary to the last 24 nucleotides of the BAR terminator.

The 5' fragment of the BAR construct was amplified using primers SM[03904]_F2 and SM[03904]_R2 to generate a 741 bp fragment, with a 27 bp overhang at the 5' end complementary to the last 27 nucleotides of the 5' homologous flank. The 3' fragment of the BAR construct was amplified using primers SM[03904]_F3 and SM[03904]_R3 to generate a 738 bp fragment complementary to the first 24 bp of the 3' homologous flank.

The 5' homologous flank and the 5' BAR fragment were joined by overlap-extension PCR with primers SM[03904]_F1 and SM[03904]_R2. This produced a '5'-BA' fragment of 2119 bp. The 3' BAR fragment and the 3' homologous flank were joined with primers SM[03904]_F3 and SM[03904]_R4 to produce a 'AR-3'' fragment of 1849 bp.

The 5'-BA and AR-3' fragments were amplified, PCR cleaned and ethanol precipitated to a final concentration of 5 µg each fragment in 10µl ddH_2O.

4.4.1.2 Generation of the *AQP2* deletion constructs

The *AQP2* deletion strategy was designed to replace the 1153 bp of the 1332 bp gene with a 1430 bp hygromycin-resistance cassette. The replaced region was 179 bp downstream of the original start codon and 288 bp downstream of the original stop codon, resulting the replacement of a 1441 bp region.

The 5' flanking region was amplified from Guy11 gDNA with SM04162F1 and SM04162R1 primers to generate a 1639 bp fragment with a 26 bp overhang at the 3' end complementary to the first 26 nucleotides of the HYG promoter. The 3' flanking region was amplified with SM04162F4 and SM04162R4 to generate a 1180 bp fragment with a 30 bp overhang at the 5' end complementary to the last 30 nucleotides of the HYG terminator.

The 5' fragment of the HYG construct was amplified from the pCB1636 plasmid using primers SM[04162]_F2 and SM[04162]_R2 to generate a 1201 fragment, with a 26 bp overhang at the 5' end complementary to the last 26 nucleotides of the 5' homologous flank. The 3' fragment of the

HYG construct was amplified using primers SM[04162]_F3 and SM[04162]_R3 to generate a 785 fragment complementary to the first 30 bp of the 3' homologous flank.

The 5' homologous flank and the 5' HYG fragment were joined by overlap-extension PCR with primers SM[04162]_F1 and SM[04162]_R2. This produced a '5'-HY' fragment of 2790 bp. The 3' HYG fragment and the 3' homologous flank were joined with primers SM[04162]_F3 and SM[04162]_R4 to produce a 'YG-3'' fragment of 1804 bp.

The 5'-HY and YG-3' fragments were amplified, PCR cleaned and ethanol precipitated to a final concentration of 5 µg each fragment in 10 µl ddH_2O.

4.4.1.3 Generation of the *AQP3* deletion constructs

The *AQP3* deletion strategy was designed to replace 1075 bp of the 1174 bp gene with a 945 bp bialophos-resistance cassette. The replaced region was 65 bp upstream of the original start codon and 79 bp upstream of the original stop codon, resulting in the replacement of a 1157 bp region.

The 5' flanking region was amplified from Guy11 gDNA with SM13332F1 and SM13332R1 primers to generate a 1605 bp fragment with a 21 bp overhang at the 3' end complementary to the first 21 nucleotides of the BAR promoter. The 3' flanking region was amplified with SM13332F4 and SM13332R4 to generate a 1246 bp fragment with a 24 bp overhang at the 5' end complementary to the last 24 nucleotides of the BAR terminator.

The 5' fragment of the BAR construct was amplified using primers SM[13332]_F2 and SM[13332]_R2 to generate a 740 bp fragment, with a 21 bp overhang at the 5' end complementary to the last 21 nucleotides of the 5' homologous flank. The 3' fragment of the BAR construct was amplified using primers SM[13332]_F3 and SM[13332]_R3 to generate a 733 bp fragment complementary to the first 24 bp of the 3' homologous flank.

The 5' homologous flank and the 5' BAR fragment were joined by overlap-extension PCR with primers SM[13332]_F1 and SM[13332]_R2. This produced a '5'-BA' fragment of 2298 bp. The 3' BAR fragment and the 3' homologous flank were joined with primers SM[13332]_F3 and SM[13332]_R4 to produce a 'AR-3'' fragment of 1932 bp.

The 5'-BA and AR-3' fragments were amplified, PCR cleaned and ethanol precipitated to a final concentration of 5 µg each fragment in 10 µl ddH_2O.

4.4.1.4 Generation of the *AGP1* deletion constructs

The *AGP1* deletion strategy was designed to replace 1183 bp of the 1435 bp gene with a 945 bp bialophos-resistance cassette. The replaced region was 252 bp downstream of the original start codon and 60 bp downstream of the original stop codon, resulting in the replacement of a 1229 bp region.

The 5' flanking region was amplified from Guy11 gDNA with SM05880F1 and SM05880R1 primers to generate a 1600 bp fragment with a 23 bp overhang at the 3' end complementary to the first 23 nucleotides of the BAR promoter. The 3' flanking region was amplified with SM05880F4 and SM05880R4 to generate a 1159 bp fragment with a 27 bp overhang at the 5' end complementary to the last 27 nucleotides of the BAR terminator.

The 5' fragment of the BAR construct was amplified using primers SM[05880]_F2 and SM[05880]_R2 to generate a 738 bp fragment, with a 23 bp overhang at the 5' end complementary to the last 23 nucleotides of the 5' homologous flank. The 3' fragment of the BAR construct was amplified using primers SM[05880]_F3 and SM[05880]_R3 to generate a 742 bp fragment complementary to the first 27 bp of the 3' homologous flank.

The 5' homologous flank and the 5' BAR fragment were joined by overlap-extension PCR with primers SM[05880]_F1 and SM[05880]_R2. This produced a '5'-BA' fragment of 2293 bp. The 3' BAR fragment and the 3' homologous flank were joined with primers SM[05880]_F3 and SM[05880]_R4 to produce a 'AR-3'' fragment of 1842 bp.

The 5'-BA and AR-3' fragments were amplified, PCR cleaned and ethanol precipitated to a final concentration of 5 µg each fragment in 10 µl ddH_2O.

4.4.2 Generation of Δ*agp2* using the 'whole' marker method

The *AGP2* deletion construct was designed to replace 271 bp of the 1255 bp gene with a 1430 bp hygromycin-resistance cassette. The replaced region was 636 bp downstream of the original start codon and 348 bp upstream of the original stop codon.

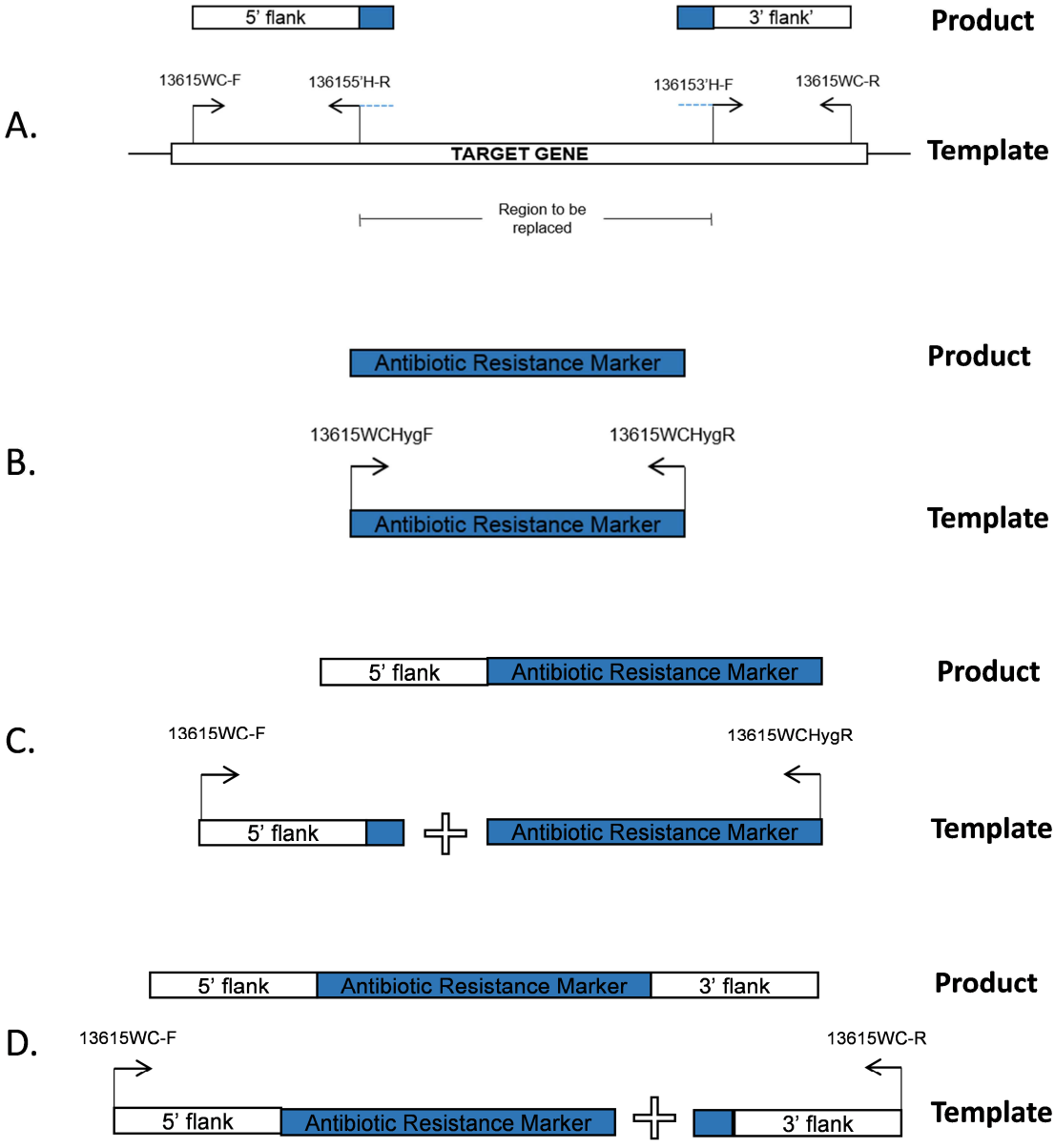

Figure 4.3: Generation of the AGP2 deletion construct using overlap-extension PCR
A*. The 5' and 3' flanking regions are amplified using primers 13615WC-F and 136155'H-R, and primers 136153'H-F and 13615WC-R, respectively.*
B*. The hygromycin resistance cassette is amplified from the pCB1636 plasmid using primers13615WCHygF and 13615WCHygR.*
C*. The 5' flank is joined to the hygromycin-resistance marker using primers 13615WC-F and 13615ECHygR.*
D*. The 3' flank is joined to the 5'flank::HYG fragment using primers 13615WC-F and 13615WC-R.*

The *AGP2* deletion strategy uses a single transformation fragment rather than the two fragments described previously. A diagrammatic overview of the PCR steps required to generate this construct is shown in Figure 4.3.

The 5' flanking region was amplified from Guy11 gDNA with 13615WCF and 136155'H-R primers to generate a 1586 bp fragment with a 28 bp overhang at the 3' end complementary to the first 28 nucleotides of the HYG promoter. The 3' flanking region was amplified with 136153'H-F and 13615WCR to generate a 1170 bp fragment with a 31 bp overhang at the 5' end complementary to the last 31 nucleotides of the HYG terminator. The HYG cassette was amplified from the pCB1636 plasmid using primers 13615WCHyg-F and 13615WCHyg-R to generate a 1484 bp fragment. The 5' homologous flank and the HYG fragment were joined by overlap-extension PCR with primers 13615WC-F and 136155'H-R to produce a '5'-HYG' fragment of 3012b. The 5'HYG fragment and the 3' flank were joined with primers were joined with primers 13615WC-F and 13615WC-R to produce a final construct of 4126 bp.

This construct was amplified, PCR cleaned and ethanol precipitated to a final concentration of 8 µg in 10 µl ddH_2O.

4.4.3 Generation and confirmation of aquaporin knockout strains

Transformations were carried out as described in chapter 2. Putative transformants were isolated from the transformation plates after 14 days growth and put through a second round of antibiotic selection to confirm uptake of the resistance marker. Low quality genomic DNA was extracted from the remaining colonies used for a PCR-based screen designed to answer two questions:

a) Has the construct integrated homologously?
b) Has the original transcript been fully disrupted?

Question a) was address using two pairs of 'integration primers'. These primers amplify are complementary to a site outside the replaced region and homologous flanks, and to a site inside the antibiotic resistance marker, as shown in Figure 4.4:

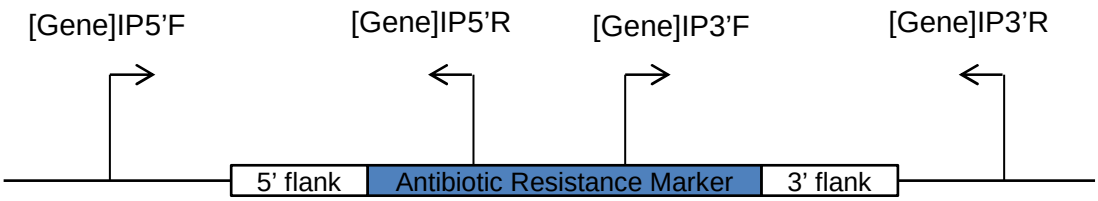

Figure 4.4: A homologously integrated deletion construct with integration primer site locations marked.

Two pairs of primers were used to reduce the possibility that no homologous recombination events were detected because the integration primers were non-functional and to ensure that the both halves of the split marker had integrated correctly.

To address question b) a primer pair that amplified inside the replaced region was used to confirm absence of the original coding region. This demonstrated that the gene was not present in multiple copies in the genome – something that might not be detected during genome sequencing. The location of this 'internal' primer pair is shown on Figure 4.5 below:

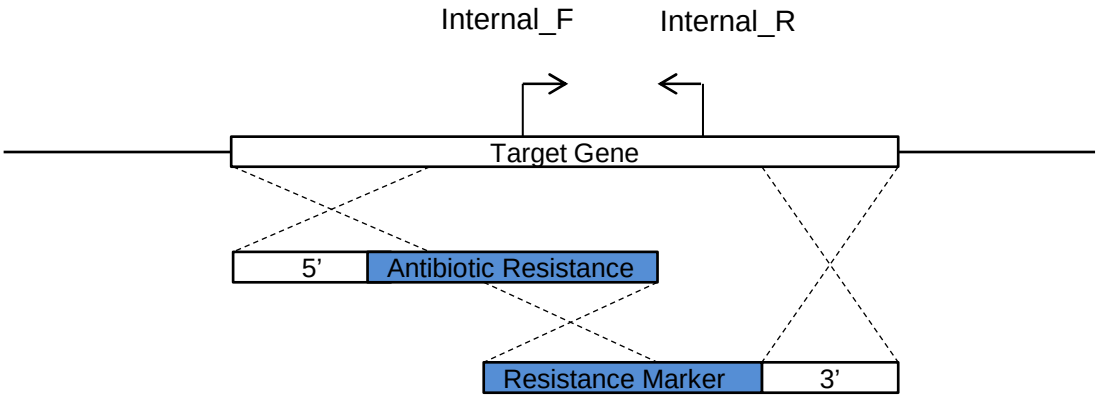

Figure 4.5: Primers amplifying in the replaced region were used to confirm absence of the original transcript.

The combination of these two sources of evidence – absence of original genomic sequence and amplification by the integration primers – strongly suggests that homologous recombination has taken place. However, this does not preclude the possibility that non-homologous recombination has also taken place, perhaps disruption genetic elements elsewhere. To preclude the possibility of additional insertion events, a Southern blot strategy was designed to detect simultaneous ectopic recombination events.

The sequence of the *M. oryzae* genome is known; therefore, we are able to predict restriction enzyme sites in the vicinity of each *AQUAPORIN* gene. The resistance marker DNA construct will therefore migrate on a DNA fragment of a known size if the genome is digested and size-separated on a DNA gel. A radiolabelled DNA probe can be used to detect the location on the gel of the resistance marker and this can be compared to the predicted band size. The presence of multiple bands indicates multiple insertion events.

For each deletion construct, restriction enzymes were selected that cut either side of the restriction marker but *at least* once outside the homologous flanks. Enzymes were selected that produced a marker-containing DNA fragment of 4-6 kb to facilitate optimum size differentiation. For each genotype, four independent transformants with putative homologous recombination events were selected for Southern blotting.

Taken together, the combination of PCR analysis and Southern blotting is strong evidence that a single, homologous recombination event has taken place. This evidence, for the five *AQUAPORIN* deletion strains used for further experiments, is shown in Figures 4.6–4.10 below:

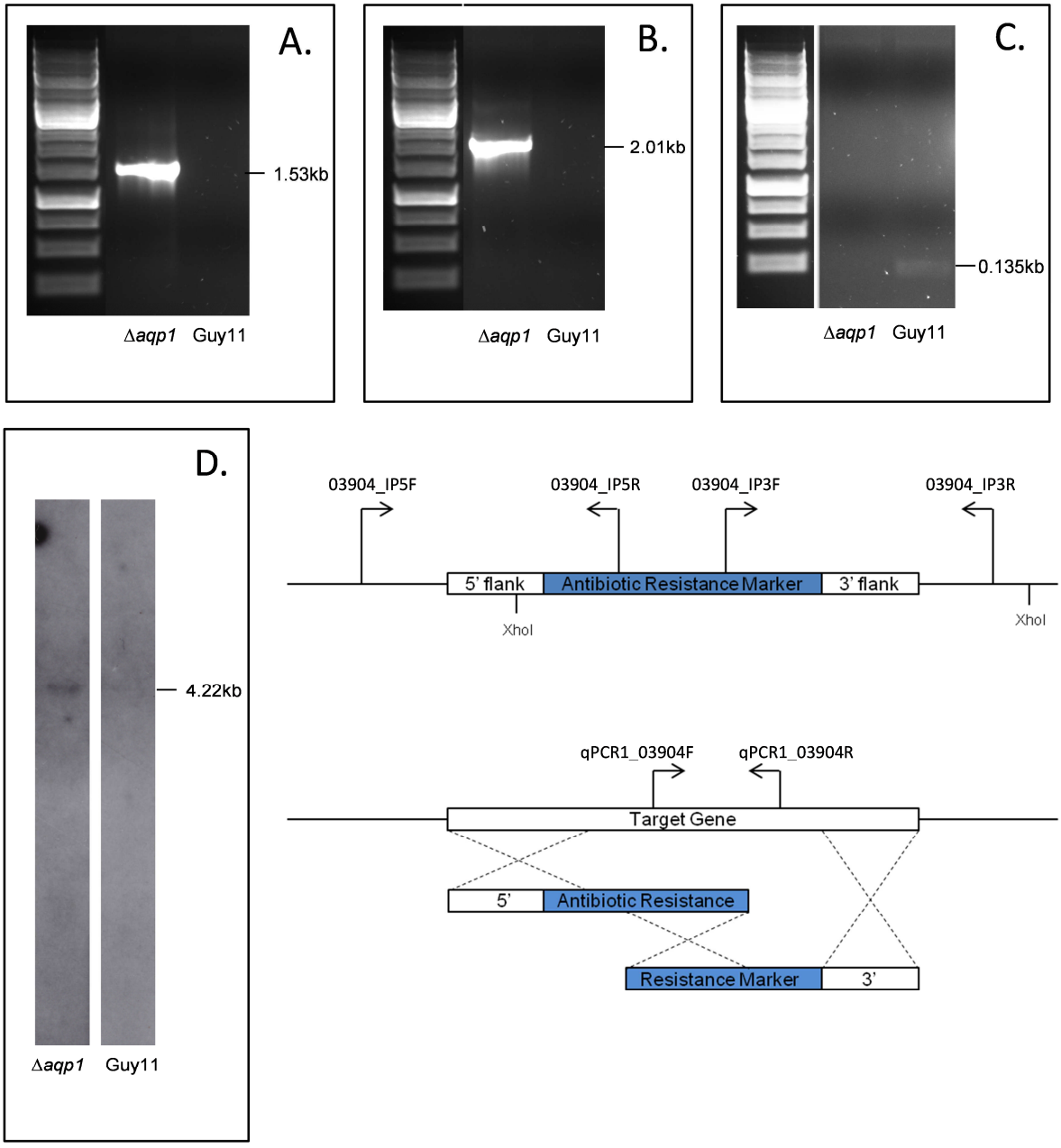

Figure 4.6: Confirmation by PCR analysis and Southern blotting of a single homologous integration event resulting in the disruption of AQP1 (MGG_03904).

A. *PCR analysis of a putative Δaqp1 transformant and wild type Guy11 with primers 03904_IP5F and 03904_IP5R. Amplification of a 1530 bp fragment confirmed the homologous replacement of the 5' region of AQP2 with the 5' sequence of BAR. In A. to C. gel markers (GeneRuler 1kb DNA ladder (Thermo Scientific)) are on LHS of gel.*

B. *PCR analysis of a putative Δaqp2 and wild type Guy11 with primers 03904_IP3F and 03904_IP3R. Amplification of a 2012 bp fragment confirmed the homologous replacement of the 3' region of AQP2 with the 3' sequence of BAR.*

C. *The absence of detectable PCR product with primers qPCR1_03904F and qPCR1_03904R indicates that AQP1 is present as a single copy in the genome.*

D. *Southern Blot analysis of DNA from the putative Δaqp1 transformant and wild type Guy11. Genomic DNA was digested with XhoI, separated by gel electrophoresis, blotted onto Hybond N^+ membrane and hybridised with an α ^{32}P [dCTP]-labelled BAR probe (945 bp). Washing conditions were as described in Materials and Methods. The presence of a single 4.2kb band verified a single Δaqp1 replacement event.*

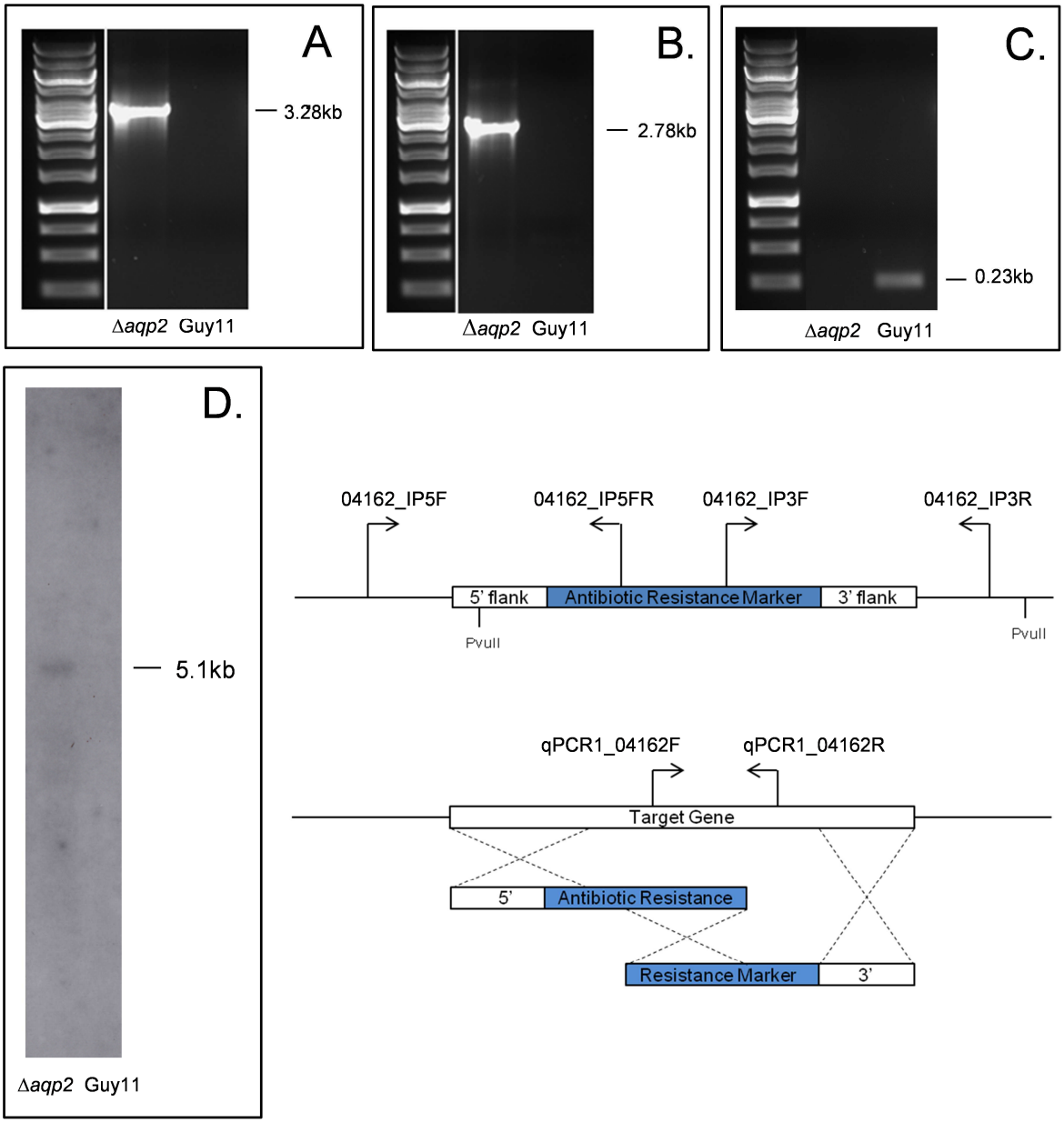

Figure 4.7: Confirmation by PCR analysis and Southern blotting of a single homologous integration event resulting in the disruption of AQP2 (MGG_04162).
A*. PCR analysis of a putative* Δaqp2 *transformant and wild type Guy11 with primers 04162_IP5F and 04162_IP5R. Amplification of a 3279 bp fragment confirmed the homologous replacement of the 5' region of AQP2 with the 5' sequence of HYG. In A. to C. gel markers (GeneRuler 1kb DNA ladder (Thermo Scientific)) are on LHS of gel.*
B*. PCR analysis of a putative Δaqp2 and wild type Guy11 with primers 04162_IP3F and 04162_IP3R. Amplification of a 2780 bp fragment confirmed the homologous replacement of the 3' region of AQP2 with the 3' sequence of HYG.*
C*. The absence of detectable PCR product with primers qPCR1_04162F and qPCR1_04162R indicates that AQP2 is present as a single copy in the genome.*
D*. Southern Blot analysis of DNA from the putative Δaqp2 transformant and wild type Guy11. Genomic DNA was digested with* PvuII*, separated by gel electrophoresis, blotted onto Hybond* N^+ *membrane and hybridised with an* $\alpha^{32}P$ *[dCTP]-labelled HYG probe (1430 bp). Washing conditions were as described in Materials and Methods The presence of a single 5.1 kb band verified a single* AQP2 *replacement event.*

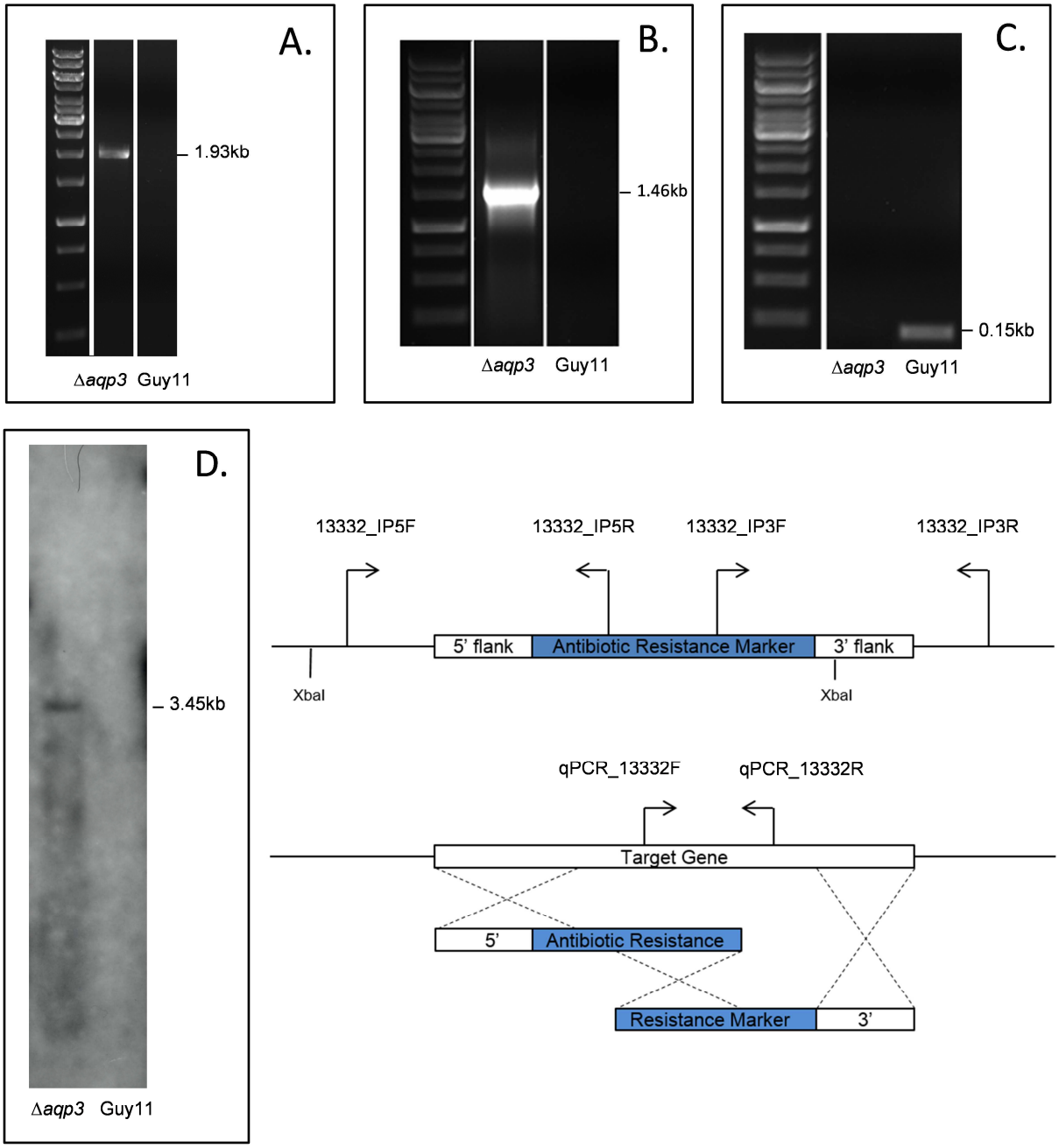

Figure 4.8: Confirmation by PCR analysis and Southern blotting of a single homologous integration event resulting in the disruption of AQP3 (MGG_13332).
A. *PCR analysis of a putative* Δaqp3 *transformant and wild type Guy11 with primers 13332_IP5F and 13332_IP5R. Amplification of a* 1930 bp *fragment confirmed the homologous replacement of the 5' region of AQP2 with the 5' sequence of BAR. In A. to C. gel markers (GeneRuler 1kb DNA ladder (Thermo Scientific)) are on LHS of gel.*
B. *PCR analysis of a putative* Δaqp2 *and wild type Guy11 with primers 13332_IP3F and 13332_IP3R. Amplification of a 1458 bp fragment confirmed the homologous replacement of the 3' region of AQP2 with the 3' sequence of BAR.*
C. *The absence of detectable PCR product with primers qPCR1_13332F and qPCR1_13332R indicates that* AQP3 *is present as a single copy in the genome.*
D. *Southern Blot of DNA from the putative Δaqp3 transformant and wild type Guy11. Genomic DNA was digested with* XbaI*, separated by gel electrophoresis, blotted onto Hybond N^+ membrane and hybridised with an α ^{32}P [dCTP]-labelled BAR probe (945 bp). Washing conditions were as described in chapter 2. The presence of a single 3.45 kb band verified a single AQP3 replacement event.*

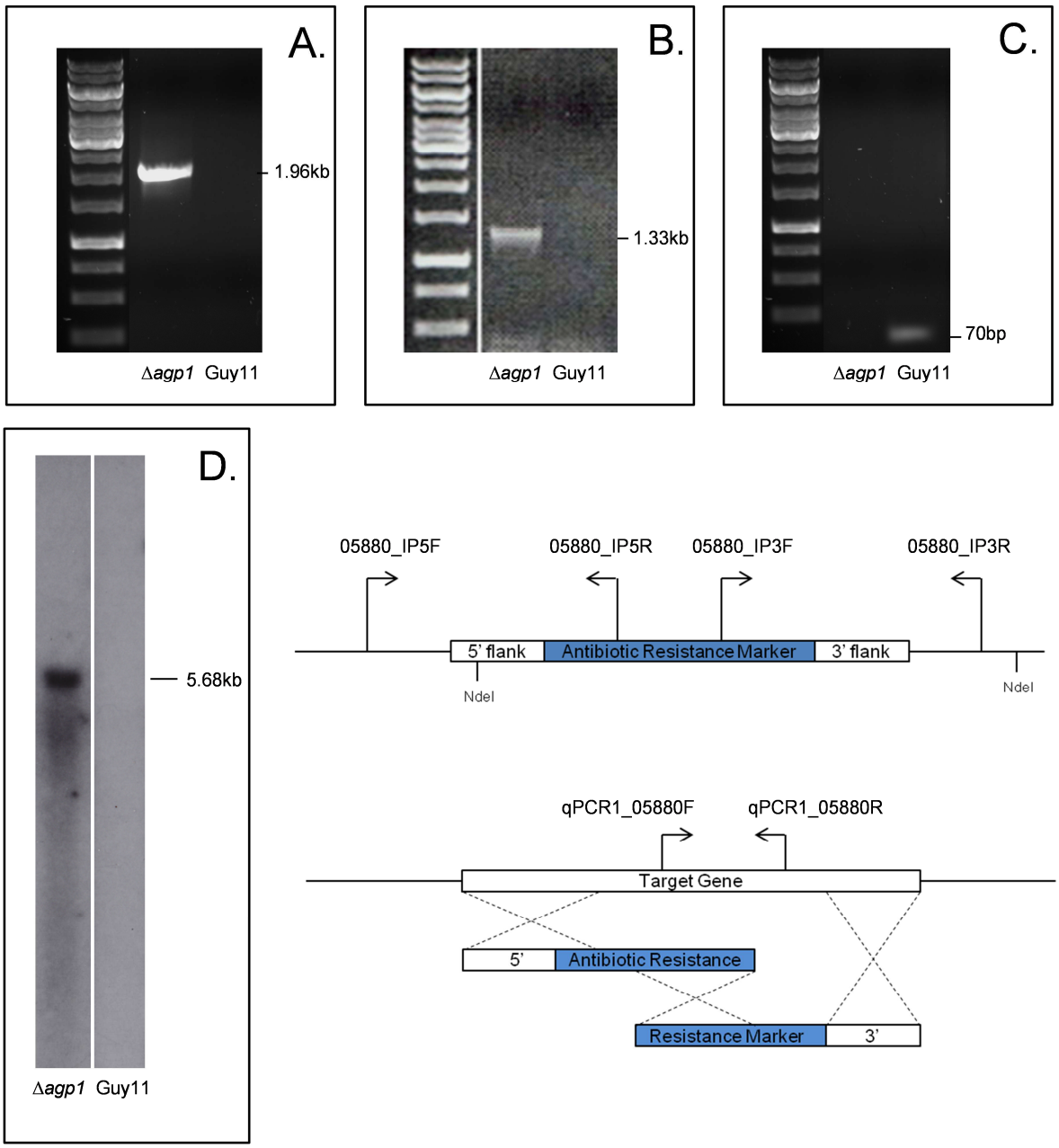

Figure 4.9 Confirmation by PCR analysis and Southern blotting of a single homologous integration event resulting in the disruption of AGP1 (MGG_05880).
A. *PCR analysis of a putative* Δagp1 *transformant and wild type Guy11 with primers 05880_IP5F and 05880_IP5R. Amplification of a 1955 bp fragment confirmed the homologous replacement of the 5' region of AQP2 with the 5' sequence of BAR. In A. to C. gel markers (GeneRuler 1kb DNA ladder (Thermo Scientific)) are on LHS of gel.*
B. *PCR analysis of a putative Δaqp2 and wild type Guy11 with primers 05880_IP3F and 05880_IP3R. Amplification of a 1331 bp fragment confirmed the homologous replacement of the 3' region of AQP2 with the 3' sequence of BAR.*
C. *The absence of detectable PCR product with primers qPCR1_05880F and qPCR1_05880R indicates that* AGP1 *is present as a single copy in the genome.*
D. *Southern Blot analysis of DNA from the putative Δagp1 transformant and wild type Guy11. Genomic DNA was digested with* NdeI*, separated by gel electrophoresis, blotted onto Hybond N^+ membrane and hybridised with an α ^{32}P [dCTP]-labelled BAR probe (945 bp). Washing conditions were as described in Materials and Methods. The presence of a single 5.68 kb band verified a single* AGP1 *replacement event.*

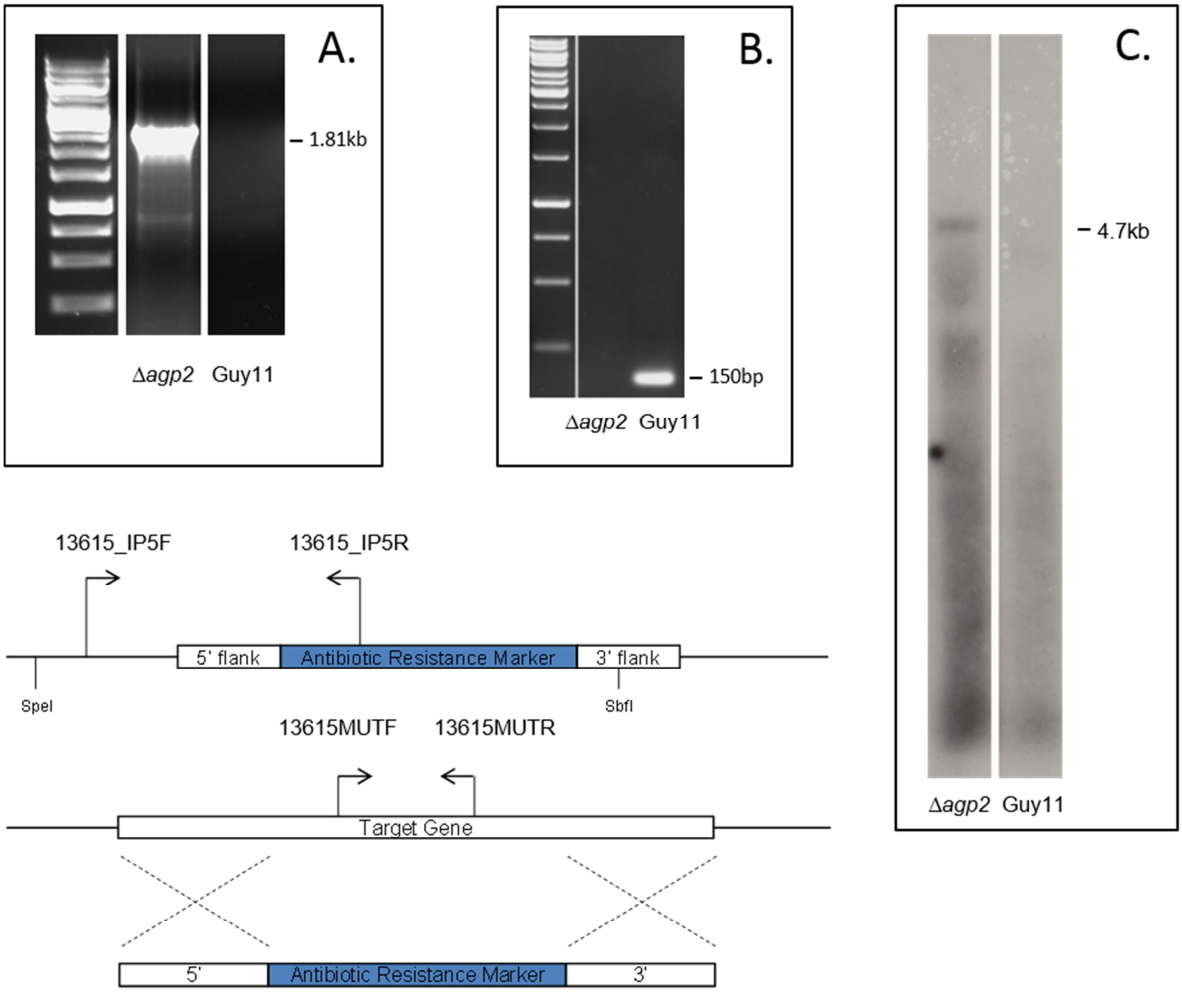

Figure 4.10: Confirmation by PCR analysis and Southern blotting of a single homologous integration event resulting in the disruption of *AGP2 (MGG_13615)*.
A. *PCR analysis of a putative* Δagp2 *transformant and wild type Guy11 with primers 13615_IP5F and 13615_IP5R. Amplification of a 1814 bp fragment confirmed the homologous replacement of the 5' region of* AQP2 *with the 5' sequence of HYG. In A. to C. gel markers (GeneRuler 1 kb DNA ladder (Thermo Scientific)) are on LHS of gel.*
B. *The absence of detectable PCR product with primers 13615MUTF and 13615MUTR indicates that* AGP2 *is present as a single copy in the genome.*
C*. Southern Blot analysis of DNA from the putative Δagp2 transformant and wild type Guy11. Genomic DNA was digested with* Spe*I and* Sbf*I, separated by gel electrophoresis, blotted onto Hybond N*$^{+}$ *membrane and hybridised with an α* ^{32}*P [dCTP]-labelled HYG probe (945 bp). Washing conditions were as described in Materials and Methods. The presence of a single 4.69 kb band verified a single* AGP2 *replacement event.*

4.4.4 Pathogenicity and virulence

Wildtype Guy11 and all knockout conidia were spray-inoculated onto 21-day old CO39 rice plants. Five to six days after inoculation, the leaves were photographed and analysed using lesion segmentation software developed by Dr. Mark Fricker (University of Oxford).

Representative images from pathogenicity assays of each genotype and the WT Guy11 are shown in Figure 4.11 and Figure 4.12. The average lesion count per unit leaf area is shown in Figure 4.13. This shows that there is no statistically significant difference between the lesion density of the wildtype Guy11 and the aquaporin null mutants. The distribution of lesion sizes and colours, as fitted by the software, was also examined and found to be equivalent between the strains (data not shown).

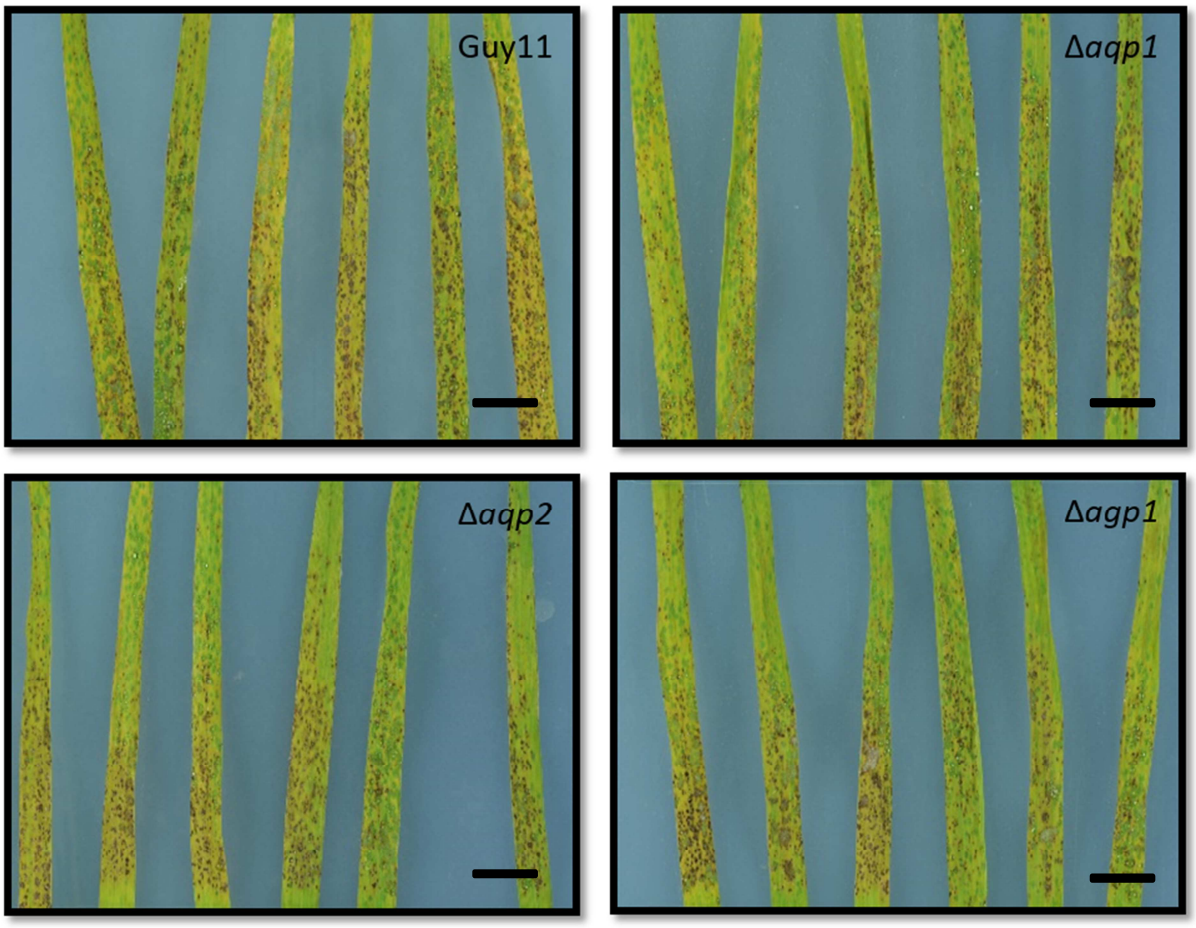

Figure 4.11: Disease lesions, 6dpi, of 27 day-old rice leaves (cv. CO39) following inoculation with wildtype Guy11 and Δaqp1, Δaqp2 and Δagp1 conidia. *Conidia were harvested and adjusted to 5x10^5 spores per ml using a haemocytometer. One millilitre of spore suspension was combined with 1ml 0.4% (w/v) gelatine and spray inoculated onto surface-sterilised rice leaves on a 2% (w/v) water agar plate. Plates were inoculated under fungal growth conditions for 6 days before being photographed. Scale bars represent 1 cm.*

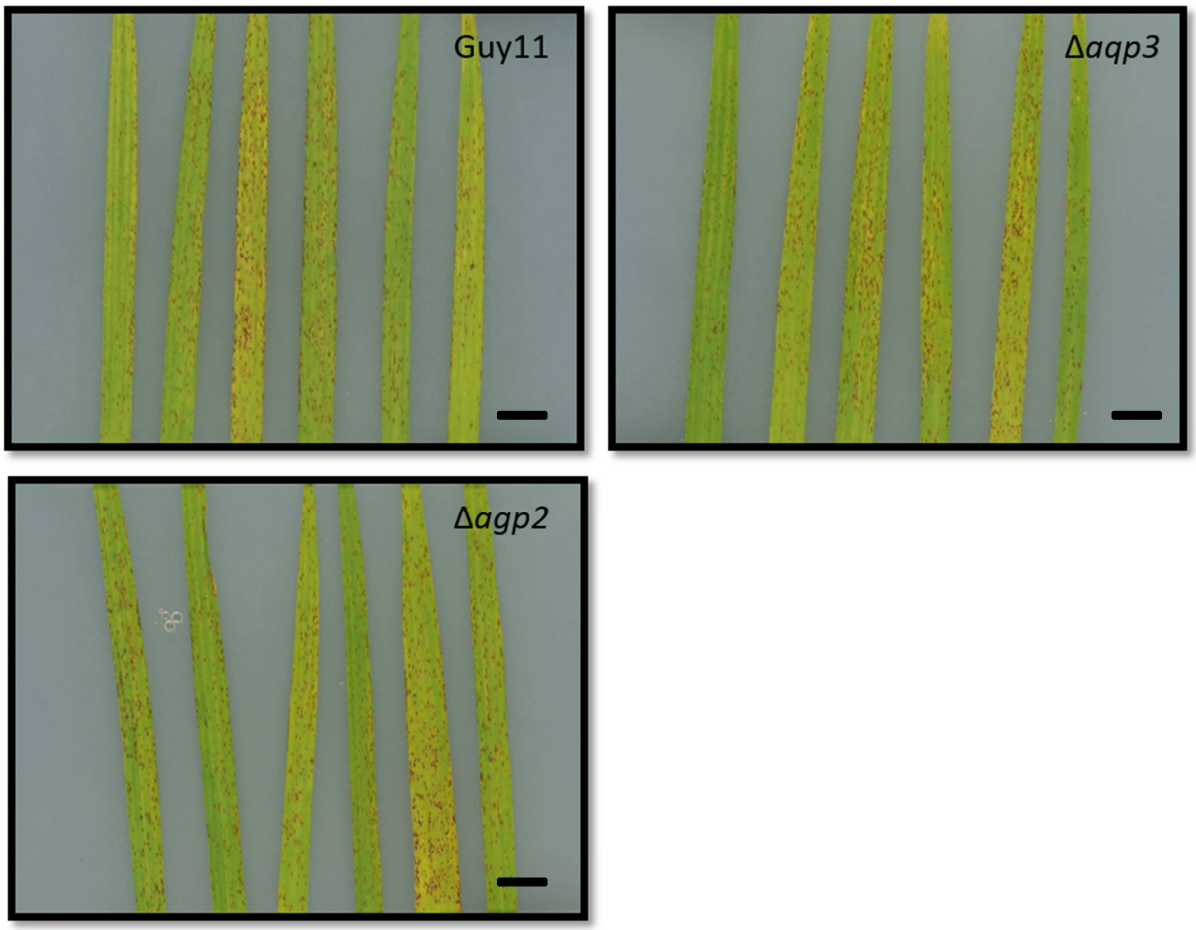

Figure 4.12: Disease lesions, 5dpi, of 26 day-old rice leaves (cv. CO39) following inoculation with wildtype Guy11, Δaqp3 and Δagp2. *Conidia were harvested and adjusted to 5x10^5 spores per ml using a haemocytometer. One millilitre of spore suspension was combined with 1ml 0.4% (w/v) gelatine and spray inoculated onto surface-sterilised rice leaves on a 2% (w/v) water agar plate. Plates were inoculated under fungal growth conditions for 5 days before being photographed. Scale bars represent 1 cm*

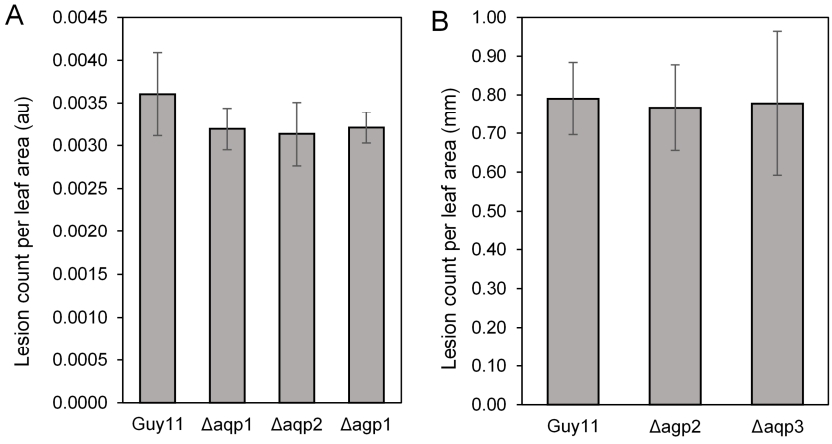

Figure 4.13: The mean lesion count per leaf area unit of the wildtype Guy11 and aquaporin null mutants in two independent pathogenicity assays. There is no statistically significant difference between the number of lesions in the null mutants, as compared with the Guy11 wildtype, in each experiment (p>0.05). Lesion counting and area measurements were performed using specialized software (M. Fricker, University of Oxford). *Each experiment represents the mean of three plates of six leaves.*

4.4.5 Infection-related development

4.4.5.1 Infection-related development on inductive surfaces

Wildtype and mutant strains were assessed for their ability to develop infection-related structures on inductive glass Menzel coverslips. Conidia were harvested and resuspended in sterile ddH_2O, and 20 µl of spore suspension was pipetted onto the inductive coverslips and incubated in a humidity chamber. At time points corresponding to specific developmental stages in the Guy11 wildtype the coverslips were photographed under a bright field microscope. Spores were photographed at 1, 2, 4 and 24 hpi, correlating with the formation of germ tubes, the hooking of the germ tubes against the inductive surface, the formation of un-melanised appressoria and the elaboration of fully melanised appressoria. An explanation of the events occurring at these developmental stages can be found in chapter 1.

Qualitative examination of the wildtype Guy11 and the five knockout lines suggests that all lines are capable of elaborating melanised appressoria and there were no obvious developmental abnormalities. A representative image of all strains at the four time points is shown in Figure 4.14.

Progression through the developmental stages was quantified by counting and categorising germlings according to their developmental state at each time point. Five developmental categories were identified from the images:

1) Absence of a germ tube
2) Germ tube
3) ‘Hooked’ germ tube
4) Un-melanised appressorium
5) Melanised appressorium

A minimum of 100 spores from each of three independent plates were scored per genotype. Hooked germ tubes were distinguished by a swelling at the tip, and melanised appressoria were identified by the dark colour of the melanin.

The percentage of spores in each category can be seen at 1 hpi (Figure 4.15), 2 hpi (Figure 4.16) 4 hpi (Figure 4.17) and 24 hpi (Figure 4.18). Quantitative analysis suggests no significant difference between the development of the wildtype and mutant germlings across the time points. *p*-values are shown in Table 4.1 below:

Table 4.1: The p-values associated with the difference between the developmental categorization of the Guy11 wild type and each aquaporin knockout strain at four time points.

Genotype	1 hpi	2 hpi	4 hpi	24 hpi
Δaqp1	0.09	0.43	0.19	0.23
Δaqp2	0.32	0.61	0.18	0.71
Δaqp3	0.31	0.24	0.27	0.12
Δagp1	0.72	0.35	0.51	0.64
Δagp2	0.23	0.10	0.70	0.23

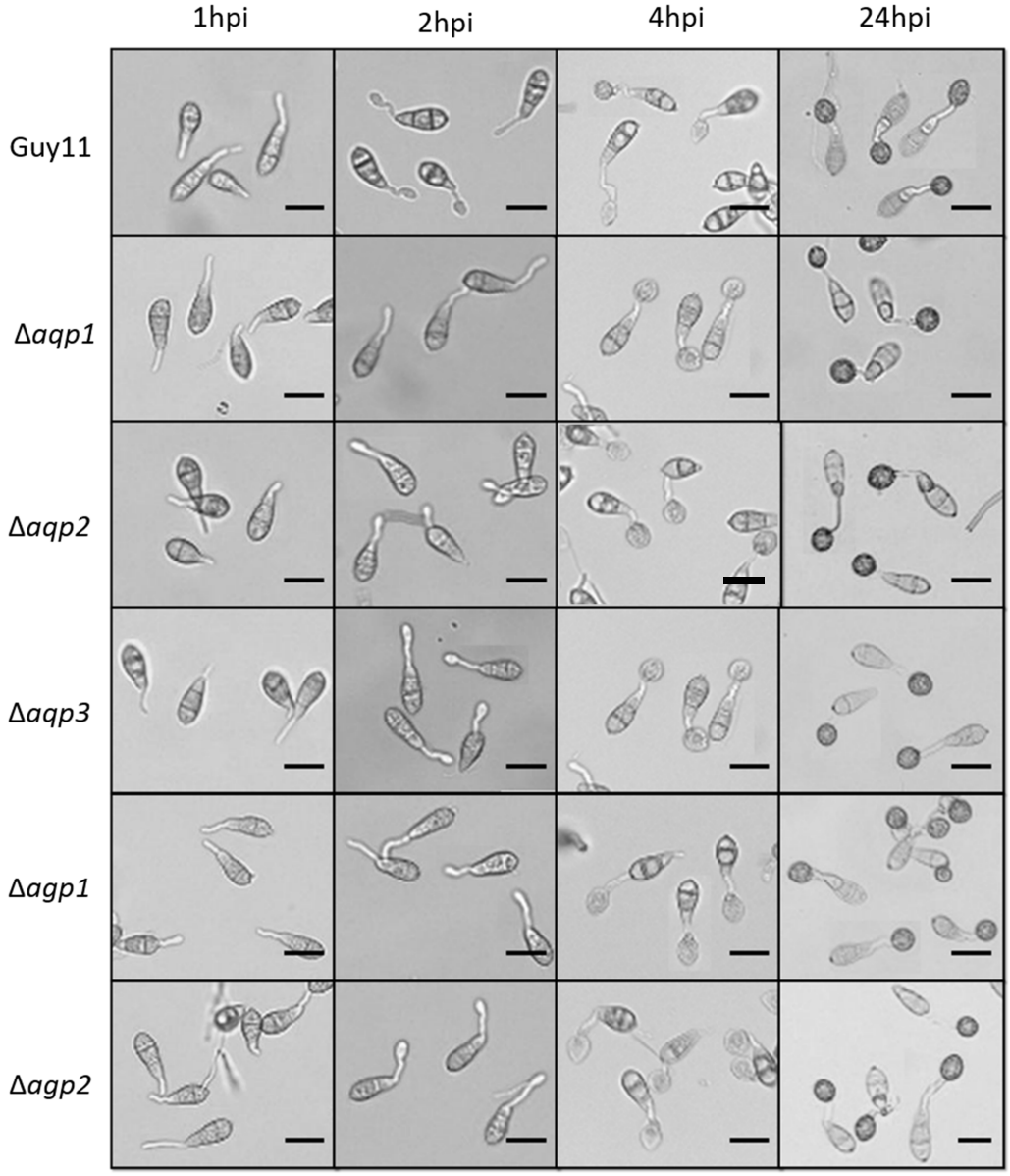

Figure 4.14 Representative images of wildtype and mutant germlings 1, 2, 4 and 24 h after inoculation on inductive Menzel coverslips. *Scale bars represent 20 µm.*

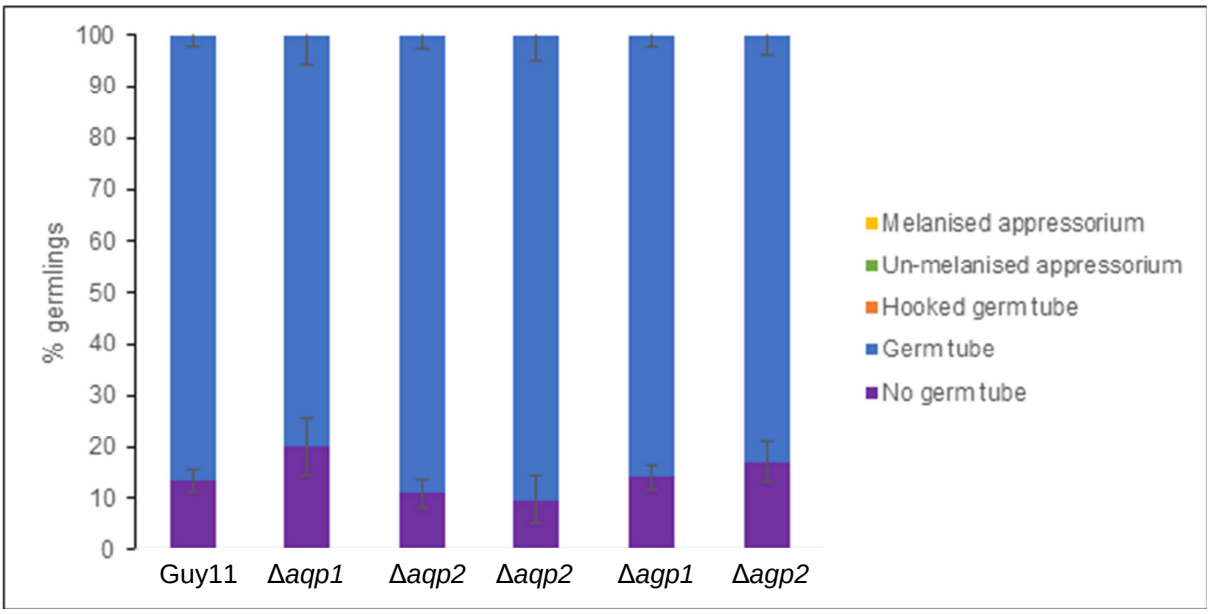

Figure 4.15: The developmental state 1 hpi of wildtype and Δaquaporin germlings. *Mean percentage germling morphologies were calculated from three independent replicates. For each replicate a minimum of 100 germlings were assessed. Error bars represent the standard deviation.*

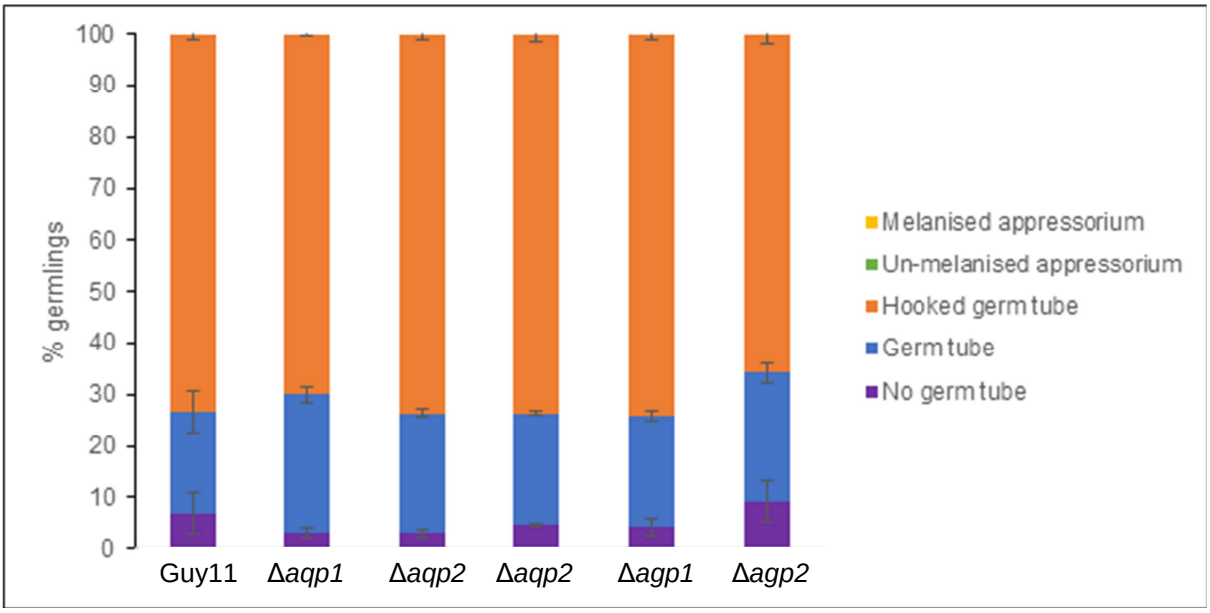

Figure 4.16: The developmental state 2 hpi of wildtype and Δaquaporin germlings. *Mean percentage germling morphologies were calculated from three independent replicates. For each replicate a minimum of 100 germlings were assessed. Error bars represent the standard deviation.*

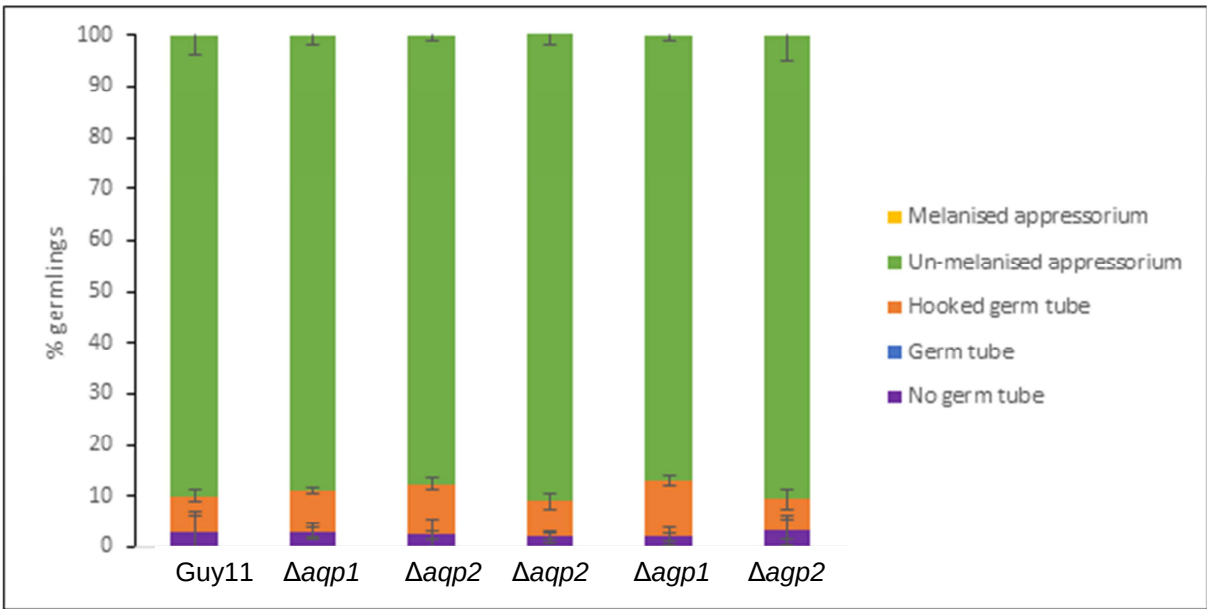

Figure 4.17: The developmental state 4 hpi of wildtype and Δaquaporin germlings. *Mean percentage germling morphologies were calculated from three independent replicates. For each replicate a minimum of 100 germlings were assessed. Error bars represent the standard deviation.*

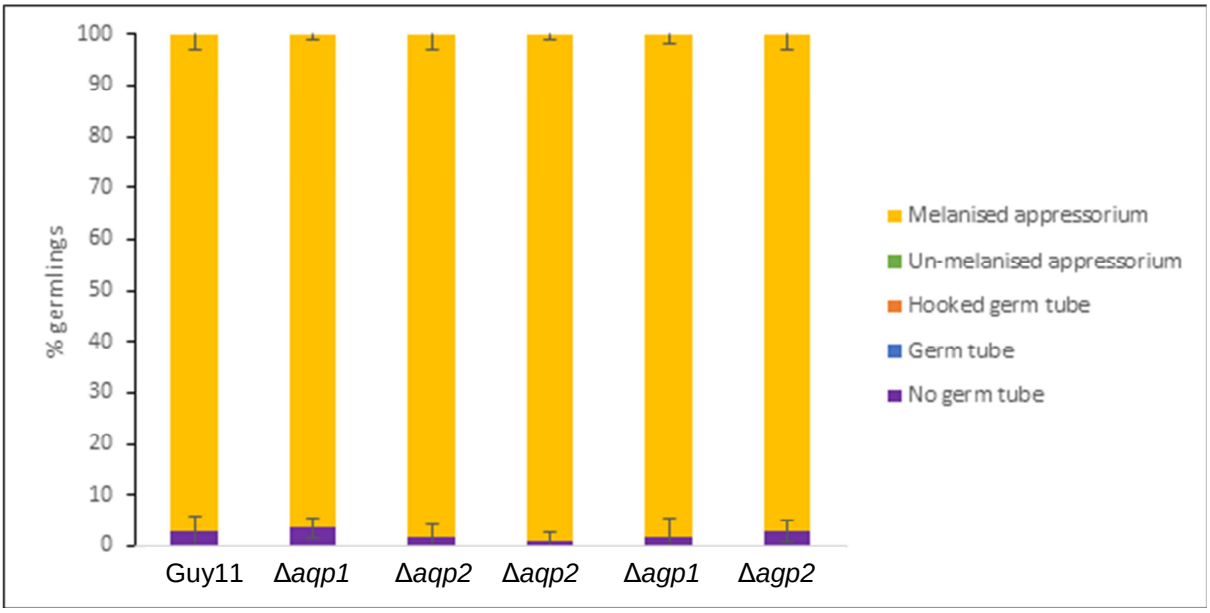

Figure 4.18: The developmental state 24 hpi of wildtype and Δaquaporin germlings. *Mean percentage germling morphologies were calculated from three independent replicates. For each replicate a minimum of 100 germlings were assessed. Error bars represent the standard deviation.*

4.4.5.2 Formation of penetration pegs on onion epidermises

Guy11 is not strictly host-limited to rice and can also infect onion epidermal cells, which are more suitable for microscopy than rice leaves as they are flat and translucent. The surface of an onion epidermis is inductive to appressorium formation and invasion hyphae form within the onion cells

24hpi. Onion epidermises can therefore be used to screen mutant lines for defects in invasion hyphae formation.

Figure 4.19 shows representative images of Guy11 and aquaporin knockout strains on onion epidermal peels 24hpi. Conidia have been inoculated onto an onion epidermises and incubated on water agar for 24h at 24°C. In all strains, melanised appressoria have formed with bulbous invasion hyphae growing in the cell beneath. There is no appreciable difference in the invasion behaviour of aquaporin knockout strains when compared with Guy11.

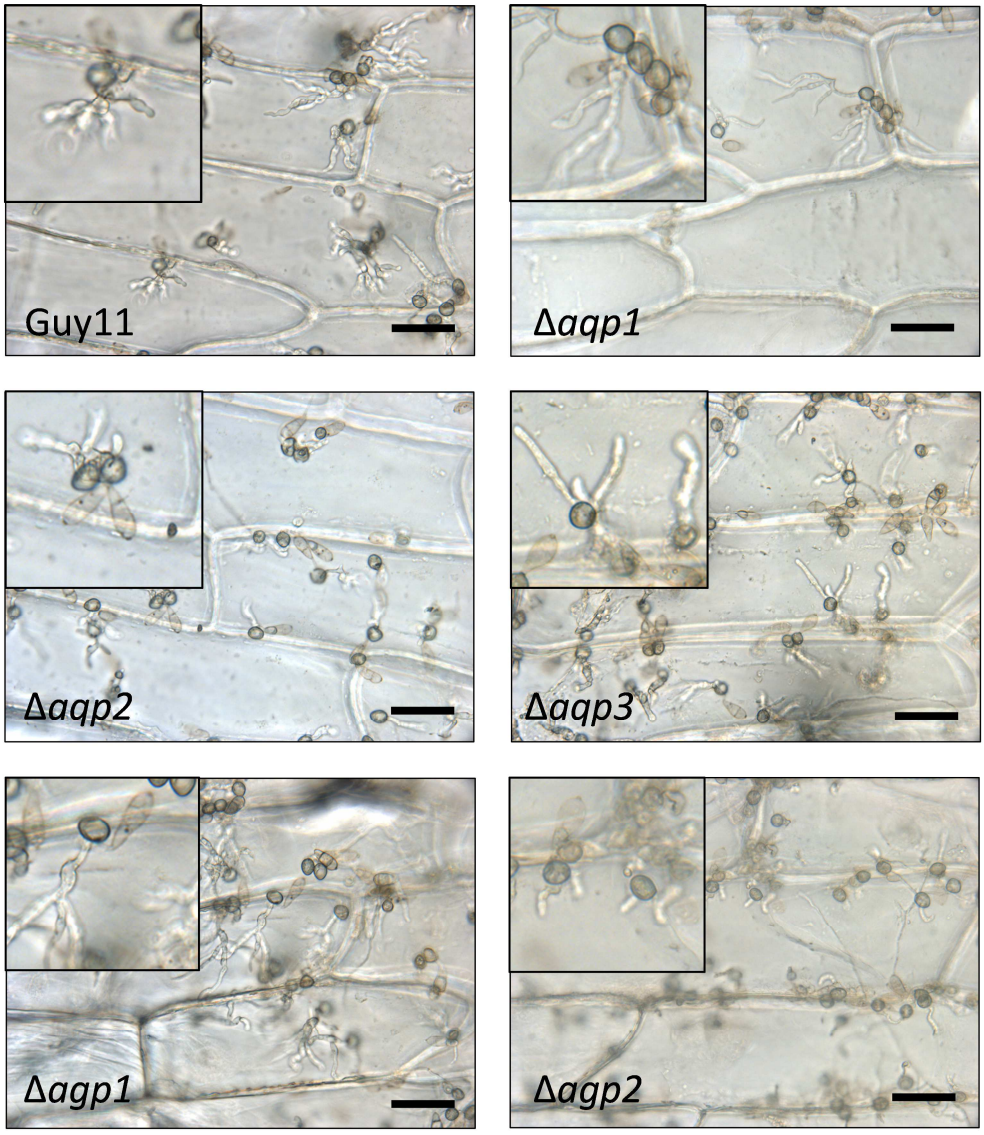

Figure 4.19: Wildtype and knockout conidia on onion epidermises 24 h post inoculation. *Conidia from a 10-day old CM plate were resuspended in 3 ml sterile ddH2O and 100 µl spore suspension was pipetted onto the adaxial side of a white onion epidermises. Scale bars represent 50 µm.*

4.4.5.3 Appressorial turgor

The external osmotic pressure required to induce collapse of 50% of appressoria can be used to approximate the internal osmotic pressure of appressoria in pure water. Assuming that glycerol is the only compatible solute within the appressorium, this measure is a proxy for the glycerol concentration within the appressorium. Data collected in this experiment indicates that the appressorium glycerol concentration for the wildtype Guy11 is 0.90 M. Glycerol concentration in the appressoria of Δ*aqp1* = 0.95 M, Δ*aqp2* = 0.93 M, Δ*aqp3* = 0.91 M, Δ*agp1* = 0.79 M and Δ*aqp1* = 0.88 M. *p*-values for the difference between each knockout and Guy11 are 0.45, 0.61, 0.73, 0.14 and 0.32 respectively. Therefore no significant difference between the appressorial glycerol concentrations of Guy11 and aquaporin mutants was demonstrated.

Previous work on *M. oryzae* spores found a concentration of 3.2 M glycerol (rather than 0.9 M) induced the collapse of 50% appressoria (Dixon et al. 1999). There are significant differences in the experimental set-up that may explain this difference. Dixon et al. germinated appressoria on the hydrophobic side of Gelbond membranes rather than glass Menzel slides, and the appressoria were tested 48 hpi rather than 8 h. Live/dead cell staining carried out in our laboratory suggested that appressoria were ‘dead’ by 24 h. Therefore it is possible that the results reported by Dixon et al. are artefactual. It is a truism amongst *M. oryzae* researchers that the appressorium can generate turgor of up to 8 MPa (de Jong et al. 1997). However, little recent work substantiates this claim.

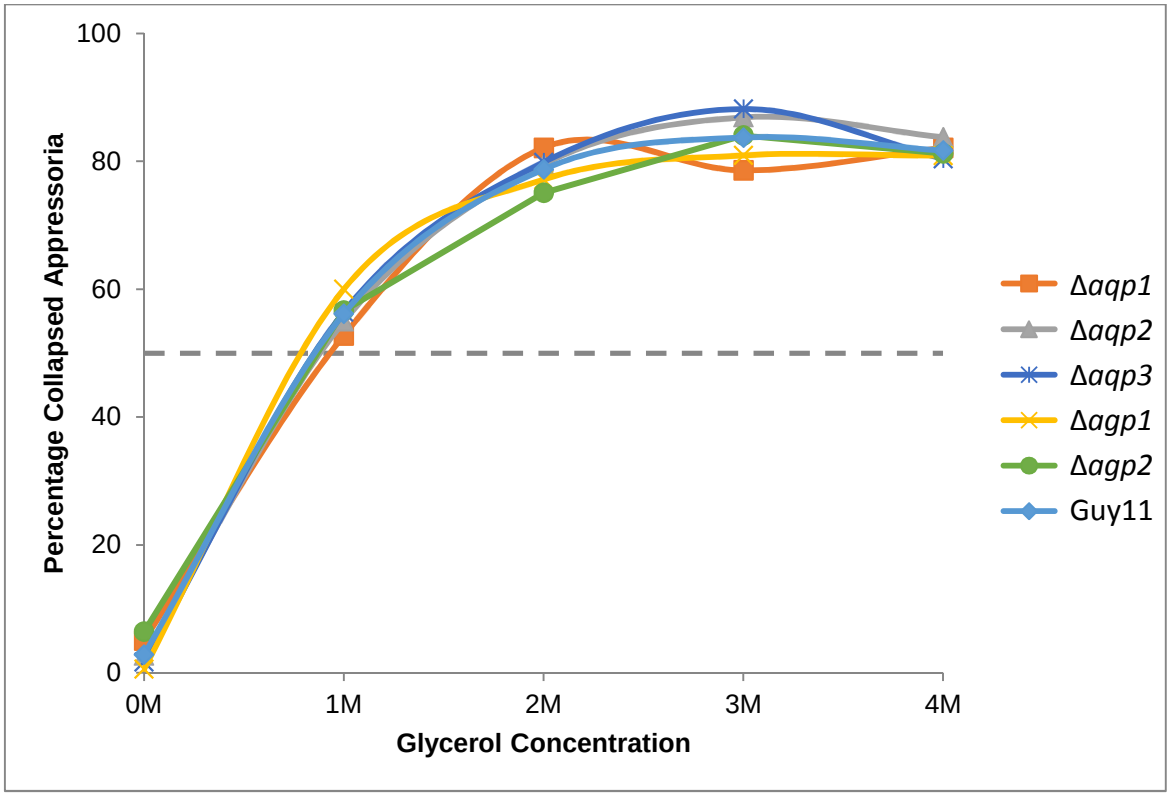

Figure 4.20: The percentage of appressoria that have undergone cytorrhysis (cell collapse) on exposure to glycerol at a range of concentrations (0-4 M). *Conidia were harvested from three independent 10-day old CM plates and inoculated onto inductive Menzel coverslips. At 8 hpi the water droplet was removed and replaced by 200 µl glycerol. After 10 min, the germlings were photographed and the number of collapsed and un-collapsed appressoria was counted. Error bars are not shown for simplicity, but all p-values are non-significant (n=3).*

4.4.6 Vegetative growth and stress tolerance

4.4.6.1 Deletion of aquaporins may affect vegetative growth on solid medium

Figure 4.21 shows the growth of the wildtype Guy11 and aquaporin knockout strains on complete and nutrient minimal medium. Student's T-test was used to compare the mutant strains to the growth of Guy11. On CM, two deletion strains are significantly different from the wildtype – Δ*aqp1* and Δ*aqp3* (p=0.01 and p=0.036) - with Δ*aqp1* growing significantly more than Guy11 and Δ*aqp3* significantly less. This pattern is replicated on minimal medium but only Δ*aqp3* is significantly different from the wildtype (p=0.016). Photographs of 10-day old CM plates with representative images of Guy11, Δ*aqp1* and Δ*aqp3* are shown in Figure 4.22.

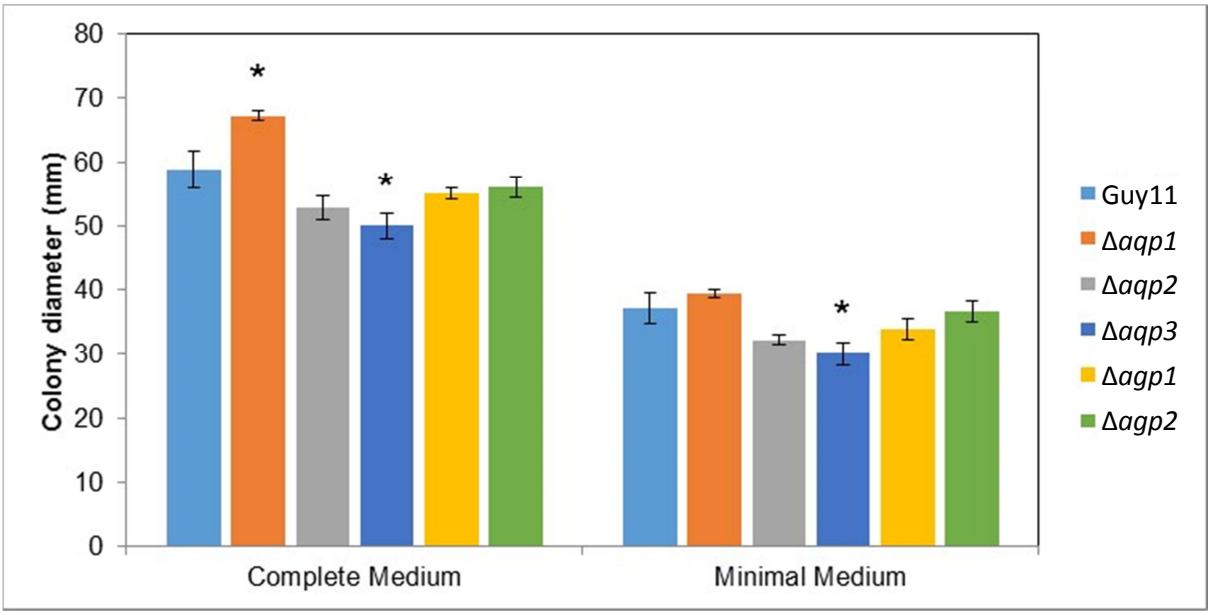

Figure 4.21: Plate growth assays of wildtype Guy11 and aquaporin knockout strains on complete medium (CM) and minimal medium (MM). *Conidia were extracted from 10 day old CM plates and adjusted to a concentration of 2.5x10^5 spores per ml. One hundred microliters of spore suspension was pipetted onto each plate and plates were incubated at 24^{o}C under a 14h/10 h light/dark regime for 10 days. Each experiment represents the mean of two technical replicates and four biological replicates. p-values for the difference on CM between* Guy11 *and* Δaqp1, Δaqp2, Δaqp3, Δagp1 *and* Δagp2 = *0.011, 0.189, 0.036, 0.235, 0.306. For MM, p-values = 0.250, 0.250, 0.016, 0.123, 0.779. Error bars represent the standard deviation (n=3).*

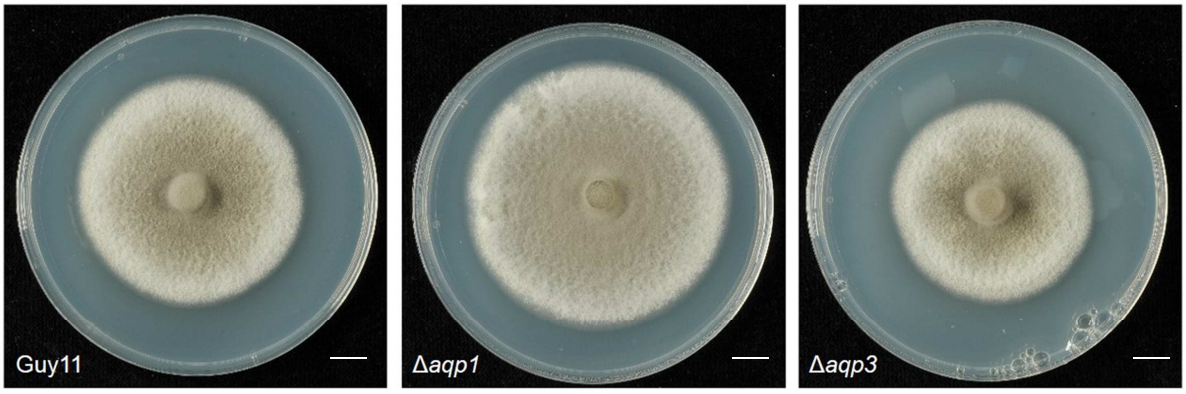

Figure 4.22: Growth of Guy11,* Δaqp1 *and* Δaqp3 *on CM 10dpi. *Eight millimeter mycelial plugs from the growing edge of a CM plate of each genotype were put on a new CM plate and grown in the dark at 24°C for 10 days. Scale bars represent 1 cm.*

4.4.6.2 Deletion of aquaporin genes does not substantially affect tolerance to osmotic stress

Increasing the concentration of osmolytes in the external environment leads to significant physiological changes to maintain osmotic balance. The loss of aquaporin channels may alter the ability of *M. oryzae* to tolerate hyperosmotic stress. I tested the ability of *M. oryzae* aquaporin deletion strains to tolerate hyperosmotic stress induced by four different osmolytes - sorbitol, glycerol, NaCl and glucose. The growth of Guy11 and each aquaporin knockout strain was

measured on CM plates supplemented with a concentration range of each osmolyte. An ANOVA was used to combine the data and test for a statistically significant difference between the wildtype and each mutant strain across the concentration range, thereby reducing the incidence of spurious significant results.

The results for plate growth on medium supplemented with sorbitol, glycerol, NaCl and glucose are in Figure 4.23, Figure 4.24, Figure 4.25 and Figure 4.26. No single gene is statistically different from Guy11 across all hyperosmotic stress conditions. Only Δ*aqp1* under glycerol and glucose stress, and Δ*aqp3* and Δ*aqp2* under NaCl stress are significantly different (p<0.05) from Guy11. However, all tests were done on CM medium, and under almost all conditions, Δ*aqp1* grows more than the wildtype and Δ*aqp3* grows less than the wildtype. If this difference in underlying growth rate on CM is eliminated, the statistical significance of differences between the wildtype and Δ*aqp1* and Δ*aqp3* disappear. The only remaining significant effect is that of NaCl stress on Δ*agp2*. Images of Guy11 and Δ*agp2* NaCl plates are shown in Figure 4.27. The strength of this effect across the concentration range can be examined using Student's T-test. At 100 mM, the difference between Guy11 and Δ*agp2* is non-significant (p=0.522). However, at 500 mM and 1 M the difference is highly significant (p<0.0001). Whilst the effect may be significant, the magnitude of the change is quite small. The mean colony diameter at 500 mM NaCl is 43.1 mm for Guy11 and 38.0 mm for Δ*agp2*. At 1 M, the mean colony diameters are 27.3 mm and 18.9 mm respectively.

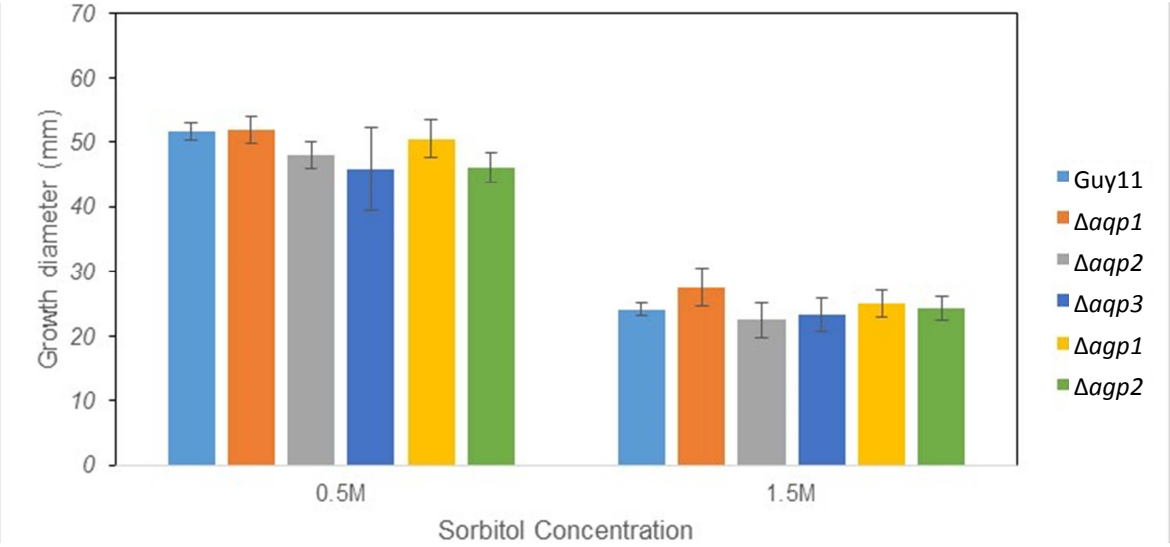

Figure 4.23: Plate growth assays of wildtype Guy11 and aquaporin knockout strains on CM supplemented with sorbitol. *Eight millimetre mycelial plugs, taken from the growing edge of a 10-day old CM plate, were placed on CM plates supplemented with sorbitol (0.5M – 1.5M). Plates were incubated at 24^{o}C in the dark for 10 days. Each experiment represents the mean of two technical replicates and four biological replicates. p-values for the difference between Guy11 and*

Δaqp1, Δaqp2, Δaqp3, Δagp1 *and* Δagp2 *are 0.0778, 0.1771, 0.0871, 0.8899 and 0.4572 Error bars represent the standard deviation (n=4).*

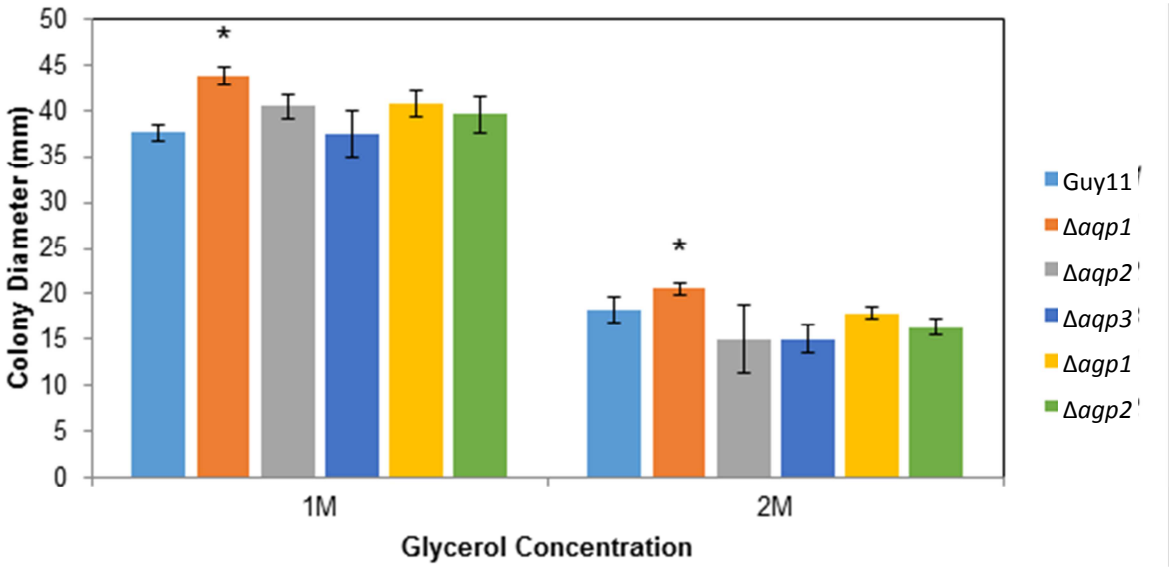

Figure 4.24 Plate growth assays of wildtype Guy11 and knockout strains on CM supplemented with glycerol. *Eight millimetre mycelial plugs, taken from the growing edge of a 10-day old CM plate, were placed on CM plates supplemented with glycerol (1 M – 2 M). Plates were incubated at 24°C in the dark for 10 days. Each experiment, with the exception of the Guy11 1 M value, represents the mean of three technical replicates and three biological replicates. Guy11 1 M represents the mean of four biological replicates with two technical replicates (n=4). Combined p-values for the difference between Guy11 and* Δaqp1, Δaqp2, Δaqp3, Δagp1 *and* Δagp2 *are* <u><.0001</u>*, 1.00, 0.0702, 0.1409, 0.150. Error bars represent the standard deviation (n=3).*

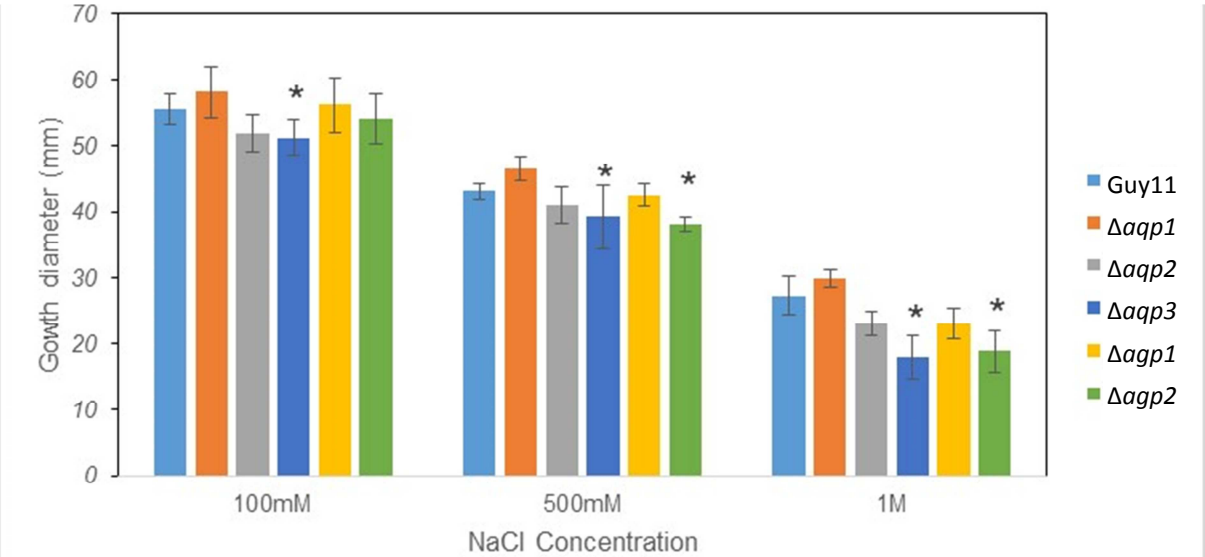

Figure 4.25: Plate growth assays of wildtype Guy11 and aquaporin knockout strains on CM supplemented with NaCl. *Eight millimetre mycelial plugs, taken from the growing edge of a 10-day old CM plate, were placed on CM plates supplemented with NaCl (100 mM – 1 M). Plates were incubated at 24°C in the dark for 10 days. Each experiment represents the mean of two technical replicates and four biological replicates. A two-way ANOVA with independent samples was used to compare the 'strain' effect across all NaCl concentrations. p-values for* Δaqp1, Δaqp2, Δaqp3, Δagp1 *and* Δagp2 are 0.889, 0.1617, <u>0.0199</u>, 0.1085 and <u>0.0002</u> respectively. *Error bars represent the standard deviation (n=4).*

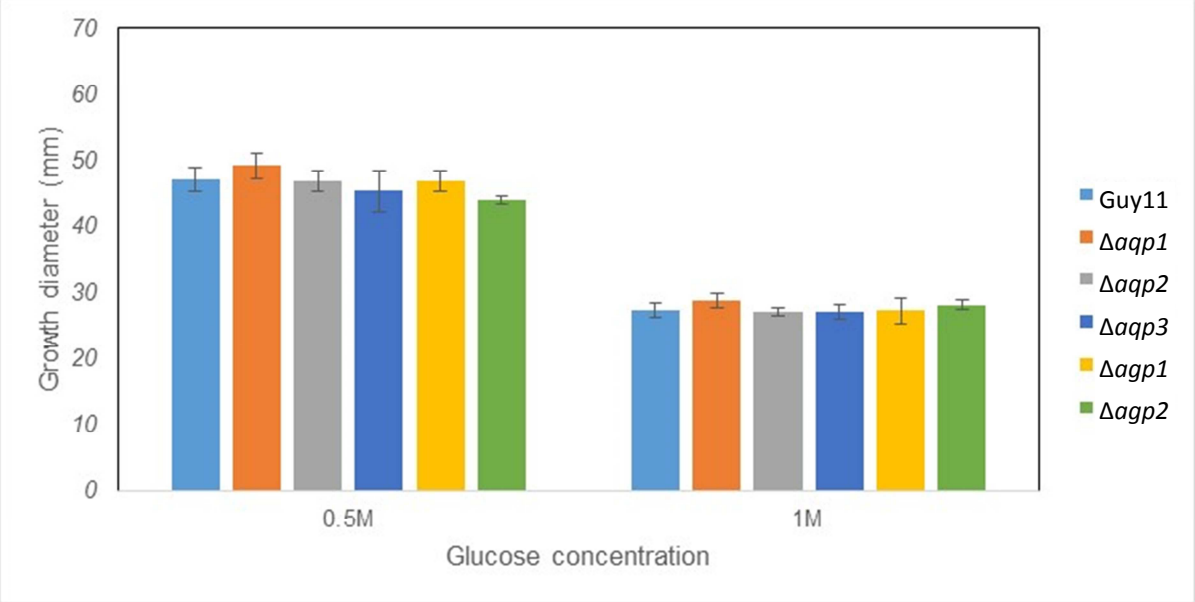

Figure 4.26: Plate growth assays of wildtype Guy11 and aquaporin knockout strains on CM supplemented with glucose. *Eight millimetre mycelial plugs, taken from the growing edge of a 10-day old CM plate, were placed on CM plates supplemented with glucose (0.5 M to 1 M). Plates were incubated at 24°C in the dark for 10 days. Each experiment represents the mean of four biological replicates and two technical replicates. P-values are 0.0617, 0.7148, 0.8268, 0.3108 and 0.0696. Error bars represent the standard deviation (n=4).*

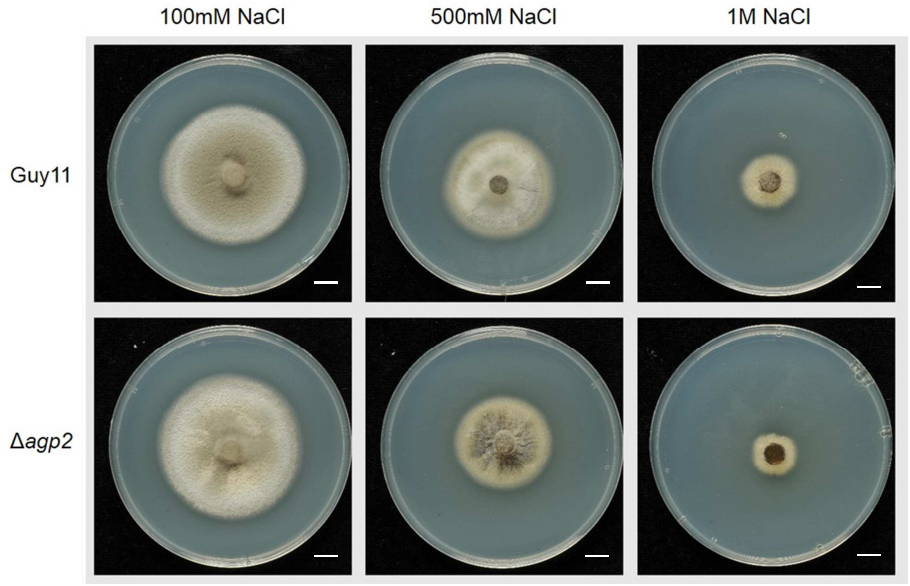

Figure 4.27: Growth of Guy11 and Δagp2 on CM supplemented with NaCl (100 mM – 1 M). *Eight millimetre mycelial plugs of each genotype were put on a CM plate with NaCl and grown in the dark at 24°C for 10 days. Scale bars represent 1 cm.*

4.4.6.3 pH stress

Complete Medium, the optimised high nutrient medium used for routine subculturing of *M. oryzae* is pH adjusted to 6.5. I cultured Guy11 and aquaporin knockout lines on agar plates adjusted to

pH 4 and pH 10 to determine if the aquaporin deletions affected the ability of *M. oryzae* to tolerate non-optimal pH conditions. As shown in Figure 4.28, the growth of knockout strains on high or low pH medium does not differ significantly from the wildtype Guy11 ($p>0.05$).

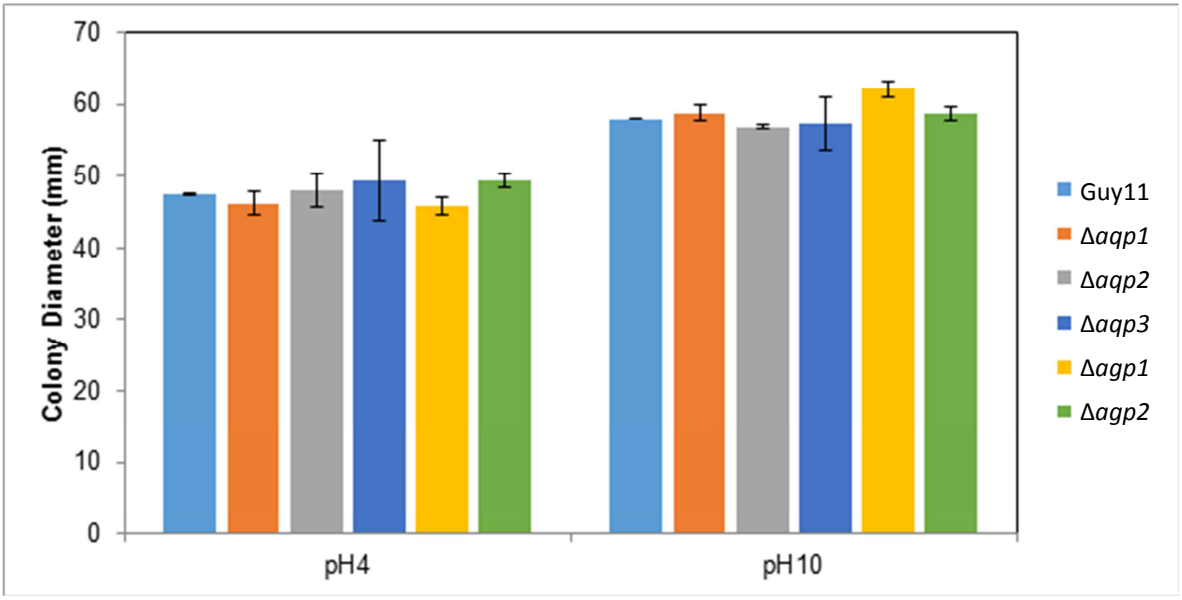

Figure 4.28: Plate growth assays of wildtype Guy11 and aquaporin knockout strains on CM supplemented with sorbitol. *Eight millimetre mycelial plugs, taken from the growing edge of a 10-day old CM plate, were placed on CM plates supplemented with sorbitol (0.5 M – 1.5 M). Plates were incubated at 24^{o}C in the dark for 10 days. Each experiment represents the mean of three technical replicates and two biological replicates. P-values at pH 4 for the difference between Guy11 and* Δaqp1, Δaqp2, Δaqp3, Δagp1 *and* Δagp2 *are 0.455, 0.815, 0.726, 0.286 and 0.205. p-values at pH 10 are 0.500, 0.090, 0.844, 0.126 and 0.500. Error bars represent the standard deviation (n=2).*

4.4.6.4 Temperature stress

The growth of Guy11 and aquaporin knockout strains at 30^{o}C is shown in Figure 4.29. Student's T-test indicates that growth of knockout strains on CM at 30^{0}C was not significantly different from the wildtype, with the exception of a significant reduction in growth of Δ*aqp3*. This difference is likely a result of the underlying growth difference on CM medium rather than a temperature-specific growth effect.

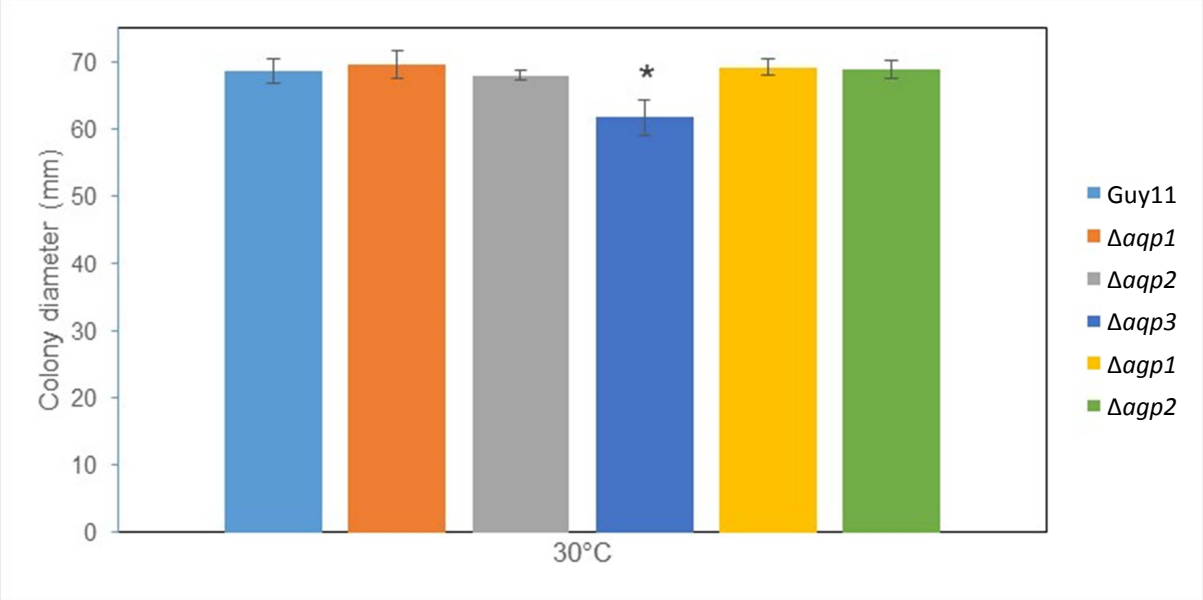

Figure 4.29: Plate growth assays of wildtype Guy11 and aquaporin knockout strains on CM at 30°C. *Eight millimetre mycelial plugs, taken from the growing edge of a 10-day old CM plate, were placed on CM plates and incubated at 30°C in the dark for 10 days. Each experiment represents the mean of three technical replicates and three biological replicates. P-values for the difference between Guy11 and* Δaqp1, Δaqp2, Δaqp3, Δagp1 *and* Δagp2 *are 0.557, 0.707, 0.027, 0.675 and 0.859. Error bars represent the standard deviation (n=3).*

4.5 Discussion

4.5.1 Single aquaporin deletion mutants are fully pathogenic and appear to have normal pathogenic development

Given the importance of osmotic turgor for the initial penetration stage of infection, I conjectured that aquaporin proteins might be involved in penetration, either as facilitators of water or glycerol. Pathogenicity assays on detached leaves from the natural host plant, rice, suggest that single deletions of aquaporin genes do not reduce disease on CO39 rice leaves. Single deletion strains of *M. oryzae* have morphologically normal infection-related development on artificial inductive surfaces and form normal invasion hyphae on onion epidermises. Appressorial turgor is also equivalent in in WT and knockout lines, albeit lower than previously reported results.

The lack of pathogenicity-associated phenotype presents two possible interpretations:

1) The function of aquaporins is not important for pathogenesis, or
2) The role of aquaporins is not detectable using single gene knockouts

A challenge for the study of aquaporins is that phenotypes are often subtle (Carbrey et al. 2001, Yang et al. 2005). Deletion of the single aquaporin ORF in the human pathogenic fungus, *Candia albicans,* had no impact on pathogenesis (Carbrey et al. 2001). As there is only a single aquaporin ORF, aquaporins in *C. albicans* are not essential for pathogenesis under the conditions tested; however, the infectious development of *C. albicans* and *M. oryzae* are profoundly different.

Different rice cultivars have a broad spectrum of susceptibility to *M. oryzae* infection (Liu et al. 2010). However, in our laboratory setting, 'virulence' is assessed only in the context of a single interaction – the ability of the Guy11 strain to infect CO39 rice. The CO39 is almost universally susceptible to *M. oryzae* isolates that are pathogenic to rice (Farman et al. 2002). Similarly, the Guy11 strain was selected for use partly because it is strongly pathogenic (Leung et al. 1988). It may be that this combination – highly susceptible plant and highly pathogenic fungus – is unsuitable for the analysis of weak effectors of pathogenesis.

Genetic redundancy is a severe limitation to studying large gene families with a hypothesis-driven reverse genetics approach. Duplicate genes and paralogous gene families are widely perceived to be sources of genetic resilience, under the assumption that functional redundancy protects against mutation (Gu et al. 2003). Yet this suggests that redundancy should be inherently unstable (Lynch and Conery 2000). Indeed, the *M. oryzae* pseudogene *MGG_10783* (*psAQP*) - a close paralog of *AQP3* (*MGG_13332*) – is no longer maintained by selection pressure and is degenerating.

The numerous reports of functionally overlapping gene families that have been conserved over extended evolutionary periods suggest that there must be a functional benefit to redundant gene families. An interesting example is the conservation of two 1,3-β-glucan synthase catalytic subunit genes *Fks1* and *Fks2* in all but one of 12 studied yeast species (Leon et al. 2002). The two genes are partially redundant, but deletions of both are synthetically lethal, as is the deletion of the single copy in *Yarrowia lipolytica* – the only yeast strain with a single copy. Interestingly deletion of *FKS1* induced transcriptional up-regulation of *FKS2.* It may be the case that transcriptional regulatory feedback circuits also operate between aquaporin genes in *M. oryzae* – a question that will be addressed in chapter 5.

4.5.2 Deletion of Δ*aqp1* and Δ*aqp3* may affect vegetative growth

On CM agar plates Δ*aqp1* grows significantly more than Guy11, and Δ*apq3* grows significantly less. This difference is observed across a wide variety of growth conditions and appears to be robust through repeated subculture of the strains (data not shown). However, in the absence of a recomplemented strain it is impossible to determine if this is due to the specific deletion of aquaporin strains. As the transformation construct is present only as a single copy in the genome, ectopic integration and disruption of another gene can be ruled out. However, we cannot discount the possibility that this change is due to random effects elsewhere in the genome. I initially planned to generate recomplementation strains with C-terminal eGFP tags. However, as discussed in chapter 7, this was fraught with problems. If the effect really is due to the effect of aquaporins it is possible to speculate as to why deletion of aquaporins might cause changes in radial growth. In both cases, the magnitude of the change is very small – less than 10 mm in all assays.

It is currently thought that the engine of mycelial growth is cytoskeleton-based polar exocytosis at the hyphal tip combined with turgor pressure that pushes the cytoplasm against the flexible wall of the tip (for a review, see Lew (2011)). Changes in cellular pressure and volume will depend on the rate of water flow across the cell membrane. This implies that the hydraulic conductivity of the membrane could determine the rate of growth – fast volume changes require rapid water flow across the membrane to maintain turgor for tip expansion. Assuming that the primary function of at least some fungal aquaporins is for water flow facilitation, there must be incidences where membrane water flux is limiting. Therefore deletion of *AQP* genes in *M. oryzae* may alter mycelial growth by changing the interplay between apical turgor and vesicle deposition.

Neurospora crassa has a single *AQP*-encoding ORF in the genome. Comparisons of hyperosmosis-induced hyphal volume shrinkage and hypoosmosis-induced tip lysis in *N. crassa* Δ*aqp* deletion mutants does not support the hypothesis that turgor regulation in hyphal tips requires aquaporins (D. McClure and M. Lim, unpublished observations). Deletion of this gene does not alter the shrink/lysis dynamics of *N. crassa* hyphal tips, indicating that during tip expansion water flows freely into (and out of) hyphal tips in the absence of aquaporins.

Whilst the Δ*aqp1* and Δ*aqp3* growth phenotypes are statistically significant, the magnitude of the effect is small. The possibility that these differences are not due to the deletion of aquaporins also cannot be discounted. Therefore any future work should prioritise the generation of recomplementation strains for these genes.

4.5.3 *AGP2* may be affected by the ion detoxification process

The growth of Δ*agp2* lines on NaCl-supplemented CM plates was reduced compared with Guy11. *M. oryzae* appears tolerant of NaCl stress at 100 mM; growth of all strains is not reduced compared with normal CM medium. However, growth of Δ*aqp2* is reduced relative to Guy11 at 500 mM and significantly reduced at 1 M NaCl. The Δ*agp2* strain is only 88% of wildtype levels at 500 mM and 67% of wildtype levels at 1 M NaCl.

This putative phenotype is somewhat cryptic, given that it does not manifest under other osmotic stress conditions. The effect might be induced by ion imbalances rather than osmotic stress. It may be the case that Agp2 is directly or indirectly involved in ion detoxification and its deletion reduces the effectiveness of this process. However, given the small magnitude of the change, the possibility that this is a type I statistical error (a ‘false positive’) remains, as does the possibility that the effect is not caused by the gene deletion, but rather an unknown clone-specific change.

4.5.4 The split marker deletion strategy is not more effective in the Guy11 background

The use of ‘split’ antibiotic resistance markers has been hypothesised to reduce the incidence of ectopic integration of DNA constructs. Whilst this appears to be the case in the Δ*ku70*/Δ*ku80* strains of *M. oryzae*, it does not apply in the Guy11 strain. This thesis used both the ‘split’ and ‘whole’ marker techniques to delete genes in the Guy11 background. In both cases, a single, homologous integration event occurred in 5-7% of colonies with the resistance marker

For split marker deletions, this suggests that the two halves of the marker must integrate ectopically together. This could occur in two ways. First, one half could integrate randomly and ‘recruit’ the second half which integrates homologously. Or, recombination and integration could occur simultaneously.

The ‘whole’ marker is easier to construct and prepare for transformation. Given that there is no apparent benefit to using the ‘split’ marker approach in Guy11, future work should consider using the whole marker approach unless working an NEHJ-impaired line.

Chapter 5 Genetic redundancy among aquaporins

5.1 Introduction

This chapter considers possibility of genetic redundancy amongst aquaporins in *Magnaporthe oryzae* and discusses reasons for their apparent dispensability. The principles behind qRT-PCR as a tool for uncovering compensatory genetic changes in single deletion mutants are explored. Using this technique, the incidence of compensatory gene regulation in *M. oryzae* single aquaporin deletion strains is investigated.

5.1.1 Redundancy in gene families

A widely-used strategy to understand the functioning of complex genetic systems is to perturb components and characterise the response. However, efforts in *Saccharomyces cerevisiae* to systematically delete all protein coding genes have yielded the surprising result that only ~18% of genes are essential for growth on rich glucose medium (Giaever et al., 2002). Similar experiments in *Caenorhabditis elegans* and *Bacillus subtilis* suggest that only 6-19% of genes are essential (Kamath et al., 2003, Kobayashi et al., 2003). Viable knockouts can even be obtained in the bacterium *Mycoplasma genitalium,* which has as few as 480 protein coding genes (Dhandayuthapani et al., 1999).

Comparative experiments between *S. cerevisiae* and the distantly-related yeast species, *Schizosaccharomyces pombe,* show that gene dispensability is highly conserved. Around 83% of genes essential for germination and colony formation, under standard laboratory conditions, are essential in both species (Kim et al., 2010). Analysis of the Gene Ontology (GO) terms in these

essential gene sets shows significant enrichment for core processes such as cellular biosynthesis (ribosome assembly, transcription initiation and translation) and macromolecular (protein, RNA, DNA and lipid) metabolism. Both budding and fission yeast essential genes are more likely to be present as a single copy (Winzeler et al., 1999) Conversely, non-essential genes are more likely to be present in multiple copies, and analysis of the GO term enrichment suggests roles in regulatory functions (cell communication and control of gene expression), and condition-specific processes such as stress response, transmembrane transport and meiosis.

There are three prevailing models that aim to rationalise the low level of lethality in genomes (Stein & Aloy, 2008)

1) Gene backup by paralogous partners
2) Environmental robustness
3) Genetic buffering

The first explanations for the prevalence of gene dispensability centred on the widespread presence of paralogs. It has been proposed that the presence of functionally overlapping paralogs introduces genetic robustness, as one paralog can substitute for the other in the event of sister gene inactivation (Gu et al., 2003). Yet this implies that the paralogous duplicate would be evolutionarily unstable as the duplicate function is masked from positive selection pressure, and there are many examples of paralog silencing (Lynch & Conery, 2000). Indeed, *MGG_10783 is* a recent duplicate of *AQP3* and appears to be in the process of degeneration (see chapter 3). Retention of truly redundant paralogs might be selected on the basis of tertiary network robustness. However, whilst this kind of network-level selection has been proposed, the evidence supporting it is weak (Wuchty et al., 2003)

Given the numerous examples of non-essential genes being retained for long evolutionary distances (see Nowak et al. (1997) for examples), two alternative models have been proposed. The idea that genes might be essential – but not under standard laboratory conditions – has been extensively studied. Analysis of metabolic networks in yeast indicate that this, so-called ‘environmental robustness’, could account for 37-68% of the dispensable metabolism genes (Papp et al., 2004). Chemical stress assays, in which every non-lethal deletion mutant in the haploid

single deletion collection (~5000 strains), was subjected to a battery of 726 different stress conditions were able to discover a measurable growth phenotype in 97% of gene deletions (Hillenmeyer et al., 2008).

Although we were not able to test 726 different conditions, in chapter 4 we aimed to test the effect of gene deletions on growth under a subset of stress conditions. There were no strong growth phenotypes, but there the third model for the widespread retention of functionally overlapping nonessential genes might explain the absence of a compelling phenotype. It has been proposed that regulatory systems exploit redundancy to achieve regulatory precision as so-called 'responsive backup circuits' (RBCs) (Kafri et al., 2006). This idea is based on the observation that paralogous pairs of genes, each of which have a neutral or very weak phenotypic effect when deleted, display multiplicative defects when deleted together. There are now many examples in the literature of RBCs in diverse organisms where a duplicate gene is up-regulated when its paralog is silenced (Zartman et al., 2008, Svenningsen et al., 2009). It has been proposed that under normal cellular conditions, this kind of feedback loop is a sophisticated device to achieve regulatory precision, by filtering nongenetic noise from transcriptional pathways (Kafri et al., 2006).

The features of the aquaporin gene family in *M. oryzae* – a large number of membrane transport proteins – supports our finding that these genes are nonessential. The absence of a strong phenotype could be caused by two factors discussed in this chapter – that the phenotypes may not manifest under the conditions tested or there may be RBCs that operate to nullify the effect of single aquaporin gene deletions. Developing an assay that would allow us to detect backup activity in the Δ*aquaporin* deletion lines, would provide an insight into the regulation of these proteins. As double knockouts of paired RBC genes often have very strong phenotypes, it might also suggest which combinations of genes should be knocked out in combination (DeLuna et al., 2010)

5.1.2 qRT-PCR

qPCR can be a very accurate and sensitive tool for measuring gene expression levels. Relative quantification, described in detail in chapter 3, measures the abundance of a target cDNA molecule relative to the abundance of stably transcribed housekeeping genes (HKGs) (Karlen et al., 2007,

Pfaffl & Hageleit, 2001). These numbers are calculated using the cycle threshold (C_T) at which the fluorescence level of a DNA-intercalating fluorescent dye reaches a specific threshold. The ratio between these two measurements can be described with the equation

$$r_1 = \frac{T_0}{R_0} = \frac{{}^{T}C_T T.E_T^{-C_T T}}{{}_{R}C_T R.E_R^{-C_R R}} = k.\frac{E_T^{-C_T T}}{E_R^{-C_R R}} \quad (1)$$

where T_0 is the initial number of target mRNA molecules, R_0 is the initial number of reference mRNA molecules, E describes the amplification efficiency of the target amplicon and k is an error constant that depends on various factors. These include the type of reagents, the size and sequence of the PCR products, and the fluorescence threshold (Livak & Schmittgen, 2001).

The constant k can be eliminated by normalisation against a calibrator sample (Pfaffl, 2001). In most experiments, the calibrator sample is an untreated control, but could also be a reference sample that is included in all runs depending on the experimental set up. The relative expression r_2 of the target gene in the sample relative to the calibrator can then be calculated by:

$$r_2 = \frac{\frac{T_0}{R_0}}{\frac{T_{0\,cal}}{R_{0\,cal}}} = \frac{k.\frac{E_T^{-C_T T}}{E_R^{-C_R R}}}{k.\frac{E_T^{-C_T T\,cal}}{E_R^{-C_R R\,cal}}} = \frac{E_T^{-C_T T\,cal - C_{tT}}}{E_R^{-C_T R\,cal - C_{tR}}} \quad (2)$$

This final simplification, known as the Pfaffl ratio, is the basis of most relative quantification work.

5.1.2.1 qRT-PCR as a tool for detecting redundancy

In a large scale study on RBCs in yeast, DeLuna et al. (2010), screened paralogous pairs of genes in yeast for evidence of RBC activity. On a 32-pair subset of genes displaying RBC activity at the protein level, they tested the transcriptional responsiveness of the paralogs to deletion of the other member using qRT-PCR. The majority (25/32) genes displayed compensatory changes at the mRNA level. This suggests that both translational and posttranslational regulation are active in RBCs, but that qRT-PCR is an appropriate tool for investigating compensatory changes in gene families.

5.1.2.2 Experimental design

In its simplest form, the question of whether reciprocal compensation occurs between a pair of genes can be addressed with four pieces of information: the abundance of Gene 1 mRNA, in the wildtype and in the Δ*gene 2* background, and the abundance of Gene 2 mRNA, in the wildtype and

in the Δ*gene 1* background. From this, a ratio of expression can be calculated which, if no compensation is occurring, will be 1. Conversely, if compensatory up-regulation is occurring then the expression of a gene in its paralogous deletion-background will be higher than in the wildtype, therefore the ratio will be greater than 1. The calibrator sample described in equation (5) would therefore be gene expression in Guy11.

With five functional aquaporin genes in *M. oryzae*, compensation can be detected by comparing the expression of each gene in each mutant background to the expression of those same genes in Guy11. This is the basis of the experiments described herein.

Analysis of 202 paired paralogous genes in yeast found that the activity of RBCs was strongly "needs-based", with compensation only occurring when the function of the gene pair was important (DeLuna et al., 2010). For example, single deletion strains of the amino acid biogenesis gene pair *LYS20* and *LYS21* are viable in the absence of exogenous lysine. However, double deletions are lethal in medium lacking lysine (Quezada et al., 2008). The same is true for paired deletions of *ASN1/ASN2* or *SER/SER33*, encoding pairs of asparagine and serine biosynthesis genes respectively (Dang et al., 1996, Jones, 1978). DeLuna et al. (2010) demonstrated that the ability of the pair to functionally compensate results from up-regulation of the remaining gene upon the deletion of the partner. However, this effect is not constitutive, and is only observed in medium lacking the amino acid in question. This suggests that RBCs may only be detectable when the genes in question are important.

Not all aquaporin genes in *M. oryzae* may be functionally important under a single developmental condition. In order to uncover any nonconstitutive RBCs between aquaporin genes, we will test for compensation at four distinct developmental stages. These are:

i) Developing germ tubes

ii) Developing appressoria

iii) Mature appressoria

iv) Liquid mycelial cultures in complete medium

Although this does not cover the full range of developmental conditions, it provides a snapshot of gene expression during pathogenesis-related development and mycelial culture. The number of

developmental conditions tested is limited by the extreme labour intensiveness of tissue collection and sample preparation.

Using qRT-PCR as a tool, we aim to measure, for all aquaporins in all mutant backgrounds, the ratio between aquaporin expression in the mutant background and expression the wildtype. To control for inherent biological variability and reduce the accuracy and specificity of the measurement, two technical replicates per C_T value and two full biological replicates were carried out. A work-flow diagram of the experimental set up, together with an overview of the data analysis steps is shown in Figure 5.1.

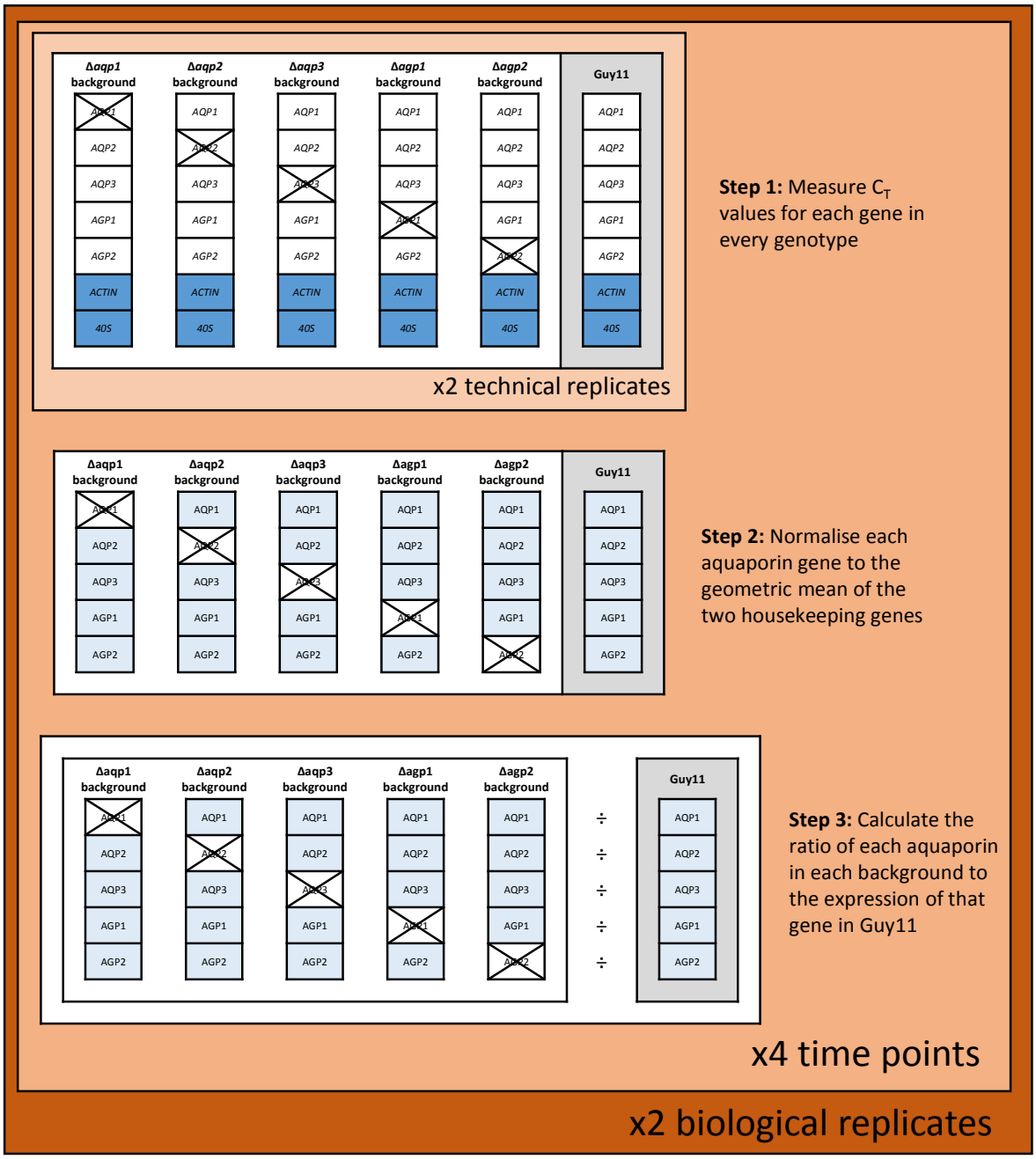

Figure 5.1: A diagrammatic overview of the major steps involved in characterising transcriptional redundancy among aquaporins in M. oryzae.

5.2 Experimental objectives

1) To examine aquaporin expression in the wild type Guy11 and Δ*aquaporin* backgrounds, using qRT-PCR
2) To calculate a ratio that describes the expression of remaining aquaporins in the Δ*aquaporin* backgrounds relative to the expression of those same genes in Guy11, at the same developmental stage

5.3 Methods specific to this chapter

5.3.1 RNA extraction from Teflon surfaces

The extraction of concentrated, high quality RNA from developing *M. oryzae* germlings from leaves is challenging. The qRT-PCR described in chapter 3 used fungal (and doubtless plant) RNA extracted from barley leaf peels. However, the C_T values obtained from that experiment were higher than is desirable for maximal accuracy. Preparation of samples from host plant peels is slow and requires a great deal of space for growth of plants. With so many independent RNA samples needed for this experiment (48 in total), we decided to use RNA extracted from germlings grown on artificial surfaces.

Published SuperSAGE analysis of developing germlings, extracted tissue from germlings on inductive microscope coverslips glued onto the bottom of square petri dishes (Soanes et al., 2012). We tried to replicate this method and found there to be numerous problems. The tiny quantity of tissue was difficult to scrape from the coverslip without cracking the glass, and the volume of liquid into which the tissue had to be scraped was very large. The large volume of liquid also slowed down the rate of freezing. Damaged cells release RNases, therefore this likely led to significant RNA template degradation. Without easy access to freeze-drying equipment, we were unable to sufficiently concentrate tissue extracted in this manner for RNA extraction.

M. oryzae produces appressoria on a variety of different surfaces. These include the hydrophobic side of GelBond membranes, PTFE (Teflon), polystyrene, Cellophane and paraffin wax (DeZwaan et al., 1999, Heupel et al., 2010). The objective of this experiment required an inductive surface on which germlings develop appressoria over an appropriate time period, and that facilitated easy removal of the germling tissue. With this in mind, we tested the inducibility of cellophane, Parafilm® (a form of paraffin wax) and Teflon. Cellophane, spread over a cutting tile, was found to be inductive over an 8h time course. However, it was impossible to get the surface completely flat and this caused problems with removal when scraping the germlings into liquid nitrogen. Contrary to previous reports we found no appressoria on Parafilm® within 12hpi. It is possible that they take longer to develop; however, felt that this delay was too significant compared to germlings on plants and other commonly used artificial surfaces. Teflon sheets (www.directplastics.co.uk) were found

to be inductive for appressorium formation. Appressoria developed more slowly than on inductive Menzel glass coverslips, but by 7h, fully melanised appressoria were elaborated. Morphology was visually normal, and the germlings were scraped easily from the surface using a razor blade. To speed up the scraping process, spore concentration was adjusted by the OD_{600} rather than using a haemocytometer. At an OD_{600} of 0.250, spores were concentrated enough for the extraction of sufficient tissue, but still developed morphologically normally.

We examined the development of appressoria on Teflon over a 24h timecourse. The optical properties of Teflon made germ tubes difficult to photograph, but by 4h, most spores had germ tubes. By 5h, un-melanised appressoria were visible and by 7h fully melanised appressoria had developed. The development time course is shown in representative images in Figure 5.2. The development time points selected for RNA extraction were

- Germ tubes (3h 45m)
- Un-melanised appressoria (5h)
- Melanised appressoria (7h)
- CM liquid medium

Spores were harvested from 8-12 10-day old CM plates of each genotype and adjusted to an OD_{600} of 0.25. This spore solution was poured onto a Teflon sheet and incubated at 24^{o}C for the requisite time. The liquid was then poured off, and the germlings scraped directly into liquid nitrogen. Samples were be stored at -80^{o}C, or used immediately.

Mycelium was harvested from CM-grown liquid culture, supplemented with 100mg/ml penicillin and streptomycin. Conical flasks with 300ml CM were innoculated with 1ml spore suspension harvested from a 10-day old CM plate, and grown at 24^{o}C in the dark, shaking at 150rpm. After three days, the mycelium was harvested by filtration through a double layer of sterile miracloth, and frozen immediately in liquid nitrogen.

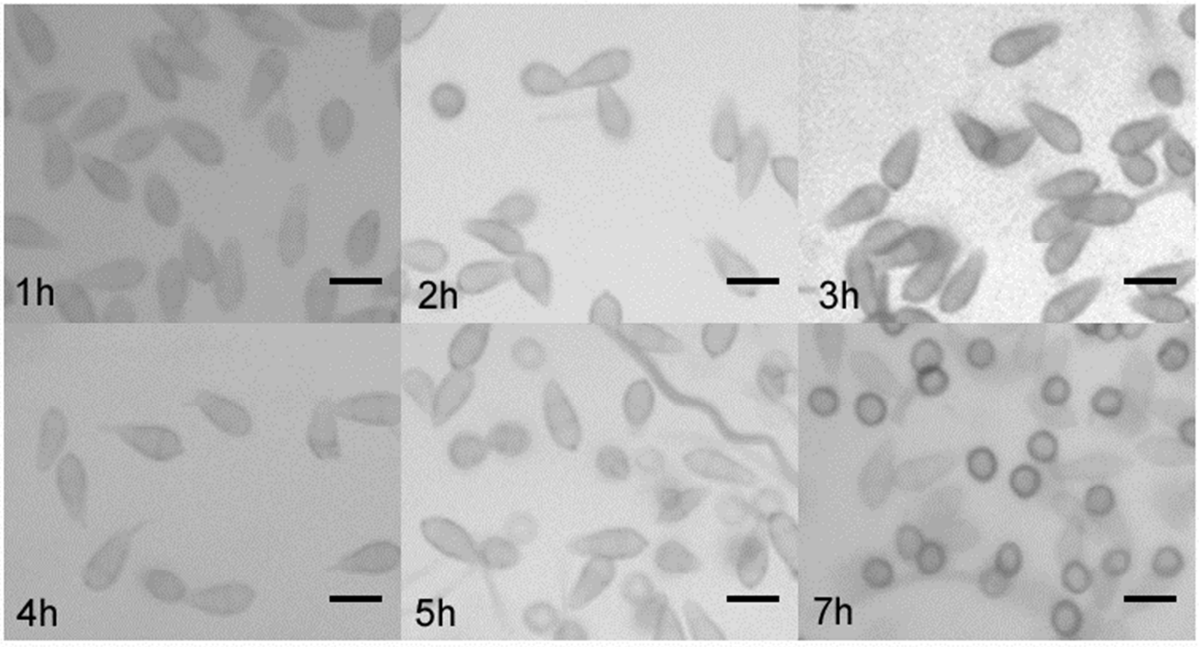

Figure 5.2: Representative images of germlings on Teflon surfaces, 1-7hpi. *Guy11 spores from a 10-day old CM plate were harvested and the concentration was adjusted to OD_{600} 0.250. Scale bars represent 20µm*

5.3.2 qRT-PCR methods in this chapter

RNA for qPCR, was harvested, as described above, and genomic DNA contamination was removed, as described in the Materials and Methods.

The quality of RNA, post gDNA removal, was analysed using an Agilent Bioanalyser. All RNA used in this experiment had a RIN > 8, with most of the samples > 9. RIN. The theoretical maximum RIN is 10.

Randomly-primed cDNA was produced using 500ng RNA per 25µl reaction with a Maxima First Strand cDNA synthesis kit (Thermo Scientific). A 'minus reverse transcriptase' (-RT) control was included for each RNA sample to check for the absence of gDNA.

qPCR primer set 2 was designed as described in the Materials and Methods. *AQ1* was amplified with qPCR1_03904F and qPCR1_03904R, *AQP2* with qPCR2_04162F and qPCR2_04162R, *AQP3* with qPCR2_13332F and qPCR2_13332R, *AGP2* with qPCR2_05880F and qPCR2_05880R, and *AGP2* with qPCR2_13615F and qPCR2_13615R. The two housekeeping

genes, Actin (MGG_03982) and ribosomal 40S (MGG_02872) were amplified with Actin_F and Actin_R, and 40S_F and 40S_R. The two housekeeping genes were selected for their transcript stability over the range of developmental conditions (Che Omar et al., manuscript in preparation). The efficiency of each primer pair was calculated on pooled cDNA from all developmental conditions

Reactions were set up in an ABI Prism 7300 thermal cycler, as described in the Materials and Methods. For each primer pair, a 'no template' control (NTC) was included to check for the presence of primer dimers. All samples for direct comparison were set up on the same plate and analysed using the same settings.

After the thermal cycler run had completed, the controls, melting curves and amplification plots were checked manually and the cycle threshold and baselines were automatically calculated by the ABI software. Where technical replicates varied by greater than 0.75 C_T units, the gene in that background and its Guy11 correspondent were repeated. Ratios were then calculated for that pair separately to control for inter-run variation.

5.4 Results

We aimed to test the hypothesis that deletion of a single *AQP* gene might result in compensatory changes in expression of one or more remaining *AQP* genes in the knockout. We designed an experimental matrix using qRT-PCR, where the transcript abundance of every *AQP* gene, normalised to two housekeeping genes, was measured in each of the five Δ*aquaporin* backgrounds and in the wildtype Guy11 strain. A ratio of the normalised expression of each gene in the Δ*aquaporin* backgrounds against the expression of the same gene in the Guy11 background could then be used to test the hypothesis. If the null hypothesis – that deletion of an *AQUAPORIN* gene does not affect the expression of the remaining family members – is true, the ratio of expression in the knockout background and the Guy11 background would be 1. This experiment was carried out at each of four developmental stages corresponding to:

i) Developing germ tubes

ii) Developing appressoria

iii) Mature appressoria

iv) Liquid mycelial cultures grown in complete medium

5.4.1 The combination of two individual biological replicates

Gene expression analysis by qRT-PCR allows accurate and highly sensitive measurements of gene expression levels (Hellemans et al., 2007). A large body of literature exists on how to reduce the technical variability of the PCR reaction, by including a template normalisation step with multiple stably expressed reference genes, and by correcting for PCR efficiency and inter-run variation (Hellemans et al., 2007, Pfaffl, 2001, Vandesompele et al., 2002). We used the equation derived in Section 5.1.2 to calculate the ratios for each data point. This involved the prior calculation of the primer pair efficiency as described in chapter 2. We normalised each gene to the geometric average of two housekeeping genes in that cDNA sample and controlled for inter-run variation by running all samples to be compared on the same plate.

However, little work has focused on how to adequately combine experimental replicates that vary because of inherent biological variability. We used the data-processing procedure described in Willems et al. (2008). This is based on a series of sequential corrections, including log transformation, mean centring and autoscaling.

Step 1. Log transform the mean normalised C_T values for each biological replicate. This makes the data distribution more symmetric and attributes equal weight to conditions of overexpression and underexpression

Step 2. For all log-transformed normalised relative quantities a_{ij} from n experiments *i* and *m* conditions *j*, calculate μ_i, the mean expression level of all conditions *j,* in experiment *i*

$$\mu_i = \frac{\sum_{j=1}^{m} a_{ij}}{m}$$

Step 3. Calculate σ_i - the standard deviation of the expression across all conditions *j* in experiment *i*

$$\sigma_i = \sqrt{\frac{\sum_{j=1}^{m} (a_{ij} - \mu_i)^2}{m-1}}$$

Step 4. Calculate the mean standard deviation of all experiments as $\overline{\sigma}$

$$\overline{\sigma} = \frac{\sum_{i=1}^{n} \sigma_i}{n}$$

Step 5. Mean centre each replicate experiment by subtracting the mean normalised relative expression level across all conditions in a given replicate experiment from that same experiment. Autoscaling also requires a final correction of the fold change by multiplying the autoscaled fold changes with the mean standard deviation of the replicate experiments before they were autoscaled. This makes the fold change reflect the initial observations, resulting in standardised and fold-change preserved log-transformed relative quantities.

$$a_{ij} = \left(\frac{a_{ij} - \mu_i}{\sigma_i}\right) . \bar{\sigma}$$

Step 6. Statistical significance can determined by calculating the 95% confidence interval for each fold-change calculation.

Performing this transformation on the two complete biological replicates gives the results shown in Figure 5.3. Data is expressed in a ‘per gene’ format rather than a ‘per genotype’ or ‘per time point’ format. This is to facilitate comparison of each gene in each background across multiple time points.

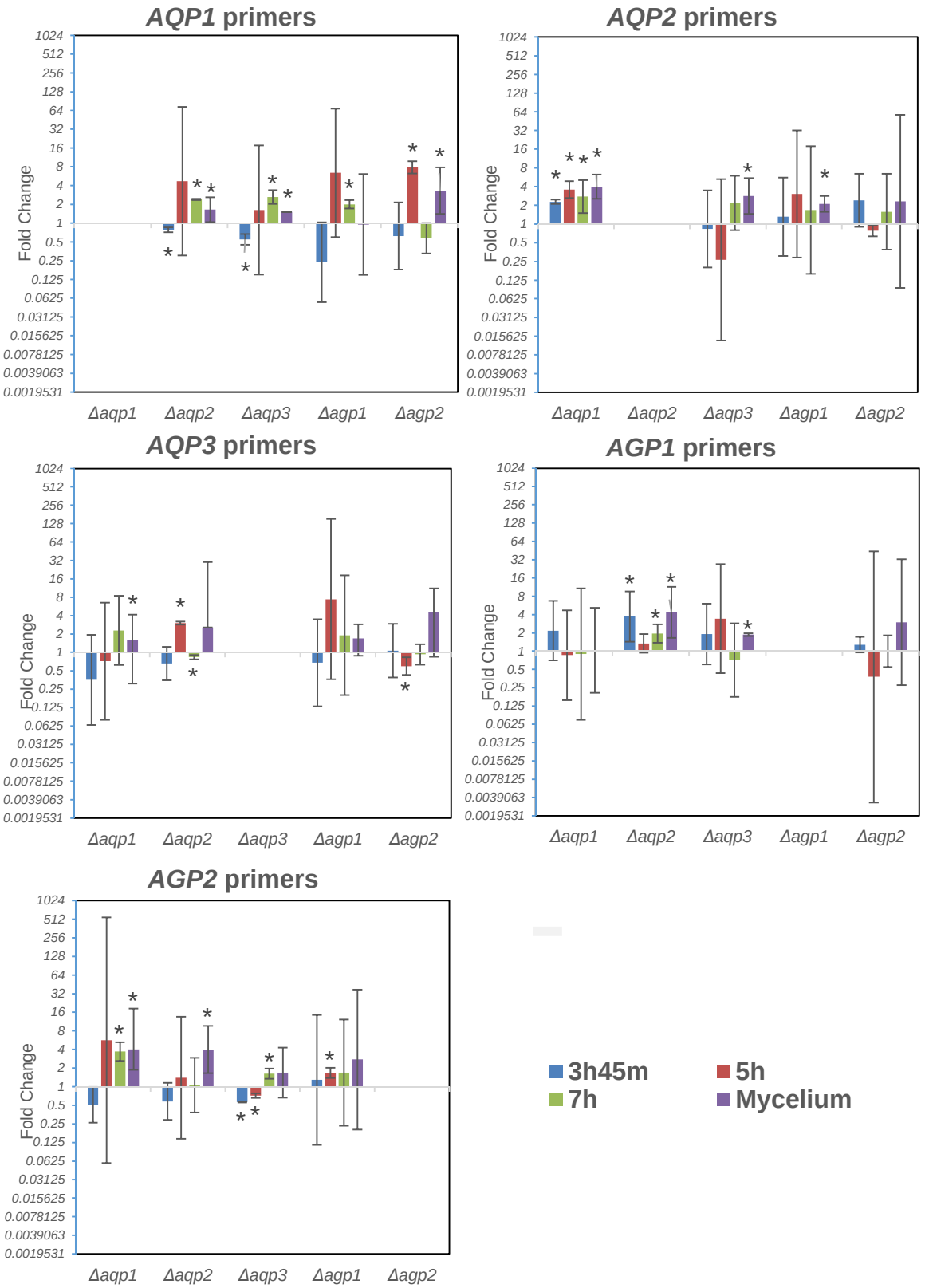

Figure 5.3: The ratio of AQUAPORIN expression in Δaquaporin backgrounds to expression in the wildtype strain, Guy11, across four developmental conditions. Data shows the combination of two experimental replicates. *Data is plotted on a $\log_2$ scale to give equal visual weight to up- and down-regulations. Error bars show the 95% confidence interval. Asterisks indicate statistically significant results*

The dataset is not without problems. Clearly some of the error values are high, and the problem of error propagation in this experiment is discussed in Section 5.5.2.1 in this chapter. However, it is encouraging that most of the data points were non-significant with a confidence interval that includes 1, indicating that the expression in the mutant background is the same as the wild type strain. This is the most parsimonious outcome and suggests that the data are valid.

The significance of the data set can be interpreted in several ways. A strong indicator of compensatory regulation is the consistent, statistically significant up-regulatory change of one or more genes in a single knockout background across all developmental conditions. This occurs in a single case – the 2 to 4-fold up-regulation of *AQP1* in the Δ*aqp2* background. This may be reciprocal, with upregulation of *AQP2* in the Δ*aqp1* background in 3 of 4 developmental conditions. A less stringent test for compensation – upregulation in at least 3 out of 4 developmental conditions, two of which are statistically significant – reveals three possible cases: *AQP2* in the Δ*agp1* background, *AQP1* in the Δ*agp2* background and *AQP1* in the *aqp*3 background.

Identifying compensation by consistent up-regulation across the developmental time course is a simplistic approach. As discussed in Section 5.1.1, compensatory regulation is sometimes only detectable when the gene product is important and the importance of different genes might vary over the developmental time course. Assuming that the importance of a gene might be detectable from a peak in its transcript abundance, an essential factor to consider is the expression profile of these genes over the time course.

The abundance of each transcript, expressed as a percentage of the geometric average of the HKGs, can be used to examine the change in each gene over the four developmental conditions. These relative abundances can only be approximated, because the constant, *k,* derived in Equation 4 in Section 5.1.2, can now no longer be eliminated by normalisation against a calibrator sample and is not necessarily equal to 1. An approximate comparison can still be made, but it should be recalled that the total transcript number required to produce the threshold fluorescence depends on the length of each amplicon which varies between genes. Furthermore, the threshold is set independently between plates, therefore comparisons between timepoints are also only

approximate. The expression in Guy11 of each gene across the four timepoints, expressed as a percentage of the HKGs is shown in Figure 5.4.

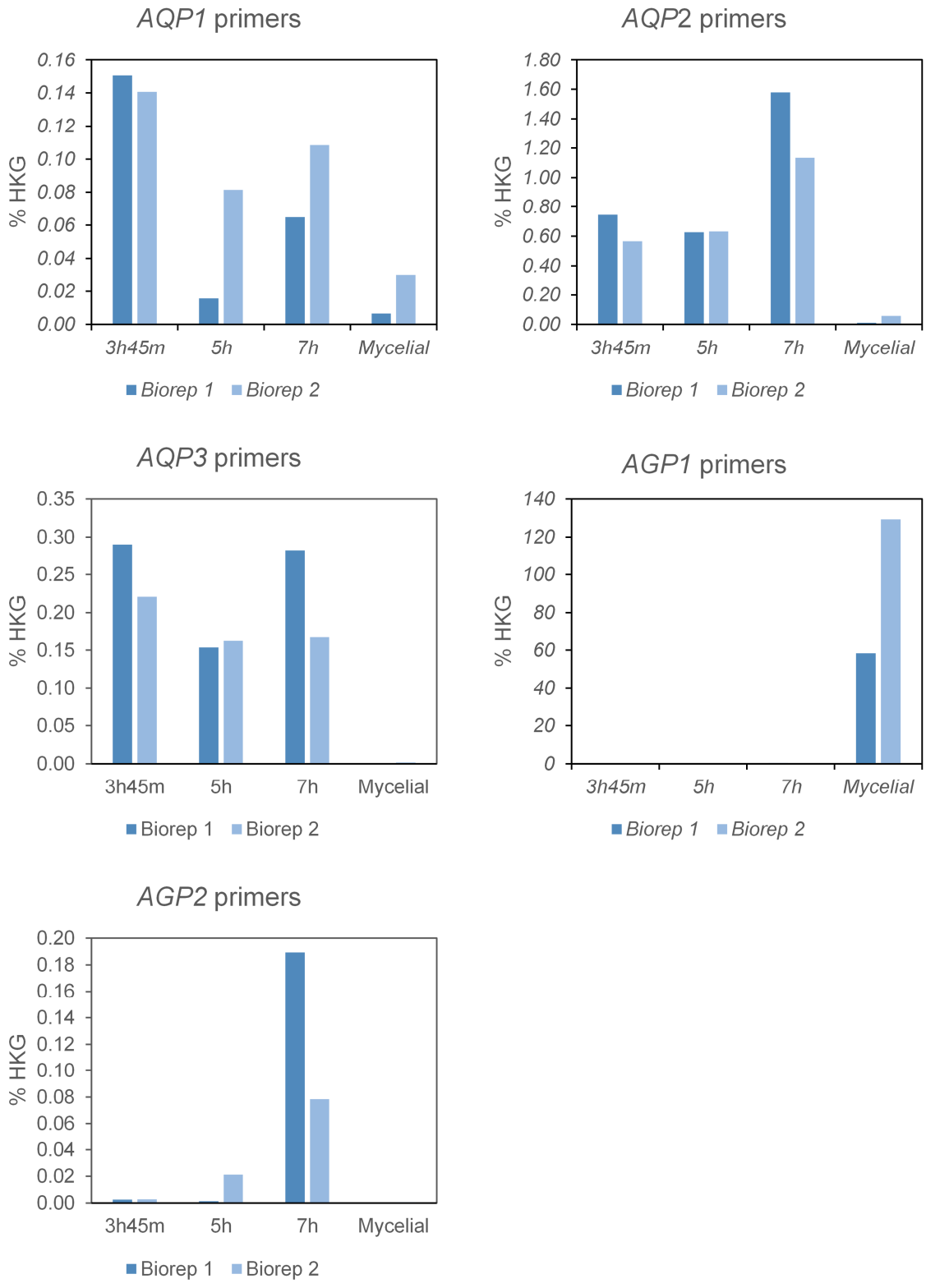

Figure 5.4: Expression of AQUAPORIN genes in the wildtype Guy11 strain, expressed as a percentage of the geometric mean of two housekeeping genes, actin and 40S. *Data from two biological replicates is shown for comparison. Note should be taken of the different axes.*

A comparison of the two biological replicates shows the underlying physiological variability. The broad outline is the same between the two replicates, but the magnitudes are different. This data reveals some interesting patterns. *AQP1, AQP2* and *AQP3* are predominantly expressed in developing germlings, but only at low levels in the mycelium. *AGP2* is expressed at low levels except for in melanised appressoria. *AGP1,* however, is expressed at very high levels in mycelium. The range observed in this experiment (60-120% of the mean expression level of actin and the 40S ribosomal subunit), whilst consistent with previous data (see chapter 3), is genuinely surprising, not only considering that it is a membrane channel protein, but also the lack of an obvious mutant phenotype.

Three genes appear to have 'peaks' at specific timepoints – *AQP2* and *AGP2* at 7hpi, and *AGP1* in mycelia. Assumption that the function of genes may be more significant when they are upregulated, and that compensation occurs when genes are more important, we looked for compensatory changes in these mutant backgrounds at these specific timepoints.

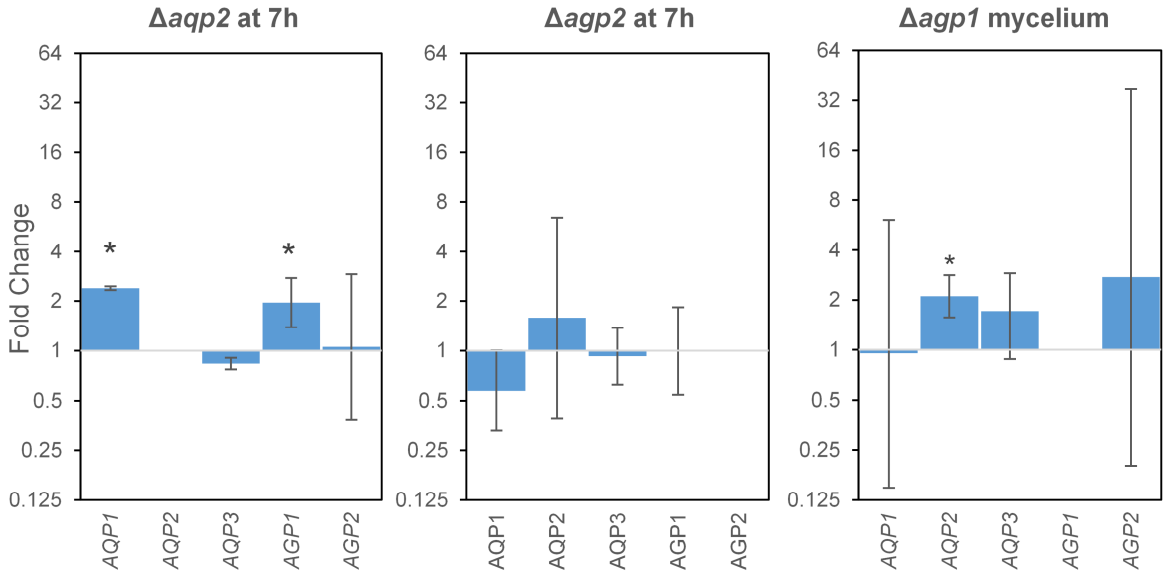

Figure 5.5: The expression of AQUAPORIN genes, relative to expression in the wildtype Guy11 strain, in a subset of genotypes at putatively important time points. Asterisks indicate statistically significant results.

The upregulation of *AQP1* and *AGP1* by about 2-fold in Δ*aqp2* is a statistically significant change. As discussed previously, *AQP1* and *AQP2* might reciprocally up-regulate – therefore the change in expression of *AQP1* is of particular interest.

There is no detectable, significant changes in the Δ*agp2* background at 7h. In the Δ*agp1* mycelium, the *AQP2* gene is potentially upregulated by 2-fold. However, in light of the high abundance of the *AGP1* transcript in mycelia, it seems unlikely that a two-fold upregulation of *AQP2* – a gene expressed at <0.02% of HKG expression in mycelia – could compensate for something with an expression potentially equivalent to the HKGs.

The enormous problem of combining biologically variable replicates means that many researchers simply present a 'representative' data sample (Willems et al., 2008). To validate the combinatorial procedure used above, we can look at the individual biological replicates to see if the same patterns are observed. This approach can also uncover systematic errors – a particular problem in this approach as all genes in a genotype are normalised to a single value, Guy11. If the Guy11 value is erroneously high, the same gene expressed in the mutant backgrounds will universally appear to be downregulated. Examination of the independent replicates can also allow us to check that there are no significant changes that have been lost during the combination of the data sets.

5.4.2 Replicates 1 and 2

The fold-change calculated for each biological replicate, plotted on a $\log_2$ scale to make the data visually symmetric, is shown in Figure 5.6. This data was calculated using equation 5 in Section 5.1.2. The data is displayed on a 'per timepoint' basis to highlight some of the issues with systematic error and high levels of variability, shown clearly in Figure 5.6. For example, in the 3h45m rep1 graph, *AGP2* is approximately four-fold down-regulated in all backgrounds. However, the most parsimonious explanation is that the Guy11 value for *AGP2* at 3h45m in rep1 (the denominator of the ratio calculation) is erroneously high. The same problems are prevalent in the mycelium dataset, particularly in rep 1. The error associated with a qPCR measurement rises as the starting transcript number tends towards zero. With the exception of *AGP2*, C_T values in mycelial extracts are low, therefore the variance of these values is likely to be high. Extreme care should be taken when drawing any inferences the mycelial extract data.

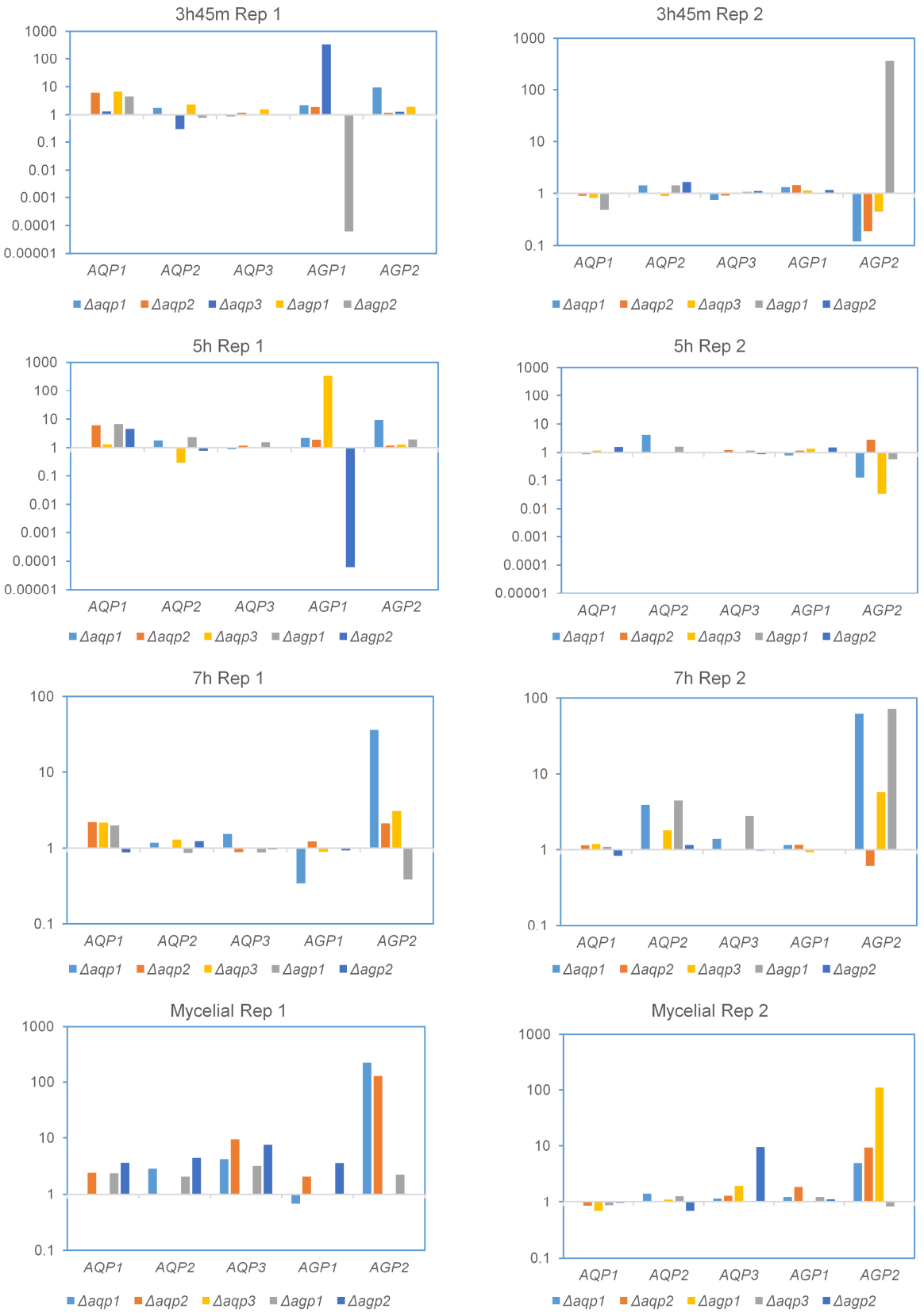

Figure 5.6: Ratio of each gene at each developmental time point, relative to the expression of that gene in Guy11. Data is plotted on a log_2 scale and each data point represents the mean of two technical replicates. Expression is normalised to the geometric mean of two housekeeping genes.

If the data is reoriented and displayed in the same manner as the combined data in Figure 5.3, it is possible to compare the individual biological replicates in the same manner as the combined data. The two biological replicates are shown side-by-side in Figure 5.7.

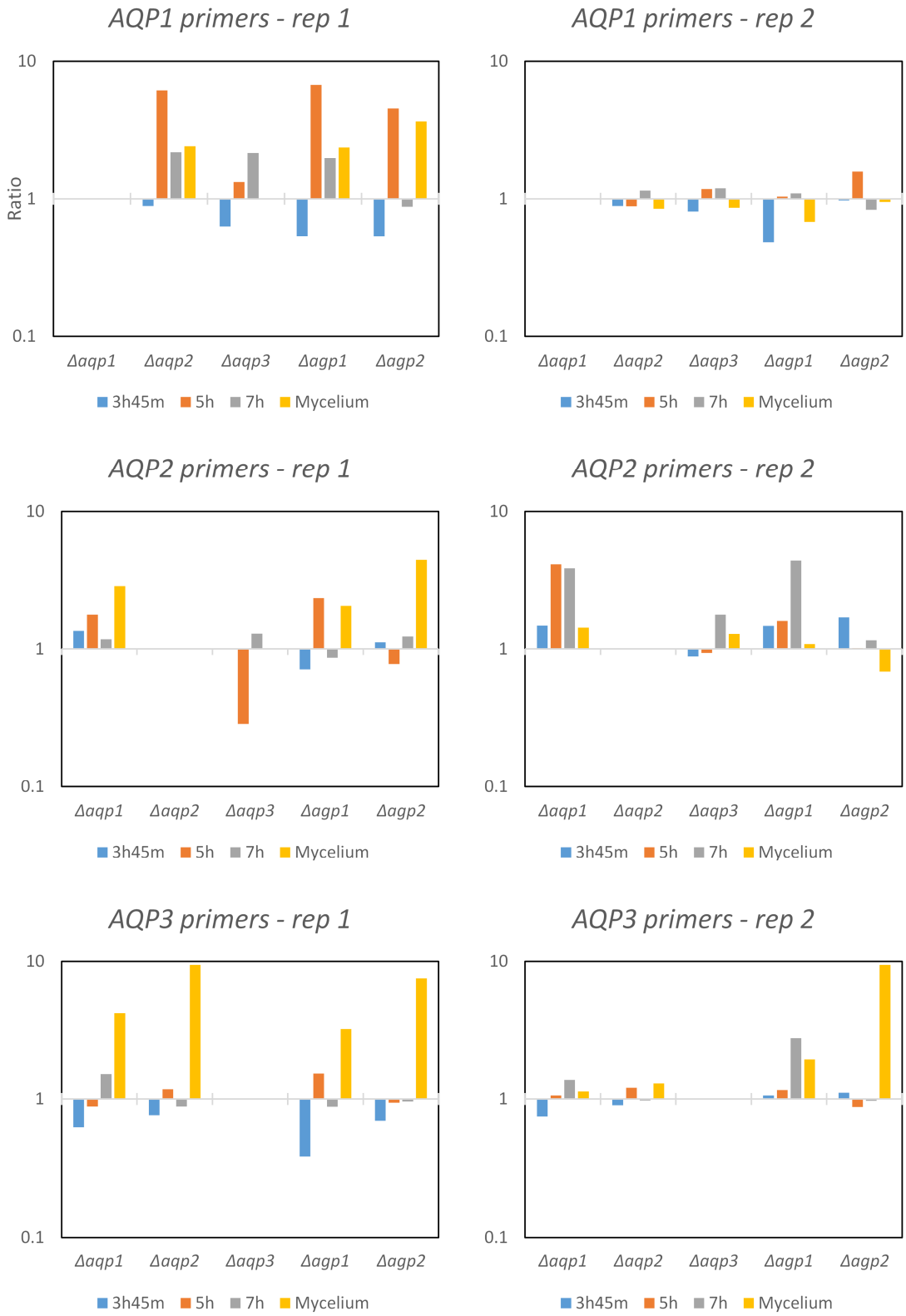

Figure 5.7 Part 1: The ratio of normalised gene expression in Δaqp backgrounds to the normalised expression of the same gene in the Guy11 background. Data shows two biological replicates.

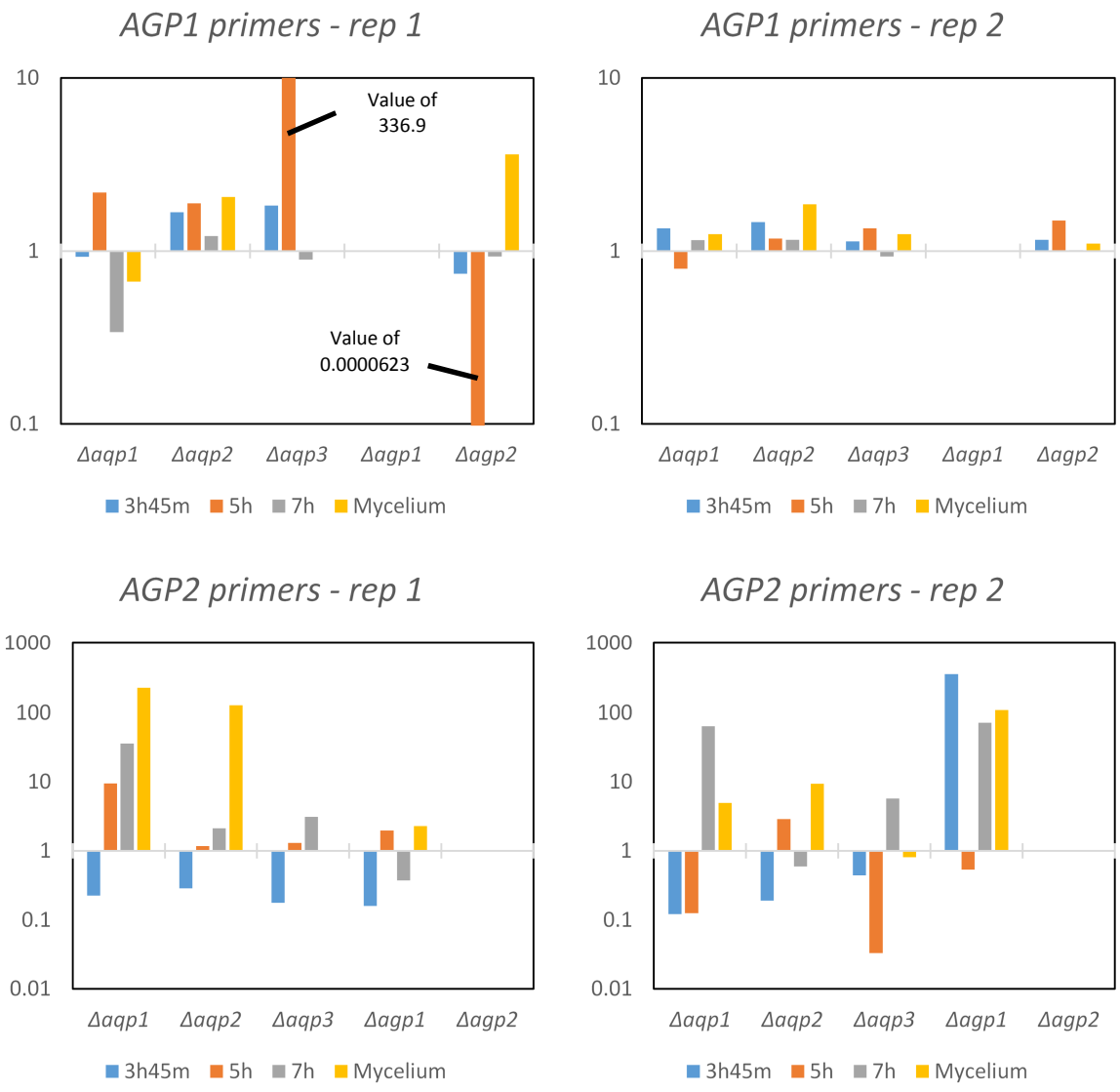

Figure 5.7 Part 2: The ratio of normalised gene expression in Δaqp backgrounds to the normalised expression of the same gene in the Guy11 background. Data shows two full biological replicates.

With the two biological replicates, the validity of the data underlying the gene-wide compensatory trends identified earlier in the chapter can be investigated. These were:

- *AQP2* in the Δ*aqp1* background
- *AQP1* in the Δ*aqp2* background
- *AQP1* in the Δ*aqp3* background
- *AQP1* in the Δ*agp2* background

The two to four-fold upregulation of *AQP2* in the Δ*aqp1* background appears robust. The trend is consistent in both biological replicates, although the magnitude of the changes is variable. There is

no evidence of systematic errors in the Guy11 values used to calculate these ratios, as can be observed by looking across all genes at all timepoints amplified with the *AQP2* primer pair in Figure 5.6.

Figure 5.7 shows the upregulation of *AQP1* in the Δ*aqp2* background in the 1st biological replicate, but this pattern is not observed in the 2nd biological replicate (where values are very close to 1). A look at Figure 5.5 suggests that the Guy11 values could be problematically low in biorep 1, but it is surprising that this could have occurred at all four time points. The situation is similar for *AQP1* in the Δ*aqp3* and Δ*agp2* backgrounds, and given the problems in the underlying data set, it is difficult to substantiate these putative compensatory changes.

As well as identifying situations of compensation across all time points, we took a second approach of looking for compensation at specific 'peaks' of transcript abundance. This is predicated on the assumption that compensation might only occur when the gene is 'important', coinciding with a transcription peak. Based on the data in Figure 5.5, we identified three genes with clear peaks of expression: *AQP2* and *AGP2* at 7pi, and *AGP1* in mycelium. Analysis of the data suggested no significant upregulation in the Δ*agp2* background at 7h, or the Δ*agp1* mycelium. However, the possibility of *AQP1* or *AGP1* upregulation in the Δ*aqp2* background could not be discounted. A breakdown of this data between the two biological replicates is shown in Figure 5.8 below:

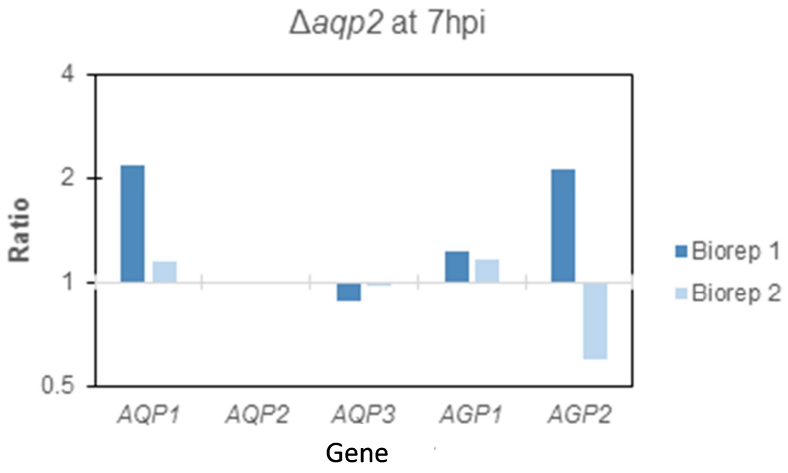

Figure 5.8: The ratio of normalised expression of each AQUAPORIN gene in RNA extracted from Δaqp2 germlings, 7hpi, to the normalised expression of the same genes in Guy11 7hpi.

Both *AQP1* and *AGP1* are upregulated in both data sets, but the magnitude of the change is small in both cases. The magnitude of the combined data is higher, likely as a consequence of the

autoscaling function of the combination process, however, based on the underlying data it is difficult to argue that the ratios are significantly different from 1.

5.5 Discussion

The data presented in this chapter suggest that in one paired combination, there may be a regulatory backup circuit that up-regulates *AQP2* in response to deletion of *AQP1.* This interaction is possibly a reciprocal one, but the strength of evidence that *AQP1* is up-regulated by the absence of *AQP2* is weaker, because the two biological replicates vary and there is evidence of problems with this particular data set.

5.5.1 A regulatory backup circuit may exist between *AQP1* and *AQP2*

If the genetic interaction between *AQP1* and *AQP1* in *M. oryzae* is a biological reality, this suggests that the function of either *AQP1* or *AQP2,* as a functionally overlapping pair, might be important for fungal growth. The up-regulation of *AQP2* in the Δ*aqp1* background can be observed at all developmental phases, with a mean fold induction of 3.2 (range: 2.3 - 4.0). This is a similar range to the fold-upregulation observed in a protein-level study in *S. cerevisiae,* where a range from 1.13-fold to 20-fold induction was observed (median 1.7-fold) (DeLuna et al., 2010)

A possible way to validate the existence of this RBC is to generate a double-knockout for both of these genes. In yeast, genes that display paralog responsiveness are very likely to display strong mutant phenotypes or be synthetically lethal (DeLuna et al., 2010). These mutants, if obtainable, could be very useful for studying the function of these aquaporin genes in *M. oryzae.* If not, they would confirm the importance of functioning aquaporins in *M. oryzae* – something that has yet to be demonstrated in any fungal species.

5.5.2 The existence of other compensatory changes cannot be ruled out

5.5.2.1 The error propagation and detection thresholds

The final output of this experiment is a ratio, based on the average of two log transformed mean centred, autoscaled ratios, each calculated from two RNA samples and normalised to the expression of two genes. Each gene has an experimentally determined efficiency term, and each value is comprised of two technical replicates.

Error terms can be divided into two groups: systematic and random errors (Skoog et al., 1988). Systematic errors cause deviation from the 'true' value, whereas random errors reduce the precision with which the 'true' value can be calculated. This experimental setup unavoidably suffers from both problems. Given the number of terms in the final output, propagation of random error results in wide confidence intervals for the observed values. Some of these errors, in practice, are not as high as might be anticipated. For example, normalisation against the geometric mean of two reference genes rather than one does not increase the overall error, as might be supposed from the introduction of an additional variable (Nordgard et al., 2006).

Karlen et al. (2007) attempted to calculate the number of experimental replicates needed to reach significance based on the reproducibility of the measures and the range of confidence that real value with within the indicated percentile. This suggests that with the approximate degree of variability displayed in our results (excluding outliers), an experimental set of two replicates is not very sensitive to changes beneath a 2-4 fold change. As the median value for compensatory change in yeast was 1.7-fold (DeLuna et al., 2010), there may be significant compensation that is beneath the detection threshold of our experiment. A larger number of biological repeats on a smaller number of samples would allow this possibility to be examined.

5.5.2.2 Compensatory up-regulation might be post-translational, or occur under different conditions

In addition to detection threshold issues, the presence of compensatory activity might be missed for two more reasons. First, as noted in the Introduction to this chapter, some compensation occurs exclusively in a post-translational manner (DeLuna et al., 2010). This was observed in 7 out of 32

cases. However, the study was designed to use the fluorescence level of a GFP-tagged paralogue as a measure of protein level in the mutant. Therefore any cases involving enhanced activation of a protein by, for example, phosphorylation would not be detected. It would not be unlikely, therefore, that cases of compensation would be missed in an exclusively transcript-based screen. Aquaporins are frequently gated (Tornroth-Horsefield et al., 2006) and in this system, regulation of the open/closed state of channels could plausibly form part of a backup circuit.

The same yeast study discovered that compensatory changes sometimes only occur when gene products are required for cell function under the experimental conditions (DeLuna et al., 2010). The authors compared the responsiveness of paralogous pairs under two conditions – rich medium and nutrient minimal medium – and found that many RBCs operate only under specific environmental conditions. Analysis of aquaporins in just four conditions may not include circumstances in which the aquaporin gene products are important.

5.5.2.3 Aquaporin expression on Teflon surfaces is congruent with SuperSAGE data from inductive glass slides, but not data collected from barley leaves

In chapter 3, we examined the expression of aquaporin genes in germlings developing on barley leaves. We compared the data with published SuperSAGE data from germlings developing on inductive glass slides (Soanes et al., 2012). The two data sets were partially congruent, with trends broadly identifiable in both studies. However, the magnitude of the expression levels, relative to the expression of HKGs, was quite different.

In this chapter, we looked at the expression of aquaporin gene during germling development on Teflon surfaces, and in CM liquid-cultured mycelium. The identifiable trends in this data are similar to those identified in the SuperSAGE data. However, this data is less similar to previous qRT-PCR data from barley leaves.

The validity of gene expression analysis done on artificial surfaces as a proxy for infectious development on leaves, is rarely questioned. To the best of our knowledge, the only documented *M. oryzae* example of differences in gene expression on leaves (and Cellophane) and two artificial surfaces, Teflon and Mylar is that of *ACE1* (Fudal et al., 2007). This gene has been implicated in

appressorium-mediated penetration. Appressoria do not form penetration pegs on Teflon, and the ability to penetrate Mylar depends on its specific surface-hardness (Howard et al., 1991). It therefore seems expression analysis on artificial surfaces is not necessarily valid for genes specifically involved in penetration.

Our experiments suggests that gene expression levels are not very similar on plants and on artificial surfaces. However, these differences may be attributable to the large technical differences between the two experiments. The RNA concentration and quality control measures, taken in the experiment in this chapter, are far superior to those performed in the experiment in chapter 3. The effect of this is two-fold: the C_T values are lower, and problem of template degradation is much reduced. Lower C_T values correspond to more accurate measurements, as they are significantly less variable (Caraguel et al., 2011). The purity and integrity of extracted RNA has been shown to be important for the accuracy of qRT-PCR (Fleige & Pfaffl, 2006). Therefore the qRT-PCR data in this study is likely to be more accurate than that of the study performed in chapter 3. The data in this chapter also represents the combination of two full biological replicates, whereas the data in chapter 3 does not.

Two further differences, the choice of housekeeping genes and the presence of plant tissue in the RNA preparations, might account for some of the differences between the two data sets. In the earlier experiment, HKGs were chosen according to those used in other *M. oryzae* studies (Skamnioti et al., 2008). However, these studies did not fully validate the stability of expression of these genes (Vandesompele et al., 2002). Che Omar et al., (manuscript in preparation) validated, in *M. oryzae*, a range of commonly-used HKGs over all the developmental conditions used in this study. Based on this information, we selected two new HKGs on the basis of improved transcriptional stability. The selection of HKGs has been shown to have a significant effect on the final calculated fold-changes in qRT-PCR experiments (Radonić et al., 2004, Dheda et al., 2004)

Another potential explanation for the differences between the tissues from which the RNA was extracted. PCR inhibitors are known to be co-purified during RNA extraction (Tichopad et al., 2003, Bustin & Nolan, 2004), and the type and concentration of PCR inhibitors varies greatly

between tissue types (Wilson, 1997). It may be the case that the presence of these inhibitors prevents proper comparison of the two data sets.

A final explanation for why the data sets are not very closely correlated is that the underlying gene expression levels are different on artificial inductive surfaces and plant host surfaces. This would undermine the widespread use of gene expression data from germlings grown on artificial inductive surfaces (Fudal et al., 2007, Soanes et al., 2012). This would be a valid study to perform; however, given the substantial experimental variation, it is not appropriate to draw this conclusion from the two studies in this thesis.

Chapter 6 Aquaporin permeability

6.1 Introduction

A large number of studies have focused on the relationship between the structure and function of aquaporin proteins (Ludewig & Dynowski, 2009, Oliva et al., 2010, Tingaud-Sequeira et al., 2010). Although the primary sequence is, at first glance, very divergent, the secondary structure, and certain spatially important amino acids are highly conserved (Soto et al., 2012). There are two major constriction zones in the hourglass-shaped aquaporin channel – the NPA region at the centre of the pore and the selectivity filter (SF) comprised of the aromatic/arginine (ar/R) region.

This chapter details the identification of these conserved residues and analysis of their properties with regard to substrate specificity. The putative function of other sequence features are also examined. I then tested the sequence-based permeability predictions using a *Saccharomyces cerevisiae* heterologous expression systems to examine each protein independently. Finally, the relevance, *in vivo*, of the demonstrated hydrogen peroxide permeability of *AQP2* was examined using a GFP-based redox reporter, Grx-roGFP2.

6.1.1 Heterologous expression of aquaporin proteins

The mild mutant phenotype of aquaporin null mutants presents a problem when studying protein function. To overcome this problem, many studies test the properties of these proteins using a heterologous expression system to isolate the proteins from their native environment. There are two systems that are commonly used in aquaporin studies – protein expression in *Xenopus laevis* oocytes, and expression in *S. cerevisiae* (Hove & Bhave, 2011). Frequently results from one system are validated with the other, but there are advantages and disadvantages of both.

Both systems rely on the controlled expression of the protein-of-interest in the exterior membrane. In *Xenopus* oocytes, this is achieved by microinjecting capped RNA transcripts directly into the oocyte (Tammaro et al., 2008), and in *S. cerevisiae* by stable transformation with a cDNA under the control of an inducible promoter (Bienert et al., 2007, Prudent et al., 2005). The introduced cDNA or cRNA is then transcribed and translated into a protein in the new cells. The promoter used in *S. cerevisiae* assays is typically the *GAL1* promoter, which is induced in as little as 4h in cells that are grown with galactose as a carbon source but strongly repressed in cells grown with glucose (Johnston & Davis, 1984).

The permeability of different molecules can be measured in oocytes either by the level of accumulation of radiolabelled compounds (Fetter et al., 2004), or by the rate of swelling following exposure to an inward gradient of an osmotically active solute (Hansen et al., 2002). Heterologous studies of aquaporins in *S. cerevisiae* fall into two categories: phenotypic complementation of an endogenous transporter or channel deletion, or enhancement of a sensitivity to a toxic substrate (Bienert et al., 2011). Assay design is therefore more complex in *S. cerevisiae,* and only a limited range of molecules have been assessed with yeast permeability assays relative to the number tested in oocytes.

Work with oocytes requires the maintenance of live amphibians and subsequently surgery to extract the oocytes from the anesthetised animals. There are specific and onerous regulations governing this type of work; a problem which is not encountered when working with *S. cerevisiae*. Each oocyte must be individually microinjected and measured and the repetition of these assays is very time consuming. Conversely, *S. cerevisiae* assays can be repeated with relative ease.

We decided to use the *S. cerevisiae* based system to circumvent problems associated with live amphibians. The yeast assays, whilst substrate-limited relative to oocytes, still cover a sufficient range of possible compounds. We will test permeability to four substrates: urea, hydrogen peroxide, ammonia/ammonium, and glycerol.

6.2 Experimental aims

i) To examine the primary structure of *Magnaporthe oryzae* aquaporin proteins and speculate on their permeability and regulation.

ii) To test the permeability of these channels to four substrates using xenologous expression in *S. cerevisiae.*

iii) To investigate the relevance *in vivo* of the permeability of these substrates.

6.3 Methods specific to this chapter

6.3.1 *S. cerevisiae* assays

For all assays, the *M. oryzae* aquaporin cDNA sequences were amplified and were cloned into the *EcoR*I and *Xho*I site of the pYES2/CT vector (Invitrogen). The coding sequence of each gene was downloaded from the Broad Institute website and primers were designed to amplify the full length sequence.

Initially, we were unable to amplify cDNA sequences from *AQP1* and *AGP1*. We resequenced these genes, finding errors in the Broad Institute (BI) annotations, as for example, revealing that the intron-exon boundary is incorrect in the AQP2 annotation. The BI annotations are partially computational and partially based on sequencing of an EST library. Moreover, the ESTs for AQP1, on which the original BI sequence was based, were found to be truncated at both the N and C-termini. We thence designed primers with homology to sequential 40 bp intervals upstream and downstream of the annotated AQP1 sequence. These were paired with primers with homology to known sequences in the middle of the gene to amplify fragments from a CDNA library and triangulate the correct START and STOP codons. This allowed us to identify a single putative START and STOP codon from which were able to amplifiy full length cDNA.

The modifications to the published cDNA sequences are validated by the subsequent release of two further genomes of *M. oryzae* strains (P131 and Y34) (Xue et al., 2012). These versions adopted the same annotation for *AQP1* and *AQP2*, but the first ~10 amino acids of the N terminus of *AGP1* were different. The permeability assays are carried out using the published *AGP1* cDNA sequence from the Broad Institute.

Table 6.1: Yeast medium notation

Medium	Carbon source	Details
SD	Glucose	Synthetic minimal medium containing glucose as a sole carbon source. Specific amino acids must be added to complement strain auxotrophies. Nitrogen minimal SD contains no added ammonium sulphate
SG	Galactose	Same as SD, but with galactose instead of glucose
YPD	Glucose	Yeast complete medium with glucose as the carbon source. No amino acid supplements are necessary
YPG	Galactose	Same as YPD, but with galactose instead of glucose

6.3.1.1 Ammonia

The *Saccharomyces cerevisiae* Δ*mep1-3* strain lacks all three endogenous ammonium transporters and has an impaired ability to grow on low concentrations of NH_3/NH_4^+ as the sole nitrogen source (Marini et al., 1997). Beitz et al. (2006) demonstrated that the expression of NH_3/NH_4^+ permeable aquaporins enhances the proliferation of Δ*mep1-3* cells under these conditions. They also demonstrated that the pH of the medium can be used to show whether the aquaporins are permeable to NH_3 or NH_4^+ by taking advantage of their relative concentration changes over a pH range (shown in Figure 6.1). If gain-of-proliferation is only detectable at pH 5.5 then it is likely that exclusively NH_4^+ is transported.

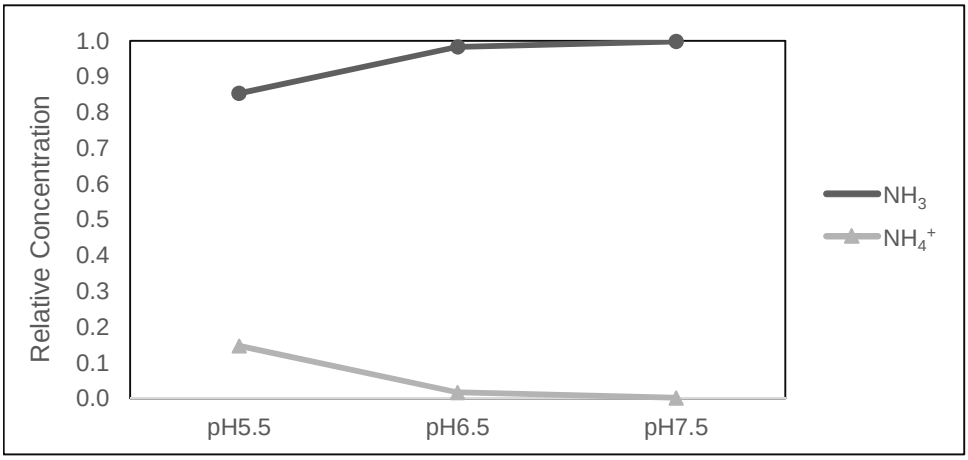

Figure 6.1: The relative concentration of ammonia (NH_3) and ammonium (NH_4^+) in aqueous medium. The pKa of NH_4^+ at each pH was calculated at 30°C according to Emerson et al. (1975). The relative concentration of NH_4^+/NH_3 was calculated according to Clément and Merlin (1995).

Growth complementation assays were carried out on nitrogen-minimal SG plates, supplemented 0.5M Tris adjusted to pH 5.5, 6.5 or 7.5 with NaOH, to a final concentration of 50 mM. An SD control was included to monitor growth under aquaporin repression and a 0.1% (w/v) proline control (a nitrogen

source with an independent uptake mechanism) was included to ensure that normal growth was not affected. The assay was carried out as follows:

1) Yeast strains were grown overnight in 50 ml SD medium supplemented with histidine and methionine at 30 mg/L, and leucine at 150 mg/L.
2) Cells were centrifuged at 931 xg (2000 rpm) and the pellet was washed with sterile ddH_2O.
3) The concentration was adjusted to an OD_{600} of 1 under sterile conditions.
4) Eight microlitres of cells were spotted at OD_{600} of 1, 0.1 and 0.01 onto plates supplemented with $(NH_4)_2SO_4$ at a concentration range of 0-5 mM. An SD control and a proline control were also performed.
5) Plates were inspected, and images were captured after 4 days at 30^oC in the dark.

Human AQP8 (hAQP8) is permeable to H_2O_2 (Bienert et al., 2007), NH_3 and NH_4^+ (Holm et al., 2005), and urea (Ma et al., 1997), and was transformed into Δ*mep1-3* to serve as a positive control. A pYES2 plasmid containing hAQP8 was provided by Dr. Pai Pedas (University of Copenhagen).

A Δ*mep1-3* strain transformed with an empty pYES2 plasmid was used as a negative control. The untransformed Δ*mep1-3* strain could not be used without the plasmid, as the untransformed are uracil auxotrophic and would not grow on the assay medium.

6.3.1.2 Urea

The urea permeability assay utilises the inability of the *DUR3* urea transporter knockout strain Δ*dur3* to grow on medium containing less than 5 mM urea as a sole nitrogen source (Liu et al., 2003). *The* Δ*dur3* strain was transformed with the pYES2 plasmids encoding each *M. oryzae* aquaporin, an empty pYES2 vector or hAQP8 as a positive control. The wildtype with a functional *DUR3* gene was included as a reference.

Cells were spotted on SG medium containing a concentration range of urea or 1 mM arginine as a nitrogen source. The medium pH was adjusted to 5.5 using 0.5 M Tris (pH 5.5) to a final concentration of 50 mM. The arginine control provides an induced growth control as arginine uptake independent of the *DUR3* transporter or aquaporins.

A high urea concentration of 20 mM was also tested, as passive diffusion across the bilayer is putatively sufficient at this concentration (Bienert et al., 2011). The experiment was performed as follows:

1) Strains were prepared at an OD_{600} of 1 as described in Section 6.3.1.1.
2) Eight microliters of cells were spotted at a dilution of 0.1, 0.01 and 0.0001 onto plates supplemented with urea (0-20 mM). An SD control and an arginine control were also performed.
3) Plates were inspected, and images were captured after 4 days at 30^{o}C in the dark.

6.3.1.3 Glycerol

S. cerevisiae adapts to high external osmolarity by accumulating glycerol to equilibrate with the environment. The yeast aquaglyceroporin deletion strain, Δ*fps1,* is unable to survive sudden hypo-osmotic shock as it cannot equilibrate with the new external osmolarity by rapidly releasing accumulated glycerol (Kayingo et al., 2001). Expression of a glycerol permeable aquaporin fully or partially restores growth after sudden osmotic shock (Prudent et al., 2005). We tested the ability of each *M. oryzae* strain to restore growth after sudden osmotic shock as follows:

1) Yeast cells were grown in 5 ml YPD broth at 30^{o}C, 200 rpm.
2) A 10 µl inoculating loop of this culture was inoculated into 50 ml SD or SG broth supplemented with 1 M sorbitol, and histidine and methionine at 30 mg/L, and leucine at 150 mg/L. The cultures were incubated at 30^{o}C, 220 rpm for 16 h.
3) The cells were centrifuged at 931 xg (2000 rpm) and a 10 µl inoculating loop of pelleted cells was resuspended in ddH_2O or ddH_2O supplemented with 1 M sorbitol.
4) The OD_{600} of each suspension was adjusted to 1, and 8 µl cells were spotted on the assay plates undiluted and at three sequential 10-fold dilutions.
    - SD-grown cultures were spotted onto SD plates with and without 1 M sorbitol.
    - SG-grown cultures were spotted onto SG plates with and without 1 M sorbitol.
5) Plates were inspected, and images were captured after 4 days at 30^{o}C in the dark.

6.3.1.4 Hydrogen peroxide

The *S. cerevisiae YAP1* gene encodes a transcription factor that regulates adaptation to oxidative stress (Semchyshyn, 2009). Δ*yap1* deletion strains are very sensitive to H_2O_2 and are have severely impaired growth on as little as 0.75 mM H_2O_2 (Bienert et al., 2007). This phenotype can be utilised to determine whether individual aquaporins are permeable to H_2O_2, as sensitivity is enhanced by the expression of an H_2O_2 permeable aquaporin in the plasma membrane.

The H_2O_2 sensitivity assay was performed as follows:

1) Yeast cells at an OD_{600} of 1 were prepared as described in Section 6.3.1.1.
2) The OD_{600} was adjusted to 1, 0.1 and 0.01, and 8 µl cells were spotted on an SD control plate and SG plates supplemented with H_2O_2 (0-1 mM).
6) Plates were inspected, and images were captured after 4 days at 30^{o}C in the dark.

Three control strains were included with the *M. oryzae* aquaporins – an isogenic wildtype strain with fully functional *FPS1*, an empty vector negative control and an hAQP8 positive control.

6.3.2 Grx-roGFP2 confocal imaging

We transformed the Δ*aqp2* single deletion strain with a plasmid containing Grx1-roGFP2, courtesy of Dr. Marketa Samalova, University of Oxford. The backbone plasmid is based on pUCAP vector that carries a pUC19 MCS and unique *Pac*I and *Asc*I restriction sites (van Engelen et al., 1995). The complete plasmid encodes Grx1, a glutathione peroxidase, conjugated to roGFP2, under the control of the strong pRP27 promoter. Transcription is terminated by the TrpC terminator, and a bialophos resistance cassette (BAR) facilitates transformation into *M. oryzae*.

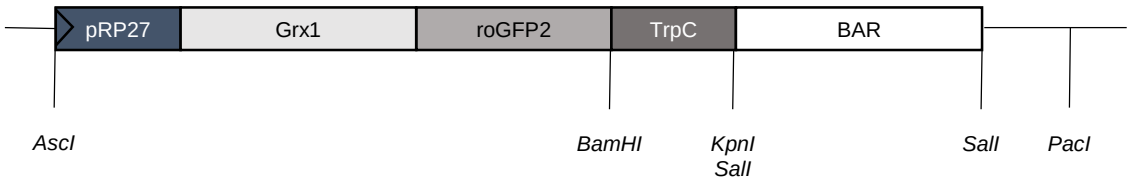

Figure 6.2: The pRP27::Grx1::roGFP construct in a modified pUCAP plasmid. *The Grx1::roGFP2 fusion protein is expressed under the control of the pRP27 promoter and terminated by the TrpC terminator. A bialophos-resistance gene is included for transformation into Magnaporthe oryzae.*

The randomly-integrating construct was transformed into Δ*aqp2* as described in the Materials and Methods. Δ*aqp2*-roGFP positive transformants were screened and found to be fluorescent, albeit at a lower level than those of the Guy11 roGFP strain, also provided by M. Samalova. The fluorescence of the brightest Δ*aqp2* strain was approximately 10-fold weaker than that of Guy11 roGFP.

Spores were harvested, washed and inoculated onto inductive Menzel coverslips as a 1:1 mixture of Guy11 and Δ*aqp2* roGFP expressing spores. The large difference between the fluorescence levels made it possible to distinguish the two genotypes and during subsequent analysis, and this ensured equal perfusion conditions for the two spore populations. After 30 m – 2 h germination, the coverslips were placed in a perfusion chamber and imaged on a Zeiss LSM510META confocal microscope.

Grx-roGFP fluorescence was excited with a 405 nm and 488 nm laser in multi-track mode with line switching. The emission spectrum (505-530 nm) was collected in parallel with an auto-fluorescence channel (excitation: 405 nm, emission 435 nm – 485 nm). Non-confocal bright field images were collected with a transmission detector. Time series were collected at 40-50 s intervals for 35-45 min as *z*-stacks of 7 sections taken at 3 µm apart using a Zeiss 40x 1.2 NA PlanApo water immersion lens. Pixel sizes were 0.23 µm in *x* and *y* and pinhole setting were adjusted for each channel to give an optical section thickness of 3 µm for each wavelength combination.

Germinating spores were imaged for approximately five minutes before they were perfused with 20 mM H_2O_2. This concentration was shown by Samalova et al (2013) (*manuscript in press*) to induce intermediate oxidation, followed by recovery, of the cellular glutathione pool. After perfusion, the H_2O_2 was washed out by perfusion with distilled water to observe the recovery rate. An *in situ* calibration of the roGFP redox couple was performed after the washout, to provide a reference for subsequent data analysis. The fluorophores were maximally reduced using 10 mM DTT before perfusion with 100 mM H_2O_2 to complete oxidation.

6.3.2.1 Image analysis

Time series were imported into a custom MatLab programme (Dr. Mark Fricker, University of Oxford). *z*-stacks were averaged in *x, y* and *z* using a 3x3x3 kernel. The image was then aligned in *x, y* and *z* to correct for movement of the sample. The *z*-position of the brightest pixel in a maximum *z*-projection of the main channel of interest was identified and the corresponding *z*-pixels for the other channels

were extracted. These average pixel intensities in a volume around the same bright pixel in *x, y* and *z* were used for subsequent analysis.

Quantitative measurements were taken from a sub-region of each spore, usually the apical cell. The average background intensity was measured from regions adjacent to the spores and subtracted. The auto-fluorescence bleed-through into the $roGFP_{405}$ channel was subtracted using the auto-fluorescence channel measurements and a scaling factor calculated from Guy11 spores (Dr M. Fricker, University of Oxford).

Each pixel was normalised to the lower DTT bound and the upper 100 mM H_2O_2 bound to correct a laser misalignment issue. Ratio images were calculated on a pixel-by-pixel basis, and the degree of oxidation was calculated according to Schwarzlander et al. (2008). For pseudo-colour display, the masked ratio was coded by hue on a spectral colour scale ranging from blue (the most reduced) to red (the most oxidised), with the limits set by the *in situ* calibration.

6.4 Results

6.4.1 Aquaporin structure/function characteristics

The primary and secondary structure of aquaporin proteins offers some insight into their function and regulation (Ludewig & Dynowski, 2009). We analysed the properties of *M. oryzae* aquaporins based on the following features:

1) The amino-acid composition of the conserved residues implicated in substrate selectivity and their putative effect on the pore properties.
2) The characteristics of the loops and termini.

6.4.1.1 The NPA region and aromatic/arginine selectivity filters

The substrate selectivity of aquaporins is linked to the physical properties of amino acids in two specific regions: the NPA motifs and surrounding amino acids on the re-enterant hemi-helices (shown in Figure 6.3), and the aromatic/arginine (ar/R) selectivity filter, which is comprised of four residues and likely serves as a size-exclusion barrier (Hove & Bhave, 2011).

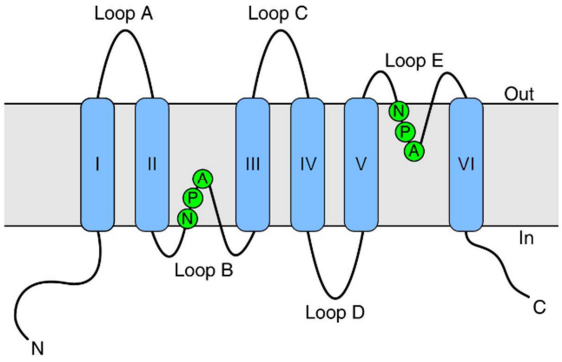

Figure 6.3: Topology of an aquaporin membrane protein. *Each protein consists of six transmembrane helices (I-VI) that span the membrane and two hemi-helices with the characteristic NPA motif that enter and re-emerge from the membrane on the same side of the bilayer. N, amino terminus; C, carboxyl terminus. The diagram is modified from Kruse et al. (2006).*

To identify important residues, we aligned the sequences of the five *M. oryzae* and a reference aquaporin (*HsAQP1*) and aquaglyceroporin (*EcGlpF*) using MUSCLE alignment software (Edgar, 2004). This alignment is shown in Figure 6.4. We used a support vector machine-based TM protein topology predictor with re-enterant helix prediction power (MEMSAT-SVM) to generate topological

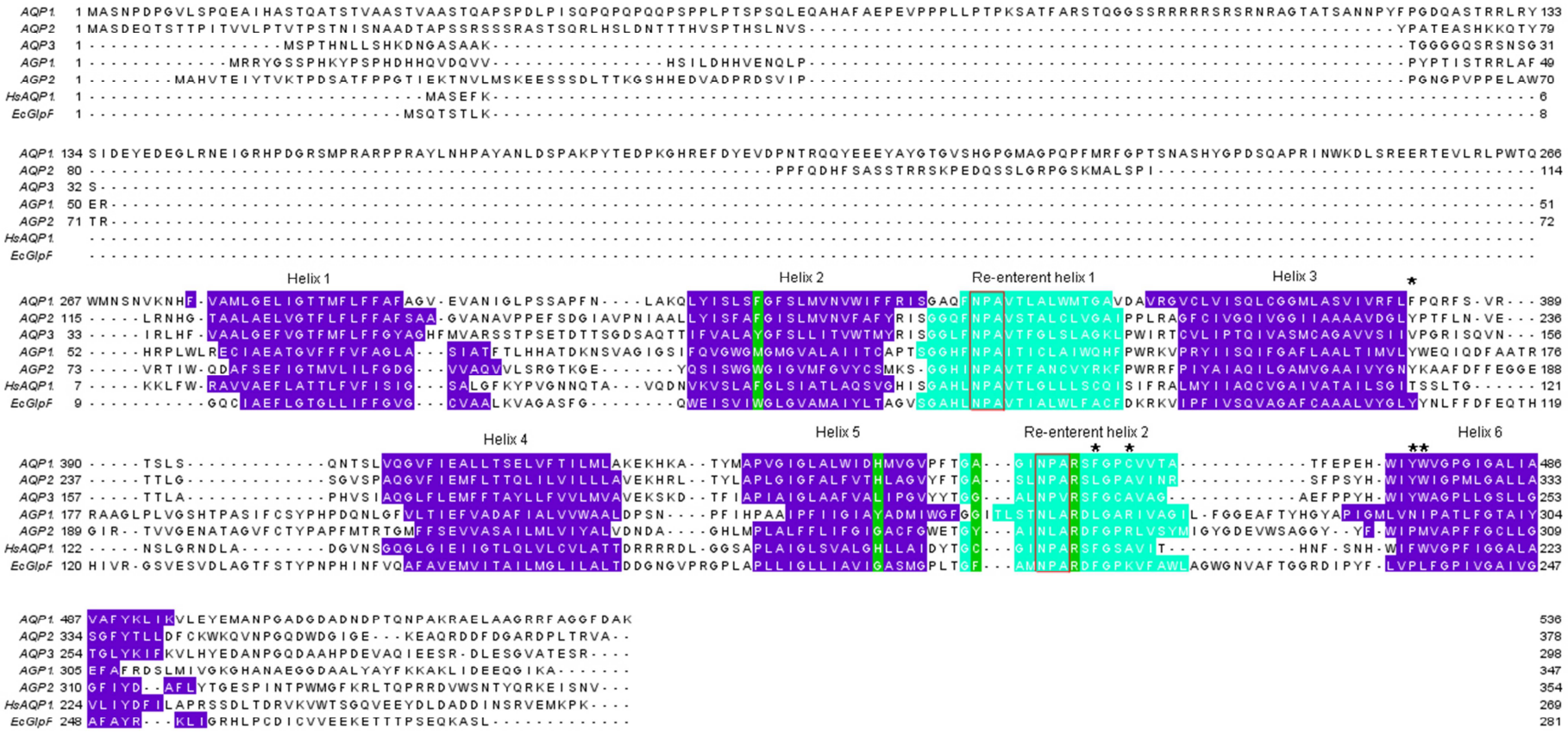

Figure 6.4: The structural features of Magnaporthe oryzae aquaporins. *The five M. oryzae aquaporins and two canonical major intrinsic proteins, Homo sapiens AQP1 (hsAQP1, accession number: O94778) as a representative of orthodox aquaporins and Escherichia coli GlfP (accession number: P0AER0) as a representative of aquaglyceroporins are aligned using MUSCLE alignment software. The transmembrane helices are shown in indigo, and the re-enterant hemi-helices are shown cyan. The secondary structure was predicted using MEMSAT_SVM prediction software. The NPA boxes are outlined in red, and amino acids forming the aromatic/arginine (ar/R) constriction are highlighted in green. The P1-P5 conserved residues are marked with asterisks. The image was generated using Jalview alignment software and Adobe Photoshop Elements 11.*

predictions of helix positions and cross-checked this with the alignment (Nugent & Jones, 2009). The amino acids surrounding the two NPA motifs and the ar/R selectivity filter are shown in Table 6.2.

A literature review by Hove and Bhave (2011) compiled experimentally tested aquaporin substrate profiles and generated consensus sequences for plant aquaporins with non-aqua permeabilities. These sequences are shown in Table 6.3.

Table 6.2: The profile of residues that are characteristically associated with substrate selectivity in Magnaporthe oryzae aquaporins and two canonical reference sequences, HsAQP1 and EcGlpF.

Gene	NPA Motifs		Selectivity Filter			
	1st NPA box	2nd NPA box	H2 Ar/R site	H5 Ar/R site	Loop E Ar/R 1	Loop E Ar/R 2
AQP1	SGAQF**NPA**VT	GAGI**NPA**RSFG	F	H	A	R
AQP2	SGGQF**NPA**VS	GASL**NPA**RSLG	F	H	A	R
AQP3	SGGLF**NPA**VT	GGAL**NPV**RSFG	Y	L	G	R
AGP1	SGGHF**NPA**IT	GG*ST**NLA**RDLG	M	Y	G	R
AGP2	SGGHI**NPA**VT	GYAI**NLA**RDFG	W	G	Y	R
HsAQP1	SGAHL**NPA**VT	GCGI**NPA**RSFG	F	H	C	R
EcGlpF	SGAHL**NPA**VT	GFAM**NPA**RDFG	W	S	F	R

* *There is a three amino acid insertion (ITL) at this position*

Table 6.3: Suggested signature sequences at the NPA and ar/R substrate selectivity sites for three substrates. *Reprinted from Springer and Plant Mol Biol, Vol 75, 2011, p413, Plant aquaporins with non-aqua functions, Hove and Bhave, Table 3 Copyright 2011, with kind permission from Springer Science and Business Media*

Substrate	1st NPA box	2nd NPA box	H2 Ar/R site	H5 Ar/R site	Loop E Ar/R 1	Loop E Ar/R 2
Ammonia	SGGH(V/L/F)**NPA**VT	G(G/A)SM**NPA**RS(F/L)G	H/W	I/V	A/G	R
H_2O_2	SG(G/A)H(V/L/I/F)**NPA**VT	G(A/G/T)(S/G)(M/I)**NP(A/G)**(V/R)(A/S)(F/L)G	H/F/W	I/H/V	A/T/G	V/R
Urea	SG(G/A)H(I/L/V/M)**NPA**VT	(G/S)(A/T/G)(G/S)(I/M)**NP(A/V)**(R/V/C)(S/A/T)(L/F)G	F/H/G/A/N	H/I/S/V	T/A/G	R/V/C

6.4.1.1.1 *AQP1*

The NPA regions of the Mo*AQP1* gene are typical of orthodox aquaporin protein family members. The NPA-regions are similar to the HsAQP1 sequence, but with a H→Q and an L→F substitution in the first NPA box, and a C→A substitution in the 2nd NPA box. The first NPA box is similar to the H_2O_2 permeability consensus sequence with only a single residue change (Q instead of H) (Hove & Bhave, 2011). The second NPA box matches the consensus sequences compiled from both H_2O_2 and urea-permeable aquaporin sequences.

The Aqp1 ar/R constriction is very similar to the HsAQP1 reference sequence, carrying FHAR instead of FHCR (Forrest & Bhave, 2007). This cysteine residue, in the HsAQP1 sequence, is

associated with sensitivity to mercury inhibition (Preston et al., 1993) but is absent from all *M. oryzae* aquaporins suggesting mercury insensitivity of aquaporins in the fungus. This cysteine residue is thought to provide a backbone carbonyl oxygen, thus is often substituted for threonine or alanine without alteration to the hydrogen bonding properties (Froger et al., 1998, Lagree et al., 1999). It is likely that this substitution does not significantly alter the permeability of *AQP1* relative to *HsAQP1*. The ar/R selectivity filter profile matches the consensus sequence of H_2O_2- and urea-transporting aquaporin proteins.

Based on analysis of the primary sequence, *AQP1* appears to be a canonical aquaporin protein with predicted permeability to H_2O_2 and perhaps to urea.

6.4.1.1.2 *AQP2*

The ar/R region of *AQP2*, an aquaporin, is identical to that of *M. oryzae AQP1,* suggesting H_2O_2 and urea permeability. The 1st NPA region has an unusual T→S substitution, the impact of which has not been tested experimentally. However, the structures of serine and threonine are relatively similar with only a single methyl group difference. This substitution may have the effect of making the pore slightly larger, perhaps affecting the size of molecules that can pass through the pore. However, the narrowest region is thought to be the ar/R selectivity filter rather than the NPA motifs (Oliva et al., 2010). If this substitution is excluded, the *M. oryzae AQP2* 1st NPA box sequence conforms well to the H_2O_2 consensus sequence. The 2nd NPA box matches the H_2O_2 consensus sequences for urea and H_2O_2 permeable aquaporins.

The primary sequence of *AQP2* – an aquaporin-type protein – suggests that it is likely to be permeable to H_2O_2 and perhaps also to urea.

6.4.1.1.3 *AQP3*

The first NPA region of *AQP3* (an aquaporin-type protein) is consistent with the ammonia and hydrogen peroxide permeable consensus sequences (with the exception of a histidine residue that is absent). However, the 2nd NPA region does not fit with any of the described consensus sequences. The NPA of the 2nd *AQP3* motif has a 'bulkier' valine residue substituted for the alanine residue (NPV instead of NPA). This substitution would result in a slightly smaller pore aperture and increased hydrophobicity compared with classical NPA-motif proteins (Wallace & Roberts, 2004).

This substitution is common amongst Nodulin-26-like intrinsic (NIPs) plant aquaporins, which are permeable to diverse substrates (Mitani-Ueno et al., 2011).

The ar/R selectivity filter is also different from the *M. oryzae AQP1* and *HsAQP1* sequences, with the exception of an almost invariant R residue that is thought to be important for proton exclusion (de Groot et al., 2003). The tyrosine residue at the H2 ar/R position has similar properties to the consensus phenylalanine. The leucine at the H5 ar/R position is present in a group of archael / bacterial aquaporins that are putatively an intermediate group between aquaporins and aquaglyceroporins (Araya-Secchi et al., 2011). The glycine residue at the E loop position 1 is atypical of strict aquaporin type proteins, but is common amongst plant ammonia facilitators (Hove & Bhave, 2011).

The selectivity residues of *AQP3* suggest that it is not a typical aquaporin protein and is likely to be functionally different from *AQP1* and *AQP2.* The residues are weakly similar to ammonia facilitators, but the primary sequence cannot be used to make strong predictions of function based on similarity to consensus sequences.

6.4.1.1.4 *AGP1*

The NPA motifs of *AGP1* and *AGP2* have a substitution in the 2nd NPA box of a 'bulkier', more hydrophobic leucine for a proline residue. The crystal structure of another aquaglyceroporin with this substitution, PfAQP from the malarial parasite *Plasmodium falciparum*, has been solved (Newby et al., 2008). In PfAQP, the bulk of the leucine residue is compensated for by covariant changes in the surrounding amino acids. It is likely that these changes also occur *AQP1,* as the regions surrounding the NPA motifs are quite divergent compared with *EcGlfP*. The typical substitutions are for smaller, more hydrophobic amino acids, perhaps reflecting accommodation of the bulkier leucine residue.

With the exception of the conserved arginine residue, the selectivity filter of *AGP1* is more hydrophobic and the amino acid residues are smaller than a typical aquaglyceroporin. Small pore-lining residues are likely to result in a wider ar/R filter. As steric restraints are known to be important for substrate exclusion, aquaporins with wide selectivity filters are likely to be permeable to larger molecules (Hub & de Groot, 2008).

6.4.1.1.5 *AGP2*

The 1st NPA region of *AGP2,* an aquaglyceroporin-type protein, is similar to that of *EcGlpF,* with only two relatively synonymous substitutions (A→G and L→I). As with *AGP2*, there is a proline-to-leucine substitution in the 2nd NPA motif (giving the sequence NLA). However, with *AGP2,* there are few significant changes in the immediate surrounding amino acids that might compensate for the bulkier residue. The changes necessary to compensate for the replacement of a proline residue with a leucine residue may therefore take place outside the immediate neighbouring amino acids.

The selectivity filter of *AGP2* is more similar than *AGP1* to that of *EcGlpF.* The first tryptophan on H2 is conserved, but the H5 serine is substituted with a glycine in *AGP2.* The effect of this change is to increase the hydrophobicity of the selectivity filter and reduce the polarity. However, the loop E1 phenylalanine to tyrosine substitution probably compensates for this change. As with all *M. oryzae* aquaporins and aquaglyceroporins, the loop E2 arginine is invariant.

The primary structure of *AGP2* suggests that it is, like *EcGlpF,* a classical aquaglyceroporin that conducts water and glycerol.

6.4.1.2 Internal loop and termini characteristics

The alignment shown in Figure 6.4 was used to determine the length of the loops and termini of each *M. oryzae* aquaporin protein and the two reference sequences, *HsAQP1* and *EcGlpF*. These are shown in Table 6.4, as labelled in Figure 6.3.

Table 6.4: The number of amino acid residues in secondary sequence features of M. oryzae aquaporins and two reference sequences

Sequence	N terminal	C terminal	A loop	C loop	D loop
AQP1	276	42	19	17	21
AQP2	120	38	23	18	10
AQP3	37	38	25	19	21
AGP1	58	40	19	42	12
AGP2	79	37	11	41	10
HsAQP1	11	39	18	21	12
EcGlpF	11	26	11	40	13

The most notable feature of *M. oryzae* aquaporins are their long N-terminal extensions as compared with those of the two reference sequences. Conversely the A, C and D loop lengths are quite typical of aquaporins.

Long terminal or loop extensions of aquaporins are frequently involved in gating or regulation (Moeller et al., 2010, von Bülow et al., 2012). The N-terminal of *Pichia pastoris* Aqy1 has a 45 aa N-terminal domain that arranges as a tight helical bundle with a tyrosine residue that occludes the channel entrance (Fischer et al., 2009). Truncation of hydrophilic N terminal of the *S. cerevisiae FPS1* protein results in a constitutively open channel (Tamás et al., 1999).

Terminal extensions of *M. oryzae* aquaporins might perform such functions. BLAST hits against the N terminal extensions of these proteins reveals that the *AQP1* long N terminal extension has significant homology to other Pezizomycete aquaporins, whilst the other aquaporin termini have no significant homology. The *AQP1*-type N-terminal extension has not been experimentally characterised, but scanning the *AQP1* terminal sequence against the 'Hits' protein domain database (http://myhits.isb-sib.ch/) reveals a significant proline-rich region (e = 0.00074) between positions 38 and 84. This region is typical of a proline rich region (PRR), with tandem glutamine-proline repeats that likely form a polyproline type II helix (Brown & Zondlo, 2012). PRRs are implicated in protein-protein interactions, typically in the assembly and targeting of protein complexes (Zarrinpar et al., 2003).

The *AQP1* gene also has a calmodulin-binding domain on the C-terminal extension (http://calcium.uhnres.utoronto.ca/ctdb/ctdb/sequence.html). Calmodulin is an intermediate messenger that integrates calcium ion fluxes and downstream target proteins (Chin & Means, 2000). Calcium/calmodulin-dependent signalling has been implicated in appressorium formation in *M. oryzae,* as calcium chelators reversibly block appressorium formation.

Two other genes, *AGP1* and *AGP2* are predicted to have calmodulin-binding domains, but these are predicted over the first NPA hemi-helix. The tertiary structure predictions in chapter 3 suggest that these regions would not be exposed to the exterior of the protein, thus may not be accessible to calmodulin.

6.4.2 *Saccharomyces cerevisiae* expression assays

The functional predictions in Section 6.4.1 are testable in the absence of a strong phenotype of single aquaporin deletion strains, by xenologous expression of individual proteins under the control of a galactose-inducible promoter in *S. cerevisiae.* The *S. cerevisiae* system is much exploited, and

the availability of inducible promoters and mutant strain libraries assist with the elucidation of the substrate specificities of individual aquaporin proteins (Hove & Bhave, 2011, Scherens & Goffeau, 2004).

6.4.2.1 *AGP1* may be permeable to ammonia

To test whether aquaporins are permeable to NH_3/NH_4^+, we grew Δ*mep1-3* yeast cells expressing individual *M. oryzae* aquaporins on nitrogen-free inductive SG medium, supplemented with a range of concentrations of ammonium sulphate. The assays (shown in Figure 6.5) were performed at pH 5.5, pH 6.5 and pH 7.5 to attempt to distinguish between NH_3 and NH_4^+ substrates. In comparison with the positive control, *hAQP8*, and the pYES2 empty vector negative control, it appears that only Agp1 is permeable to NH_3/NH_4^+. It is not possible to conclude whether the substrate is NH_3 or NH_4^+ as the growth effect is not significantly higher at pH5.5.

Growth of glucose controls indicates that the initial inoculum of all strains is comparable under repressive conditions. There is an apparent pH-dependent growth effect on all strains including the wildtype, which grows better at pH 5.5 and pH 6.5 than at pH 7.5 Growth of strains on the proline control – a nitrogen source whose uptake should not be affected by aquaporins or absence of *MEP1-3* - is equivalent across all strains at pH 5.5 and pH 6.5, but at pH 7.5 the AQP3- and hAQP8-expressing strains and the wildtype appear to grow better. The structure of proline makes it extremely unlikely that the proline is taken up by an aquaporin. It is possible that there may be another source of NH_3/NH_4^+ in the medium that is made more apparent by the weak growth of other aquaporin strains at this pH. The agar used in these assays was standard laboratory grade agar. However, highly purified varieties are available, reportedly with lower concentrations of "naturally occurring pigments, salts and miscellaneous matter" (source: Sigma Aldrich). It may be the case that these impurities release ammonium at a very low level.

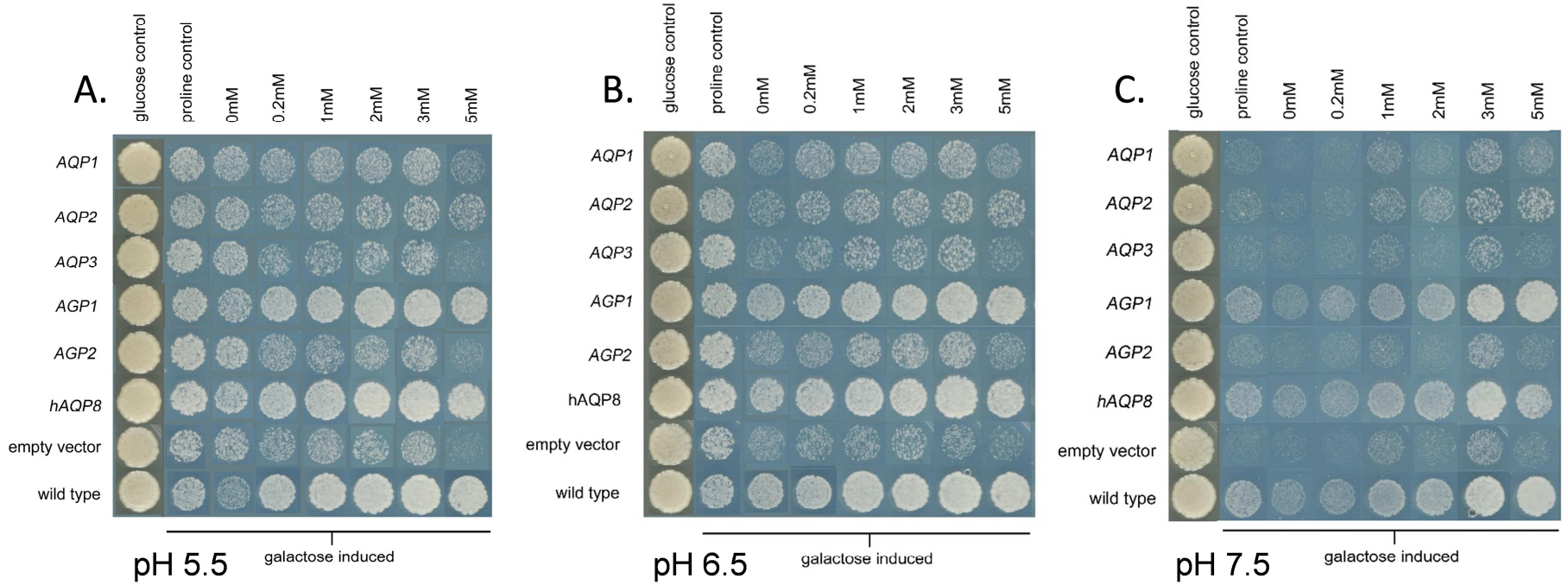

***Figure 6.5:* Yeast growth complementation on plates supplemented with a concentration range of ammonium sulphate.** *Δmep1-3 strains expressing Magnaporthe oryzae aquaporins, the empty pYES2 vector or hAQP8, and the isogenic wildtype strain were spotted at OD_{600} 0.1 onto SD plates or nitrogen-minimal SG containing 0.1% proline or ammonium sulphate. The concentrations represent the concentration of the NH_4^+ group, not the $(NH_4)_2SO_4$. The experiments were performed at pH 5.5 (A), pH 6.5 (B) and pH 7.5 (C).*

6.4.2.2 *AQP1, AQP2, AGP1* and *AGP2* may be permeable to urea

The urea permeability assay utilises the inability of the *S. cerevisiae* Δ*dur3* strain to grow on concentrations of urea below 4 mM. Expression of urea-permeable aquaporins in Δ*dur3* cells restores the ability to grow below 4 mM. Three control growth conditions were included: a glucose control to ensure that aquaporin-repressed growth is normal, an arginine control to ensure that normal nitrogen metabolism is not adversely affected, and a 20mM urea control at which diffusion of urea across the membrane should be sufficient for growth of all strains. An *hAQP8* positive control was included to provide a reference, and the pYES2 empty vector is a negative control. The results are shown in Figure 6.6.

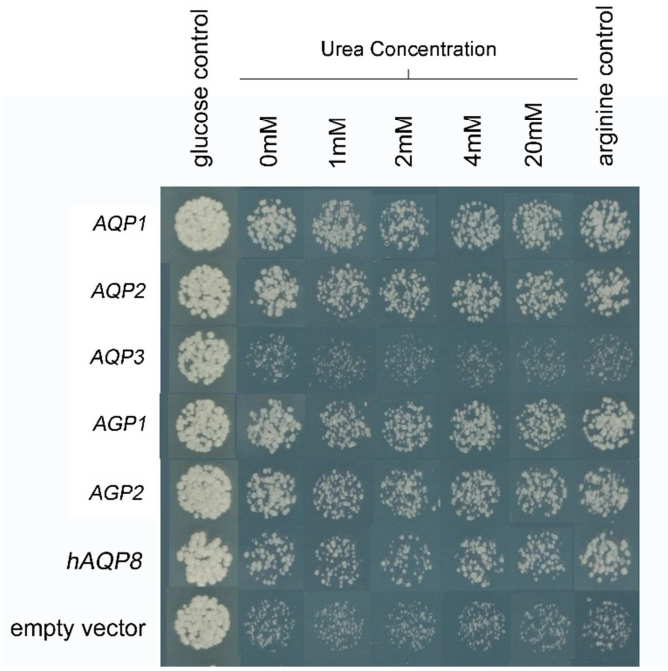

Figure 6.6: Functional complementation of the Saccharomyces cerevisiae Δdur3 deletion by Magnaporthe oryzae aquaporin genes. *Δdur3 strains expressing Magnaporthe oryzae aquaporins and the empty pYES2 vector or hAQP were spotted at OD_{600} of 0.01 onto SD plates or nitrogen-minimal SG plates containing 1 mM arginine or urea (0-20 mM) as a sole nitrogen source. The medium pH was adjusted to 5.5.*

On comparison with *hAQP8* and the empty vector, it superficially appears that all genes with the exception of *AQP3* are permeable to urea. However, a closer look at the controls reveals that this conclusion is problematic. The glucose control suggests that the initial inoculum is the same. However, growth on the arginine control and growth at 20 mM urea, both of which should be substantial and equivalent for all strains, is reduced in *AQP3* and the pYES2 empty vector line,

relative to the other aquaporin-expressing strains. For the other aquaporin-expressing lines, growth is not significantly enhanced at 20 mM relative to 0 mM urea, indicating that the experiment is not operating correctly. Similar results were obtained when the experiment was replicated.

As the strains do not behave as described, it would be unwise to conclude that these aquaporins are permeable to urea without validating the conclusion using a different experimental set-up.

6.4.2.3 *AQP1* and *AQP2* may be permeable to hydrogen peroxide

The severely-impaired oxidative response of *S. cerevisiae* Δ*yap1* makes the mutant hypersensitive to oxidative stress, therefore expression of an H_2O_2 permeable aquaporin causes a detectable growth reduction.

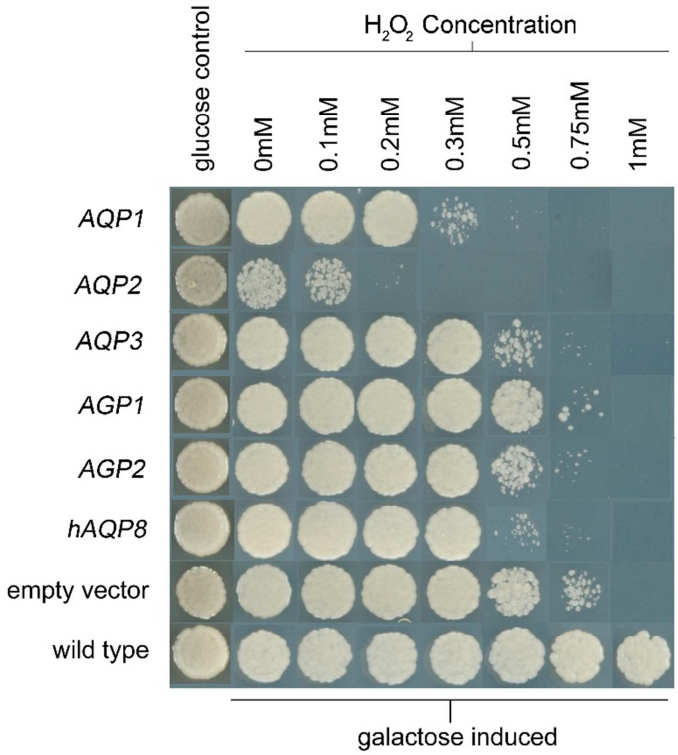

Figure 6.7: Growth of Saccharomyces cerevisiae Δyap1 cells on medium supplemented with H_2O_2. *Cells expressing Magnaporthe oryzae aquaporins, the hAQP8 positive control and the pYES2 empty vector, or the isogenic wildtype progenitor were spotted at an OD_{600} of 0.1 onto SD plates, or SG plates supplemented with a concentration range of H_2O_2. Plates were imaged after 4 days at 30°C.*

Comparison of the *M. oryzae* aquaporin expressing lines with the *hAQP8* positive control and the empty vector negative control line suggests that Aqp2 is highly permeable to H_2O_2, with significant

growth inhibition at as low as 0.1 mM H_2O_2. Aqp1 also appears to be permeable, with growth inhibition at 0.3 mM H_2O_2.

Examination of the glucose control lines indicates that the initial inoculum was comparable, but growth of Aqp2-expressing cells is reduced, even at 0mM H_2O_2. This was also observed in the repeat assay. As H_2O_2 is produced endogenously, the presence of a highly permeable peroxyporin might still reduce growth even in the absence of exogenous H_2O_2.

6.4.2.4 No aquaporins can compensate for *FPS1*

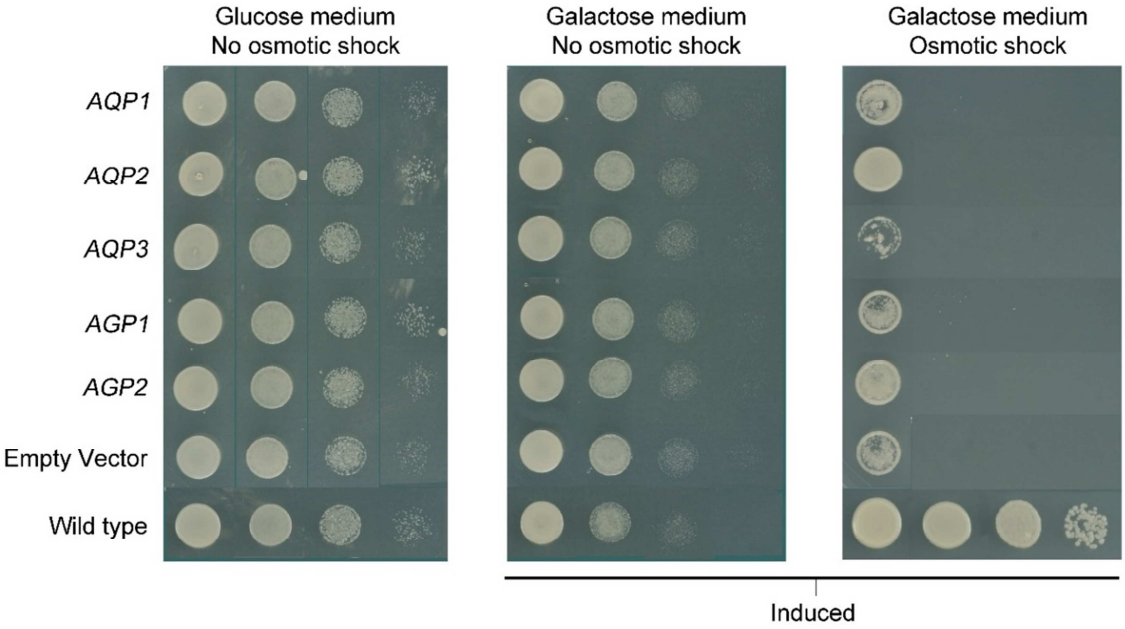

Figure 6.8: Growth of Saccharomyces cerevisiae Δfps1 cells and the isogenic wildtype FPS1 on glucose and galactose medium with or without a hypo-osmotic shock following equilibration at high osmolarity. *Cells transformed with Magnaporthe oryzae aquaporin or the pYES2 empty vector and the wildtype strain were pre-grown in inductive (galactose) or repressive (glucose) medium supplemented with 1M sorbitol for 16 h. Cultures were adjusted to an OD_{600} of 1 in water or water supplemented with 1M sorbitol and serially 10-fold diluted. Eight microliters of each dilution (left to right) was spotted onto SG or SD plates, with or without 1M sorbitol. Plates were imaged after 4 days at 30°C.*

The yeast Fps1 protein is responsible for rapidly releasing glycerol in response to sudden hypo-osmotic shock (Beese et al., 2009). We expressed the *M. oryzae* aquaporin genes in the *S. cerevisiae* Δ*fps1* background and cultured these cells in inductive SG medium, supplemented with 1 M sorbitol, overnight to induce glycerol accumulation. The cells were subsequently plated out onto SG plates with or without 1 M sorbitol. The induced cells that were not exposed to osmotic shock grew comparatively with the wild type and empty vector. This indicates that none of the

proteins function as constitutive glycerol channels, as these would be unable to retain internal glycerol and would therefore display a growth defect on high osmolarity medium.

The growth of induced proteins following hypo-osmotic shock also indicates that none of the proteins can compensate for Fps1 and rescue the phenotype.

The glucose controls indicate that the growth of each strain is normal under repressive conditions, and that the initial inoculum is the same between strains. However, no glycerol permeation of aquaporins could be detected using this assay.

6.4.3 Deletion of an H_2O_2 permeable aquaporin does not affect the rate of roGFP-redox response to H_2O_2 perfusion

Many publications have utilised xenologous expression in *Saccharomyces cerevisiae* or *Xenopus laevis* oocytes to test the substrate specificity of aquaporin proteins (Bertl & Kaldenhoff, 2007, Bienert et al., 2007, Liu et al., 2003). Few of these demonstrable permeabilities have been linked subsequently to phenotypes *in vivo.* The results of the H_2O_2 permeability assay indicate that *M. oryzae AQP2* is permeable to H_2O_2. If *AQP2* is present as a constitutive peroxyporin in the plasma membrane, the rate of diffusion of H_2O_2 across the PM could be reduced if the *AQP2* gene is deleted.

M. oryzae has extensive oxidative stress response pathways that are activated by to exogenous oxidative stress (Guo et al., 2011, Guo et al., 2010). One of these responses involves glutathione - a tripeptide cytoplasmic antioxidant that is normally present in its reduced form, but in response to severe oxidative stress prevents damage to cellular components by acting as a reducing agent (Belozerskaya & Gessler, 2007, Gessler et al., 2007).

The balance between cellular glutathione (GSH) and its reduced form, glutathione disulphide (GSSG) can be used as a measure of redox status in response to oxidative stress (Meyer et al., 2007). The electrochemical potential of the GSH:GSSG redox couple can be measured in fungi using transgenic redox GFP-based reporters (Heller et al., 2012). One such reporter, roGFP2 has two cysteine residues on adjacent β-strands in the protein barrel (Dooley et al., 2004). The formation of disulphide bridges between these residues causes structural changes in the protein

barrel, and the two forms are preferentially excited at two different wavelengths (ox = 405 nm, red = 488 nm). roGFP specifically senses the redox potential of the cellular glutathione pool using glutaredoxin (GRX) as a facilitator of electron movement between Grx and roGFP. This property allows ratiometric quantification of the GSH:GSSG redox couple. The fusion of a Grx subunit to the roGFP protein improves response kinetics (Gutscher et al., 2008).

The rate of oxidation of the glutathione pool in response to H_2O_2 challenge provides a proxy for diffusion of H_2O_2 across the plasma membrane. We compared the rate of ratio change following H_2O_2 perfusion of Guy11 and Δ*aqp2* spores expressing roGFP. Imaging and image processing are described in the Materials and Methods section of this chapter.

Data is shown in figures 6.10 – 6.11 from three independent perfusion experiments. Data was collected from a mixed group of spores, and the two genotypes were distinguished by the different emission intensities. As can be seen in all experiments, the average intensity of the roGFP signal is approximately 10-fold lower in the Δ*aqp2* transformant than in the wild type Guy11 transformant. However, the ratio data shows that the probe still behaves correctly in response to oxidation and reduction.

We compared the difference in % oxidation between the the Δ*aqp2* and the Guy11 roGFP-expressing strains at five conditions:

A. Resting oxidation levels
B. Maximum response to 20 mM H_2O_2 perfusion
C. Recovery following washout
D. Reduction following 10 mM DTT
E. Oxidation following 100 mM H_2O_2

The data shows no difference between the rate of oxidation or reduction between spores with a functional *AQP2* gene and those with a disrupted *AQP2* gene.

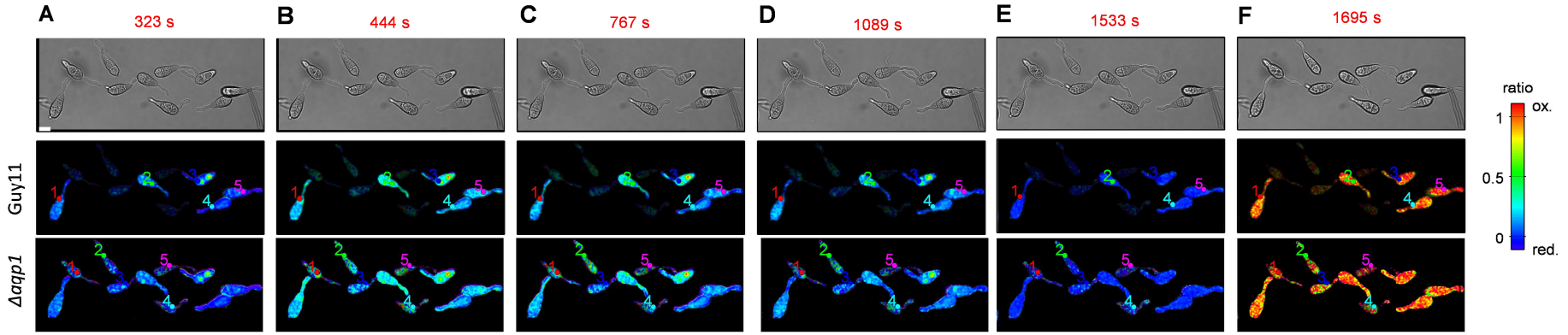

Figure 6.9: Response of the redox poise of the glutathione to transient oxidative stress during development of Guy11 and Δaqp2 germlings. *Guy11 and Δaqp2 germlings expressing Grx1-roGFP were sequentially imaged with excitation at 405nm and 488nm as z-stacks at 40s intervals and processed as described in the Materials and Methods of this chapter. This figure shows the resting redox poise of a mixed population of spores (**A**) response to 20mM H_2O_2 perfusion (**B**), recovery following perfusion of H_2O_2 (**C**), washout of the H_2O_2 (**D**). An internal calibration of complete reduction by 10mM DTT (E) followed by complete oxidation by 100mM H_2O_2 was performed (**F**). This calibration was used to generate the false colour display. The regions from which data was extracted in each genotype are shown as numbered, coloured dots.*

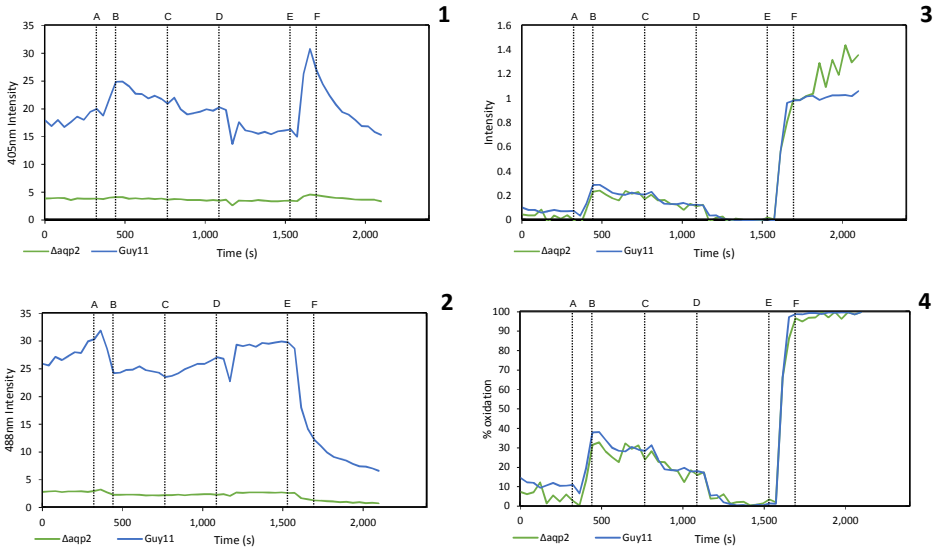

Figure 6.10: Graphs 1-4 show the data collected in Figure 6.9 averaged across all spores of each genotype. Labelled time points on the graphs correspond to the conditions described in Figure 6.9.

Graph 1 *shows the averaged signal intensity following 405 nm laser excitation, corresponding to the oxidised Grx1-roGFP2 signal.*
Graph 2 *shows the averaged signal intensity following 488 nm laser excitation, corresponding to the reduced Grx1-roGFP2 signal.*
Graph 3 *shows the ratio of oxidised to reduced roGFP signal. This data treatment corrects for signal bleaching and intensity differences between the two spore populations.*
Graph 4 *shows the average % oxidation of the glutathione pool in each genotype. The % oxidation is calculated using the internal calibration, where reduction following 10 mM DTT is fully reduced, and oxidation following 100mM H_2O_2 corresponds to fully oxidised.*

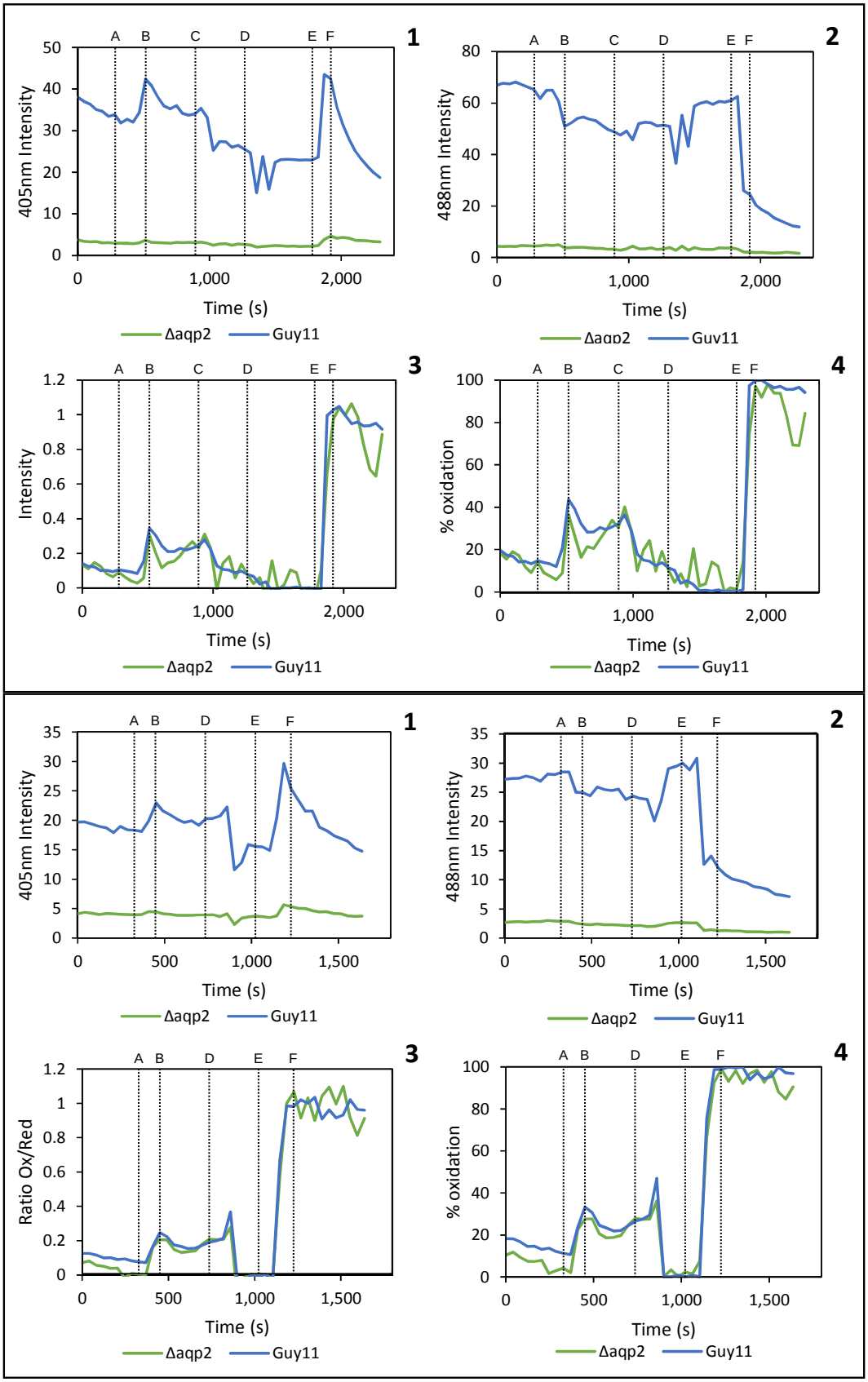

Figure 6.11: Box 1 and 2 are two independent experiments showing the redox poise of glutathione to transient oxidative stress during development of M. oryzae wildtype Guy11 and Δaqp2 germlings. *Legend continues overleaf…*

Figure 6.11 legend continued…*Guy11 and Δaqp2 germlings expressing Grx1-roGFP were sequentially imaged with excitation at 405 nm and 488 nm as z-stacks at 40 s intervals and processed as described in the Materials and Methods of this chapter. This figure shows the resting redox poise of a mixed population of spores (**A**) response to 20mM H_2O_2 perfusion (**B**), recovery following perfusion of H_2O_2 (**C**), washout of the H_2O_2 (**D**). An internal calibration of complete reduction by 10 mM DTT (E) followed by complete oxidation by 100 mM H_2O_2 was performed (**F**). This calibration was used to generate the false colour display. The regions from which data was extracted in each genotype are shown as numbered, coloured dots.*

1. *shows the averaged signal intensity following 405 nm laser excitation, corresponding to the oxidised Grx1-roGFP2 signal.*
2. *shows the averaged signal intensity following 488 nm laser excitation, corresponding to the reduced Grx1-roGFP2 signal.*
3. *shows the ratio of oxidised to reduced roGFP signal. This data treatment corrects for signal bleaching and intensity differences between the two spore populations.*
4. *shows the average % oxidation of the glutathione pool in each genotype. The % oxidation is calculated using the internal calibration, where reduction following 10 mM DTT is fully reduced, and oxidation following 100 mM H_2O_2 corresponds to fully oxidised.*

The Guy11 and Δaqp2 data in Box 1 is the average of data from four independent spores. The Guy11 data in Box 2 is the average of data from two spores, and the Δaqp2 data is the average from five spores. No washout was performed in the experiment shown in Box 1.

6.5 Discussion

6.5.1 The *Magnaporthe oryzae* 70-15 gene annotations are of poor quality

Pre-spliced cDNA sequences must be used for *S. cerevisiae* expression assays as *M. oryzae* genes would not necessarily be spliced correctly (Juneau et al., 2009). Amplification of these sequences necessitated validation and sequencing of the amplified cDNA sequences. In 3/5 amplified sequences, the annotated gene coding sequence was incorrect in the widely-used 70-15 reference sequence (Dean et al., 2005).

The quality of the annotation in the recently-released P131 and Y34 genome releases (Xue et al., 2012) appears much improved, as all erroneous annotations discovered in the 70-15 release are correct in these versions. Any future work, where the gene sequence is important, should cross-reference the 70-15 gene sequences with the P131 and Y34 versions.

6.5.2 Predictions based on the primary sequence are partially correct

In Section 6.4.1, we made the following predictions based on the primary sequence of each *M. oryzae* aquaporin protein:

i) Aqp1 permeability to H_2O_2

ii) Aqp2 permeability to H_2O_2

iii) Aqp1 permeability to urea

iv) Aqp2 permeability to urea

v) Agp2 permeability to glycerol

Predictions i) and ii) proved to be correct. However, predictions iii) and iv) could not be substantiated because the assay did not function as expected, and prediction v) could not be supported by the results of the assay.

Xenologous expression assays, if carried out with the correct controls, can be used to infer permeability to specific substrates. The assays used in this experiment have been validated using other techniques (Bienert et al., 2011, Bienert et al., 2007, Liu et al., 2003, Prudent et al., 2005). However, absence of evidence of permeability does not demonstrate impermeability. Xenologous expression assays with aquaporins are predicated on several assumptions:

- The proteins are translated and folded correctly in *S. cerevisiae.*
- The proteins are plasma membrane localized.
- The proteins are constitutively active.
- They do not function as heterotetramers.

A positive result in one or more assays indicates that those specific proteins fold correctly, are active and are correctly trafficked to the PM. It also suggests that that specific substrate does not permeate through heterotetrameric protein complexes. However, in the case of *AQP3* and *AGP2*, which were not demonstrably permeable to any of the substrates tested, these possibilities cannot be excluded.

The first two assumptions can be tested using immunolocalisation assays. We cloned a variant of the cDNA coding sequences with a MYC epitope tag at the C-terminal. Immunolocalisation with anti-c-MYC antibodies could have been used to check for expression of the construct and localisation of the signal to the plasma membrane. This experiment was not carried out due to the imminent submission deadline, but would serve as a useful augmentation to any future expression assays.

The final two assumptions are more challenging to test experimentally. Gating properties are typically investigated by site directed mutatgenesis and molecular dynamic simulation (Jozefkowicz et al., 2013, von Bülow et al., 2012). Otto et al. (2010) used co-expression of two *Nicotiana tabacum,* NtAQP1 and NtPIP2;1, in *S. cerevisiae* to demonstrate that tetramer composition affected transport activity. However, all of these options are technically challenging and were not performed for these proteins.

Yeast drop test assays can provide a qualitative measure of substrate permeability. However, could be improved by making more quantitative measures of substrate permeability. Expression in *Xenopus laevis* oocytes, or stopped flow spectrophotometry with yeast cells can provide a more quantitative measure (Bertl & Kaldenhoff, 2007, Virkki et al., 2002). Future analysis of these proteins should consider these techniques as an augmentation to the project.

6.5.3 Deletion of the H_2O_2 permeable *AQP2* does not affect the rate of H_2O_2 diffusion across germling plasma membranes

The *M. oryzae* aquaporin, *AQP2*, appears to be highly permeable to hydrogen peroxide. We tested the rate of diffusion of H_2O_2 across the plasma membrane by measuring the redox state of the cellular glutathione pool, with a roGFP reporter, following H_2O_2 challenge.

The results suggest that the rate of diffusion of H_2O_2 across the plasma membrane is not altered by the absence of the Aqp2 protein. There are four possible interpretations of this result:

1) There is no Aqp2 in the plasma membrane.
2) There are compensatory changes that restore the wildtype diffusion rate.
3) Aqp2 in the plasma membrane does not affect the rate of diffusion of hydrogen peroxide.
4) The change in the rate of diffusion is not detected by this assay.

The first interpretation could be explained by two factors. First, that Aqp2 protein is at very low abundance in the membranes of developing germlings, and second, that Aqp2 does not localise to the plasma membrane. Transcript abundance data from chapter 3 and 5 indicates that the transcript is present during the early stages of germling development when the assay was

performed. However, the relationship between transcript abundance and protein abundance is not necessarily linear (Greenbaum et al., 2003, Vogel & Marcotte, 2012). If the Aqp2 protein is rare, deletion of the gene may not have a detectable effect. Alternatively, the Aqp2 protein may be present, but not localise to the plasma membrane. If the protein is expressed on an internal membrane, the assay would not show a change in the rate of diffusion across the plasma membrane.

The issue of compensatory genetic regulation is discussed at length in chapter 5. It is particularly interesting that the proposed compensatory feedback loop identified in that chapter concerns Aqp1 and Aqp2, both of which have been demonstrated in this chapter to be permeable to H_2O_2. It is plausible that the compensatory up-regulation of Aqp2 in the Δ*aqp1* background obscures the effect on the rate of diffusion of H_2O_2.

The third possibility is simply that Aqp2 does not have a significant effect on the rate of diffusion of H_2O_2 relative to diffusion across the lipid bilayer. The diffusion coefficient of H_2O_2 across membranes is a subject of debate (Antunes & Cadenas, 2000, Miller et al., 2010, Sousa-Lopes et al., 2004), but it plausible that the magnitude of the direct diffusion conceals the loss of facilitated diffusion.

The final potential explanation of this result, is there is a genuine difference between the H_2O_2 diffusion rate, but that it is not detected by the assay. However, this is unlikely. The difference in midpoint potential of the GSH:GSSG redox couple and the Grx1-roGFP redox couple makes the Grx1-roGFP extremely sensitive to small increases in the proportion of oxidised roGFP (Meyer & Dick, 2010). The Grx-roGFP2 conjugate senses redox potential changes between -240mV and -320mV, but the midpoint potential of glutathione is approximately -180mV (Lukyanov & Belousov). The Grx-roGFP2 range therefore corresponds to very small increases from the baseline state; therefore, the probe is highly responsive, and a slower or less pronounced response (as might be predicted in the absence of Agp2) would certainly be detected.

The only direct evidence that aquaporins influence H_2O_2 diffusion *in vivo* comes from an overexpression study in mammalian cells (Miller et al., 2010). Here, individual aquaporins were overexpressed in HeLa cells, and the response measured of a chemoselective fluorescent

indicator for H_2O_2, Peroxy Yellow 1 Metthyl-Ester (PY1-ME), to H_2O_2 perfusion. This research is, to our knowledge, the first study of the effect of an aquaporin protein on H_2O_2 diffusion in its native context. Given the recent interest in H_2O_2 as a signalling molecule (for a review see Gough and Cotter (2011)), further work on this aspect of the project should be a priority.

Two key experiments should be carried out. First, a double knockout for the two peroxyporins, *AQP1* and *AQP2* should be constructed. The roGFP construct should be introgressed, and the experiments described in this chapter repeated. Second, the Δ*aqp2* background should be complemented with an epitope-tagged *AQP2* gene, and the localisation of the protein examined using immunofluorescence or immunoblotting. The combination of these two experiments would help address the first two interpretations of the negative result described in this chapter. No change in the rate of diffusion was observed in these assays supports the conclusion that aquaporins do not affect the rate of diffusion of H_2O_2 across the PM in *M. oryzae* germlings.

Chapter 7 GFP tagging of aquaporins in *M. oryzae*

7.1 Introduction

In chapter 4, we examined the phenotype of aquaporin single-deletion strains in *M. oryzae* and found minor, but statistically significant growth differences between the wild type Guy11 and mutant strains. This chapter details the attempt to recomplement the aquaporin mutants with eGFP-aquaporin fusion constructs. A functional recomplementation strain would allow us to distinguish 'real' phenotypes caused by the gene deletion from cryptic unrelated differences. These fusion proteins would also provide an insight into the membrane localisation of the MIPs. With these aims in mind, I generated C- and N- terminal, and internal loop, aquaporin-eGFP fusions with both the native and constitutive promoters. I also attempted to characterise the activity of aquaporin promoters using cytosolic eGFP as a reporter. The problems detailed herein demonstrate the challenge of working with membrane fusion proteins.

7.1.1 Aquaporin localisation

There are two primary mechanisms for investigating protein localisation – epitope tagging and fluorescent-protein tagging (Terpe, 2003). Heavily melanised fungal cells are impervious to many antibodies, therefore epitope tagging is problematic when looking at *M. oryzae* germlings. Fluorescent proteins are a genetically-encoded alternative to immunolocalisation and are extensively used in *M. oryzae* (Campos-Soriano et al., 2012, Dagdas et al., 2012). Fluorescent fusion proteins also offer the possibility of studying turnover, transport and protein-protein interactions, using techniques such as FRET, fluorescence recovery after photobleaching,

fluorescence lifetime imaging, or bimolecular fluorescence complementation (see Fricker et al. (2006) for a review) (Moore & Murphy, 2009).

Very little is known about the subcellular localisation of aquaporin proteins in fungi. This chapter details the attempt to generate *M. oryzae* strains expressing aquaporin proteins fused to the 'enhanced' GFP variant (eGFP). This variant is brighter and has a lower tendency to oligomerise that native GFP (Zhang et al., 1996).

7.2 Experimental aims

1) To recomplement aquaporin single deletion strains using eGFP-aquaporin fusion proteins.
2) To examine the subcellular localisation of aquaporins by confocal microscopy.

7.3 Methods specific to this chapter

7.3.1 Yeast recombinational cloning

Yeast recombinational cloning is a technique used to create modular DNA constructs; it requires regions of homology at the ends of the fragments to be joined. These fragments, and the *S. cerevisiae* / *E. coli* dual expression vector 1284 pNEB-Nat-Yeast, are thence transformed into *S. cerevisiae* and recombination occurs between the homologous regions, so yielding a contiguous DNA plasmid. The backbone plasmid carries ampicillin resistance marker for selection in *E. coli,* and the URA3 gene, encoding uracil prototrophy, for selection in *S. cerevisiae.* PCR primers were designed to include 25-30 bp of homology between the fragments to be joined and terminal fragments were designed with homology to the 1284 pNEB-Nat-Yeast cloning vector. All DNA fragments were amplified with a high-fidelity polymerase.

S. cerevisiae (strain DS94) was transformed with 300-500 ng each DNA fragment as described in the Materials and Methods. Colonies were selected for uracil prototrophy.

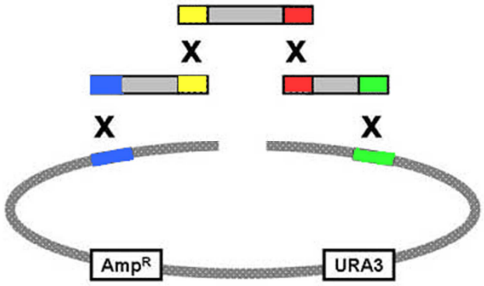

Figure 7.1: Yeast Recombinational Cloning (YRC) to assemble modular constructs with regions of 25-30 bp homology. Overlapping inserts recombine when co-transformed into yeast. *Fragments must be amplified using high fidelity polymerases and the vector must be linearised with Hind*III *and dephosphorylated to prevent recircularisation.*

Ten to fifteen colonies per DNA construct were inoculated into 50ml selective SD liquid medium (see general Materials and Methods) and grown for 16 h at 30^{o}C and 150 rpm. Plasmids were extracted as follows:

1. After incubation, cells were centrifuged at 1500 rpm and the pellet was resuspended in 0.5 ml sterile distilled water.
2. This suspension was transferred to a 1.5 ml Eppendorf tube and centrifuged for 5 sec at maximum speed 13,000 rpm.
3. The supernatant was removed and 250 µl yeast lysis buffer, 250 µl phenol: chloroform: isoamylalcohol (25:24:1) and 0.3 g acid washed glass beads (425-600 µm) were added.
4. Tubes were vortexed for 30 m and 250 µl TE buffer (pH 8) was added after vortexing.
5. The mixture was centrifuged at 13,000 rpm for 15 min and the aqueous phase was transferred to a new tube. To this, 1/10th volume of 3 M sodium acetate pH 5.5 and 1 ml 96% ethanol was added and the tubes were incubated at -20^{o}C for not less than 30 min.
6. The tubes were centrifuged at 13,000 rpm for 30 min at 4^{o}C and the supernatant was discarded.
7. The pellet was resuspended in 400 µl TE buffer pH 8 and 4 µl RNase A (10 mg/ml) was added. This was incubated at 37^{o}C until the pellet dissolved.
8. 10 µl of 4 M ammonium acetate and 1 ml 96% (w/v) ethanol were added.
9. The tubes were centrifuged for 15 min at 13,000 rpm and the supernatant was discarded.
10. The pellet was washed with 500 µl ice cold 70% (w/v) ethanol and air dried before resuspension in 50 µl distilled water.

After extraction, the plasmids were amplified using ultra-competent *E. coli* cells as described in the Materials and Methods. Plasmids were digested to confirm correct assembly of the construct and transformed into *M. oryzae.*

7.3.2 Confocal microscopy

Spores (100 µl; 2.5x10^5 per ml) were inoculated onto inductive Menzel coverslips and germinated for the time indicated. Germlings were viewed using the C-Apochromat x40/1.2 water immersion lens of a Zeiss LSM 510 Meta Microscope, with argon laser excitation at 488 nm and emission collected at 500-530 nm. Simultaneous nonconfocal transmission 3D (*x, y, z*) images were collected as z-stacks with a pixel spacing of 0.22 µm x 0.22 µm x 1-2 µm or 0.12 µm x 0.12 µm x 1-2 µm with 6-18 optical sections. Images are displayed as maximum projections along the z-axis unless specified otherwise.

7.3.3 Western blots

7.3.3.1 Total protein extraction from *Magnaporthe oryzae*

A sterile pestle and mortar was pre-cooled using liquid nitrogen and the surface tissues scraped from a 10 day old CM culture directly into liquid nitrogen, using a sterile scalpel. The frozen tissue was ground into a fine powder and approximately 200 mg tissue was placed into a 1.5 ml Eppendorf tube on ice before 1 ml ice cold 1x RIPA buffer was added to each tube. The tubes were vortexed until the powder had dispersed into the buffer. These tubes were packed into an ice-filled beaker and this beaker was securely-sealed and attached to the head of a vortex. The samples were vortexed, at maximum speed, for 45 min. Samples were centrifuged at 4^{o}C for 20 min at 17,900 xg (13,000 rpm) and the supernatant was pipetted into a pre-cooled 1.5 ml Eppendorf tube. Protein samples were stored at -80^{o}C or used immediately.

7.3.3.2 Electrophoresis of proteins using SDS-PAGE

SDS-PAGE was carried out using a Mini-PROTEAN 3 Cell and blot module (BioRad). Gels were hand-cast, as detailed below.

Two 12% (w/v) acrylamide running gels were prepared with 9.2 ml sterile dH2O, 4.8 ml 1.5 M Tris pH 8.8, 6 ml of 40% (w/v) acrylamide and 200 µl 10% (w/v) SDS. To polymerise, 12 µl of TEMED (BioRad) was added whilst mixing followed by 180 µl 10% (w/v) ammonium persulphate (BioRad) as a co-catalyser. Water-saturated butanol was poured over the upper edge of the gel to create an anoxic medium and facilitate faster polymerisation. When polymerisation was complete, the stacking gel was prepared as follows: 8.3 ml H_2O, 3.8 ml 0.5 M Tris buffer pH 6.8, 1.9 ml 40% acrylamide (w/v), 150 µl 10% SDS; 15 µl TEMED whilst mixing followed by 150 µl 10% (w/v) ammonium persulfate. The stacking gel was then carefully pipetted onto the running gel and the comb placed on top.

Samples were pre-mixed to a final concentration of 1x protein loading dye and pipetted into the wells. 10 µl SeeBlue Plus2 Pre-Stained Standard protein ladder (Invitrogen) was included in each blot. Samples were run in 1x western running buffer at a constant 150 V for 30 m - 1 h or until the loading dye reached the lower edge of the gel.

7.3.3.3 Electrophoretic transfer

The PVDF transfer membrane [Immobilon P, Millipore) was initially hydrophilised by gentle agitation for 30 min at room temperature, in 20 ml methanol and 80 ml sterile dH_2O.

Proteins were transferred to the hydrophilised membrane using the Mini-PROTEAN electrophoresis transfer cell (Biorad) in 1x western Transfer buffer. The electrophoretic transfer was performed at 100 mA for 1h 30m. The membrane was rinsed for five min in 1x TBS-T before blocking in 1x blocking buffer (30 ml per blot) for 30-60 min.

7.3.3.4 Detection of proteins

The primary anti-GFP rabbit polyclonal antibody (ab290, AbCam) was diluted in 1x blocking buffer to 1:2500 in a final volume of 10 ml per 15 cm^2 membrane area. The membrane was incubated in the antibody for 1h at room temperature, with gentle agitation. The membrane was washed three times in 1x TBS-T for 1x 10 min and 2x 5 min. After the final wash an alkaline phosphatase-conjugated anti-rabbit antibody A3687 (Sigma Aldrich) was diluted to 1:10,000 in 10ml TBS-T. The

membrane was agitated for 30 min before washing in 1x TBS-T buffer for 1x 10 min and 2x 5 min. The membrane was rinsed in 1x TBS before developing.

A SIGMAFAST^{TM} BCIP/NBT tablet (Sigma Aldrich) was dissolved in 10ml sterile ddH_2O and vortexed until the tablet dissolved. The membrane was submerged in the developing solution and gently agitated in the dark until sufficient colour had developed (1-5 min). Finally, the membrane was rinsed with water and the reaction stopped by submersion in 20mM EDTA, in the dark for 2 min.

7.4 Results

7.4.1 C-terminal aquaporin fusion proteins are not expressed or mislocalise

C-terminal eGFP fusions mislocalise less frequently, as localisation signals, predominantly located at the N-terminus, are less likely to be disrupted (Palmer & Freeman, 2004). We designed a construct, shown in Figure 7.2, to express each aquaporin protein under the control of its native promoter, as a fusion with eGFP at the C-terminus. A flexible 5x glycine linker was included between the two proteins to prevent steric hindrance of protein-folding and subsequent misfolding of one or both proteins (Iwakura & Nakamura, 1998). Downstream of the fusion protein, an *Aspergillus nidulans* TrpC terminator was included to ensure correct termination of transcription, and an antibiotic resistance gene was included in the construct to facilitate transformation of the construct into *M. oryzae*. We used the native promoters in order to understand endogenous protein levels and timing of protein expression.

To generate the constructs, the aquaporin protein coding regions and approximately 1.5 kb of upstream promoter region was cloned with the STOP codon deleted, in frame with eGFP, into the *Asc*I and *Sbf*I sites of a modified pUCAP19 expression vector. This vector contained the eGFP, a TrpC terminator from *A. nidulans* and either hygromycin resistance (HYGR) or bialophos resistance (BAR) as *M. oryzae* selectable markers.

Individual proteins were constructed as follows:

- The *AQP1* coding region, and 1562 bp of upstream promoter sequence were amplified by the C03904F and C03904R primers. The PCR product was then digested and cloned into the *Asc*I and *Sbf*I sites of a HYGR-containing expression vector.
- The *AQP2* coding region and 1416 bp of promoter sequence, amplified by C04162F and C04162R primers, was cloned into the *Asc*I and *Sbf*I sites of a BAR vector.
- The *AQP3* coding region and 1541 bp of promoter sequence was amplified with C13332F and C13332R primers, also with *Asc*I and *Sbf*I restriction sites of a HYGR vector.
- The *AGP1* coding region was only amplified with 369 bp of promoter sequence as there are only 471 bp separating *AGP1* and *MGG_05881*. The *AGP1* promoter also had an *Sbf*I site, therefore the *AGP1* primers, C05880F and C05880R, were flanked with two *Asc*I sites and the *AGP1* construct was cloned into the single site of a HYGR vector. The orientation of the insert was checked with restriction enzyme digestion.
- The *AGP2* coding region, and 1570 bp of promoter sequence, was amplified using C13615F and C13615R primers and cloned into the *Asc*I and *Sbf*I sites of a BAR vector.

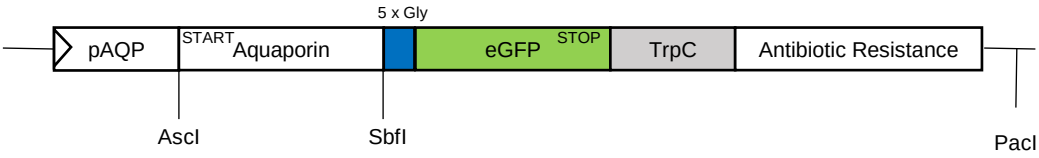

Figure 7.2: A schematic of the C-terminal eGFP fusion construct. *The aquaporin protein and approximately 1.5 kb of the upstream promoter region was cloned, in frame with eGFP and before a 5x glycine flexible linker domain, into the* Asc*I and* Sbf*I sites. The transcription was terminated by the Aspergillus nidulans TrpC terminator. A selectable marker was used for identifying positive transformants after transformation into the fungus. The plasmid backbone is a modified pUCAP19 vector (courtesy of Dr. M. Samalova, University of Oxford).*

The constructs were amplified using competent *E. coli* cells and transformed into the aquaporin single deletion line that corresponded to their protein fusion. Six to twelve resistant lines were selected per construct and screened for fluorescence using confocal microscopy at three developmental stages (spores, developing germ tubes and mature appressoria). Representative images are shown in Figure 7.3 - Figure 7.8.

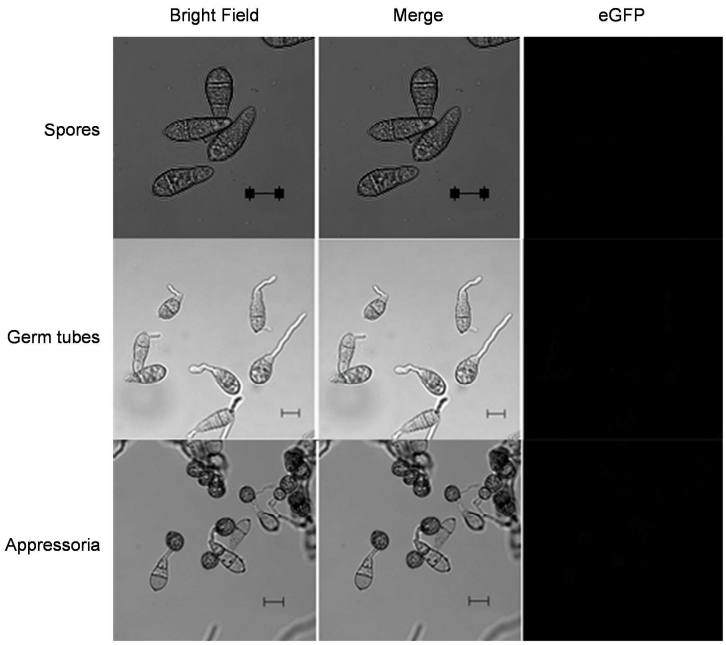

Figure 7.3: Confocal images of Guy11 germlings at three developmental stages. *Conidia were inoculated on inductive Menzel slides and viewed using the C-Apochromat x40 / 1.2 water immersion lens of a Zeiss LSM 510 Meta Microscope, with argon laser excitation at 488 nm and emission collected at 500-530 nm. Simultaneous nonconfocal transmission 3D (x, y, z) images were collected as z-stacks with a pixel spacing of 0.22 µm x 0.22 µm x 1-2 µm or 0.12 µm x 0.12 µm x 1-2 µm with 6-18 optical sections. Images are displayed as maximum projections along the z-axis. Scale bars = 10 µm.*

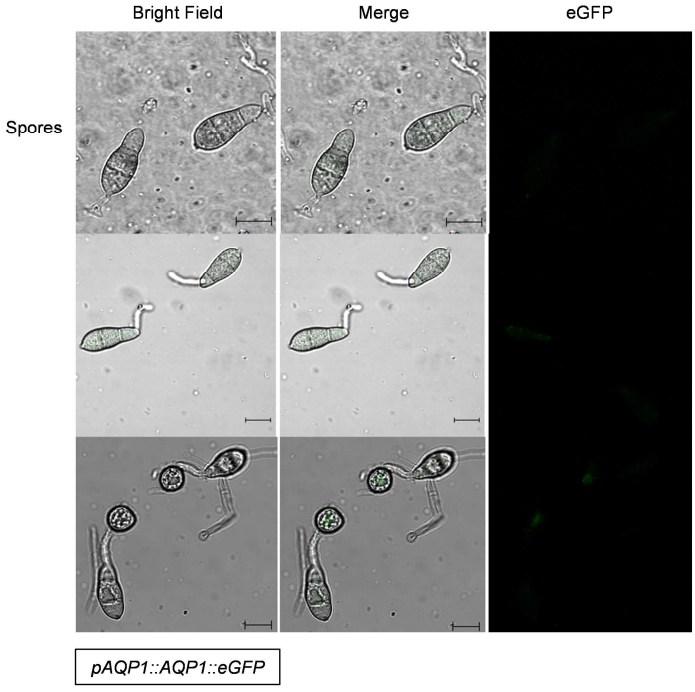

Figure 7.4: Confocal images of Δaqp1 germlings expressing pAQP1::AQP1::eGFP at three developmental time points. *Conidia were inoculated on inductive Menzel slides and viewed using the C-Apochromat x40 / 1.2 water immersion lens of a Zeiss LSM 510 Meta Microscope, with argon laser excitation at 488 nm and emission collected at 500-530 nm. Simultaneous nonconfocal transmission 3D (x, y, z) images were collected as z-stacks with a pixel spacing of 0.22 µm x 0.22 µm x 1-2 µm or 0.12 µm x 0.12 µm x 1-2 µm with 6-18 optical sections. Images are displayed as maximum projections along the z-axis. Scale bars = 10 µm.*

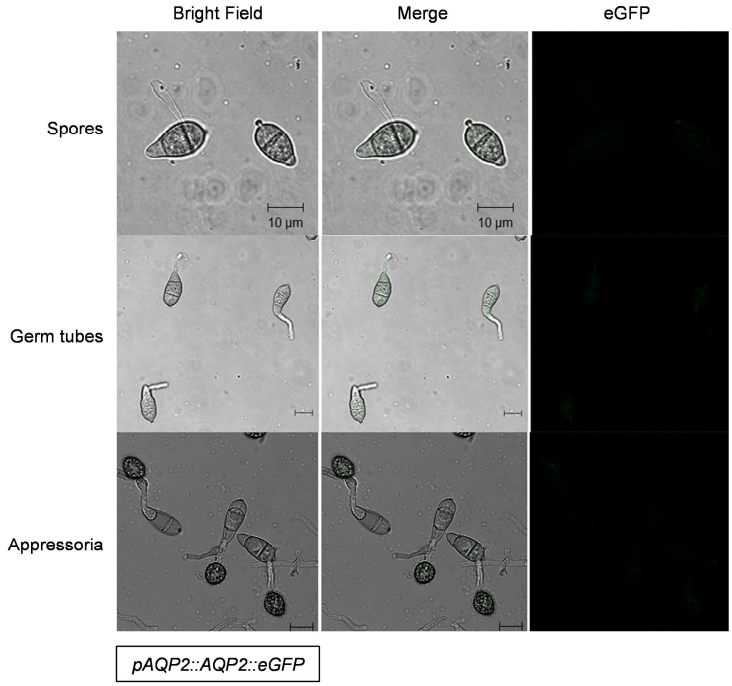

Figure 7.5 Confocal images of Δaqp2 germlings expressing pAQP2::AQP2::eGFP at three developmental time points. *Conidia were inoculated on inductive Menzel slides and viewed using the C-Apochromat x40 / 1.2 water immersion lens of a Zeiss LSM 510 Meta Microscope, with argon laser excitation at 488 nm and emission collected at 500-530 nm. Simultaneous nonconfocal transmission 3D (*x, y, z*) images were collected as z-stacks with a pixel spacing of 0.22 µm x 0.22 µm x 1-2 µm or 0.12 µm x 0.12 µm x 1-2 µm with 6-18 optical sections. Images are displayed as maximum projections along the z-axis. Scale bars = 10 µm.*

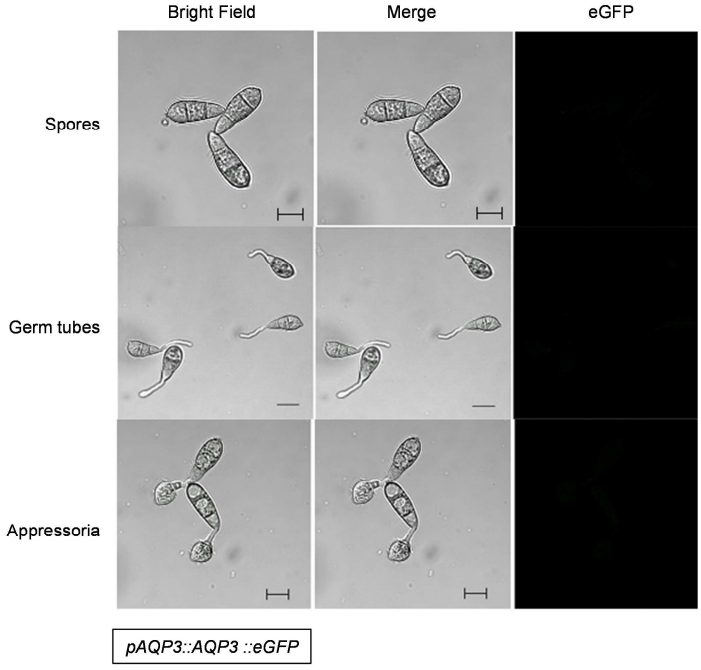

Figure 7.6: Confocal images of Δaqp3 germlings expressing pAQP3::AQP3::eGFP at three developmental time points. *Conidia were inoculated on inductive Menzel slides and viewed using the C-Apochromat x40 / 1.2 water immersion lens of a Zeiss LSM 510 Meta Microscope, with argon laser excitation at 488 nm and emission collected at 500-530 nm. Simultaneous nonconfocal transmission 3D (*x, y, z*) images were collected as z-stacks with a pixel spacing of 0.22 µm x 0.22 µm x 1-2 µm or 0.12 µm x 0.12 µm x 1-2 µm with 6-18 optical sections. Images are displayed as maximum projections along the z-axis. Scale bars = 10 µm.*

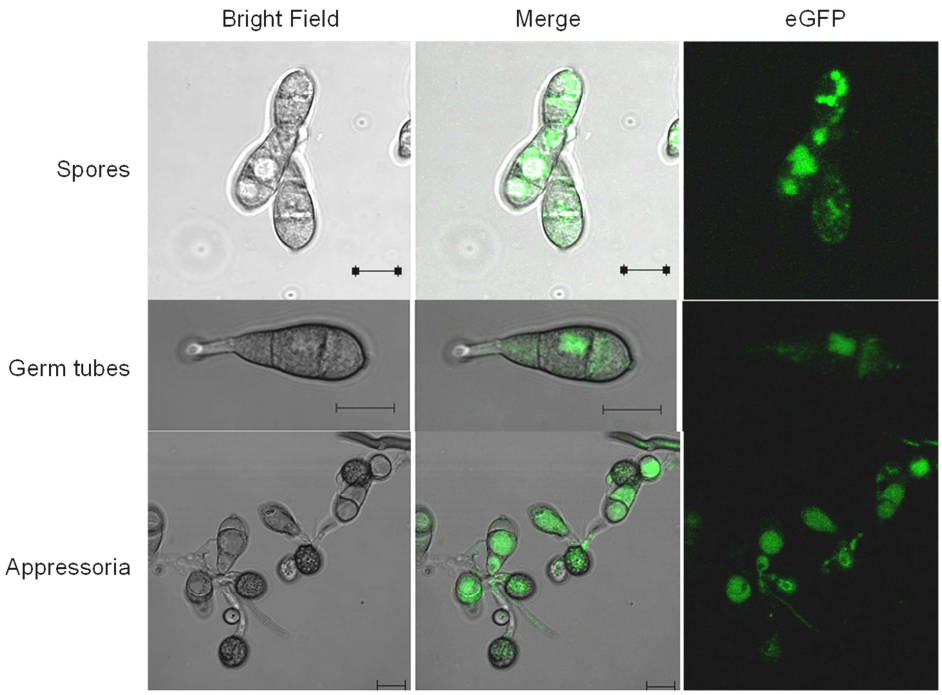

Figure 7.7: Confocal images of Δagp1 germlings expressing pAGP2::AGP2::eGFP at three developmental time points. *Conidia were inoculated on inductive Menzel slides and viewed using the C-Apochromat x40 / 1.2 water immersion lens of a Zeiss LSM 510 Meta Microscope, with argon laser excitation at 488 nm and emission collected at 500-530 nm. Simultaneous nonconfocal transmission 3D (x, y, z) images were collected as z-stacks with a pixel spacing of 0.22 µm x 0.22 µm x 1-2 µm or 0.12 µm x 0.12 µm x 1-2 µm with 6-18 optical sections. Images are displayed as maximum projections along the z-axis. Scale bars = 10 µm.*

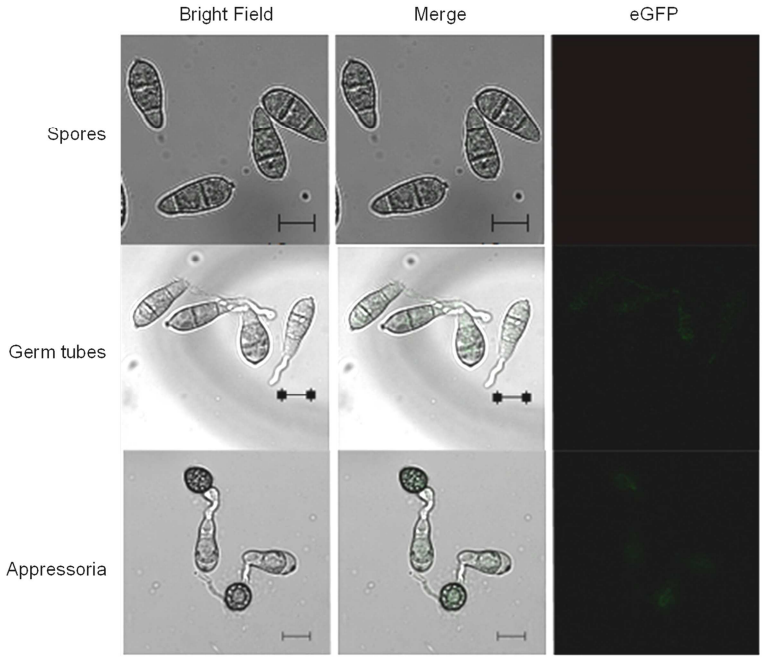

Figure 7.8: Confocal images of Δagp2 germlings expressing pAGP2::AGP2::eGFP at three developmental time points. *Conidia were inoculated on inductive Menzel slides and viewed using the C-Apochromat x40 / 1.2 water immersion lens of a Zeiss LSM 510 Meta Microscope, with argon laser excitation at 488 nm and emission collected at 500-530 nm. Simultaneous nonconfocal transmission 3D (x, y, z) images were collected as z-stacks with a pixel spacing of 0.22 µm x 0.22 µm x 1-2 µm or 0.12 µm x 0.12 µm x 1-2 µm with 6-18 optical sections. Images are displayed as maximum projections along the z-axis. Scale bars = 10 µm.*

The levels of protein fluorescence are below the detectable threshold for all fusion proteins, with the exception *AGP1*. But this is not uncommon when working with fluorescent proteins (Rizzo et al., 2009). The absence of detectable fluorescence can be caused by a number of factors:

- The localised environment of the target organelle (primarily pH)
- Improper folding of the chimaera
- Silencing of the fusion expression
- High levels of protein turnover that degrade the chimeric complex before the fusion protein is fully mature
- Low expression from the promoter
- Mutations in the construct

Many of these problems can be addressed by western blot analysis which is, itself considerably more sensitive to eGFP than fluorescence microscopy, and can detect immature and improperly folded eGFP that could otherwise not be visualised (Chalfie & Kain, 2005). We performed a western blot with anti-GFP antibodies on the total protein extract from these fusion lines. The blot is shown in Figure 7.9.

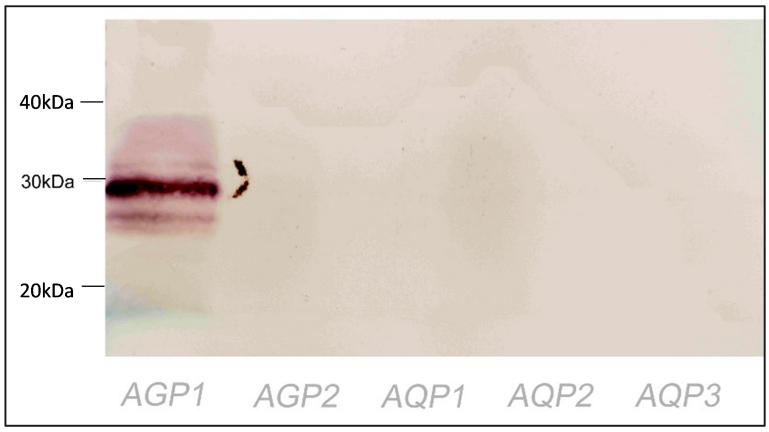

Figure 7.9: A western blot with anti-GFP polyclonal antibodies on total protein extract from pAQP C-terminal eGFP fusion lines. *The AGP1 band corresponds to the size of the un-conjugated eGFP monomer. No signal is detected in the non-fluorescent lines.*

The blot shows that there is no expression of eGFP in the *AGP2, AQP1, AQP2* and *AQP3* fusion lines. It also reveals that the *AGP1* eGFP fluorescence results from cleaved eGFP rather than a complete fusion protein. The expected band size for the *AGP1::eGFP* fusion protein is predicted to be 65 kDa, but the eGFP signal migrates as a ~30 kDa band. This corresponds well with the size of free eGFP (28 kDa). The *AGP1::eGFP* fluorescent signal in Figure 7.7 appears to localise to the vacuoles, consistent with a non-membrane associated protein.

For *AQP1-3* and *AGP2*, the absence of detectable expression by western blot analysis allows us to eliminate several possible explanations as to why no fluorescence is be detected. A western signal would be detected if the protein were in an acidic organelle, and if proteins were folding improperly or being rapidly degraded. We cannot eliminate the possibility that the construct was silenced, the promoter expression was low, or that there are inactivating mutations in the construct. To address the issue of introduced mutations, we sequenced a sample construct - the full length *AGP2::eGFP* construct - and found it to carry no mutations.

For *AGP1,* the promoter is clearly driving expression of the construct, but the chimeric protein is likely being degraded and sequestered in the vacuoles. The *Agp2* protein is relatively small (approximately 38 kDa), therefore the addition of a 28 kDa eGFP tag could cause improper folding and subsequent rapid degradation (Goldberg, 2003). Chimeric proteins where the FP is cleaved often localise correctly when the FP is placed in a different position (Rizzo et al., 2009). Experiments with human *AQP4* provide an example of correctly-localised *AQP4* with an internal eGFP tag on the C-loop (Tajima et al., 2010). We therefore attempted to generate an *AGP1* fusion with an internal eGFP fluorescence tag.

7.4.2 An *AGP1* fusion with *eGFP* on an internal loop has no detectable fluorescence

The *AGP1::eGFP* C-terminal chimera from Section 7.4.1 was expressed, but could only be detected as degradation products of the fusion. We generated an FP fusion protein with eGFP on an internal loop to determine whether this breakdown was caused by tag-induced misfolding of the protein. The topology of the protein was predicted using MEMSAT_SVM (see chapter 3). We selected the longest internal loop as the site for eGFP localisation to maximise the distance between the membrane core of the protein and the FP tag. The structure of the eGFP fusion protein is shown in Figure 7.10.

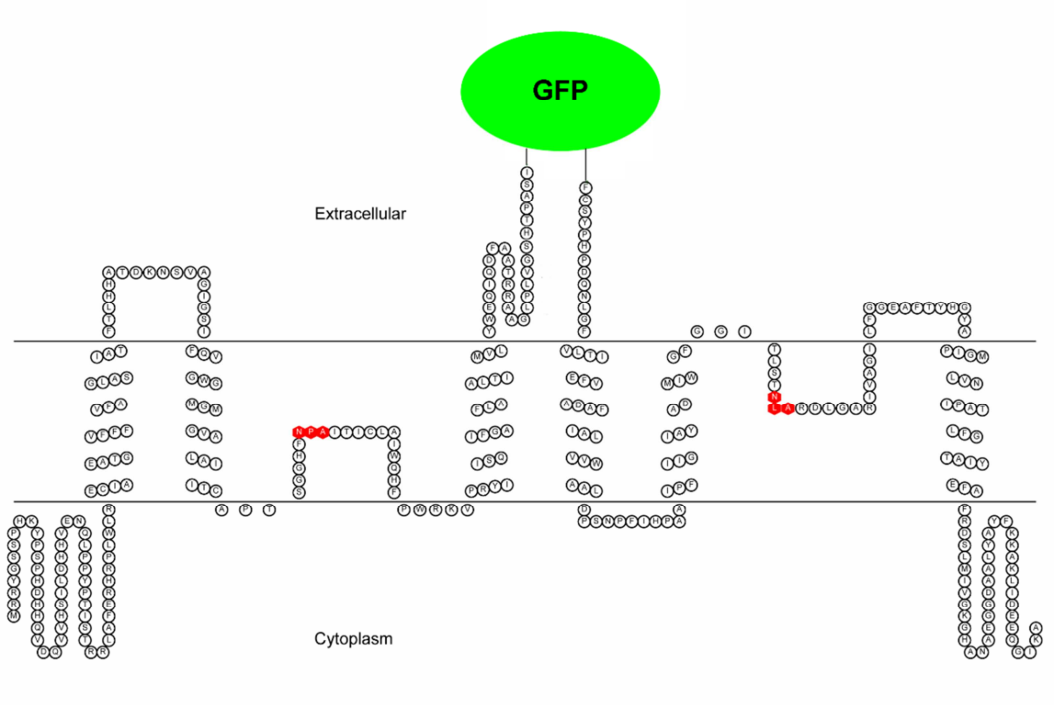

Figure 7.10: The topology of the AGP1 eGFP internal fusion protein. *The eGFP monomer is fused with the C-loop sequence, as predicted by MEMSAT_SVM topology prediction software.*

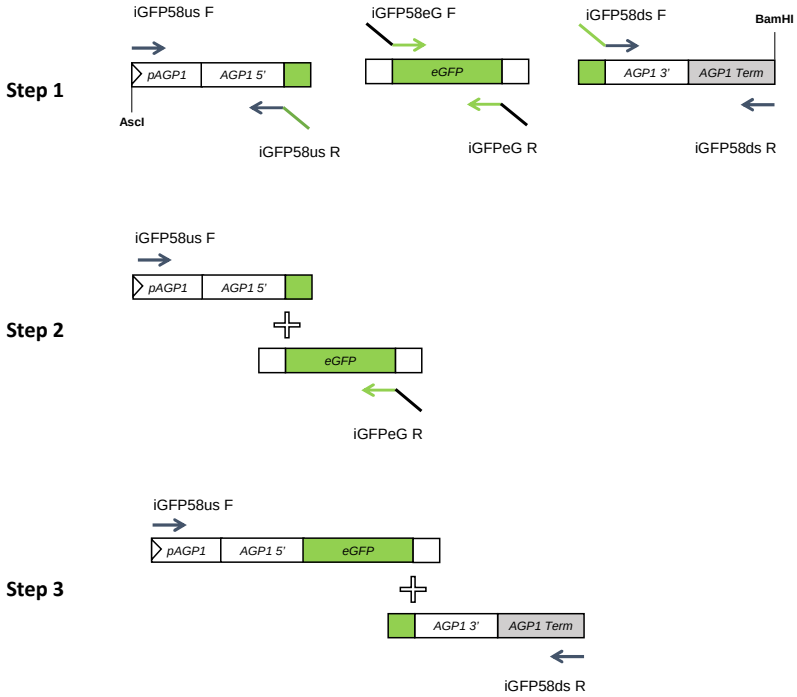

Figure 7.11: Construction of the internal AGP1 eGFP chimera using overlap extension PCR.
Step 1: *Amplify the upstream coding and promoter region, the eGFP coding region, and the downstream coding and terminator region using primer pairs iGFP58usF and iGFP58usR, iGFPeGF and iGFPrGR, and iGFP58dsF and iGFP58dsR, respectively.*
Step 2: *Join the promoter and 5' coding region fragment and the eGFP fragment using overlap extension PCR with primers iGFP58usF and iGFPeGR.*
Step 3: *Join the 'promoter and 5'coding region::eGFP' fragment to the 3' coding region and terminator fragment using primers iGFP58usF and iGFP58dsR.*

The construct was created using overlap extension PCR and cloned into the *Asc*I and *BamH*I sites of a modified pUCAP19 vector. The PCR steps are shown in Figure 7.11.

The first step in the creation of the construct involved amplification of the three fragments to be subsequently joined. The upstream 702 bp of promoter sequence and the first 986 bp of genomic coding sequence was amplified from Guy11 gDNA using primers iGFP58usF and iGFP58usR. The downstream iGFP58usR primer was designed with 18 bp overlap with the 5' region of eGFP to facilitate overlap extension PCR and the upstream primer was designed with an *Asc*I site for ease of cloning into the vector. The 720 bp eGFP fragment, with the STOP codon removed, was amplified from the C-terminal tagging vector using primers iGFPeGF and iGFPeGR. The 966bp 3' coding region and downstream terminator sequence was amplified using the iGFP58dsF and iGFP58dsR primers. The iGFP58dsF primer had 18 bp overlap with the 3' end of the eGFP sequence, and the iGFP58dsR primer carried a *BamH*I site for cloning into the vector.

Step 2 joined the 5' promoter and coding sequence with the eGFP coding sequence, using overlap extension PCR with the iGFP58usF and iGFP58eGR primers and equal quantities of both fragments as a template.

Step 3 joined the 5'::eGFP construct to the 3' coding sequence and terminator fragment. The PCR reaction used equal quantities of each fragment and primers iGFP58usF and iGFPdsR to assemble the complete construct.

Once the whole fragment was assembled, it was digested with *BamH*I and *Asc*I and cloned into a modified pUCAP19 vector, containing the HYGR gene. This vector was amplified using competent *E. coli* cells and transformed into the *M. oryzae* strain, Δ*agp1,* as described in the Materials and Methods.

After transformation, 12 independent hygromycin-resistant clones were selected for imaging. Representative images are shown in Figure 7.12.

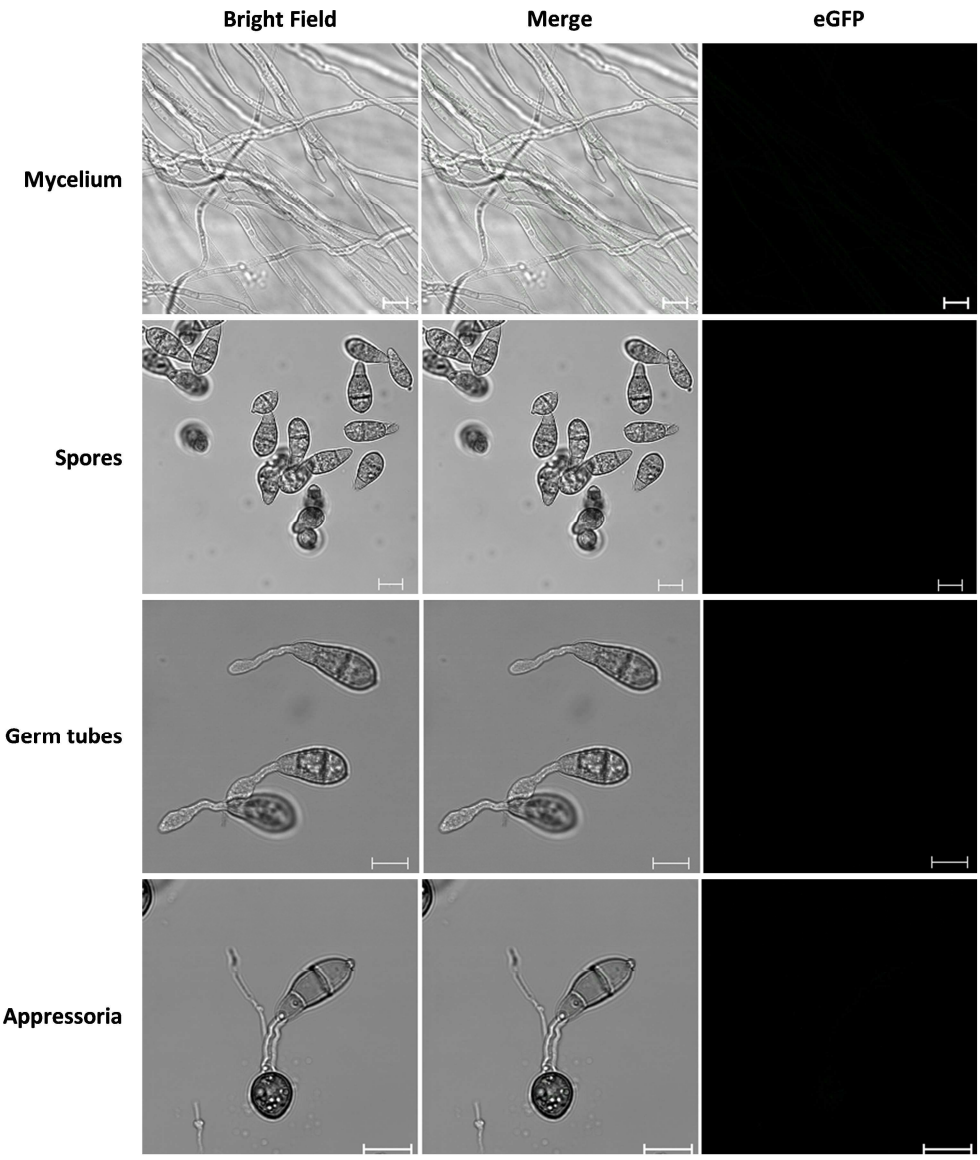

Figure 7.12: Confocal images at four developmental stages of Δagp1 transformed with AGP1 with eGFP on an internal loop under the control of the AGP1 promoter. Spores were imaged on inductive Menzel coverslips. Scale bars represent 10 µm.

The pAPG1::*5'AGP1:: eGFP:: 3'AGP1* construct is not detectably fluorescent. From the gene expression analysis (chapter 3 and chapter 5), we know that *AGP1* transcript abundance is high in mycelium, and this same promoter drives expression of the C-terminal fusion in germlings. Therefore the complete absence of fluorescence is unexpected. The construct was fully sequenced to preclude the possibility of disruptive mutations and found to be error free. A western blot was not carried out to detect improperly folded or immature eGFP, so these, and the possibility that the protein is located in the lumen of an acidic cellular compartment cannot be discounted. The latter case is less likely, because the fluorescence of eGFP is not completely abolished at low pH, but is instead substantially reduced (Haupts et al., 1998).

7.4.3 Some aquaporin promoters drive the expression of cytosolic eGFP

In chapters 3 and 5, I investigated the transcript abundance of aquaporins in *M. oryzae*. Although previous work in our laboratory suggested that fluorescence can be detected from transcripts of equivalent or lower abundance, the possibility remains that these promoters do not drive expression of aquaporin proteins under the conditions described. To test the activity of these promoters, I generated constructs to express a cytosolic eGFP reporter under the control of the native aquaporin promoters and terminated by the native aquaporin terminators.

These constructs were generated by yeast recombinational cloning. A generic construct and the primers used to amplify each of the fragments is shown in Figure 7.13. The eGFP gene was flanked by approximately 3 kb of promoter sequence and 1 kb of downstream terminator sequence. A 2.8 kb sulphonylurea resistance cassette was included for selection in *M. oryzae.* Each fragment was amplified using the primer pairs shown in Table 7.1.

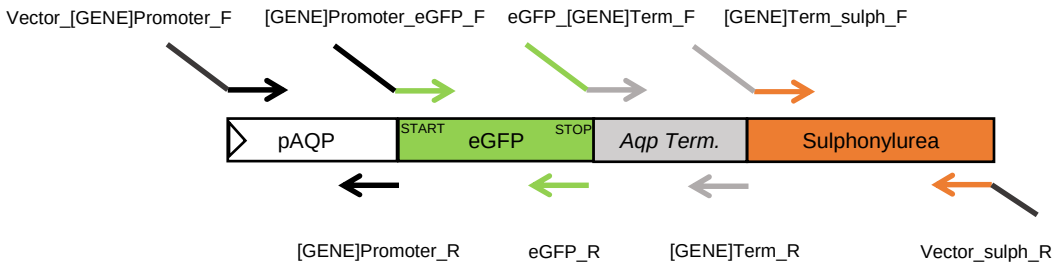

Figure 7.13: The generic construct design to express eGFP with approximately 3 kb of the native aquaporin promoter. Transcription is terminated by ~1 kb downstream native terminator sequence. Sulphonylurea resistance is included as a selectable marker for Magnaporthe oryzae transformation.

Table 7.1: The fragments used to construct the eGFP promoter reporter constructs. Primer sequences are listed in the general Materials and Methods.

Gene	Fragment	F primer	R primer	Fragment size (bp)
AQP1	Promoter	FG Vector_[03904]Promoter_F	FG [03904]Promoter_R	2930
	eGFP	FG [03904]Promoter_eGFP_F	FG eGFP_R	750
	Terminator	FG eGFP_[03904]Term_F	FG [03904]Term_R	1107
	Sulphonylurea	FG [03904]Term_sulph_F	FG Vector_sulph_R	2879
AQP2	Promoter	FG Vector_[04162]Promoter_F	FG [04162]Promoter_R	3060
	eGFP	FG [04162]Promoter_eGFP_F	FG eGFP_R	744
	Terminator	FG eGFP_[04162]Term_F	FG [04162]Term_R	1065
	Sulphonylurea	FG [04162]Term_sulph_F	FG Vector_sulph_R	2878
AQP3	Promoter	FG Vector_[13332]Promoter_F	FG [13332]Promoter_R	3764
	eGFP	FG [13332]Promoter_eGFP_F	FG eGFP_R	744

	Terminator	FG eGFP_[13332]Term_F	FG [13332]Term_R	1063
	Sulphonylurea	FG [13332]Term_sulph_F	FG Vector_sulph_R	2874
AGP1	Promoter	FG Vector_[05880]Promoter_F	FG [05880]Promoter_R	3067
	eGFP	FG [05880]Promoter_eGFP_F	FG eGFP_R	745
	Terminator	FG eGFP_[05880]Term_F	FG [05880]Term_R	1054
	Sulphonylurea	FG [05880]Term_sulph_F	FG Vector_sulph_R	2874
AGP2	Promoter	FG Vector_[13615]Promoter_F	FG [13615]Promoter_R	2042
	eGFP	FG [13615]Promoter_eGFP_F	FG eGFP_R	744
	Terminator	FG eGFP_[13615]Term_F	FG [13615]Term_R	1038
	Sulphonylurea	FG [13615]Term_sulph_F	FG Vector_sulph_R	2878

The constructs were assembled using yeast recombinational cloning and the plasmids were amplified using competent *E. coli* cells. These constructs were transformed into the wildtype strain Guy11. Representative confocal images of each transformed strain are shown in Figure 7.14 - Figure 7.18.

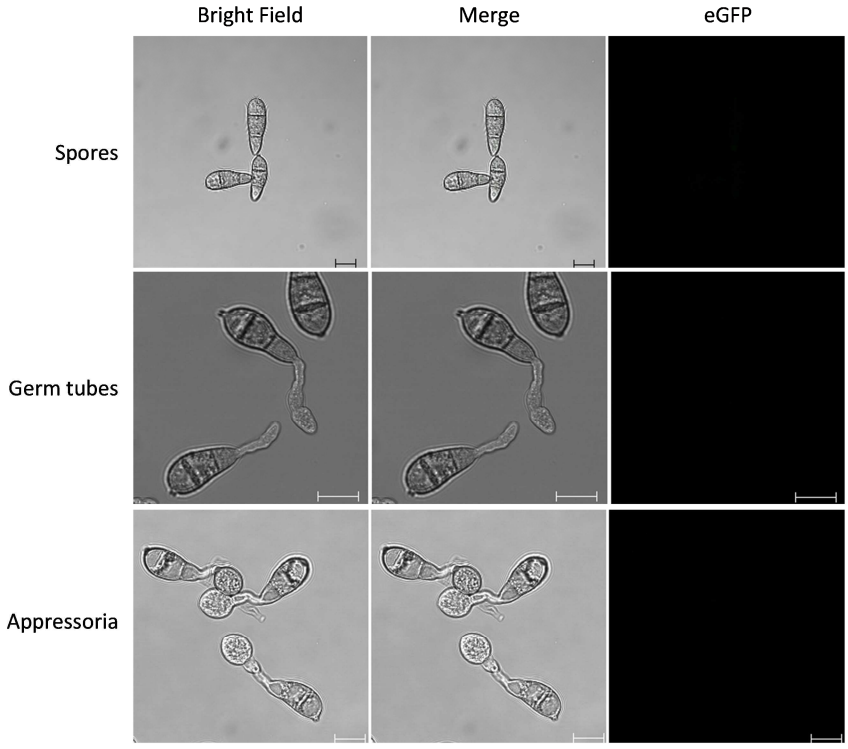

Figure 7.14: Confocal images showing Guy11 transformed with pAQP1::eGFP under 488nm laser excitation. Infection-related development is induced and imaged on Menzel coverslips. Scale bars = 10 nm.

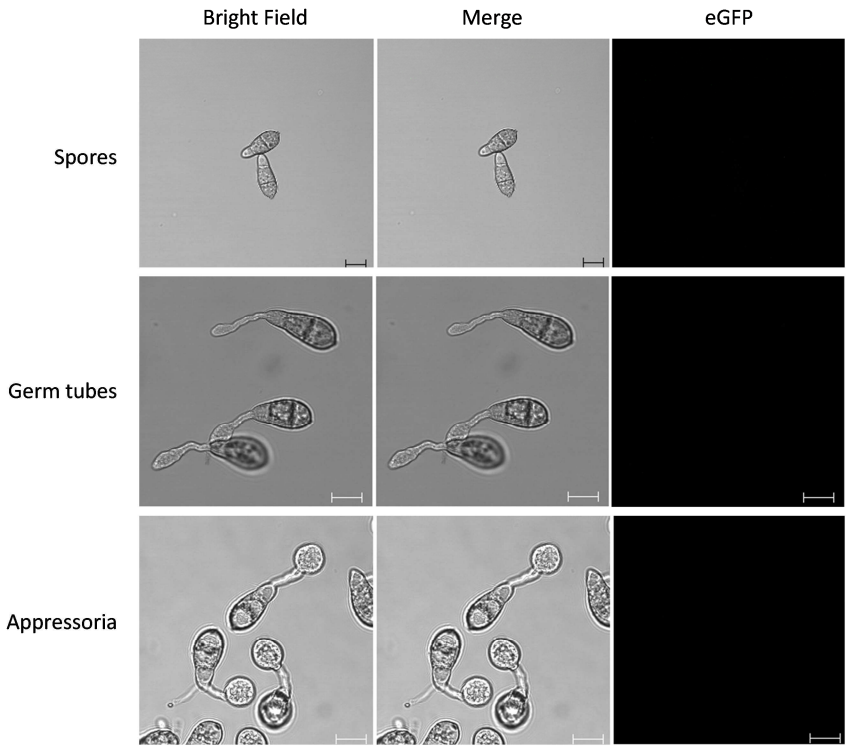

Figure 7.15: Confocal images showing Guy11 transformed with pAQP2::eGFP under 488nm laser excitation. Infection-related development is induced and imaged on Menzel coverslips. Scale bars = 10 nm.

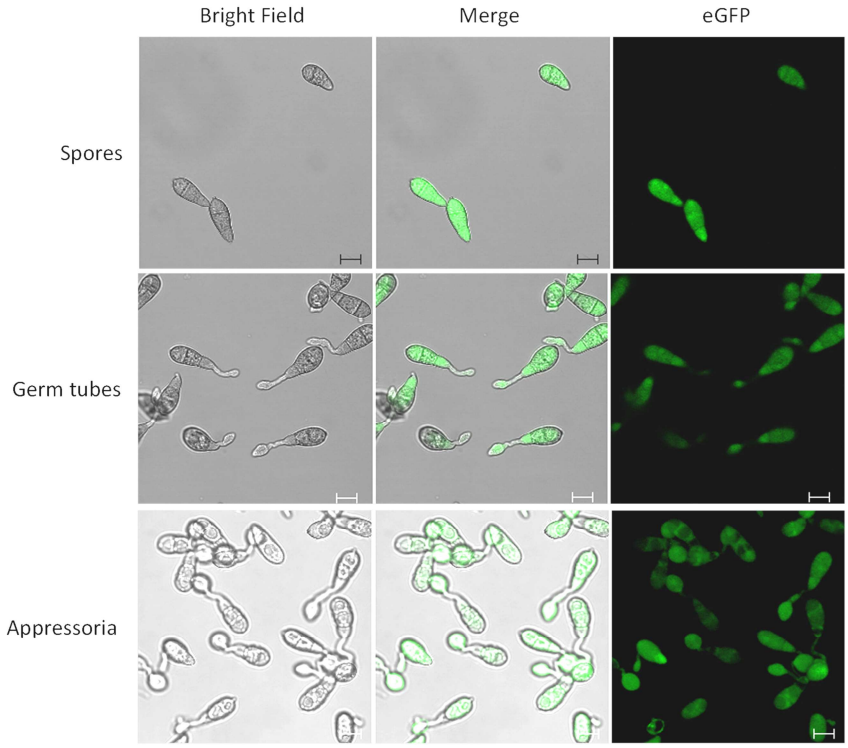

Figure 7.16: Confocal images showing Guy11 transformed with pAQP3::eGFP under 488nm laser excitation. Infection-related development is induced and imaged on Menzel coverslips. Scale bars = 10 nm.

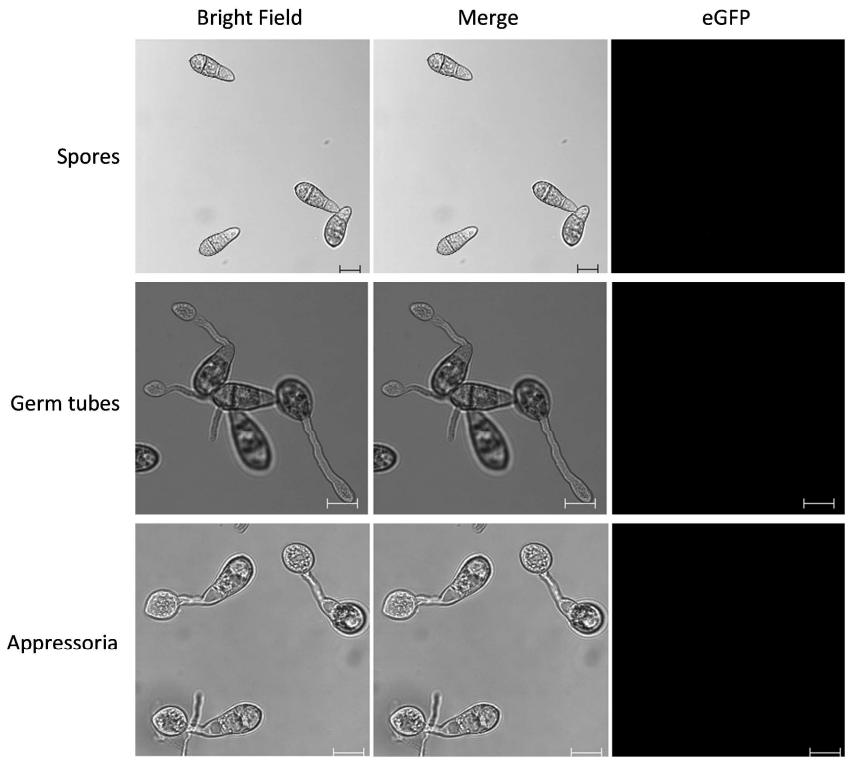

Figure 7.17: Confocal images showing Guy11 transformed with pAGP1::eGFP under 488nm laser excitation. Infection-related development is induced and imaged on Menzel coverslips. Scale bars = 10 nm.

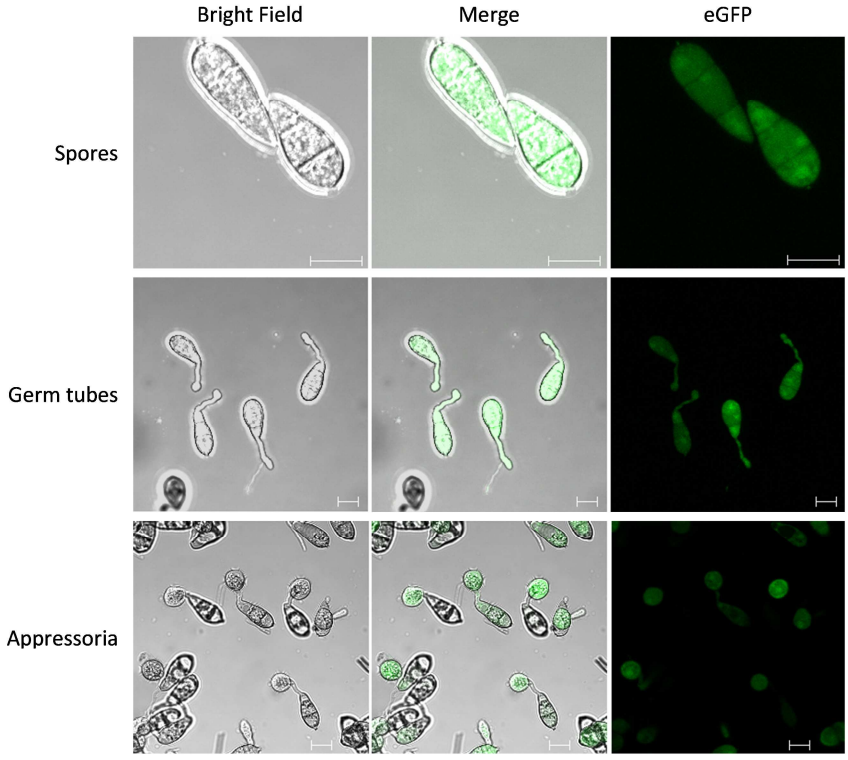

Figure 7.18: Confocal images showing Guy11 transformed with pAGP2::eGFP under 488nm laser excitation. Infection-related development is induced and imaged on Menzel coverslips. Scale bars = 10 nm.

This data suggests that only *AQP3* and *AGP2* promoters drive expression of the eGFP reporter. This is surprising considering the transcript abundance data from chapters 3 and 5, and the observation that the *AGP1* promoter drives (misfolded) expression of a C-terminal eGFP construct. It is possible that there are mutations in the constructs; however, the probability of this occurring in the assembly of three constructs is low.

7.4.4 Only *AGP2* is expressed by the pRP27 promoter with a C-terminal eGFP tag

If the result in Section 7.4.3 is correct, it suggests that the eGFP:: aquaporin chimeras must be expressed under the control of a strong promoter to investigate their localisation. I constructed a C-terminal eGFP fusion construct expressed using the pRP27 strong constitutive promoter (Bhadauria et al., 2013). The construct was created using yeast recombinational cloning, and a generic schematic with the primers used to amplify different fragments is shown in Figure 7.19.

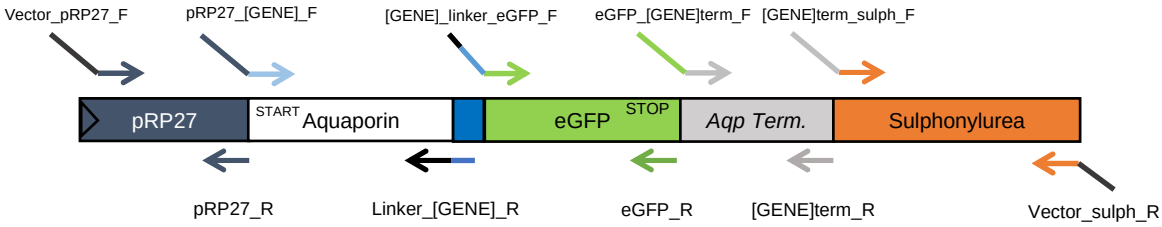

Figure 7.19: The generic construct design to express an aquaporin::eGFP C-terminal fusion under the control of a strong pRP27 promoter. Transcription is terminated by ~1 kb downstream native terminator. A sulphonylurea resistance gene is included as a selectable marker for Magnaporthe oryzae transformation.

The terminal primers, Vector_pRP27F and vector_sulph_R were designed with 25-30 bp homology with the yeast vector at the flanks. The *pRP27* promoter was amplified using the Vector_pRP27_F and pRP27_R primers. The aquaporin coding region (with stop codon removed) was amplified from genomic DNA with 25-30 bp 5' homology to the *pRP27* promoter and the flexible linker sequence encoded in the 3' R primer. The eGFP sequence was amplified with homology to the 5' linker at the 5' flank. The ~1 kb aquaporin terminator sequence was amplified from Guy11 gDNA with 25-30 bp homology to the eGFP 3' sequence. The sulphonylurea resistance gene was amplified using the [GENE]term_sulph_F and Vetor_sulph_R primers, with 25-30 bp homology to the aquaporin terminator at the 5' end and 25-30 bp homology to the yeast vector at the 3' end.

The primers and fragment sizes for amplifying each module of the construct for each gene are shown in Table 7.2. The constructs were assembled using yeast recombination cloning, and the constructs were transformed into Guy11. Five to eight independent clones from each construct transformation were screened for fluorescence. Representative images of spores from each line are shown in Figure 7.20.

Table 7.2: The fragments used to construct the C-terminal eGFP fusion proteins with a strong constitutive promoter. *Primer sequences are listed in the general Materials and Methods.*

Gene	Fragment	F primer	R primer	Fragment size (bp)
AQP1	Promoter	CSVector_pRP27_F	CSpRP27_R	508
	Coding region	CSpRP27_[39]_F	CSLinker_[39]_R	1868
	eGFP	CS[39]_linker_eGFP_F	CSeGFP_R	759
	Terminator	CSeGFP_[39]term_F	CS[39]term_R	1150
	Sulphonylurea	CS[39]term_sulph_F	CSVector_sulph_R	2849
AQP2	Promoter	CSVector_pRP27_F	CSpRP27_R	508
	Coding region	CSpRP27_[41]_F	CSLinker_[41]_R	1354
	eGFP	CS[41]_linker_eGFP_F	CSeGFP_R	742
	Terminator	CSeGFP_[41]term_F	CS[41]term_R	1064
	Sulphonylurea	CS[41]term_sulph_F	CSVector_sulph_R	2879
AQP3	Promoter	CSVector_pRP27_F	CSpRP27_R	508
	Coding region	CSpRP27_[133]_F	CSLinker_[133]_R	1198
	eGFP	CS[133]_linker_eGFP_F	CSeGFP_R	742
	Terminator	CSeGFP_[133]term_F	CS[133]term_R	1060
	Sulphonylurea	CS[133]term_sulph_F	CSVector_sulph_R	6299
AGP1	Promoter	CSVector_pRP27_F	CSpRP27_R	508
	Coding region	CSpRP27_[58]_F	CSLinker_[58]_R	1457
	eGFP	CS[58]_linker_eGFP_F	CSeGFP_R	743
	Terminator	CSeGFP_[58]term_F	CS[58]term_R	1055
	Sulphonylurea	CS[58]term_sulph_F	CSVector_sulph_R	2879
AGP2	Promoter	CSVector_pRP27_F	CSpRP27_R	508
	Coding region	CSpRP27_[136]_F	CSLinker_[136]_R	1295
	eGFP	CS[39]_linker_eGFP_F	CSeGFP_R	742
	Terminator	CSeGFP_[136]term_F	CS[136]term_R	1041
	Sulphonylurea	CS[136]term_sulph_F	CSVector_sulph_R	2872

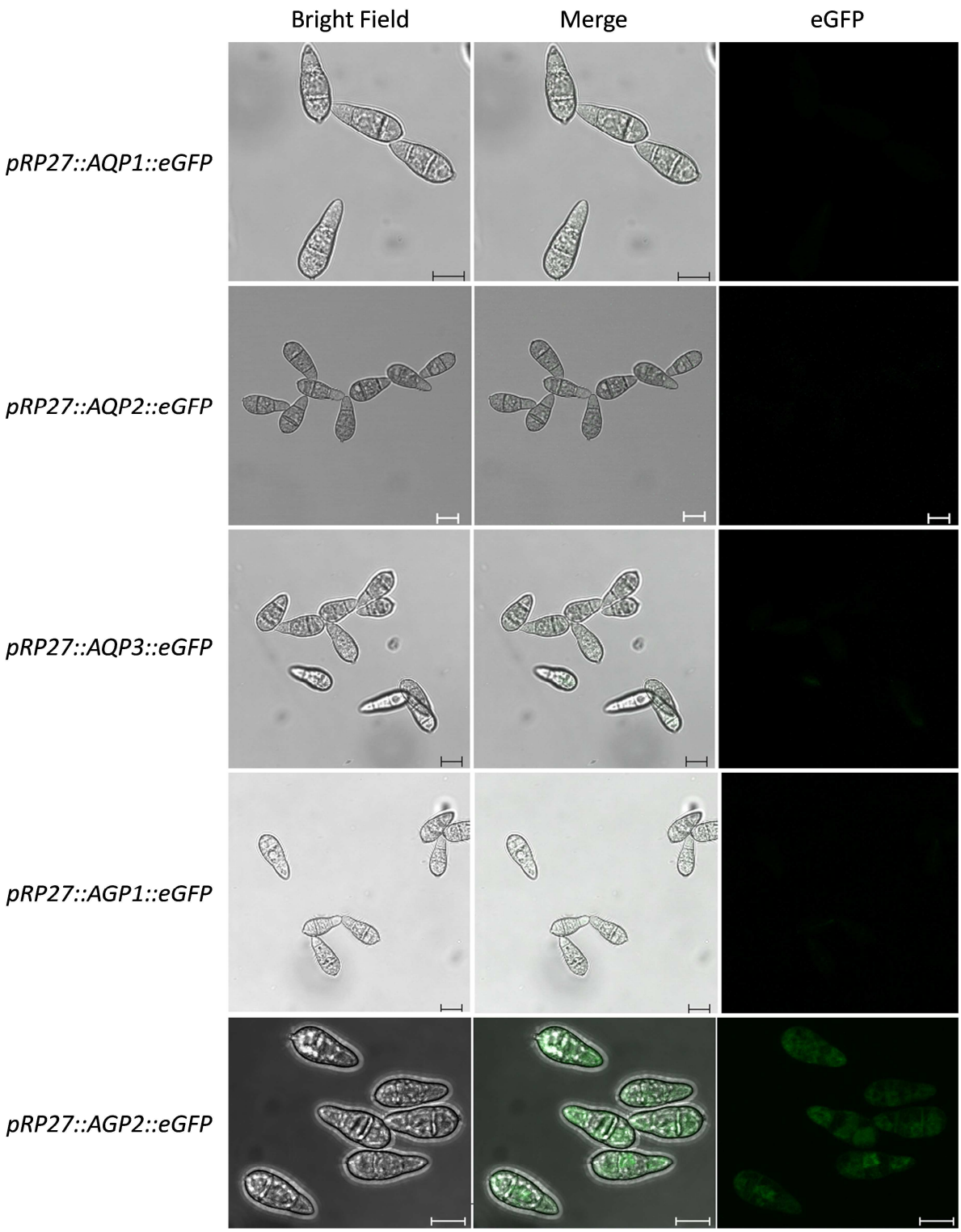

Figure 7.20: Confocal images showing spores of Guy11 transformed with pRP27::AQUAPORIN::eGFP constructs under 488 nm laser excitation. Infection-related development is induced and imaged on Menzel coverslips. Scale bars = 10 nm.

Only a single line, *AGP2*, was fluorescent in this assay. No fluorescence was detected from any transformants of *AGP1, -2, -3* or *AGP2.* Higher resolution images of the *pRP27::AGP2::eGFP* lines are shown in Figure 7.22. The internal membrane structure is clear from these images, although

some vacuolar localisation is also apparent. It is likely that the membrane-associated fluorescence is, at least partially, associated with the endoplasmic reticulum (ER) as the nuclei are clearly outlined and the ER is contiguous with the nuclear envelope. No co-localisation assays were performed so the actual membrane association cannot be confirmed, but predominantly ER-association, together with breakdown products in the vacuoles, appears the most likely option.

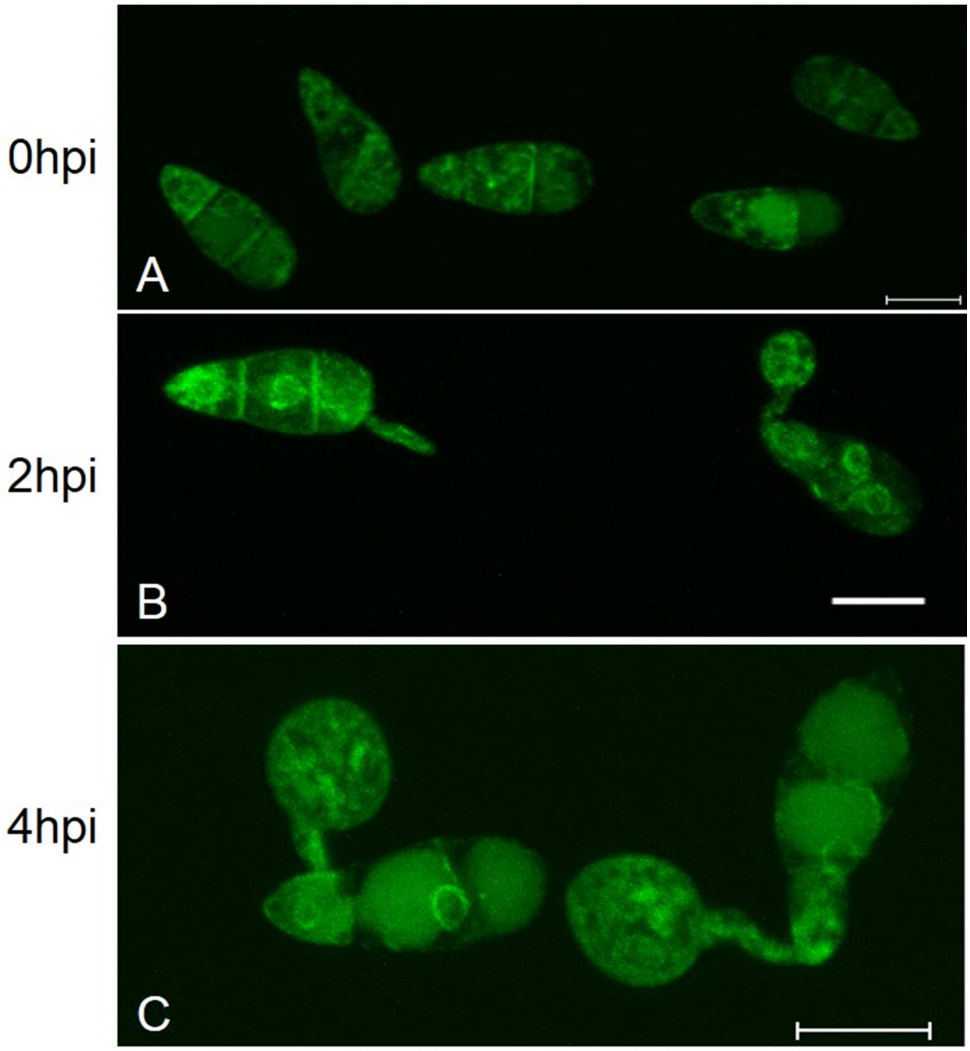

Figure 7.21: Confocal images of Guy11 transformed with pRP27::AGP2::eGFP under 488 nm laser excitation. Images are representative z-stacks of the eGFP fluorescence at 0, 2 and 4 hpi after inoculation onto inductive Menzel coverslips. Scale bars = 10 µm.

7.4.4.1 *The eGFP::AGP2* overexpressing construct causes aberrant germ tube emergence

Curiously, the *AGP2::eGFP* overexpressing lines appeared to have unusual appressorium formation. The site of germ tube emergence was predominantly the side of the apical cell rather than the tip of the apical cell. The difference is shown in Figure 7.22 with Guy11 spores (A) and the

AGP2::eGFP overexpressor spores (B). We categorised a minimum of 250 spores from six independent *AGP2::eGFP* overexpressor strains and the Guy11 wild type strain, according to the emergence point of their germ tubes after 4 h on inductive Menzel slides. The six independent *pRP27::AGP2::eGFP* lines had a range of fluorescence levels (very fluorescent = lines 1 and 5, no fluorescence = lines 2 and 4). The results are shown in Figure 7.23. The *AGP2*-overexpressing lines clearly differ from Guy11, and this difference does not appear to correlate with fluorescence level. The change cannot be the result of the random integration event disrupting another gene as the phenotype is consistent between different lines.

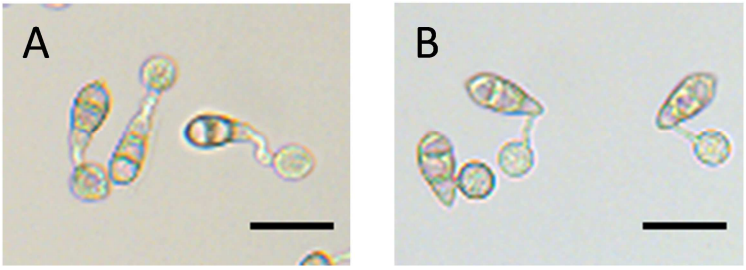

Figure 7.22: Wild type Guy11 germlings (A) and pRP27::AGP2::eGFP-expressing germlings (B) 4 hpi on inductive Menzel slides. Scale bar = 20 µm.

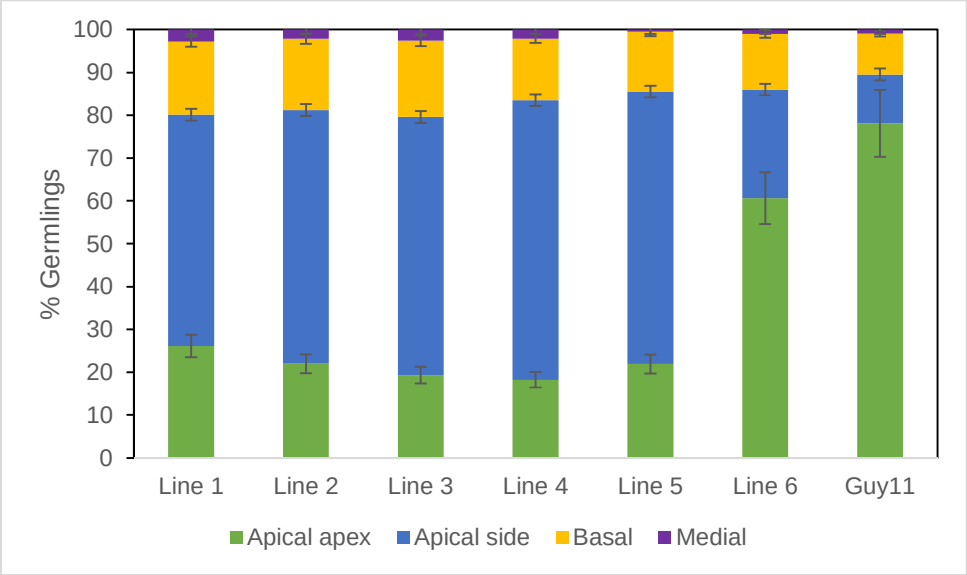

Figure 7.23: Germ tube emergence point of wildtype and six independent transformant lines expressing pRP27::AGP2::eGFP on inductive Menzel coverslips 4 hpi. Mean percentage germling morphologies were calculated from three independent slides and at least 250 germlings per line were counted. Error bars represent the standard error of the mean.

7.4.5 N-terminal aquaporin eGFP fusion proteins mislocalise

Previous work with human *AQP2* suggests that N-terminal fusions can localise and fold correctly (Umenishi et al., 2000). Little is known about the localisation or tetramerisation signals on fungal aquaporins and it is possible that we cannot obtain C-terminal fusions because these sequences are located on the C-terminal. We generated N-terminal eGFP aquaporin fusion proteins under the control of a strong constitutive ribosomal subunit promoter: pRP27 (Bhadauria et al., 2013). The promoter was selected over the native aquaporin promoters because previous experimental work suggested that three aquaporin promoters do not drive the expression of fluorescent reporter proteins.

A generic example of the constructs used to create N-terminal fusions is shown in Figure 7.24. The pRP27 promoter drives transcription of eGFP (stop codon deleted) followed by the *AQUAPORIN* sequence, separated by a flexible 5x glycine linker domain. Transcription is terminated by the TrpC terminator from *A. nidulans* and the construct includes an antibiotic resistance domain (either HYGR or BAR) for selection of *M. oryzae* transformants. The vector, into which the aquaporin coding sequences are cloned, was designed and constructed by Dr. M. Samalova (University of Oxford).

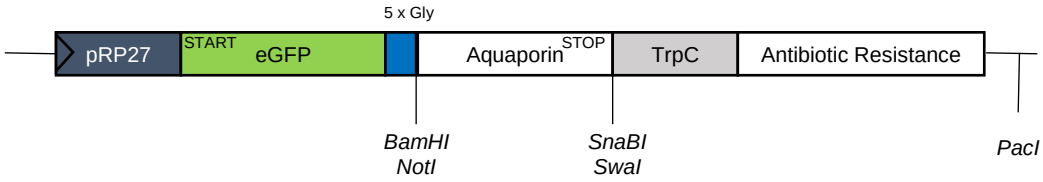

Figure 7.24: A schematic of the N-terminal eGFP aquaporin fusion construct. *The aquaporin protein was cloned, in frame with eGFP and after a 5x glycine flexible linker domain, into the* BamHI/Not*I and* SnaBI/Swa*I sites. The fusion protein was under the control of the strong pRP27 promoter and transcription was terminated by the Aspergillus nidulans TrpC terminator. A* Magnaporthe oryzae *selectable marker was used for identifying positive transformants after transformation into the fungus. The plasmid backbone is a modified pUCAP19 vector (courtesy of Dr. M. Samalova, University of Oxford).*

The primers used to amplify the coding regions are shown in Table 7.3. All F primers contained a *BamH*I or a *Not*I site, and all R primers contained a *SnaB*I site or a *Swa*I site. The fragments were amplified from the wild type gDNA and were cloned in frame with eGFP. *AQP1, AQP3 and AGP1* were cloned into a vector with a HYGR selectable marker and *AQP2* and *AGP2* were cloned into a

vector with a BAR selectable marker. Positive clones were digested to confirm correct assembly and amplified with competent *E. coli* cells before being transformed into *M. oryzae.*

Table 7.3: Primers used to amplify coding regions for N-terminal eGFP fusions.

Gene	F Primer	R Primer	PCR fragment size (bp)
AQP1	N03904F	N03904R	1895
AQP2	N04162F	N04162R	1348
AQP3	N13332F	N13332R	1194
AGP1	N05880F	N05880R	1452
AGP2	N13615F	N13615R	1272

Each vector was transformed into the single aquaporin knockout background corresponding to the gene encoded on the plasmid. After transformation, 5-10 independent clones were screened for fluorescence. Representative images of each genotype are shown in Figure 7.25.

With the exception of the *AQP2* fusion, all constructs are strongly fluorescent. However, the fluorescence is diffused throughout the hyphae indicating cytoplasmic, rather than membrane associated, localisation. It may be that the overexpression is so strong that the breakdown products of the fusion protein are diffused throughout the cytoplasm, and this fluorescence masks the fluorescence of the membrane localised product. If this is the case, the two forms of eGFP – the membrane-localised conjugate and the cleaved degradation product – would be different molecular weights and could be distinguished by western blot analysis. A western blot on total protein extract from N-terminal *AQP2, AQP3, AGP1* and *AGP2* chimeric overexpression lines is shown in Figure 7.26.

The western blot clearly shows a single eGFP band at ~28 kDa: the cleaved cytosolic protein molecular weight. Therefore no detectable fusion protein is expressed in the membrane-associated form before the eGFP is cleaved.

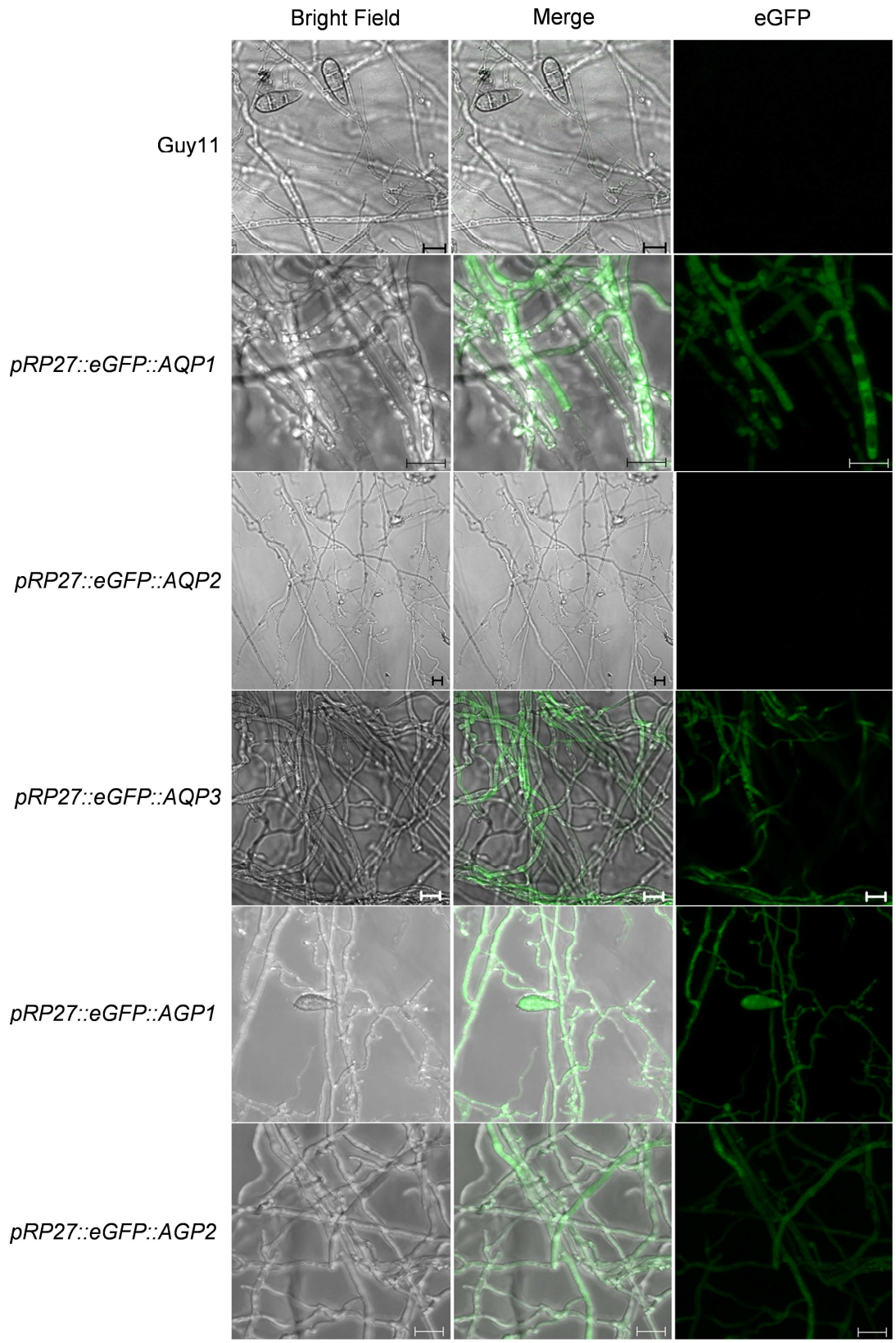

Figure 7.25: Confocal z-stack projections of the wild type strain, Guy11, expressing N-terminal eGFP aquaporin fusions under the control of the pRP27 promoter. Mycelium was grown on solid complete medium. *Images are displayed as maximum projections along the z-axis. Scale bars = 10 µm.*

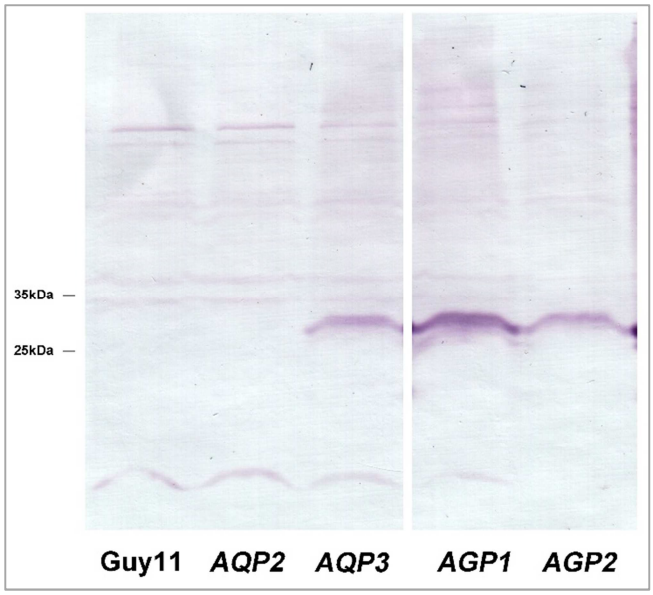

Figure 7.26: A western blot with anti-GFP antibodies on total protein extract from N-terminal eGFP fusion lines. *The AQP3, AGP1 and AGP2 bands corresponds to the size of the un-conjugated eGFP monomer. No signal is detected in the non-fluorescent lines. The western blot was performed as described in the materials and methods specific to this chapter.*

7.5 Discussion

The stated aims of this chapter were to recomplement the Δ*aquaporin* deletion strains with eGFP-aquaporin fusions and to understand the localisation of aquaporin protein in *M. oryzae* using FP tagging. Extensive technical problems meant that most of these aims were not completed.

The most disruptive issue encountered is the apparent lack of expression of many of the constructs. For example, the *AQP3* promoter drives expression of a fluorescent reporter, but the C-terminal fusion protein is not expressed, either with the native promoter or a strong constitutive promoter. These observations represent either the effect of cryptic silencing mechanisms, or they are caused by as-yet-unknown technical problems.

Some of the constructs used in these experiments, particularly the promoter reporter constructs and the C-terminal fusions with the pRP27 promoter are very large (up to 8 kb) – much bigger than constructs described in chapter 3. It may be the case that these constructs integrate only partially, perhaps giving them an antibiotic-resistant phenotype but lacking part of all of the fluorescence module. This problem may be exacerbated by the fact that the sulphonylurea resistance marker is an allele of an *M. oryzae* acetolactate synthase gene (Zhang et al., 2010). It is plausible that the

resistance phenotype may be associated with homologous recombination between the endogenous susceptible allele and the introduced resistant allele. This hypothesis would fit with the observation that some lines in sulphonlyurea-selected *M. oryzae* strains were completely non-fluorescent whereas others of the same expression construct were very fluorescent. A future experiment could involve swapping the sulhphonylurea resistance gene for a smaller BAR or HYGR cassette on a subset of constructs.

The issue of possible silencing still remains. The *pRP27* promoter caused strong expression of the N-terminal fusion construct, albeit resulting in eGFP cleavage. Why, therefore, does the same promoter not have the same effect on C-terminal fusions? If the protein cannot fold properly, we should see the same fluorescence as with the N-terminal fusions, but instead, apart from *AGP2,* we see no fluorescence at all. We did not perform a western blot, so it is possible that these proteins are localised in acidic compartments or are degraded rapidly. This seems an unlikely explanation for such a large number of fusions. The most plausible explanation is that the proteins are never made, with either transcription or translation not occurring.

We know that for randomly integrating constructs, genomic location is an important determinant of expression level (Dror & Winston, 2004, Smith & Boeke, 1997). It may be the case that screening 6-12 lines is not enough to identify lines where the construct integrates into an actively transcribed region of the genome. However, this does not fit with our observation that at least weak fluorescence is observed in ~60% of independent clones where any one line is fluorescent. It should be noted that this applies to BAR- and HYGR-selected strains. The percentage of SUR-selected independent clones that displayed fluorescence in any strain where at least one other line with the same construct was fluorescent was very variable, including incidences where only 1/5 lines were fluorescent.

7.5.1 The *pRP25*::*AGP2*::*eGFP*-expressing strains display membrane-localised fluorescence and a germ tube emergence phenotype

An *AGP2* C-terminal fusion under the control of the pRP27 strong constitutive promoter was the only fluorescent line with apparent membrane localisation. The fusion protein has an ER-like

localisation pattern, as indicated by the cytoplasmic membrane structure and outlining of the nuclei. A similar pattern is observed with *Mo*Tsc13p-GFP, another ER-localised GFP-tagged protein in *M. oryzae* (He et al., 2012). A fluorescent signal is also detected in the vacuoles, but this is likely to be where the degradation products of the chimeric protein are sequestered. The localisation of this protein in the ER could be confirmed by co-staining with $DIOC_6(3)$, a dye which, in high concentrations, stains the ER and perinuclear membrane of filamentous fungi (Hickey et al., 2004, Levin & Carson, 2004).

Little is known about the normal localisation of fungal aquaporins; however, an ER-like localisation pattern is not without precedent. The *S. cerevisiae Aqy1* putatively localises partly to the ER (Sidoux-Walter et al., 2004) as do the 'superaquaporins' – the AQP11-like/SIP clade in animals and plants (Soto et al., 2012, Ishibashi, 2006).

This ER localisation could alternatively be an overexpression artefact, or result from partial misfolding of the protein and subsequent retention by quality control mechanisms (Moore & Murphy, 2009). It is disappointing that the C-terminal fusion with the native promoter did not function, especially considering that the promoter was capable of driving strong fluorescence of a cytosolic reporter and the C-terminal fusion is appears capable of folding correctly. The localisation pattern does not suggest complete misfolding as, unlike the N-terminal fusions, the protein is still associated with membranes.

Without further validation, this expression pattern is interesting, but does not represent conclusive proof that the protein is expressed on internal membranes. Generation of an epitope tagged Agp2 fusion and expression in the Δ*agp2* background under the native promoter would provide an opportunity to validate this expression. The tagged protein localisation could then be examined using immunostaining techniques in fixed specimens or specific membrane fractions.

The apparent overexpression phenotype is unexpected. Germ tube emergence in *M. oryzae* predominantly occurs from the apical cell, but about 20% of germ tubes emerge from the basal cell. The apical germ tubes usually emerge from the tip of the apex, but in the overexpressing

lines, these germ tubes appear predominantly at the side of the apical cell. The phenotype does not appear to be strongly dosage dependent, as evidenced by the lack of phenotype response to differing levels of fluorescence. However, it may be the case that the level of membrane-associated fluorescence is distinct from the vacuolar signal, therefore total fluorescence is not a good measure of fusion protein dosage. Nevertheless, the phenotype manifests in lines with a complete absence of fluorescence.

In other fungal species with similar three-celled macrospores, germ tube emergence is subject to precise spatial controls and is tightly coupled to nuclear division and growth (Harris, 2005). The events that determine the site of germ tube emergence are very poorly studied in *M. oryzae*, with most attention focused on appressorium formation and elaboration. There is an emerging role in other fungal species for septin proteins in the selection of sites for germ tube emergence (Berepiki & Read, 2013, Li et al., 2012). Quite how overexpression of an aquaglyceroporin protein could disrupt this process is unclear, and is worthy of further investigation.

Chapter 8 Discussion

The individual chapters of this thesis each carry a discussion relevant to the findings described therein. This general discussion describes these findings and attempts to draw the results together in a wider sense. Finally, it generates a hypothesis and details further work necessary to better understand the role of this diverse family of genes in *M. oryzae*.

8.1 Summary

Research on aquaporins has focussed predominantly on elucidating their role in animal and plant cells. Given the essentiality of turgor pressure for filamentous growth and plant infection by *M. oryzae*, I speculated that these proteins maybe important to fungi generally and, more specifically, to the lifestyle of this appressorium-forming fungus. I attempted to characterise the transport capabilities, cellular localisation and transcript abundance of this family of rice blast genes, as well as the impact of their deletion on pathogenicity and growth.

In chapter 3, I identified MIP-domain containing genes across the fungal kingdom, and generated an improved phylogeny of fungal aquaporins. From this, I proposed an evolutionary history that explains the topology of the resultant evolutionary tree. The evidence thus unmasked supports a single AQP-type gene, and between 1 and 3 AGP-type genes in the last common ancestor of extant fungi, with subsequent clade-specific gene expansions (Soto et al., 2012). In the same chapter, I examined the transcript abundance of aquaporin genes during the early stages of germling morphogenesis and pathogenic development, and found the expression of aquaporin genes to be differentially regulated.

In chapter 4, I detailed efforts to generate null mutant strains for each individual aquaporin gene in the *M. oryzae* genome. The virulence and infection-related development of each aquaporin null mutant was characterised, and found to be indistinguishable from *M. oryzae* wild type strain Guy11. The axenic growth of each mutant strain, relative to wildtype growth, was characterised under a variety of different stress conditions and predominantly found to be the same as the wild type. Some mild putative phenotypes were uncovered by plate growth assays.

In chapter 5, I considered the possibility that there is functional redundancy between members of the aquaporin gene family, conjecturing that this may explain the absence of strong mutant phenotypes in null mutants. I used qRT-PCR to look for evidence of compensatory changes in transcript abundance, in germlings growing on artificial inductive surfaces, inductive to appressorium formation in wild type strain Guy11, over a range of developmental conditions. The results indicate the possibility of reciprocal genetic linkage between two genes, *AQP1* and *AQP2.*

In chapter 6, the properties of each individual aquaporin protein were examined, computationally and experimentally. I analysed their respective primary and secondary sequence characteristics in order to make functional predictions of channel permeability and regulation. Such predictions were then tested in heterologous expression assays in *Saccharomyces cerevisiae,* exploiting the *GAL1* galactose-inducible promoter construct (West et al., 1984). I thus tested the permeability of the heterologous *M. oryzae* genes to exposure to glycerol, hydrogen peroxide, ammonia/ammonium and urea. I was able to demonstrate that hydrogen peroxide permeability was influenced by transformation with two *M. oryzae* genes, *AQP1* and *AQP2*, and ammonia permeability with *AGP1*. I further tested the physiological relevance of Aqp2*,* using a genetically-encoded cellular redox reporter, Grx1-roGFP1 in the Δ*aqp2* background (Gutscher et al., 2008). This showed no difference between the Δ*aqp2* and wild type strain Guy11 in the rate of redox shift in response to H_2O_2 challenge, indicating that the rate of H_2O_2 flux across the plasma membrane is not altered in the absence of Aqp2.

In chapter 7, I attempted to characterise the subcellular localisation of aquaporins in *M. oryzae* and generate fluorescent-tagged re-complementation strains of null mutants. The *AGP2* C-terminal

eGFP fusion putatively localises to the ER and perinuclear membranes. However, I was unable to generate membrane-localised fusions for the other proteins.

8.2 MIP family expansions

The large expansion in the number of MIP-domain containing proteins in the Basidiomycetes and pezizomycetes is striking, relative to the small numbers in Saccharomycetes and fungal outgroups to the dikarya. In plants and animals, the large number of genes is thought to be concomitant with an increase in the physiological significance of these proteins. The same is true in bacteria, where, for example, the six AGP-like genes in the gram positive lactic acid bacterium, *Lactobacillus plantarum,* are thought to contribute to lactic acid metabolism (Bienert et al., 2013). This contrasts with a typical AGP-like complement of 1-2 genes in most Gram positive bacteria (Tanghe et al., 2006). My finding that some fungi have as many as 17 MIP genes (considerably more than most animals) allows us to hypothesise that a similar 'importance-driven' expansion may have occurred in certain fungal taxa.

This hypothesis is supported by evidence of putative neo- or sub-functionalisation of MIPs in *M. oryzae*. Sequence analysis and permeability assays suggest that even the most closely-related genes are likely to have substantially different properties. For example, the two most sequence-similar sequences, *AQP1* and *AQP2* (42% similarity at the amino acid level) are likely to be subject to different regulatory processes, as indicated by the long putative regulatory domains in the termini of Aqp1, but not Aqp2. This is further substantiated by evidence, at the transcript level, that the abundance of MIP transcripts is regulated differently during infection related development and mycelial growth. In particular, the extremely high transcript abundance of *AGP1* in mycelial culture is notably different from other MIP genes.

The evidence in this thesis suggests that aquaporins have evolved to have independent physiological roles. Therefore it is surprising that I was unable to detect significant phenotypic changes in aquaporin null mutants as compared with wild type strain Guy11, under the wide range of experimental conditions tested. If the role of aquaporin proteins has diversified over the course of their evolution, the likelihood that they have functional roles that overlap significantly is reduced.

This functional diversification might therefore, in turn, be expected to reduce the chances of direct redundancy between members of the aquaporin gene family.

8.3 Regulation of expression

In chapter 5, I considered the possibility that there may be regulatory changes in the transcript abundance of other aquaporin genes in null backgrounds, thereby abrogating the physiological effect of deleting that gene. These 'responsive backup circuits' (RBCs) are thought to have evolved to facilitate transcriptional plasticity in response to normal transcriptional 'noise', and may explain the absence of a mutant phenotype (Kafri et al., 2006). The possible RBC-activity between *AQP1* and *AQP2* is particularly interesting in light of the demonstrable H_2O_2 permeability of these two proteins. It is possible that this is their primary physiological role; this raises the question, why would *M. oryzae* require 'peroxyporins'?

In the interaction between plants and pathogens, hydrogen peroxide, a form of reactive oxygen species (ROS), is actively produced by both the plant and the fungus (Dat et al., 2000, Kuźniak & Urbanek, 2000). It has been hypothesised that the production of large quantities of H_2O_2 by the plant is a defensive response (Shetty et al., 2007). However, recent evidence suggests that invading pathogens, even when unable to infect, do not experience substantial redox challenge (M. Samalova, *in press* 2013).

The H_2O_2 molecule is cytotoxic in high concentrations, but is now thought to be more important in its capacity as a signalling molecule (for a review, see Gough and Cotter (2011)). Indeed, H_2O_2-mediated signalling appears to be an important role of the molecule in *M. oryzae*. A recent paper by Ryder et al. (2013), demonstrates that the reorientation of the cytoskeleton prior to penetration peg formation, requires synthesis of ROS by NADPH oxidases. Furthermore, the application of antioxidants severely delays the development of appressorium formation, indicating a role for ROS at earlier developmental stages (Egan et al., 2007). The frequency of malformed appressoria is also much higher in the presence of antioxidants.

Interesting recent evidence from the mammalian literature suggests that aquaporins may be important *in vivo* for H_2O_2-mediated signalling (Miller et al., 2010, Vieceli Dalla Sega et al., 2012). Despite its highly reactive nature and correspondent short half-life, H_2O_2 was long thought to be freely diffusible across biological membranes (Bienert et al., 2006, Giorgio et al., 2007). However, a study by Miller et al. (2010), showed that overexpression of the H_2O_2-permeable human Aqp3 in HeLa cell plasma membranes results in substantial amplification of downstream signalling pathways that rely on ROS as the physiological messenger (King et al., 2004, Miller et al., 2010). This implies that diffusion constrains can significantly affect the signalling capabilities of H_2O_2.

From such findings, I speculated that the peroxyporins in *M. oryzae* may facilitate diffusion of H_2O_2 from the site of production to the site of action. I did not observe the morphological abnormalities or delayed appressorium formation upon addition of exogenous antioxidants, as described by Egan et al. (2007). However, if there is functional complementation between Aqp1 and Aqp2 then our findings are not unexpected.

8.4 Further Work

To substantiate the hypothesis laid out above, the generation of a double knockout of *AQP1* and *AQP2* should be prioritised. The effect of these deletions on appressorium formation should be evaluated and compared with the antioxidant phenotypic effect. The Grx1-roGFP2 assay should also be repeated with this double knockout mutant, necessitating the introgression of the roGFP construct into the double deletion strain.

Evaluation of the *in vivo* permeability of the double knockout is potentially of wide interest. Evidence is only just emerging of a significant role for aquaporins in ROS diffusion, and, to our knowledge, the work presented in this thesis represents the only study of the ‘diffusibility’, *in vivo*, of H_2O_2 in the presence and absence of native H_2O_2-permeable aquaporins. The roGFP system is perfectly suited for this purpose, and this study validates its reproducibility, even when the signal strength is very low.

At the outset of this study, we defined our aim to be to understand the role of and to evaluate the importance of aquaporins to the lifestyle of the rice blast fungus, *M. oryzae*. To-date, this has not been achieved. The literature reveals that a function for some plant aquaporins has been designated based on their transcript regulatory patterns (Ma et al., 2006). Zhang (2012) performed an interesting comparative study of the expression of maize aquaporin genes between different tissues over a developmental time course, using available SuperSAGE and RNAseq information. They used linkage analysis to look for co-expression of aquaporins and other transmembrane solute transporters. The profiles of these linkages are highly suggestive of other channel permeants and physiological roles.

Although SuperSAGE studies of that scale are likely beyond the scope of this project, a further *M. oryzae* qRT-PCR screen could be carried out under different stress conditions. These could include, but not be limited to, nutrient stress (i.e. the sequential removal of individual nutrients), drought stress, and the stress conditions described in chapter 4. Like significant up-regulation of NIP2 in silicon-deficient rice plants (Ma et al., 2007), any substantial variations in transcript abundance would be worthy of further evaluation.

It would be of great interest to better understand the transport capabilities of the *M. oryzae* proteins. In this thesis, we did not measure the permeability of these channels to their canonical substrate, water. Measurement of water transport properties is technologically challenging in *Saccharomyces cerevisiae* expression assays. The assay involves enzymatic digestion of the cell wall and subsequent analysis of the rate of swelling and shrinking following osmotic shift, performed in a stopped-flow spectrophotometer (Suga & Maeshima, 2004). These assays were planned, but were not performed due to the absence of suitable technical help and the impending submission deadline.

An alternative method for measuring water permeability involves heterologous expression in *Xenopus oocytes*. The rate of swelling of protein-expressing oocytes in response to osmotic shift is used to calculate their permeability coefficients (Siefritz et al., 2001). Expression in oocytes would

also provide a platform to validate the *S. cerevisiae* expression work, and would allow an expansion in the number of compounds that could potentially be tested.

The final augmentation to this project concerns the intracellular localisation of the aquaporins. Despite substantial efforts, I was not able to suggest localisation patterns for the majority of aquaporins in *M. oryzae*. This could be rectified with the use of epitope-tagged aquaporin lines, in combination with immunofluorescence. An small protein tag, such as the c-MYC or 6x His sequences, should cloned into the C-terminals of each aquaporin gene, then randomly integrated, together with their native promoters, into the genome of the corresponding deletion strain. The use of fluorescent secondary antibodies on protoplasted *M. oryzae* cells would circumvent the problems associated with immunostaining heavily melanised cells. These tagged re-complemented lines could also be used to validate the small phenotypic differences uncovered in chapter 4.

8.5 Concluding remarks

The work detailed in this thesis represents a considerable effort to unmask the function of *M. oryzae* MIP genes. Whilst it goes some way towards a better understanding of their expression and provides substantial descriptive detail, it does not ascribe a specific function to each *M. oryzae* gene. The reverse genetics approach first taken during this project can be a powerful tool; however, it is subject to substantial limitations, most notably in multi-gene families, where (as in this case) no mutant phenotype may be detectable. It is clear that the generation of more null mutants alone does not represent the future for this project. However, the co-ordinated use of expression analysis and descriptive functional information could yet yield insights into the question that remains unanswered – why does *M. oryzae* retain a large, diverse family of MIP genes?

References

Adachi K, Hamer JE, 1998. Divergent cAMP signaling pathways regulate growth and pathogenesis in the rice blast fungus *Magnaporthe grisea*. *Plant Cell* **10**, 1361-73.

Agre P, 2006. The aquaporin water channels. *Proc. Amer. Thoracic Society* **3**, 5.

Allen E, Allison M, Sparkes D, Sylvester-Bradley R, Wiseman J. Physiological and technological limits to yield improvement of potatoes. *Proceedings of the Yields of farmed species: constraints and opportunities in the 21st century. Proceedings of a University of Nottingham Easter School Series, June 2004, Sutton Bonington, UK.*, *2005*: Nottingham University Press, 289-309.

Altschul SF, Madden TL, Schaffer AA., 1997. Gapped BLAST and PSI-BLAST: a new generation of protein database search programs. *Nucleic Acids Res* **25**, 3389-402.

Anderberg H, Danielson J, Johanson U, 2011. Algal MIPs, high diversity and conserved motifs. *BMC Evolu. Biol.* **11**, 1-15.

Antunes F, Cadenas E, 2000. Estimation of H_2O_2 gradients across biomembranes. *FEBS Letters* **475**, 121-6.

Araya-Secchi R, Garate J, Holmes D, Perez-Acle T, 2011. Molecular dynamics study of the archaeal aquaporin AqpM. *BMC Genom.* **12**, S8.

Backhus LE, Derisi J, Brown PO, Bisson LF, 2001. Functional genomic analysis of a commercial wine strain of *Saccharomyces cerevisiae* under differing nitrogen conditions. *FEMS Yeast Res* **1**, 111-25.

Bansal A, Sankararamakrishnan R, 2007. Homology modeling of major intrinsic proteins in rice, maize and Arabidopsis: comparative analysis of transmembrane helix association and aromatic/arginine selectivity filters. *BMC Structural Biology* **7**, 27.

Barr ME, 1977. *Magnaporthe, Telimenella*, and *Hyponectria* (*Physosporellaceae*). *Mycologia*, 952-66.

Bartnicki-Garcia S, 2006. Chitosomes: past, present and future. *FEMS Yeast Res* **6**, 957-65.

Bartnicki-Garcia S, Bracker CE, Gierz G, Lopez-Franco R, Lu H, 2000. Mapping the growth of fungal hyphae: orthogonal cell wall expansion during tip growth and the role of turgor. *Biophys J.* **79**, 2382-90.

Beese SE, Negishi T, Levin DE, 2009. Identification of positive regulators of the yeast Fps1 glycerol channel. *PLoS Genet* **5**, e1000738.

Beitz E, Wu B, Holm LM, Schultz JE, Zeuthen T, 2006. Point mutations in the aromatic/arginine region in aquaporin 1 allow passage of urea, glycerol, ammonia, and protons. *Proc Natl Acad Sci U S A* **103**, 269-74.

Belozerskaya TA, Gessler NN, 2007. Reactive oxygen species and the strategy of antioxidant defense in fungi: A review. *Appl. Bioch. and Microbiol.* **43**, 506-15.

Berepiki A, Read ND, 2013. Septins are important for cell polarity, septation and asexual spore formation in *Neurospora crassa* and show different patterns of localisation at germ tube tips. *PLoS ONE* **8**, e63843.

Bertl A, Kaldenhoff R, 2007. Function of a separate NH_3-pore in aquaporin TIP2;2 from wheat. *FEBS Lett* **581**, 5413-7.

Bhadauria V, Banniza S, Vandenberg A, SelvaraJ. G, Wei Y, 2013. Overexpression of a novel biotrophy-specific *Colletotrichum truncatum* effector, CtNUDIX, in hemibiotrophic fungal phytopathogens causes incompatibility with their host plants. *Eukaryot Cell* **12**, 2-11.

Bienert GP, Bienert MD, Jahn TP, Boutry M, Chaumont F, 2011. Solanaceae XIPs are plasma membrane aquaporins that facilitate the transport of many uncharged substrates. *Plant J.* **66**, 306-17.

Bienert GP, Desguin B, Chaumont F, Hols P, 2013. Channel-mediated lactic acid transport: a novel function for aquaglyceroporins in bacteria. *BioChem. J*. **15**, 559-70

Bienert GP, Møller ALB, Kristiansen KA*, et al.*, 2007. Specific aquaporins facilitate the diffusion of hydrogen peroxide across membranes. *J. Biol. Chem.* **282**, 1183-92.

Bienert GP, Schjoerring JK, Jahn TP, 2006. Membrane transport of hydrogen peroxide. *Biochim. Biophys. Acta (BBA) - Biomembranes* **1758**, 994-1003.

Bonhivers M, Carbrey JM, Gould SJ, Agre P, 1998. Aquaporins in *Saccharomyces*. Genetic and functional distinctions between laboratory and wild-type strains. *J. Biol. Chem.* **273**, 27565-72.

Bonman JM, 1992. Durable resistance to rice blast disease — environmental influences. In: Johnson R, Jellis GJ, eds. *Breeding for Disease Resistance.* Springer Netherlands, 115-23. (Developments in Plant Pathology; vol. 1.)

Bourett TM, Howard RJ, 1990. In vitro development of penetration structures in the rice blast fungus *Magnaporthe grisea*. *Can. J. Bot.* **68**, 329-42.

Brown A, 1990. *Microbial water stress physiology. Principles and perspectives*. John Wiley & Sons.

Brown AM, Zondlo NJ, 2012. A propensity scale for type ii polyproline helices (PPII): aromatic amino acids in proline-rich sequences strongly disfavor PPII due to proline–aromatic interactions. *BioChem.* **51**, 5041-51.

Burghardt B, Elkaer ML, Kwon TH*, et al.*, 2003. Distribution of aquaporin water channels AQP1 and AQP5 in the ductal system of the human pancreas. *Gut* **52**, 1008-16.

Bustin SA, Benes V, Garson JA*, et al.*, 2009. The MIQE guidelines: minimum information for publication of quantitative real-time PCR experiments. *Clin Chem.* **55**, 611-22.

Bustin SA, Nolan T, 2004. Pitfalls of quantitative real-time reverse-transcription polymerase chain reaction. *J. biomolecular techniques: JBT* **15**, 155.

Campos-Soriano L, Valè G, Lupotto E, San Segundo B, 2012. Investigation of rice blast development in susceptible and resistant rice cultivars using a gfp-expressing *Magnaporthe oryzae* isolate. *Plant Patholoy*

Caraguel CG, Stryhn H, Gagné N, Dohoo IR, Hammell KL, 2011. Selection of a cutoff value for real-time polymerase chain reaction results to fit a diagnostic purpose: analytical and epidemiologic approaches. *J. Vet.Diag. Investig.* **23**, 2-15.

Carbrey JM, Bonhivers M, Boeke JD, Agre P, 2001a. Aquaporins in *Saccharomyces*: characterization of a second functional water channel protein. *Proc. Nat. Acad. Sci. USA* **98**, 1000-5.

Carbrey JM, Cormack BP, Agre P, 2001b. Aquaporin in *Candida*: characterization of a functional water channel protein. *Yeast* **18**, 1391-6.

Carvalho ND, Arentshorst M, Jin Kwon M, Meyer V, Ram AF, 2010. Expanding the ku70 toolbox for filamentous fungi: establishment of complementation vectors and recipient strains for advanced gene analyses. *Appl MicroBiol. Biotechnol* **87**, 1463-73.

Chalfie M, Kain SR, 2005. *Methods of BioChem. Analysis, Green Fluorescent Protein: Properties, Applications and Protocols*. Wiley-Liss.

Cheetham J, Smith DA, Da Silva Dantas A, 2007. A single MAPKKK regulates the Hog1 MAPK pathway in the pathogenic fungus *Candida albicans*. *Mol Biol. Cell* **18**, 4603-14.

Chi M-H, Park S-Y, Kim S, Lee Y-H, 2009. A novel pathogenicity gene is required in the rice blast fungus to suppress the basal defenses of the host. *PLoS Pathog* **5**, e1000401.

Chin D, Means AR, 2000. Calmodulin: a prototypical calcium sensor. *Trends Cell Biol.* **10**, 322-8.

Choi J, Park J, Jeon J*, et al.*, 2007. Genome-wide analysis of T-DNA integration into the chromosomes of *Magnaporthe oryzae*. *Mol. Microbiol.***66**, 371-82.

Choi W, Dean RA, 1997. The adenylate cyclase gene MAC1 of *Magnaporthe grisea* controls appressorium formation and other aspects of growth and development. *Plant Cell* **9**, 1973-83.

Choi WG, Roberts DM, 2007. Arabidopsis NIP2;1, a major intrinsic protein transporter of lactic acid induced by anoxic stress. *J. Biol. Chem.* **282**, 24209-18.

Chu S, Derisi J, Eisen M, 1998. The transcriptional program of sporulation in budding yeast. *Science* **282**, 699-705.

Chumley FG, Valent B, 1990. Genetic analysis of melanin-deficient, nonpathogenic mutants of *Magnaporthe grisea*. *Mol. Plant-Microbe Interact* **3**, 135-43.

Clément B, Merlin G, 1995. The contribution of ammonia and alkalinity to landfill leachate toxicity to duckweed. *Science of The Total Environment* **170**, 71-9.

Cliften PF, Fulton RS, Wilson RK, Johnston M, 2006. After the duplication: gene loss and adaptation in *Saccharomyces* genomes. *Genetics* **172**, 863-72.

Collingridge PW, Kelly S, 2012. MergeAlign: improving multiple sequence alignment performance by dynamic reconstruction of consensus multiple sequence alignments. *BMC Bioinformatics* **13**.

Cosgrove DJ, 1981. Analysis of the dynamic and steady-state responses of growth rate and turgor pressure to changes in cell parameters. *Plant Physiology* **68**, 1439-46.

Dagdas YF, Yoshino K, Dagdas G,, 2012. Septin-mediated plant cell invasion by the rice blast fungus, *Magnaporthe oryzae*. *Science* **336**, 1590-5.

Dang V-D, Valens M, Bolotin-Fukuhara M, Daignan-Fornier B, 1996. Cloning of the ASN1 and ASN2 genes encoding asparagine synthetases in *Saccharomyces cerevisiae*: differential regulation by the CCAAT-box-binding factor. *Mol. Microbiol.* **22**, 681-92.

Danielson J, Johanson U, 2008. Unexpected complexity of the aquaporin gene family in the moss *Physcomitrella patens*. *BMC Plant Biol.* **8**, 45.

Danielson JA, Johanson U, 2010. Phylogeny of major intrinsic proteins. *Adv Exp Med Biol.* **679**, 19-31.

Dat J, Vandenabeele S, Vranová E, Van Montagu M, Inzé* D, Van Breusegem F, 2000. Dual action of the active oxygen species during plant stress responses. *Cell. Mol. Life Sci. CMLS* **57**, 779-95.

De Groot BL, Frigato T, Helms V, Grubmüller H, 2003. The Mechanism of Proton Exclusion in the Aquaporin-1 Water Channel. *J. Molecular Biology* **333**, 279-93.

De Jong JC, Mccormack BJ, Smirnoff N, Talbot NJ, 1997. Glycerol generates turgor in rice blast. *Nature* **389**, 244-.

De Lucena RM, Elsztein C, Simões DA, De Morais MA, 2012. Participation of CWI, HOG and Calcineurin pathways in the tolerance of *Saccharomyces cerevisiae* to low pH by inorganic acid. *J. Applied Microbiology* **113**, 629-40.

Dean RA, Talbot NJ, Ebbole DJ, 2005. The genome sequence of the rice blast fungus *Magnaporthe grisea*. *Nature* **434**, 980-6.

Deising HB, Werner S, Wernitz M, 2000. The role of fungal appressoria in plant infection. *Microbes and Infect.* **2**, 1631-41.

Deluna A, Springer M, Kirschner MW, Kishony R, 2010. Need-based up-regulation of protein levels in response to deletion of their duplicate genes. *PLoS Biol.* **8**, e1000347.

Dezwaan TM, Carroll AM, Valent B, Sweigard JA, 1999. *Magnaporthe grisea* pth11p is a novel plasma membrane protein that mediates appressorium differentiation in response to inductive substrate cues. *The Plant Cell* **11**, 2013-30.

Dhandayuthapani S, Rasmussen WG, Baseman JB, 1999. Disruption of gene mg218 of *Mycoplasma genitalium* through homologous recombination leads to an adherence-deficient phenotype. *Proc. Nat. Acad. USA* **96**, 5227-32.

Dheda K, Huggett JF, Bustin SA, Johnson MA, Rook G, Zumla A, 2004. Validation of housekeeping genes for normalizing RNA expression in real-time PCR. *Biotechniques* **37**, 112-4, 6, 8-9.

Dietz S, Von Bulow J, Beitz E, Nehls U, 2011. The aquaporin gene family of the ectomycorrhizal fungus *Laccaria bicolor*: lessons for symbiotic functions. *New Phytol* **190**, 927-40.

Dimmic MW, Rest JS, Mindell DP, Goldstein RA, 2002. rtREV: An amino acid substitution matrix for inference of retrovirus and reverse transcriptase phylogeny. *J. Mol Evol* **55**, 65-73.

Dixon KP, Xu J-R, Smirnoff N, Talbot NJ, 1999. Independent signaling pathways regulate cellular turgor during hyperosmotic stress and appressorium-mediated plant infection by *Magnaporthe grisea*. *The Plant Cell* **11**, 2045-58.

Doheny JG, Mottus R, Grigliatti TA, 2008. Telomeric Position Effect—A Third Silencing Mechanism in Eukaryotes. *PLoS One* **3**, e3864.

Donofrio NM, Oh Y, Lundy R*, et al.*, 2006. Global gene expression during nitrogen starvation in the rice blast fungus, *Magnaporthe grisea*. *Fungal Genet. and Biol.* **43**, 605-17.

Dooley CT, Dore TM, Hanson GT, Jackson WC, Remington SJ, Tsien RY, 2004. Imaging dynamic redox changes in mammalian cells with green fluorescent protein indicators. *J. Biol. Chem.* **279**, 22284-93.

Dror V, Winston F, 2004. The Swi/Snf chromatin remodeling complex is required for ribosomal dna and telomeric silencing in *Saccharomyces cerevisiae*. *Mol. Cell. Biol.* **24**, 8227-35.

Dudasova Z, Dudas A, Chovanec M, 2004. Non-homologous end-joining factors of Saccharomyces cerevisiae. *FEMS MicroBiol. Rev* **28**, 581-601.

Duvick DN, Cassman KG, 1999. Post-green revolution trends in yield potential of temperate maize in the north-central United States. *Crop Science* **39**, 1622-30.

Ebersberger I, De Matos Simoes R, Kupczok A,, 2011. A Consistent Phylogenetic Backbone for the Fungi. *Mol Biol. Evol*.

Echevarria M, Windhager EE, Tate SS, Frindt G, 1994. Cloning and expression of AQP3, a water channel from the medullary collecting duct of rat kidney. *Proc Natl Acad Sci U S A* **91**, 10997-1001.

Eddy SR, 1998. Profile hidden Markov models. *Bioinformatics* **14**, 755-63.

Edgar RC, 2004. MUSCLE: multiple sequence alignment with high accuracy and high throughput. *Nucleic Acids Res* **32**, 1792-7.

Egan MJ, Wang ZY, Jones MA, Smirnoff N, Talbot NJ, 2007. Generation of reactive oxygen species by fungal NADPH oxidases is required for rice blast disease. *Proc Natl Acad Sci U S A* **104**, 11772-7.

Egerton-Warburton LM, Querejeta JI, Allen MF, 2007. Common mycorrhizal networks provide a potential pathway for the transfer of hydraulically lifted water between plants. *J. Exp Bot* **58**, 1473-83.

Emerson K, Russo RC, Lund RE, Thurston RV, 1975. Aqueous ammonia equilibrium calculations: effect of pH and temperature. *J. Fish. Board Can.* **32**, 2379-83.

Endeward V, Musa-Aziz R, Cooper GJ*, et al.*, 2006. Evidence that aquaporin 1 is a major pathway for CO_2 transport across the human erythrocyte membrane. *FASEB J.* **20**, 1974-81.

Engel A, Stahlberg H, 2002. Aquaglyceroporins: channel proteins with a conserved core, multiple functions, and variable surfaces. *Int Rev Cytol* **215**, 75-104.

Fang EG, Dean RA, 2000. Site-directed mutagenesis of the magB gene affects growth and development in *Magnaporthe grisea*. *Mol Plant Microbe Interact* **13**, 1214-27.

Farman ML, Eto Y, Nakao T*, et al.*, 2002. Analysis of the structure of the AVR1-CO39 avirulence locus in virulent rice-infecting isolates of *Magnaporthe grisea*. *Mol Plant Microbe Interact* **15**, 6-16.

Felsenstein J, 1985. Confidence limits on phylogenies: an approach using the bootstrap. *Evolution*, 783-91.

Fetter K, Van Wilder V, Moshelion M, Chaumont F, 2004. Interactions between plasma membrane aquaporins modulate their water channel activity. *Plant Cell* **16**, 215-28.

Fischer G, Kosinska-Eriksson U, Aponte-Santamaría C*, et al.*, 2009. Crystal structure of a yeast aquaporin at 1.15 å reveals a novel gating mechanism. *PLoS Biol.* **7**, e1000130.

Fleige S, Pfaffl MW, 2006. RNA integrity and the effect on the real-time qRT-PCR performance. *Mol. Asp. Med.* **27**, 126-39.

Flexas J, Ribas-Carbo M, Hanson DT, 2006. Tobacco aquaporin NtAQP1 is involved in mesophyll conductance to CO2 in vivo. *Plant J.* **48**, 427-39.

Forrest K, Bhave M, 2007. Major intrinsic proteins (MIPs) in plants: a complex gene family with major impacts on plant phenotype. *Funct. Integ. Gen.* **7**, 263-89.

Foster A, Talbot N, 2000. The role of carbohydrates in the pathogenicity of the rice blast fungus *Magnaporthe grisea*. *Dev. Plant Path.*, 271-80.

Foster AJ, Jenkinson JM, Talbot NJ, 2003. Trehalose synthesis and metabolism are required at different stages of plant infection by *Magnaporthe grisea*. *EMBO J.* **22**, 225-35.

Fricker M, Runions J, Moore I, 2006. Quantitative fluorescence microscopy: from art to science. *Annu Rev Plant Biol.* **57**, 79-107.

Froger A, Thomas D, Delamarche C, Tallur B, 1998. Prediction of functional residues in water channels and related proteins. *Protein Sci.* **7**, 1458-68.

Fudal I, Collemare J, Bohnert HU, Melayah D, Lebrun MH, 2007. Expression of M*agnaporthe grisea* avirulence gene ACE1 is connected to the initiation of appressorium-mediated penetration. *Eukaryot Cell* **6**, 546-54.

Garcia-Perez A, Burg MB, 1991. Renal medullary organic osmolytes. *Physiol Rev* **71**, 1081-115.

Gaspar M, Bousser A, Sissoeff I, Roche O, Hoarau J, Mahe A, 2003. Cloning and characterization of ZmPIP1-5b, an aquaporin transporting water and urea. *Plant Sci.* **165**, 21-31.

Gessler NN, Aver'yanov AA, Belozerskaya TA, 2007. Reactive oxygen species in regulation of fungal development. *BioChem. (Mosc)* **72**, 1091-109.

Ghatak A, Willocquet L, Savary S, Kumar J, 2013. Variability in aggressiveness of rice blast (*Magnaporthe oryzae*) isolates originating from rice leaves and necks: a case of pathogen specialization? *PloS One* **8**, e66180.

Giaever G, Chu AM, Ni L*, et al.*, 2002. Functional profiling of the *Saccharomyces cerevisiae* genome. *Nature* **418**, 387-91.

Gilbert R, Johnson A, Dean R, 1996. Chem. signals responsible for appressorium formation in the rice blast fungus *Magnaporthe grisea. Physiol. Mol. Plant Path.***48**, 335-46.

Giorgio M, Trinei M, Migliaccio E, Pelicci PG, 2007. Hydrogen peroxide: a metabolic by-product or a common mediator of ageing signals? *Nat Rev Mol Cell Biol.* **8**, 722-8.

Giraldo MC, Dagdas YF, Gupta YK*, et al.*, 2013. Two distinct secretion systems facilitate tissue invasion by the rice blast fungus *Magnaporthe oryzae*. *Nat Commun* **4**.

Godfray HCJ, Beddington JR, Crute IR*, et al.*, 2010. Food security: the challenge of feeding 9 billion people. *Science* **327**, 812-8.

Goff SA, 1999. Rice as a model for cereal genomics. *Curr. Op. Plant Biol.* **2**, 86-9.

Goff SA, Ricke D, Lan T-H*, et al.*, 2002. A draft sequence of the rice genome (*Oryza sativa* L. ssp. japonica). *Science* **296**, 92-100.

Goldberg AL, 2003. Protein degradation and protection against misfolded or damaged proteins. *Nature* **426**, 895-9.

Goldoni M, Azzalin G, Macino G, Cogoni C, 2004. Efficient gene silencing by expression of double stranded RNA in *Neurospora crassa*. *Fungal Genet. Biol.* **41**, 1016-24.

Gough D, Cotter T, 2011. Hydrogen peroxide: a Jekyll and Hyde signalling molecule. *Cell Death dis.* **2**, e213.

Greenbaum D, Colangelo C, Williams K, Gerstein M, 2003. Comparing protein abundance and mRNA expression levels on a genomic scale. *Geno. Biol.* **4**, 117.

Gribaldo S, Poole AM, Daubin V, Forterre P, Brochier-Armanet C, 2010. The origin of eukaryotes and their relationship with the Archaea: are we at a phylogenomic impasse? *Nat Rev Microbiol.* **8**, 743-52.

Gu Z, Steinmetz LM, Gu X, Scharfe C, Davis RW, Li W-H, 2003. Role of duplicate genes in genetic robustness against null mutations. *Nature* **421**, 63-6.

Guo M, Chen Y, Du Y, 2011. The bZIP transcription factor MoAp1 mediates the oxidative stress response and is critical for pathogenicity of the rice blast fungus *Magnaporthe oryzae*. *PLoS Pathog* **7**, e1001302.

Guo M, Guo W, Chen Y, 2010. The basic leucine zipper transcription factor Moatf1 mediates oxidative stress responses and is necessary for full virulence of the rice blast fungus *Magnaporthe oryzae*. *Mol Plant Microbe Interact* **23**, 1053-68.

Gupta A, Sankararamakrishnan R, 2009a. Genome-wide analysis of major intrinsic proteins in the tree plant *Populus trichocarpa*: Characterization of XIP subfamily of aquaporins from evolutionary perspective. *BMC Plant Biol.* **9**, 134.

Gupta AB, Sankararamakrishnan R, 2009b. Genome-wide analysis of major intrinsic proteins in the tree plant *Populus trichocarpa*: characterization of XIP subfamily of aquaporins from evolutionary perspective. *BMC Plant Biol.* **9**, 134.

Gustavsson S, Lebrun A-S, Nordén K, Chaumont F, Johanson U, 2005. A novel plant major intrinsic protein in *Physcomitrella patens* most similar to bacterial glycerol channels. *Plant Physiol.* **139**, 287-95.

Gutscher M, Pauleau A-L, Marty L, 2008. Real-time imaging of the intracellular glutathione redox potential. *Nat. Meth.* **5**, 553-9.

Hachez C, Chaumont F, 2010. Aquaporins: a family of highly regulated multifunctional channels. In: Jahn T, Bienert G, eds. *MIPs and Their Role in the Exchange of Metalloids.* Springer New York, 1-17. (Advances in Experimental Medicine and Biology; vol. 679.)

Hachez C, Moshelion M, Zelazny E, Cavez D, Chaumont F, 2006. Localization and quantification of plasma membrane aquaporin expression in maize primary root: a clue to understanding their role as cellular plumbers. *Plant Mol. Biol.* **62**, 305-23.

Haddoub R, Rutzler M, Robin A, Flitsch SL, 2009. Design, synthesis and assaying of potential aquaporin inhibitors. *Handb Exp Pharmacol*, 385-402.

Hamer JE, Howard RJ, Chumley FG, Valent B, 1988. A mechanism for surface attachment in spores of a plant pathogenic fungus. *Science* **239**, 288-90.

Hampl V, Hug L, Leigh JW, 2009. Phylogenomic analyses support the monophyly of Excavata and resolve relationships among eukaryotic “supergroups”. *Proc. Nat.Acad. Sci. USA* **106**, 3859-64.

Han J, Lee J, Bibbs L, Ulevitch R, 1994. A MAP kinase targeted by endotoxin and hyperosmolarity in mammalian cells. *Science* **265**, 808-11.

Han J, Choi Y, Brey T, Lee J, 1998. Molecular cloning and characterization of a *Drosophila* p38 mitogen-activated protein kinase. *J. Biol. Chem.* **273**, 369-74.

Hansen M, Kun JFJ, Schultz JE, Beitz E, 2002. A Single, Bi-functional Aquaglyceroporin in Blood-stage *Plasmodium falciparum* Malaria Parasites. *J. Biol. Chem.* **277**, 4874-82.

Hara-Chikuma M, Sohara E, Rai T*, et al.*, 2005. Progressive adipocyte hypertrophy in aquaporin-7-deficient mice: adipocyte glycerol permeability as a novel regulator of fat accumulation. *J. Biol. Chem.* **280**, 15493-6.

Hara-Chikuma M, Verkman AS, 2005. Aquaporin-3 functions as a glycerol transporter in mammalian skin. *Biol. Cell* **97**, 479-86.

Harish A, Tunlid A, Kurland CG, 2013. Rooted phylogeny of the three superkingdoms. *Biochimie* **95**, 1593-604.

Harries WE, Akhavan D, Miercke LJ, Khademi S, Stroud RM, 2004. The channel architecture of aquaporin 0 at a 2.2-Å resolution. *Proc Natl Acad Sci U S A* **101**, 14045-50.

Harris SD, 2005. Morphogenesis in germinating *Fusarium graminearum* macroconidia. *Mycologia* **97**, 880-7.

Harrison P, Kumar A, Lan N, Echols N, Snyder M, Gerstein M, 2002. A small reservoir of disabled ORFs in the yeast genome and its implications for the dynamics of proteome evolution. *J. Mol Biol.* **316**, 409-19.

Haupts U, Maiti S, Schwille P, Webb WW, 1998. Dynamics of fluorescence fluctuations in green fluorescent protein observed by fluorescence correlation spectroscopy. *Proc. Nat. Acad. Sci. USA* **95**, 13573-8.

He M, Kershaw MJ, Soanes DM, Xia Y, Talbot NJ, 2012. Infection-associated nuclear degeneration in the rice blast fungus *Magnaporthe oryzae* requires non-selective macro-autophagy. *PLoS One* **7**, e33270.

Hedfalk K, Bill RM, Mullins JGL, 2004. A regulatory domain in the C-terminal extension of the yeast glycerol channel Fps1p. *J. Biol. Chem.* **279**, 14954-60.

Hellemans J, Mortier G, De Paepe A, Speleman F, Vandesompele J, 2007. qBase relative quantification framework and software for management and automated analysis of real-time quantitative PCR data. *Genome Biol.* **8**, R19.

Heller J, Meyer AJ, Tudzynski P, 2012. Redox-sensitive GFP2: use of the genetically encoded biosensor of the redox status in the filamentous fungus *Botrytis cinerea*. *Mol Plant Pathol* **13**, 935-47.

Herrera M, Hong NJ, Garvin JL, 2006. Aquaporin-1 transports NO across cell membranes. *Hypertension* **48**, 157-64.

Heupel S, Roser B, Kuhn H, Lebrun MH, Villalba F, Requena N, 2010. Erl1, a novel era-like GTPase from *Magnaporthe oryzae*, is required for full root virulence and is conserved in the mutualistic symbiont Glomus intraradices. *Mol Plant Microbe Interact* **23**, 67-81.

Heymann JB, Engel A, 2000. Structural clues in the sequences of the aquaporins. *J. Mol Biol.* **295**, 1039-53.

Hibuse T, Maeda N, Funahashi T, 2005. Aquaporin 7 deficiency is associated with development of obesity through activation of adipose glycerol kinase. *Proc Natl Acad Sci U S A* **102**, 10993-8.

Hickey PC, Swift SR, Roca MG, Read ND, 2004. Live-cell imaging of filamentous fungi using vital fluorescent dyes and confocal microscopy. *Meth. Microbiol.* **34**, 63-87.

Hillenmeyer ME, Fung E, Wildenhain J*, et al.*, 2008. The chemical genomic portrait of yeast: uncovering a phenotype for all genes. *Science* **320**, 362-5.

Hohmann S, 2002. Osmotic stress signaling and osmoadaptation in yeasts. *Microbiol. Mol. Biol. Rev.* **66**, 300-72.

Holm LM, Jahn TP, Moller AL, 2005. NH_3 and NH_4^+ permeability in aquaporin-expressing *Xenopus* oocytes. *Pflugers Arch* **450**, 415-28.

Hove RM, Bhave M, 2011. Plant aquaporins with non-aqua functions: deciphering the signature sequences. *Plant Mol Biol.* **75**, 413-30.

Howard RJ, Ferrari MA, Roach DH, Money NP, 1991. Penetration of hard substrates by a fungus employing enormous turgor pressures. *Proc. Nat. Acad. Sci. USA* **88**, 11281-4.

Howard RJ, Valent B, 1996. Breaking and entering: host penetration by the fungal rice blast pathogen *Magnaporthe grisea*. *Annu. Rev. Microbiol.***50**, 491-512.

Hub JS, De Groot BL, 2008. Mechanism of selectivity in aquaporins and aquaglyceroporins. *Proc. Nat. Acad. Sci. USA* **105**, 1198-203.

Huertas P, 2010. DNA resection in eukaryotes: deciding how to fix the break. *Nat Struct Mol Biol.* **17**, 11-6.

Ikeda M, Beitz E, Kozono D, Guggino WB, Agre P, Yasui M, 2002. Characterization of aquaporin-6 as a nitrate channel in mammalian cells. Requirement of pore-lining residue threonine 63. *J. Biol. Chem.* **277**, 39873-9.

Ishibashi K, 2006. Aquaporin subfamily with unusual NPA boxes. *Biochimica et Biophysica Acta (BBA)-Biomembranes* **1758**, 989-93.

Ishibashi K, 2009**.** New members of mammalian aquaporins: AQP10-AQP12**.** *Handb Exp Pharmacol***,** 251-62.

Ishibashi K, Hara S, Kondo S, 2009. Aquaporin water channels in mammals. *Clin. Exp. Nephrol.***13**, 107-17.

Ishibashi K, Kuwahara M, Gu Y, 1997. Cloning and functional expression of a new water channel abundantly expressed in the testis permeable to water, glycerol, and urea. *J. Biol. Chem.* **272**, 20782-6.

Ishibashi K, Morinaga T, Kuwahara M, Sasaki S, Imai M, 2002. Cloning and identification of a new member of water channel (AQP10) as an aquaglyceroporin. *Biochimi. Biophys. Acta* **1576**, 335-40.

Ishibashi K, Sasaki S, Fushimi K, 1994. Molecular cloning and expression of a member of the aquaporin family with permeability to glycerol and urea in addition to water expressed at the basolateral membrane of kidney collecting duct cells. *Proc Natl Acad Sci U S A* **91**, 6269-73.

Ishikawa F, Suga S, Uemura T, Sato MH, Maeshima M, 2005. Novel type aquaporin SIPs are mainly localized to the ER membrane and show cell-specific expression in *Arabidopsis thaliana*. *FEBS Lett* **579**, 5814-20.

Iwakura M, Nakamura T, 1998. Effects of the length of a glycine linker connecting the N-and C-termini of a circularly permuted dihydrofolate reductase. *Protein Eng* **11**, 707-13.

Jaggard KW, Qi A, Ober ES, 2010. Possible changes to arable crop yields by 2050. *Philosophical Transactions of the Royal Society B: Biol. Sciences* **365**, 2835-51.

Jahn TP, Møller ALB, Zeuthen T, 2004. Aquaporin homologues in plants and mammals transport ammonia. *FEBS Lett.* **574**, 31-6.

Jeon J, Choi J, Lee GW, Dean RA, Lee YH, 2013. Experimental Evolution Reveals Genome-Wide Spectrum and Dynamics of Mutations in the Rice Blast Fungus, *Magnaporthe oryzae*. *PLoS ONE* **8**.

Jeong JS, Mitchell TK, Dean RA, 2007. The *Magnaporthe grisea* snodprot1 homolog, MSP1, is required for virulence. *FEMS Microbiology Letters* **273**, 157-65.

Johnston M, Davis RW, 1984. Sequences that regulate the divergent GAL1-GAL10 promoter in *Saccharomyces cerevisiae*. *Mol Cell Biol.* **4**, 1440-8.

Jones GE, 1978. L-Asparagine auxotrophs of *Saccharomyces cerevisiae*: genetic and phenotypic characterization. *J. Bacteriol* **134**, 200-7.

Jozefkowicz C, Rosi P, Sigaut L*, et al.*, 2013. Loop A is critical for the functional interaction of two *Beta vulgaris* PIP aquaporins. *PLoS One* **8**, e57993.

Juneau K, Nislow C, Davis RW, 2009. Alternative Splicing of PTC7 in *Saccharomyces cerevisiae* Determines Protein Localization. *Genetics* **183**, 185-94.

Kafri R, Levy M, Pilpel Y, 2006. The regulatory utilization of genetic redundancy through responsive backup circuits. *Proc. Nat. Acad. Sci. USA* **103**, 11653-8.

Kamath RS, Fraser AG, Dong Y, 2003. Systematic functional analysis of the *Caenorhabditis elegans* genome using RNAi. *Nature* **421**, 231-7.

Kankanala P, Czymmek K, Valent B, 2007. Roles for rice membrane dynamics and plasmodesmata during biotrophic invasion by the blast fungus. *Plant Cell* **19**, 706-24.

Karlen Y, Mcnair A, Perseguers S, Mazza C, Mermod N, 2007. Statistical significance of quantitative PCR. *BMC Bioinformatics* **8**, 131.

Karpel JE, Bisson LF, 2006. Aquaporins in *Saccharomyces cerevisiae* wine yeast. *FEMS MicroBiol. Lett* **257**, 117-23.

Katoh K, Kuma K, Miyata T, Toh H, 2005. Improvement in the accuracy of multiple sequence alignment program MAFFT. *Genome Inform* **16**, 22-33.

Katsuhara M, Akiyama Y, Koshio K, Shibasaka M, Kasamo K, 2002. Functional analysis of water channels in barley roots. *Plant Cell Physiol.* **43**, 885-93.

Kayingo G, Kilian SG, Prior BA, 2001. Conservation and release of osmolytes by yeasts during hypo-osmotic stress. *Archives of microbiology* **177**, 29-35.

Kershaw MJ, Talbot NJ, 2009. Genome-wide functional analysis reveals that infection-associated fungal autophagy is necessary for rice blast disease. *Proc. Nat. Acad. Sci. USA* **106**, 15967-72.

Khush G, Jena KK, 2009. Current status and future prospects for research on blast resistance in rice (*Oryza sativa* L.). In: Wang G-L, Valent B, eds. *Advances in Genetics, Genomics and Control of Rice Blast Disease.* Springer Netherlands, 1-10.

Kim DU, Hayles J, Kim D*, et al.*, 2010a. Analysis of a genome-wide set of gene deletions in the fission yeast *Schizosaccharomyces pombe*. *Nat Biotechnol* **28**, 617-23.

Kim KS, Lee Y-H, 2012. Gene Expression Profiling during Conidiation in the Rice Blast Pathogen *Magnaporthe oryzae*. *PloS one* **7**, e43202.

Kim S, Hu J, Oh Y*, et al.*, 2010b. Combining ChIP-chip and Expression Profiling to Model the *MoCRZ1* Mediated Circuit for Ca^{2+}/Calcineurin Signaling in the Rice Blast Fungus. *PLoS Pathog* **6**, e1000909.

King LS, Kozono D, Agre P, 2004. From structure to disease: the evolving tale of aquaporin biology. *Nat Rev Mol Cell Biol.* **5**, 687-98.

Kjer KM, 1995. Use of ribosomal-RNA secondary structure in phylogenetic studies to identify homologous positions - an example of alignment and data presentation from the frogs. *Molecular Phylogenet. Evol.* **4**, 314-30.

Kobayashi K, Ehrlich SD, Albertini A*, et al.*, 2003. Essential *Bacillus subtilis* genes. *Proc. Nat. Acad. Sci. USA* **100**, 4678-83.

Koga H, Nakayachi O, 2004. Morphological studies on attachment of spores of *Magnaporthe grisea* to the leaf surface of rice. *J. Gen. Plant Path.* **70**, 11-5.

Koide Y, Kobayashi N, Xu D, Fukuta Y, 2009. Resistance genes and selection DNA markers for blast disease in rice (*Oryza sativa* L.). *Jpn Agric Res Q* **43**, 255-80.

Kojima S, Bohner A, Von Wiren N, 2006. Molecular mechanisms of urea transport in plants. *J. Memb. Biol.* **212**, 83-91.

Kolaczkowski B, Thornton JW, 2004. Performance of maximum parsimony and likelihood phylogenetics when evolution is heterogeneous. *Nature* **431**, 980-4.

Kozono D, Ding X, Iwasaki I*, et al.*, 2003. Functional Expression and Characterization of an Archaeal Aquaporin: AqpM *Methanothermobacter marburgensis*. *J. Biol. Chem.* **278**, 10649-56.

Krogh BO, Symington LS, 2004. Recombination proteins in yeast. *Annu Rev Genet* **38**, 233-71.

Kronstad J, 1997. Virulence and cAMP in smuts, blasts and blights. *Trends Plant Sci* **2**, 193-9.

Kruse E, Uehlein N, Kaldenhoff R, 2006. The aquaporins. *Genome Biol.* **7**, 206.

Kumari SS, Eswaramoorthy S, Mathias RT, VaradaraJ. K, 2011. Unique and analogous functions of aquaporin 0 for fiber cell architecture and ocular lens transparency. *Biochim Biophys Acta* **1812**, 1089-97.

Kuźniak E, Urbanek H, 2000. The involvement of hydrogen peroxide in plant responses to stresses. *Acta Physiologiae Plantarum* **22**, 195-203.

Lacroix H, Spanu PD, 2009. Silencing of six hydrophobins in *Cladosporium fulvum*: complexities of simultaneously targeting multiple genes. *Appl. Envir. Microbiol.* **75**, 542-6.

Lagree V, Froger A, Deschamps S, 1999. Switch from an aquaporin to a glycerol channel by two amino acids substitution. *J. Biol. Chem.* **274**, 6817-9.

Laizé V, Tacnet F, Ripoche P, Hohmann S, 2000. Polymorphism of *Saccharomyces cerevisiae* aquaporins. *Yeast* **16**, 897-903.

Lartillot N, Philippe H, 2004. A Bayesian mixture model for across-site heterogeneities in the amino-acid replacement process. *Mol Biol. Evol* **21**, 1095-109.

Leon M, Sentandreu R, Zueco J, 2002. A single FKS homologue in *Yarrowia lipolytica* is essential for viability. *Yeast* **19**, 1003-14.

Leung H, Borromeo E, Bernardo M, Notteghem J, 1988a. Genetic analysis of virulence in the rice blast fungus *Magnaporthe grisea*. St. Paul, MN, ETATS-UNIS: Amer. Phytopatholog. Soc.

Leung H, Borromeo ES, Bernardo MA, Notteghem JL, 1988b. Genetic analysis of virulence in the rice blast fungus *Magnaporthe grisea*. *Phytopathology* **78**, 1227-33.

Levin MK, Carson JH, 2004. Fluorescence correlation spectroscopy and quantitative cell biology. *Differentiation* **72**, 1-10.

Lew RR, 2010. Turgor and net ion flux responses to activation of the osmotic MAP kinase cascade by fludioxonil in the filamentous fungus *Neurospora crassa*. *Fung. Genet Biol.* **47**, 721-6.

Lew RR, 2011. How does a hypha grow? The biophysics of pressurized growth in fungi. *Nat Rev Microbiol.* **9**, 509-18.

Lew RR, Levina NN, Shabala L, Anderca MI, Shabala SN, 2006. Role of a mitogen-activated protein kinase cascade in ion flux-mediated turgor regulation in fungi. *Eukaryot Cell* **5**, 480-7.

Li LF, Zhang CD, Konopka JB, 2012. A *Candida albicans* temperature-sensitive cdc12-6 mutant identifies roles for septins in selection of sites of germ tube formation and hyphal morphogenesis. *Eukaryot Cell* **11**, 1210-8.

Litman T, Sogaard R, Zeuthen T, 2009. Ammonia and urea permeability of mammalian aquaporins. *Handb Exp Pharmacol*, 327-58.

Liu H, Suresh A, Willard FS, Siderovski DP, Lu S, Naqvi NI, 2007a. Rgs1 regulates multiple G[alpha] subunits in *Magnaporthe* pathogenesis, asexual growth and thigmotropism. *EMBO J.* **26**, 690-700.

Liu J, Wang X, Mitchell T, 2010. Recent progress and understanding of the molecular mechanisms of the rice–*Magnaporthe oryzae* interaction. *Mol. Plant Path.***11**, 419-27.

Liu L-H, Ludewig U, Gassert B, Frommer WB, Von Wirén N, 2003. Urea transport by nitrogen-regulated tonoplast intrinsic proteins in *Arabidopsis*. *Plant Physiol.* **133**, 1220-8.

Liu W, Zhou X, Li G*, et al.*, 2011. Multiple plant surface signals are sensed by different mechanisms in the rice blast fungus for appressorium formation. *PLoS Pathog* **7**, e1001261.

Liu XH, Lu JP, Zhang L, Dong B, Min H, Lin FC, 2007. Involvement of a *Magnaporthe grisea* serine/threonine kinase gene, MgATG1, in appressorium turgor and pathogenesis. *Eukaryot Cell* **6**, 997-1005.

Livak KJ, Schmittgen TD, 2001. Analysis of relative gene expression data using real-time quantitative PCR and the $2^{-\Delta\Delta Ct}$ Method. *Methods* **25**, 402-8.

Lloyd DJ, Hall FW, Tarantino LM, Gekakis N, 2005. Diabetes insipidus in mice with a mutation in Aquaporin-2. *PLoS Genet* **1**, e20.

Lobell DB, Cassman KG, Field CB, 2009. Crop yield gaps: their importance, magnitudes, and causes. *Annu Rev Environ Res* **34**, 179-204.

Lockhart JA, 1965. An analysis of irreversible plant cell elongation. *J. Theoretical Biol.* **8**, 264-75.

Loque D, Ludewig U, Yuan L, Von Wiren N, 2005. Tonoplast intrinsic proteins AtTIP2;1 and AtTIP2;3 facilitate NH3 transport into the vacuole. *Plant Physiol* **137**, 671-80.

Loreto C, Reggio E, 2010. Aquaporin and vascular diseases. *Current neuropharmacology* **8**, 105.

Lu DC, Zhang H, Zador Z, Verkman AS, 2008. Impaired olfaction in mice lacking aquaporin-4 water channels. *FASEB J.* **22**, 3216-23.

Ludevid D, Hofte H, Himelblau E, Chrispeels MJ, 1992. The expression pattern of the tonoplast intrinsic protein gamma-TIP in *Arabidopsis thaliana* is correlated with cell enlargement. *Plant Physiol* **100**, 1633-9.

Ludewig U, Dynowski M, 2009. Plant aquaporin selectivity: where transport assays, computer simulations and physiology meet. *Cell. Mol. Life Sci.* **66**, 3161-75.

Lukyanov KA, Belousov VV. Genetically encoded fluorescent redox sensors. *Biochimica et Biophysica Acta (BBA) - General Subjects*.

Lutfiyya LL, Iyer VR, Derisi J, Devit MJ, Brown PO, Johnston M, 1998. Characterization of three related glucose repressors and genes they regulate in *Saccharomyces cerevisiae*. *Genetics* **150**, 1377-91.

Lynch M, Conery JS, 2000. The evolutionary fate and consequences of duplicate genes. *Science* **290**, 1151-5.

Ma JF, Tamai K, Yamaji N, 2006. A silicon transporter in rice. *Nature* **440**, 688-91.

Ma JF, Yamaji N, Tamai K, Mitani N, 2007. Genotypic difference in silicon uptake and expression of silicon transporter genes in rice. *Plant Physiol* **145**, 919-24.

Ma T, Jayaraman S, Wang KS, 2001. Defective dietary fat processing in transgenic mice lacking aquaporin-1 water channels. *Am J. Physiol Cell Physiol* **280**, C126-34.

Ma T, Song Y, Yang B, 2000. Nephrogenic diabetes insipidus in mice lacking aquaporin-3 water channels. *Proc Natl Acad Sci U S A* **97**, 4386-91.

Ma T, Yang B, Verkman AS, 1997. Cloning of a novel water and urea-permeable aquaporin from mouse expressed strongly in colon, placenta, liver, and heart. *BioChem. Biophys Res Commun* **240**, 324-8.

Maciaszczyk-Dziubinska E, Migdal I, Migocka M, Bocer T, Wysocki R, 2010. The yeast aquaglyceroporin Fps1p is a bidirectional arsenite channel. *FEBS Lett* **584**, 726-32.

Maeda T, Takekawa M, Saito H, 1995. Activation of yeast PBS2 MAPKK by MAPKKKs or by binding of an SH3-containing osmosensor. *Science* **269**, 554-8.

Maeshima M, Ishikawa F, 2008. ER membrane aquaporins in plants. *Pflügers Archiv – Europ. J. Physiol.* **456**, 709-16.

Magni F, Chinello C, Raimondo F, Mocarelli P, Kienle MG, Pitto M, 2008. AQP1 expression analysis in human diseases: implications for proteomic characterization. *Expert Rev Proteomics* **5**, 29-43.

Marcel S, Sawers R, Oakeley E, Angliker H, Paszkowski U, 2010. Tissue-adapted invasion strategies of the rice blast fungus *Magnaporthe oryzae*. *Plant Cell* **22**, 3177-87.

Marini AM, Soussi-Boudekou S, Vissers S, Andre B, 1997. A family of ammonium transporters in Saccharomyces cerevisiae. *Mol Cell Biol.* **17**, 4282-93.

Martins AP, Marrone A, Ciancetta A, 2012. Targeting aquaporin function: potent inhibition of Aquaglyceroporin-3 by a gold-based compound. *PLoS ONE* **7**, e37435.

Mathai JC, Agre P, 1999. Hourglass pore-forming domains restrict aquaporin-1 tetramer assembly. *BioChem.* **38**, 923-8.

Mathioni S, Belo A, Rizzo C, Dean R, Donofrio N, 2011. Transcriptome profiling of the rice blast fungus during invasive plant infection and in vitro stresses. *BMC Genom.* **12**, 49.

Matsumura K, Chang BH, Fujimiya M, 2007. Aquaporin 7 is a beta-cell protein and regulator of intraislet glycerol content and glycerol kinase activity, beta-cell mass, and insulin production and secretion. *Mol Cell Biol.* **27**, 6026-37.

Maurel C, 2007. Plant aquaporins: novel functions and regulation properties. *FEBS Lett* **581**, 2227-36.

Maurel C, Verdoucq L, Luu D-T, Santoni V, 2008. Plant aquaporins: membrane channels with multiple integrated functions. *Ann. Rev. Plant Biol.* **59**, 595-624.

Meyer AJ, Brach T, Marty L, *et al.*, 2007. Redox-sensitive GFP in *Arabidopsis thaliana* is a quantitative biosensor for the redox potential of the cellular glutathione redox buffer. *Plant J.* **52**, 973-86.

Meyer AJ, Dick TP, 2010. Fluorescent protein-based redox probes. *Antioxidants and Redox Signaling* **13**, 621-50.

Meyrial V, Laizé V, Gobin R, Ripoche P, Hohmann S, Tacnet F, 2001. Existence of a tightly regulated water channel in *Saccharomyces cerevisiae*. *European J. BioChem.* **268**, 334-43.

Miah G, Rafii MY, Ismail MR, 2013. Blast resistance in rice: a review of conventional breeding to molecular approaches. *Mol. Biol. Rep.* **40**, 2369-88.

Miki D, Itoh R, Shimamoto K, 2005. RNA silencing of single and multiple members in a gene family of rice. *Plant Physiol* **138**, 1903-13.

Miller EW, Dickinson BC, Chang CJ, 2010. Aquaporin-3 mediates hydrogen peroxide uptake to regulate downstream intracellular signaling *Proc. Nat. Acad. Sci. USA* **107**, 15681-6.

Mitani-Ueno N, Yamaji N, Zhao F-J, Ma JF, 2011. The aromatic/arginine selectivity filter of NIP aquaporins plays a critical role in substrate selectivity for silicon, boron, and arsenic. *J. Experim. Bot.* **62**, 4391-8.

Mitchel A, 2002. Molecular and Cellular Biology of Filamentous Fungi; A Practical Approach. *Mycopathologia* **154**, 107-8.

Mitchell TK, Dean RA, 1995. The cAMP-dependent protein kinase catalytic subunit is required for appressorium formation and pathogenesis by the rice blast pathogen *Magnaporthe grisea*. *Plant Cell* **7**, 1869-78.

Mizutani M, Watanabe S, Nakagawa T, Maeshima M, 2006. Aquaporin NIP2;1 is mainly localized to the ER membrane and shows root-specific accumulation in *Arabidopsis thaliana*. *Plant Cell Physiol.* **47**, 1420-6.

Moeller HB, Praetorius J, Rützler MR, Fenton RA, 2010. Phosphorylation of aquaporin-2 regulates its endocytosis and protein–protein interactions. *Proc. Nat. Acad. Sci. USA* **107**, 424-9.

Mollapour M, Piper PW, 2007. Hog1 mitogen-activated protein kinase phosphorylation targets the yeast Fps1 aquaglyceroporin for endocytosis, thereby rendering cells resistant to acetic acid. *Mol. Cell. Biol.* **27**, 6446-56.

Money N, 1998. Mechanics of invasive fungal growth and the significance of turgor in plant infection. In: Kohmoto K, Yoder O, eds. *Molecular Genetics of Host-Specific Toxins in Plant Disease.* Springer Netherlands, 261-71. (Developments in Plant Pathology; vol. 13.)

Money NP, Harold FM, 1992. Extension growth of the water mold *Achlya*: interplay of turgor and wall strength. *Proc Natl Acad Sci U S A* **89**, 4245-9.

Moore I, Murphy A, 2009. Validating the location of fluorescent protein fusions in the endomembrane system. *Plant Cell* **21**, 1632-6.

Morinaga T, Nakakoshi M, Hirao A, Imai M, Ishibashi K, 2002. Mouse aquaporin 10 gene (AQP10) is a pseudogene. *BioChem. Biophys Res Commun* **294**, 630-4.

Morishita Y, Matsuzaki T, Hara-Chikuma M, 2005. Disruption of aquaporin-11 produces polycystic kidneys following vacuolization of the proximal tubule. *Mol Cell Biol.* **25**, 7770-9.

Morrison DA, Ellis JT, 1997. Effects of nucleotide sequence alignment on phylogeny estimation: a case study of 18S rDNAs of apicomplexa. *Mol Biol. Evol* **14**, 428-41.

Mosquera G, Giraldo MC, Khang CH, Coughlan S, Valent B, 2009. Interaction transcriptome analysis identifies Magnaporthe oryzae BAS1-4 as biotrophy-associated secreted proteins in rice blast disease. *Plant Cell* **21**, 1273-90.

Motoyama T, Kadokura K, Ohira T*, et al.*, 2005. A two-component histidine kinase of the rice blast fungus is involved in osmotic stress response and fungicide action. *Fung. Genet. Biol.* **42**, 200-12.

Motoyama T, Ochiai N, Morita M, Iida Y, Usami R, Kudo T, 2008. Involvement of putative response regulator genes of the rice blast fungus *Magnaporthe oryzae* in osmotic stress response, fungicide action, and pathogenicity. *Curr. Genet.* **54**, 185-95.

Nagase H, Agren J, Saito A*, et al.*, 2007. Molecular cloning and characterization of mouse aquaporin 6. *BioChem. Biophys Res Commun* **352**, 12-6.

Negishi T, Oshima K, Hattori M, 2012. Tonoplast- and plasma membrane-localized aquaporin-family transporters in blue hydrangea sepals of aluminum hyperaccumulating plant. *PLOS One* **7**, e43189.

Nellemann C, 2009. *The Environmental Food Crisis: The Environment's Role in Averting Future Food Crises: a UNEP Rapid Response Assessment*. UNEP/Earthprint.

Newby ZER, O'connell Iii J, Robles-Colmenares Y, Khademi S, Miercke LJ, Stroud RM, 2008. Crystal structure of the aquaglyceroporin PfAQP from the malarial parasite *Plasmodium falciparum*. *Nat Struct Mol Biol.* **15**, 619-25.

Nguyen QB, Itoh K, Van Vu B, Tosa Y, Nakayashiki H, 2011. Simultaneous silencing of endo-β-1,4 xylanase genes reveals their roles in the virulence of *Magnaporthe oryzae*. *Mol. Microbiol.* **81**, 1008-19.

Nguyen QB, Kadotani N, Kasahara S, Tosa Y, Mayama S, Nakayashiki H, 2008. Systematic functional analysis of calcium-signalling proteins in the genome of the rice-blast fungus, *Magnaporthe oryzae*, using a high-throughput RNA-silencing system. *Molecular Microbiology* **68**, 1348-65.

Niemietz CM, Tyerman SD, 2002. New potent inhibitors of aquaporins: silver and gold compounds inhibit aquaporins of plant and human origin. *FEBS Letters* **531**, 443-7.

Nordgard O, Kvaloy JT, Farmen RK, Heikkila R, 2006. Error propagation in relative real-time reverse transcription polymerase chain reaction quantification models: the balance between accuracy and precision. *Anal BioChem.* **356**, 182-93.

Nowak MA, Boerlijst MC, Cooke J, Smith JM, 1997. Evolution of genetic redundancy. *Nature* **388**, 167-71.

Nugent T, Jones D, 2009. Transmembrane protein topology prediction using support vector machines. *BMC Bioinform.* **10**, 159.

Oerke EC, 2006. Crop losses to pests. *J. Agricultural Science* **144**, 31-43.

Ogden TH, Rosenberg MS, 2006. Multiple sequence alignment accuracy and phylogenetic inference. *System. Biol.* **55**, 314-28.

Oh Y, Donofrio N, Pan H, 2008. Transcriptome analysis reveals new insight into appressorium formation and function in the rice blast fungus *Magnaporthe oryzae*. *Genome Biol* **9**, R85.

Oliva R, Calamita G, Thornton JM, Pellegrini-Calace M, 2010. Electrostatics of aquaporin and aquaglyceroporin channels correlates with their transport selectivity. *Proc. Nat. Acad. Sci. USA* **107**, 4135-40.

Oshio K, Watanabe H, Yan D, Verkman AS, Manley GT, 2006. Impaired pain sensation in mice lacking Aquaporin-1 water channels. *BioChem. Biophys Res Commun* **341**, 1022-8.

Otto B, Uehlein N, Sdorra S*, et al.*, 2010. Aquaporin tetramer composition modifies the function of tobacco aquaporins. *J. Biol. Chem.* **285**, 31253-60.

Palmer E, Freeman T, 2004. Investigation into the use of C-and N-terminal GFP fusion proteins for subcellular localization studies using reverse transfection microarrays. *Comp. Funct. Genom.* **5**, 342-53.

Pao GM, Wu LF, Johnson KD, 1991. Evolution of the MIP family of integral membrane transport proteins. *Mol MicroBiol.* **5**, 33-7.

Papadopoulos MC, Verkman AS, 2007. Aquaporin-4 and brain edema. *Pediatr Nephrol* **22**, 778-84.

Papadopoulos MC, Verkman AS, 2013. Aquaporin water channels in the nervous system. *Nat Rev Neurosci* **14**, 265-77.

Papp B, Pal C, Hurst LD, 2004. Metabolic network analysis of the causes and evolution of enzyme dispensability in yeast. *Nature* **429**, 661-4.

Park JH, Saier JMH, 1996. Phylogenetic Characterization of the MIP Family of Transmembrane Channel Proteins. *J. Memb. Biol.* **153**, 171-80.

Pettersson N, Filipsson C, Becit E, Brive L, Hohmann S, 2005. Aquaporins in yeasts and filamentous fungi. *Biol. Cell* **97**, 487-500.

Pfaffl MW, 2001. A new mathematical model for relative quantification in real-time RT-PCR. *Nucleic Acids Res.* **29**.

Pfaffl MW, Hageleit M, 2001. Validities of mRNA quantification using recombinant RNA and recombinant DNA external calibration curves in real-time RT-PCR. *Biotechnology Letters* **23**, 275-82.

Philippe H, Brinkmann H, Lavrov DV*, et al.*, 2011. Resolving difficult phylogenetic questions: why more sequences are not enough. *PLoS Biol.* **9**, e1000602.

Philippe H, Zhou Y, Brinkmann H, Rodrigue N, Delsuc F, 2005. Heterotachy and long-branch attraction in phylogenetics. *BMC Evol Biol* **5**, 50.

Philips J, Herskowitz I, 1997. Osmotic balance regulates cell fusion during mating in *Saccharomyces cerevisiae*. *J. Cell Biol.* **138**, 961-74.

Pina C, Pinto F, Feijo JA, Becker JD, 2005. Gene family analysis of the *Arabidopsis* pollen transcriptome reveals Biol. implications for cell growth, division control, and gene expression regulation. *Plant Physiol* **138**, 744-56.

Plamboeck AH, Dawson TE, Egerton-Warburton LM, North M, Bruns TD, Querejeta JI, 2007. Water transfer via ectomycorrhizal fungal hyphae to conifer seedlings. *Mycorrhiza* **17**, 439-47.

Popping B, Gibbons T, Watson MD, 1996. The *Pisum sativum* MAP kinase homologue (PsMAPK) rescues the Saccharomyces cerevisiae hog1 deletion mutant under conditions of high osmotic stress. *Plant Mol Biol* **31**, 355-63.

Posas F, Witten EA, Saito H, 1998. Requirement of STE50 for Osmostress-Induced Activation of the STE11 Mitogen-Activated Protein Kinase Kinase Kinase in the High-Osmolarity Glycerol Response Pathway. *Molecular and Cellular Biology* **18**, 5788-96.

Posas F, Wurgler-Murphy SM, Maeda T, Witten EA, Thai TC, Saito H, 1996. Yeast HOG1 MAP kinase cascade is regulated by a multistep phosphorelay mechanism in the SLN1–YPD1–SSK1 "two-component" osmosensor. *Cell* **86**, 865-75.

Preston GM, Jung JS, Guggino WB, Agre P, 1993. The mercury-sensitive residue at cysteine 189 in the CHIP28 water channel. *J. Biol. Chem.* **268**, 17-20.

Price MN, Dehal PS, Arkin AP, 2010. FastTree 2 – Approximately maximum-likelihood trees for large alignments. *PLoS ONE* **5**, e9490.

Prudent S, Marty F, Charbonnier M, 2005. The yeast osmosensitive mutant *fps1* Δ transformed by the cauliflower BobTIP1; 1 aquaporin withstand a hypo-osmotic shock. *FEBS Lett* **579**, 3872-80.

Querejeta JI, Egerton-Warburton LM, Allen MF, 2003. Direct nocturnal water transfer from oaks to their mycorrhizal symbionts during severe soil drying. *Oecologia* **134**, 55-64.

Quezada H, Aranda C, Deluna A, 2008. Specialization of the paralogue LYS21 determines lysine biosynthesis under respiratory metabolism in *Saccharomyces cerevisiae*. *Microbiology* **154**, 1656-67.

Radonić A, Thulke S, Mackay IM, Landt O, Siegert W, Nitsche A, 2004. Guideline to reference gene selection for quantitative real-time PCR. *BioChem Biophys Res Comm* **313**, 856-62.

Raitt DC, Posas F, Saito H, 2000. Yeast Cdc42 GTPase and Ste20 PAK-like kinase regulate Sho1-dependent activation of the Hog1 MAPK pathway. *EMBO J.* **19**, 4623-31.

Ray DK, Mueller ND, West PC, Foley JA, 2013. Yield trends are insufficient to double global crop production by 2050. *PloS one* **8**, e66428.

Reilly JM, Fuglie KO, 1998. Future yield growth in field crops: what evidence exists? *Soil Tillage Res* **47**, 275-90.

Reiser V, D'aquino KE, Ee LS, Amon A, 2006. The stress-activated mitogen-activated protein kinase signaling cascade promotes exit from mitosis. *Mol Biol. Cell* **17**, 3136-46.

Ringler P, Borgnia MJ, Stahlberg H, Maloney PC, Agre P, Engel A, 1999. Structure of the water channel AqpZ from *Escherichia coli* revealed by electron crystallography. *J. Mol Biol.* **291**, 1181-90.

Rizzo MA, Davidson MW, Piston DW, 2009. Fluorescent protein tracking and detection: applications using fluorescent proteins in living cells. *Cold Spring Harbor Protocols* **2009**, pdb.top64.

Rojek AM, Skowronski MT, Fuchtbauer EM, 2007. Defective glycerol metabolism in aquaporin 9 (AQP9) knockout mice. *Proc Natl Acad Sci U S A* **104**, 3609-14.

Roumen EC, 1992. Partial resistance to neck blast influenced by stage of panicle development and rice genotype. *Euphytica* **64**, 173-82.

Ryder LS, Dagdas YF, Mentlak TA, 2013. NADPH oxidases regulate septin-mediated cytoskeletal remodeling during plant infection by the rice blast fungus. *Proc Natl Acad Sci U S A* **110**, 3179-84.

Saito H, Tatebayashi K, 2004. Regulation of the osmoregulatory HOG MAPK cascade in yeast. *J. BioChem.* **136**, 267-72.

Saitoh H, Fujisawa S, Mitsuoka C*, et al.*, 2012. Large-scale gene disruption in *Magnaporthe oryzae* identifies MC69, a secreted protein required for infection by monocot and dicot fungal pathogens. *PLoS Pathog* **8**, e1002711.

Saleh D, Milazzo J, Adreit H, Tharreau D, Fournier E, 2012. Asexual reproduction induces a rapid and permanent loss of sexual reproduction capacity in the rice fungal pathogen *Magnaporthe oryzae*: results of in vitro experimental evolution assays. *BMC Evolutionary Biology* **12**, 42.

Satoh K, Narita T, Matsuki-Fukushima M*, et al.*, 2013. E2f1-deficient NOD/SCID mice have dry mouth due to a change of acinar/duct structure and the down-regulation of AQP5 in the salivary gland. *Pflugers Arch* **465**, 271-81.

Saunders DG, Aves SJ, Talbot NJ, 2010. Cell cycle-mediated regulation of plant infection by the rice blast fungus. *Plant Cell* **22**, 497-507.

Scherens B, Goffeau A, 2004. The uses of genome-wide yeast mutant collections. *Genome Biol* **5**, 229.

Schwarzlander M, Fricker MD, Müller C*, et al.*, 2008. Confocal imaging of glutathione redox potential in living plant cells. *J. Microscop* **231**, 299-316.

Semchyshyn H, 2009. Hydrogen peroxide-induced response in *E. coli* and *S. cerevisiae*: different stages of the flow of the genetic information. *Central Eur J. Biol* **4**, 142-53.

Shetty NP, Mehrabi R, Lutken H*, et al.*, 2007. Role of hydrogen peroxide during the interaction between the hemibiotrophic fungal pathogen *Septoria tritici* and wheat. *New Phytol* **174**, 637-47.

Sidoux-Walter F, Pettersson N, Hohmann S, 2004. The *Saccharomyces cerevisiae* aquaporin Aqy1 is involved in sporulation. *Proc Natl Acad Sci U S A* **101**, 17422-7.

Siefritz F, Biela A, Eckert M, Otto B, Uehlein N, Kaldenhoff R, 2001. The tobacco plasma membrane aquaporin NtAQP1. *J. Exp Bot* **52**, 1953-7.

Silvey V. 1994. Plant breeding in improving crop yield and quality in recent decades. *Proc. Plant Breed Mankind-Symp Agribex **94** 355* 19-34.

Skamnioti P, Furlong RF, Gurr SJ, 2008. Evolutionary history of the ancient cutinase family in five filamentous Ascomycetes reveals differential gene duplications and losses and in *Magnaporthe grisea* shows evidence of sub- and neo-functionalization. *New Phytol.* **180**, 711-21.

Skamnioti P, Gurr SJ, 2007. *Magnaporthe grisea* cutinase2 mediates appressorium differentiation and host penetration and is required for full virulence. *Plant Cell* **19**, 2674-89.

Skamnioti P, Gurr SJ, 2009. Against the grain: safeguarding rice from rice blast disease. *Trends Biotechnol* **27**, 141-50.

Skamnioti P, Henderson C, Zhang Z, Robinson Z, Gurr SJ, 2007. A novel role for catalase B in the maintenance of fungal cell-wall integrity during host invasion in the rice blast fungus *Magnaporthe grisea*. *Mol Plant Microbe Interact* **20**, 568-80.

Skoog DA, West DM, Holler FJ, 1988. Fundamentals of analytical chemistry.

Smith JS, Boeke JD, 1997. An unusual form of transcriptional silencing in yeast ribosomal DNA. *Gen. Dev.* **11**, 241-54.

Smith SE, Read DJ, 2010. *Mycorrhizal symbiosis*. Access Online via Elsevier.

Smythe AB, Sanderson MJ, Nadler SA, 2006. Nematode small subunit phylogeny correlates with alignment parameters. *System. Biol.***55**, 972-92.

Soanes DM, Chakrabarti A, Paszkiewicz KH, Dawe AL, Talbot NJ, 2012. Genome-wide transcriptional profiling of appressorium development by the rice blast fungus *Magnaporthe oryzae*. *PLoS Pathog* **8**, e1002514.

Sohara E, Rai T, Sasaki S, Uchida S, 2006. Physiological roles of AQP7 in the kidney: lessons from AQP7 knockout mice. *Biochim Biophys Acta* **1758**, 1106-10.

Soto G, Alleva K, Amodeo G, Muschietti J, Ayub ND, 2012. New insight into the evolution of aquaporins from flowering plants and vertebrates: Orthologous identification and functional transfer is possible. *Gene* **503**, 165-76.

Sousa-Lopes A, Antunes F, Cyrne L, Marinho HS, 2004. Decreased cellular permeability to H_2O_2 protects *Saccharomyces cerevisiae* cells in stationary phase against oxidative stress. *FEBS lett.* **578**, 152-6.

Soveral G, Madeira A, Loureiro-Dias MC, Moura TF, 2008. Membrane tension regulates water transport in yeast. *Bioch. Biophys. Acta* **1778**, 2573-9.

Soveral G, Prista C, Moura TF, Loureiro-Dias MC, 2010. Yeast water channels: an overview of orthodox aquaporins. *Biol. Cell* **103**, 35-54.

Soveral G, Veiga A, Loureiro-Dias MC, Tanghe A, Van Dijck P, Moura TF, 2006. Water channels are important for osmotic adjustments of yeast cells at low temperature. *Microbiology* **152**, 1515-21.

Spink J, Street P, Sylvester-Bradley R, Berry P, 2009. The potential to increase productivity of wheat and oilseed rape in the UK. *See http://dius. gov. uk*.

Stein A, Aloy P, 2008. A molecular interpretation of genetic interactions in yeast. *FEBS Lett.* **582**, 1245-50.

Suga S, Maeshima M, 2004. Water channel activity of radish plasma membrane aquaporins heterologously expressed in yeast and their modification by site-directed mutagenesis. *Plant Cell Physiol* **45**, 823-30.

Sukumaran J, Holder MT, 2010. DendroPy: a Python library for phylogenetic computing. *Bioinformatics* **26**, 1569-71.

Sumaila UR, Cheung W, Dyck A, 2012. Benefits of rebuilding global marine fisheries outweigh costs. *PloS One* **7**, e40542.

Svenningsen SL, Tu KC, Bassler BL, 2009. Gene dosage compensation calibrates four regulatory RNAs to control *Vibrio cholerae* quorum sensing. *EMBO J.* **28**, 429-39.

Tajima M, Crane JM, Verkman AS, 2010. Aquaporin-4 (AQP4) associations and array dynamics probed by photobleaching and single-molecule analysis of green fluorescent protein-AQP4 chimeras. *J. Biol. Chem.* **285**, 8163-70.

Takano J, Wada M, Ludewig U, Schaaf G, Von Wiren N, Fujiwara T, 2006. The Arabidopsis major intrinsic protein NIP5;1 is essential for efficient boron uptake and plant development under boron limitation. *Plant Cell* **18**, 1498-509.

Talavera G, Castresana J, 2007. Improvement of phylogenies after removing divergent and ambiguously aligned blocks from protein sequence alignments. *Systematic Biology* **56**, 564-77.

Talbot NJ, 2003. On the trail of a cereal killer: exploring the biology of *Magnaporthe grisea*. *Ann Rev Microbiol* **57**, 177-202.

Talbot NJ, Ebbole DJ, Hamer JE, 1993. Identification and characterization of MPG1, a gene involved in pathogenicity from the rice blast fungus *Magnaporthe grisea*. *Plant Cell* **5**, 1575-90.

Tamás MJ, Karlgren S, Bill RM, 2003. A Short Regulatory Domain Restricts Glycerol Transport through Yeast Fps1p. *J. Biol. Chem.* **278**, 6337-45.

Tamas MJ, Luyten K, Sutherland FC, 1999. Fps1p controls the accumulation and release of the compatible solute glycerol in yeast osmoregulation. *Mol MicroBiol.* **31**, 1087-104.

Tammaro P, Shimomura K, Proks P, 2008. *Xenopus* oocytes as a heterologous expression system for studying ion channels with the patch-clamp technique. *Methods Mol Biol.* **491**, 127-39.

Tamura K, Peterson D, Peterson N, Stecher G, Nei M, Kumar S, 2011. MEGA5: molecular evolutionary genetics analysis using maximum likelihood, evolutionary distance, and maximum Parsimony Methods. *Mol Biol. Evol*.

Tanghe A, Carbrey JM, Agre P, Thevelein JM, Van Dijck P, 2005a. Aquaporin Expression and Freeze Tolerance in *Candida albicans*. *Appl. Environ. Microbiol.* **71**, 6434-7.

Tanghe A, Kayingo G, Prior BA, Thevelein JM, Van Dijck P, 2005b. Heterologous aquaporin (AQY2-1) expression strongly enhances freeze tolerance of *Schizosaccharomyces pombe*. *J. Mol MicroBiol. Biotechnol* **9**, 52-6.

Tanghe A, Van Dijck P, Thevelein JM, 2006. Why do microorganisms have aquaporins? *Trends MicroBiol.* **14**, 78-85.

Terpe K, 2003. Overview of tag protein fusions: from molecular and bioChem. fundamentals to commercial systems. *Appl MicroBiol. Biotechnol* **60**, 523-33.

Thines E, Weber RW, Talbot NJ, 2000. MAP kinase and protein kinase A–dependent mobilization of triacylglycerol and glycogen during appressorium turgor generation by *Magnaporthe grisea*. *Plant Cell* **12**, 1703-18.

Thorsen M, Di Y, Tangemo C, 2006. The MAPK Hog1p modulates Fps1p-dependent arsenite uptake and tolerance in yeast. *Mol Biol. Cell* **17**, 4400-10.

Tichopad A, Dilger M, Schwarz G, Pfaffl MW, 2003. Standardized determination of real-time PCR efficiency from a single reaction set-up. *Nucleic Acids Res* **31**, e122.

Tilman D, Balzer C, Hill J, Befort BL, 2011. Global food demand and the sustainable intensification of agriculture. *Proc. Nat. Acad. Sci. USA* **108**, 20260-4.

Tingaud-Sequeira A, Calusinska M, Finn RN, Chauvigné F, Lozano J, Cerdà J, 2010. The zebrafish genome encodes the largest vertebrate repertoire of functional aquaporins with dual paralogy and substrate specificities similar to mammals. *BMC Evolutionary Biology* **10**, 38.

Tornroth-Horsefield S, Wang Y, Hedfalk K, 2006. Structural mechanism of plant aquaporin gating. *Nature* **439**, 688-94.

Tradtrantip L, Tajima M, Li L, Verkman AS, 2009. Aquaporin water channels in transepithelial fluid transport. *J. Med Invest* **56 Suppl**, 179-84.

Trail F, 2007. Fungal cannons: explosive spore discharge in the Ascomycota. *FEMS MicroBiol. Lett* **276**, 12-8.

Tsukaguchi H, Shayakul C, Berger UV, 1998. Molecular characterization of a broad selectivity neutral solute channel. *J. Biol. Chem.* **273**, 24737-43.

Uehlein N, Lovisolo C, Siefritz F, Kaldenhoff R, 2003. The tobacco aquaporin NtAQP1 is a membrane CO2 pore with physiological functions. *Nature* **425**, 734-7.

Umenishi F, Verbavatz JM, Verkman AS, 2000. cAMP regulated membrane diffusion of a green fluorescent protein-aquaporin 2 chimera. *Biophys J.* **78**, 1024-35.

Urban M, Bhargava T, Hamer JE, 1999. An ATP-driven efflux pump is a novel pathogenicity factor in rice blast disease. *EMBO J.* **18**, 512-21.

Valent B, Farrall L, Chumley FG, 1991. *Magnaporthe grisea* genes for pathogenicity and virulence identified through a series of backcrosses. *Genetics* **127**, 87-101.

Valent B, Khang CH, 2010. Recent advances in rice blast effector research. *Cur Op Plant Biol* **13**, 434-41.

Van Engelen FA, Molthoff JW, Conner AJ, Nap JP, Pereira A, Stiekema WJ, 1995. pBINPLUS: an improved plant transformation vector based on pBIN19. *Transgenic Res* **4**, 288-90.

Vandesompele J, De Preter K, Pattyn F, 2002. Accurate normalization of real-time quantitative RT-PCR data by geometric averaging of multiple internal control genes. *Genom Biol.* **3**.

Veneault-Fourrey C, Barooah M, Egan M, Wakley G, Talbot NJ, 2006. Autophagic fungal cell death is necessary for infection by the rice blast fungus. *Science* **312**, 580-3.

Verkman AS, 2005. Novel roles of aquaporins revealed by phenotype analysis of knockout mice. *Rev Physiol BioChem. Pharmacol* **155**, 31-55.

Verkman AS, 2011. Aquaporins at a glance. *J. Cell Sci* **124**, 2107-12.

Vieceli Dalla Sega F, Zambonin L, Fiorentini D, Rizzo B, Landi L, Prata C, 2012. Aquaporins can facilitate Nox-produced hydrogen peroxide transport through plasma membrane in leukaemia cell lines. *Free Radical Biology and Medicine* **53, Supplement 1**, S158-S9.

Villalba F, Collemare J, Landraud P*, et al.*, 2008. Improved gene targeting in *Magnaporthe grisea* by inactivation of MgKU80 required for non-homologous end joining. *Fung Genet Biol* **45**, 68-75.

Virkki LV, Franke C, Somieski P, Boron WF, 2002. Cloning and functional characterization of a novel aquaporin from *Xenopus laevis* Oocytes. *J. Biol. Chem.* **277**, 40610-6.

Vogel C, Marcotte EM, 2012. Insights into the regulation of protein abundance from proteomic and transcriptomic analyses. *Nat Rev Genet* **13**, 227-32.

Von Bülow J, Müller-Lucks A, Kai L, Bernhard F, Beitz E, 2012. Functional characterization of a novel aquaporin from *dictyostelium discoideum* amoebae implies a unique gating mechanism. *J. Biol. Chem.* **287**, 7487-94.

Wallace IS, Roberts DM, 2004. Homology modeling of representative subfamilies of *Arabidopsis* major intrinsic proteins. Classification based on the aromatic/arginine selectivity filter. *Plant Physiology* **135**, 1059-68.

Wallace IS, Roberts DM, 2005a. Distinct transport selectivity of two structural subclasses of the nodulin-like intrinsic protein family of plant aquaglyceroporin channels. *BioChem.* **44**, 16826-34.

Wallace IS, Wills DM, Guenther JF, Roberts DM, 2002. Functional selectivity for glycerol of the nodulin 26 subfamily of plant membrane intrinsic proteins. *FEBS Lett* **523**, 109-12.

Wang H, Xu Z, Gao L, Hao B, 2009. A fungal phylogeny based on 82 complete genomes using the composition vector method. *BMC Evol Biol* **9**, 195.

Wang Z-Y, Soanes DM, Kershaw MJ, Talbot NJ, 2007. Functional analysis of lipid metabolism in *Magnaporthe grisea* reveals a requirement for peroxisomal fatty acid β-oxidation during appressorium-mediated plant infection. *Mol Plant-Microb Interact* **20**, 475-91.

Wang ZY, Thornton CR, Kershaw MJ, Debao L, Talbot NJ, 2003. The glyoxylate cycle is required for temporal regulation of virulence by the plant pathogenic fungus *Magnaporthe grisea*. *Mol Microbiol* **47**, 1601-12.

Weld RJ, Plummer KM, Carpenter MA, Ridgway HJ, 2006. Approaches to functional genomics in filamentous fungi. *Cell Res* **16**, 31-44.

West RW, Yocum RR, Ptashne M, 1984. *Saccharomyces cerevisiae* GAL1-GAL10 divergent promoter region: location and function of the upstream activating sequence UASG. *Mol Cell Biol* **4**, 2467-78.

Will JL, Kim HS, Clarke J, Painter JC, Fay JC, Gasch AP, 2010. incipient balancing selection through adaptive loss of aquaporins in natural *Saccharomyces cerevisiae* populations. *PLoS Genet* **6**, e1000893.

Willems E, Leyns L, Vandesompele J, 2008. Standardization of real-time PCR gene expression data from independent Biol. replicates. *Anal BioChem.* **379**, 127-9.

Wilson IG, 1997. Inhibition and facilitation of nucleic acid amplification. *Appl Environ Microbiol* **63**, 3741.

Wilson RA, Talbot NJ, 2009a. Fungal physiology – a future perspective. *Microbiol* **155**, 3810-5.

Wilson RA, Talbot NJ, 2009b. Under pressure: investigating the biology of plant infection by *Magnaporthe oryzae*. *Nat Rev MicroBiol.* **7**, 185-95.

Winzeler EA, Shoemaker DD, Astromoff A*, et al.*, 1999. functional characterization of the *S. cerevisiae* genome by gene deletion and parallel analysis. *Science* **285**, 901-6.

Wu B, Beitz E, 2007. Aquaporins with selectivity for unconventional permeants. *Cell Mol Life Sci* **64**, 2413-21.

Wu M, Chatterji S, Eisen JA, 2012. Accounting for alignment uncertainty in phylogenomics. *PLoS One* **7**, e30288.

Wuchty S, Oltvai ZN, Barabasi AL, 2003. Evolutionary conservation of motif constituents in the yeast protein interaction network. *Nat Genet* **35**, 176-9.

Xia X, Xie Z, Kjer KM, 2003. 18S Ribosomal RNA and tetrapod phylogeny. *System Biol* **52**, 283-95.

Xiong L, Zhu JK, 2002. Molecular and genetic aspects of plant responses to osmotic stress. *Plant Cell Environ* **25**, 131-9.

Xu H, Cooke J, Zwiazek J, 2013. Phylogenetic analysis of fungal aquaporins provides insight into their possible role in water transport of mycorrhizal associations. *Botany*.

Xu J-R, Hamer JE, 1996. MAP kinase and cAMP signaling regulate infection structure formation and pathogenic growth in the rice blast fungus *Magnaporthe grisea*. *Genes Devel* **10**, 2696-706.

Xue M, Yang J, Li Z*, et al.*, 2012. Comparative analysis of the genomes of two field isolates of the rice blast fungus *Magnaporthe oryzae*. *PLoS Genet* **8**, e1002869.

Yafetto L, Carroll L, Cui Y, 2008. The fastest flights in nature: high-speed spore discharge mechanisms among fungi. *PloS one* **3**, e3237.

Yakata K, Tani K, Fujiyoshi Y, 2011. Water permeability and characterization of aquaporin-11. *J. Struct Biol.* **174**, 315-20.

Yang B, Song Y, Zhao D, Verkman AS, 2005. Phenotype analysis of aquaporin-8 null mice. *Amer J. Physiol - Cell Physiology* **288**, C1161-C70.

Yang B, Zhang H, Verkman AS, 2008. Lack of aquaporin-4 water transport inhibition by antiepileptics and arylsulfonamides. *Bioorg Med Chem.* **16**, 7489-93.

Yool AJ, Weinstein AM, 2002. New roles for old holes: Ion channel function in aquaporin-1. *News Physiol Sci* **17**, 68-72.

Yu J, Yool AJ, Schulten K, Tajkhorshid E, 2006. Mechanism of Gating and Ion Conductivity of a Possible Tetrameric Pore in Aquaporin-1. *Structure* **14**, 1411-23.

Zardoya R, 2005. Phylogeny and evolution of the major intrinsic protein family. *Biol Cell* **97**, 397-414.

Zardoya R, Ding X, Kitagawa Y, Chrispeels MJ, 2002. Origin of plant glycerol transporters by horizontal gene transfer and functional recruitment. *Proc Natl Acad Sci U S A* **99**, 14893-6.

Zardoya R, Villalba S, 2001. A phylogenetic framework for the aquaporin family in eukaryotes. *J. Mol Evol* **52**, 391-404.

Zarrinpar A, Bhattacharyya RP, Lim WA, 2003. The structure and function of proline recognition domains. *Sci Signal* **2003**

Zartman JJ, Yakoby N, Bristow CA, 2008. Cad74A is regulated by BR and is required for robust dorsal appendage formation in *Drosophila* oogenesis. *Devel Biol* **322**, 289-301.

Zeigler RS, Leong SA, Teng P, 1994. *Rice blast disease*. IRRI

Zhang G, Gurtu V, Kain SR, 1996. An enhanced green fluorescent protein allows sensitive detection of gene transfer in mammalian cells. *BioChem. Biophys Res Comm* **227**, 707-11.

Zhang H, Liu K, Zhang X, 2010a. A two-component histidine kinase, MoSLN1, is required for cell wall integrity and pathogenicity of the rice blast fungus, *Magnaporthe oryzae*. *Curr Genet* **56**, 517-28.

Zhang S, Fan Y, Xia YX, Keyhani NO, 2010b. Sulfonylurea resistance as a new selectable marker for the entomopathogenic fungus *Beauveria bassiana*. *Appl MicroBiol. Biotechnol* **87**, 1151-6.

Zhang X, 2012. Correlation of aquaporins and transmembrane solute transporters revealed by genome-wide analysis in developing maize leaf. *International J. Genomics* **2012**.

Zhao X, Kim Y, Park G, Xu J-R, 2005. A mitogen-activated protein kinase cascade regulating infection-related morphogenesis in *Magnaporthe grisea*. *Plant Cell* **17**, 1317-29.

Zuckerkandl E, Pauling L, 1965. Evolutionary divergence and convergence in proteins. *Evol Genes Prot* **97**, 97-166.